Physicochemical
Problems
of Mineral Processing
44 (2010)

Instructions for preparation of manuscripts

It is recommended that the following guidelines be followed by the authors of the manuscripts:

- Original papers dealing with the principles of mineral processing and papers on technological aspects of mineral processing will be published in the journal which appears once a year
- The manuscript should be sent to the Editor for reviewing before February 15 each year
- The manuscript should be written in English. For publishing in other languages an approval of the editor is necessary
- Contributors whose first language is not the language of the manuscript are urged to have their manuscript competently edited prior to submission.
- The manuscript should not exceed 10 pages
- Two copies of the final manuscript along with an electronic version should be submitted for publication before April 15
- There is a 80 USD fee for printing the paper. No fee is required for the authors participating in the Annual Symposium on Physicochemical Problems on Mineral Processing
- Manuscripts and all correspondence regarding the symposium and journal should be sent to the editor.

Address of the Editorial Office
Wrocław University of Technology
Wybrzeże Wyspiańskiego 27, 50-370 Wrocław, Poland
Institute of Mining Engineering
Laboratory of Mineral Processing

Location of the Editiorial Office:
pl. Teatralny 2, Wrocław, Poland
phone: (071) 320 68 79, (071) 320 68 78
fax: (071) 344 81 23
pawel nowak <ncnowak@cyf-kr.edu.pl>
jan.drzymala@pwr.wroc.pl
andrzej.luszczkiewicz@pwr.wroc.pl
zygmunt.sadowski@pwr.wroc.pl
http://www.ig.pwr.wroc.pl/minproc
http://www.minproc.pwr.wroc.pl/journal

Physicochemical Problems of Mineral Processing 44 (2010)

www.ig.pwr.wroc.pl/minproc
www.minproc.pwr.wroc.pl/journal

WROCŁAW 2010

The papers published in the Physicochemical Problems of Mineral Processing journal are abstrated in Chemical Abstracts, Thomson Reuters (Science Citation Index Expanded, Materials Science Citation Index, Journal Citation Reports), Coal Abstracts, Google Scholar and other sources

This publication was supported in different forms by:
Komitet Górnictwa PAN
(Sekcja Wykorzystania Surowców Naturalnych)
Akademia Górniczo-Hutnicza w Krakowie
Politechnika Śląska w Gliwicach
Politechnika Wrocławska

ISSN 1643-1049
OFICYNA WYDAWNICZA POLITECHNIKI WROCŁAWSKIEJ
WYBRZEŻE WYSPIAŃSKIEGO 27, 50-370 WROCŁAW, POLAND

CONTENTS

A.M. Amer, Hydrometallurgical processing of low grade Egyptian magnesite . 5

R. Aranowski, J. Hupka, Ch. Jungnickel, Changes in rheological properties during anaerobic digestion of activated sludge 13

M. Brozek, A. Mlynarczykowska, Probability of detachment of particle determined according to the stochastic model of flotation kinetics 23

J. Grodzka, A. Pomianowski, Hydrogen-bond puzzle 35

Y.S. Haroun, M.F. Raslan, Occurrence of barite mineralization in Bahariya Depression, Western Desert, Egypt 41

A. Heim, A. Obraniak, T. Gluba, Change in the properties of beds granulated in disc granulators 53

S.S. Ibrahim, A.A. El-Midany, T.R. Boulos, Economic preferences of mechanical activation over mineral beneficiation for phosphate rock direct applications 63

S.S. Ibrahim, A.A. El-Midany, T.R. Boulos, Effect of intensive mechanical stresses on phosphate chemistry as a way to increase its solubility for fertilizer application 79

A. Kolodziejczak-Radzimska, T. Jesionowski, A. Krysztafkiewicz, Obtaining zinc oxide from aqueous solutions of KOH and $Zn(CH_3COO)_2$ 93

A. Korkosz, M. Janczarek, R. Aranowski, J. Rzechula, J. Hupka, Efficiency of deep bed filtration in treatment of swimming pool water 103

P.B. Kowalczuk, T. Chmielewski, Changes of electrode potential in the non-oxidative leaching 115

I. Kursun, Determination of flocculation and adsorption-desorption characteristics of Na-feldspar concentrate with different polymers..... 127

W. Malewski, T. Jesionowski, F. Ciesielczyk, A. Krysztafkiewicz, Dispersion characterisation of colloidal silica at subsequent stages of silica sol preparation 143

A. Malicka-Soczka, L. Domka, A. Kozak, Kaolin modified with silane compounds as a filler used in rubber industry 151

F. Modrzejewska-Sikorska, A. Ciesielczyk, A. Krysztafkiewicz, T. Jesionowski, Synthesis and characterisation of precipitated copper(II) silicates 157

R. Modrzewski, P. Wodzinski, The results of process investigations of a double-frequency screen 169

A. Nowik-Zajac, C. Kozlowski, W. Walkowiak, Transport of perrhenate anions across plasticizer membranes with basic ion carriers 179

T.P. Olejnik, Kinetics of grinding ceramic bulk considering grinding media contact points 187

B. Pospiech, W. Walkowiak, Studies on iron(III) removal from chloride aqueous solutions by solvent extraction and transport through polymer inclusion membranes with D2EHPA 195

Z. Sadowski, I. Polowczyk, A. Frackowiak, T. Kozlecki, S. Chibowski, Bioinspired synthesis of calcium carbonate colloid particles 205

A.M. Saleh, A study on the performance of second order models and two phase models in iron ore flotation 215

K. Siwinska-Stefanska, A. Krysztafkiewicz, F. Ciesielczyk, D. Paukszta, J. Sojka-Ledakowicz, T. Jesionowski, Physicochemical and structural properties of TiO_2 precipitated in an emulsion system 231

M. Ulewicz, U. Lesinska, M. Bochenska, Transport of lead across polymer inclusion membrane with p-tert -butylcalix[4]arene derivative 245

M. Yildirim, H. Akarsu, Preparation of magnesium oxide (MgO) from dolomite by leach-precipitation-pyrohydrolysis process 257

Physicochem. Probl. Miner. Process. 44(2010) 5-12

journal homepage
www.minproc.pwr.wroc.pl/journal/

Physicochemical Problems of Mineral Processing

Index No. 32213X ISSN 1643-1049

A.M. Amer*

HYDROMETALLURGICAL PROCESSING OF LOW GRADE EGYPTIAN MAGNESITE

Received December 20, 2008; reviewed; accepted March 16, 2009

The pressure leaching with carbon-dioxide for the production of high purity magnesium oxide from low grade magnestie oxide from (Halaib) deposit (Eastern Desert) has been studied. It was found that more than 90% of magnesium can be extracted under the following conditions: calcinations temperature 700° C, leaching temperature 50° C, carbon dioxide pressure 600 kPa and leaching time 120 min. The kinetics of the carbonation process was investigated and the activation energy of the process was determined (30 kg/mole).

key words: magnesite, leaching, calcinations, kinetics

INTRODUCTION

Magnesite ($MgCO_3$) is a basic raw material for manufacturing of the alkaline refractories. It is used in the iron-steel, cement, glass, sugar, paper, and pharmaceutical industries as well as in the production of many magnesium chemicals (Whaley, 1981; Van Staden, 1994).

Beneficiation of magnesite is carried out using physical and chemical methods. The physical methods of upgrading low-grade magnesite rely on the physical differences between magnesium carbonate and impurities. The chemical beneficiation relies on chemical leaching of magnesite with the use of common inorganic acids such

* Environmental Science Dept. Fac. of Science; Alexandria University, 21511 Moharrem Bek, Alexandria , Egypt; e-mail: ashrafamer0408@yahoo.com

as hydrochloric (Tunley, 1992) sulfuric (Treushchenko et al., 1991) and nitric acid (Ekmekyapar, 1989; Li, 1991). The use of these acids in benefication of low grade magnesites have not been commericalised because of complexity of purification and acid generation.

Carbon dioxide (Sheila, 1991; Amer, 1996) has been used as a leaching agent to selectively dissolve magnesia and form soluble magnesium bicarbonate leaving the impurities unaffected. The solution is decomposed by heating to form basic magnesium carbonate, which is next processed to obtain high purity magnesia.

A rapid growth of the steel industry in Egypt and particularly the increased use of oxygen in steel making has created heavy demands for high grade magnesite and refractories. Therefore, an increased attention is being paid in Egypt to the upgrading of low grade and submarginal magnesite by chemical treatment.

In Egypt, magnesite deposits are found in the Southern part of the Eastern Desert in Halaib, Gabal Mudargag and G. El-Mayit. The talc-magnesite deposits of the Barramyia area appear to be of low grade magnesite rocks which, by the removal of talc, might become valuable as a refractory material and in the production of magnesium compounds (Said, 1991).

The extraction of magnesium from magnesite involves a thermal decomposition of magnesite and leaching of the calcinated magnesite in an autoclave under carbon-dioxide pressure to produce soluble magnesium bicarbonate. The solution is subsequently decomposed by heating to precipitate basic magnesium carbonate, which is then thermally decomposed to produce high purity magnesium oxide.

MATERIAL AND METHODS

In this study low-grade magnesite (Halaib deposit), from the Southern Eastern Desert, was used. Its chemical composition is given in Table 1. It is clear that magnesite contains 37.2% of MgO while the theoretical MgO content in pure magnesite is 47.82%. This indicates that the studied magnesite samples are of low-grade ore.

The X-ray diffraction analysis indicated, that in addition to magnesite, which is present as a major mineral, there are dolomite (Ca,Mg_2,CO_3) and antigorite ($3MgO{\cdot}2SiO_2{\cdot}2H_2O$) which are present as minor constituents.

The calcination of magnesite samples was carried out in an electric muffle furnace. Representative samples of magnesite ore (-12+3 mm in diameter) were calcinated at 750°C for 2 hrs, crushed and ground to 100% passing through a 150 μm screen for the leaching experiments.

All pressure leaching experiments were performed in a laboratory 2 dm^3 volume autoclave (Amer and Ibrahim, 1997). It had a maximum working pressure of 2 kPa, a temperature of 140° C and a maximum stirring speed of 800 min^{-1}. The experiments

were carried out with circulating cold water through the cooling coils of the autoclave. The stirrer used maintained good dispersion of carbon dioxide in the pulp. The slurry samples were taken through a capillary tube, filtered, and chemically analysed.

Table 1. Chemical analysis of representative sample of Halaib magnesite

Constituent	%
MgO	37.32
CO_2	50.41
CaO	5.38
SiO_2	3.78
Fe_2O_3	0.47
Al_2O_3	0.36
Cl^-	0.33
SO_3	0.24
Na_2O	0.22
MnO_2	0.14
K_2O	0.08
P_2O_5	0.05
Moisture	0.39
L.O.I.* (1000^o C)	49.75

*Loss on ignition

RESULTS AND DISCUSSION

EFFECT OF CARBON DIOXIDE PRESSURE

The effect of CO_2 partial pressure in the range from 200 to 900 kPa was studied. CO_2 was bubbled into the slurry under different partial pressures where the dissolution of magnesium increased with the increase of carbon dioxide pressure and leach time as illustrated in Figure 1.

EFFECT OF TEMPERATURE

Leaching temperature has a considerable influence on the dissolution of magnesium. Its influence was studied over the temperature range from 20 to 50^{o}C using a CO_2 pressure of 800 kPa, particle size of –44 μm and a solid liquid ratio of 15 g/dm^3. The results are shown in Fig. 2. It can be concluded that the magnesium conversion increases with the increase of temperature from 20 to 40^{o}C.

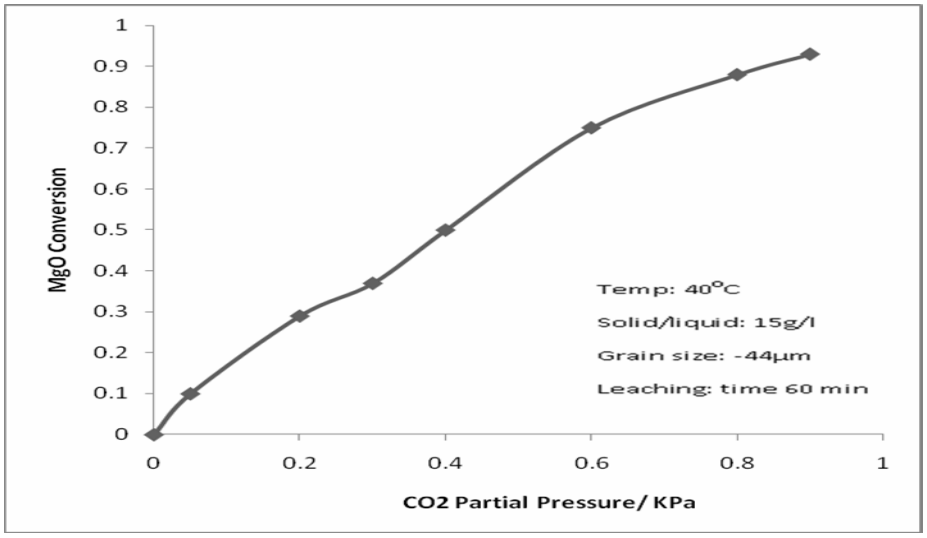

Fig. 1. Effect of CO_2 partial pressure on MgO conversion

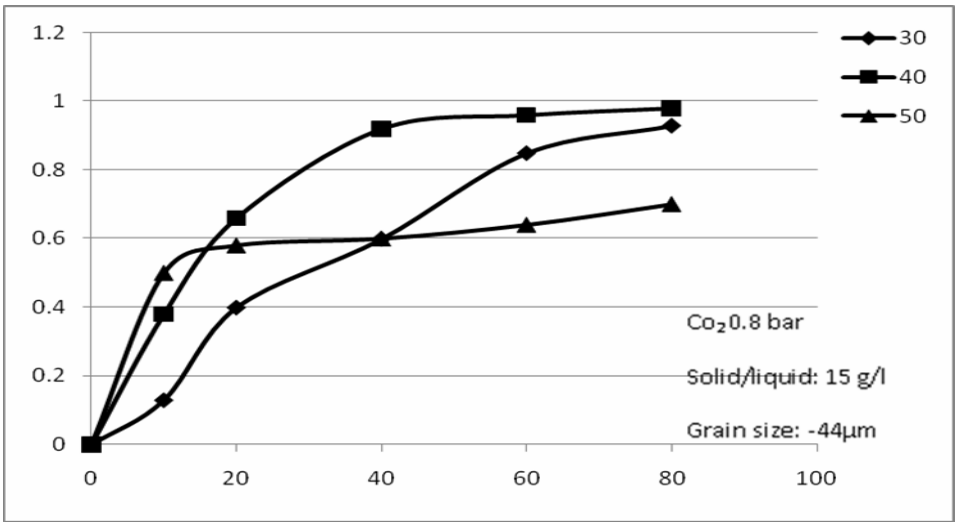

Fig. 2. Effect of leaching temperature

The observed decrease of MgO conversion at 50° C may be due to a low solubility of MgO and precipitation of basic magnesium carbonate (Sheila et al., 1991).

EFFECT OF SOLID LIQUID RATIO

Figure 3 ilustrates the conversion of magnesium oxide as a function of solid-liquid ratio at 40° C and CO_2 pressure of 800 kPa. For a solid-liquid ratio of 50 g/dm^3, the

precipitation of basic magnesium carbonate occurs due to a high magnesium concentration.

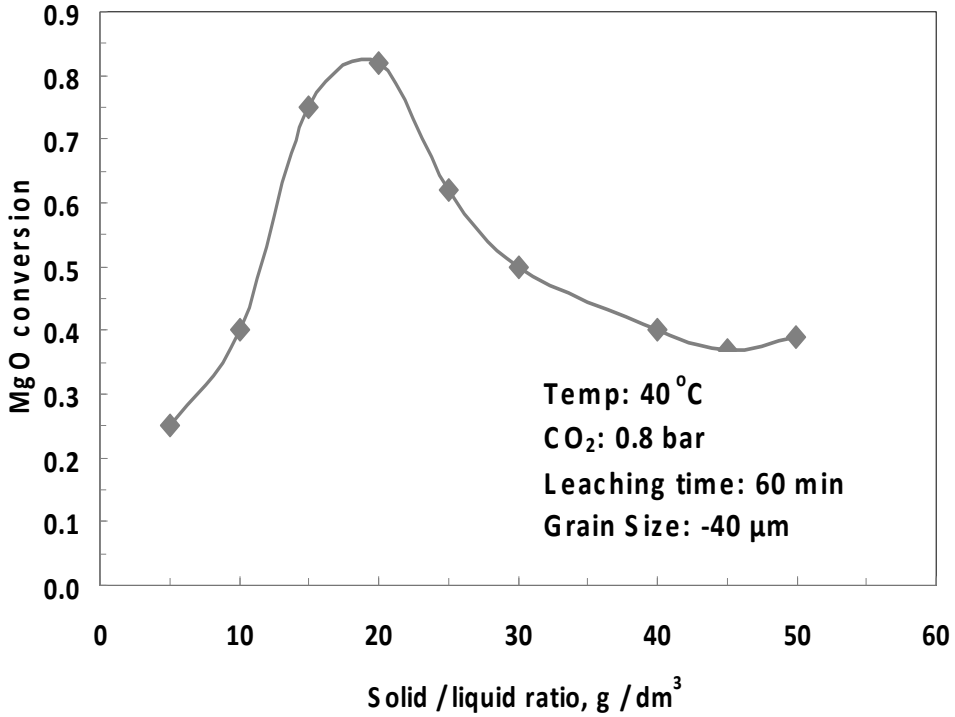

Fig. 3. Effect of solid/liquid

EFFECT OF PARTICLE SIZE

The effect of particle size on the dissolution of magnesium is shown in Fig. 4. In these experiments different size fractions of calcinate (from 75 to 50 µm, 44-75 µm and below 44 µm) were leached in the CO_2 atmosphere and all three size fractions showed similar response to dissolution. It can be attributed to the hydration of calcinated magnesite prior to carbonation. The $Mg(OH)_2$ particles have different surface properties from these of MgO. The $Mg(OH)_2$ particles are finer than MgO and hence the surface of MgO has no remarkable effect on the rate of magnesium dissolution.

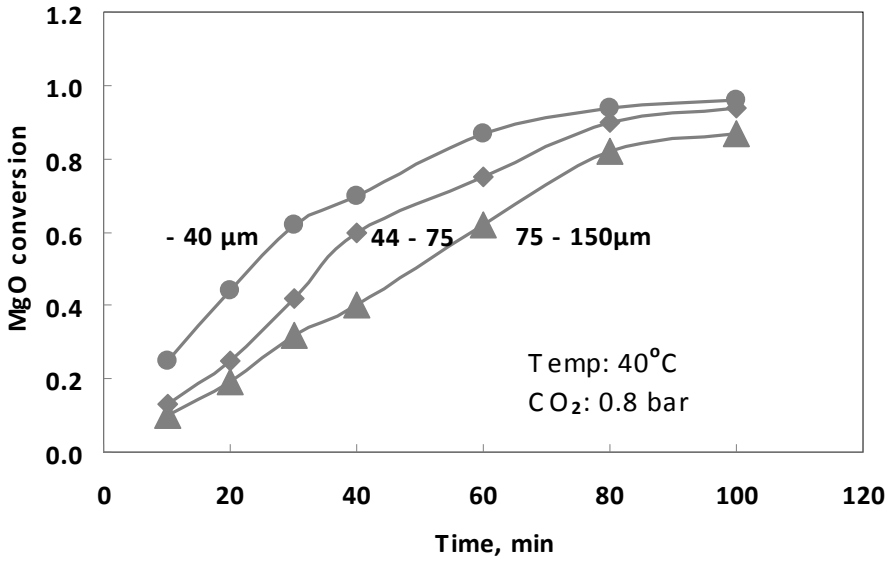

Fig. 4. Effect of particle size on MgO conversion

KINETICS AND MECHANISM OF LEACHING PROCESS

The magnesium extraction from calcined magnesite in the presence of CO_2 can be expressed by the following reactions:

$$MgO + H_2O \text{ ---> } Mg(OH)_2 \quad \text{hydration} \tag{1}$$

$$Mg(OH)_2 + 2CO_2 \text{ ---> } Mg(HCO_3)_2 \tag{2}$$

To determine the reaction rate constant, the following model was used:

$$1-(1-\alpha MgO)^{1/3} = kt \tag{3}$$

where k is apparent rate reaction constant, α fraction of leached magnesium oxide from magnesite and t reaction time.

Plots of this model equation, using the experimental data of MgO in solution, is shown in Fig. 4. According to Fig. 4. the dissolution is controlled by chemical surface reactions for different particle sizes. Figure 5 shows the Arrhenius plot, while the reaction rate constant k, calculated from the experiments, is shown in Fig. 6. The activation energy of 30 kJ/mol was calculated from the slope. This value falls above the maximum theoretical values for chemical reaction (Krik-Othmer, 1995).

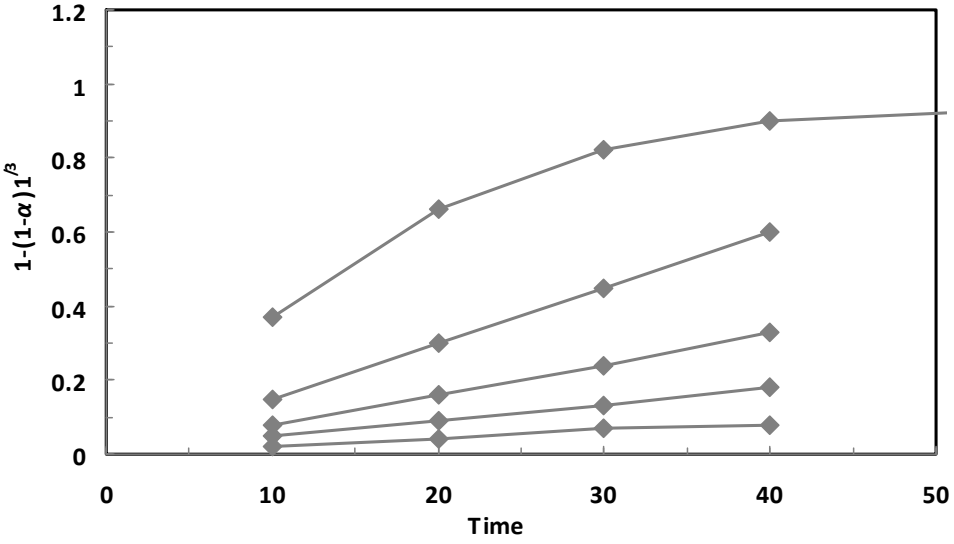

Fig. 5. Plot of 1-(1-α)1/3 against leaching time

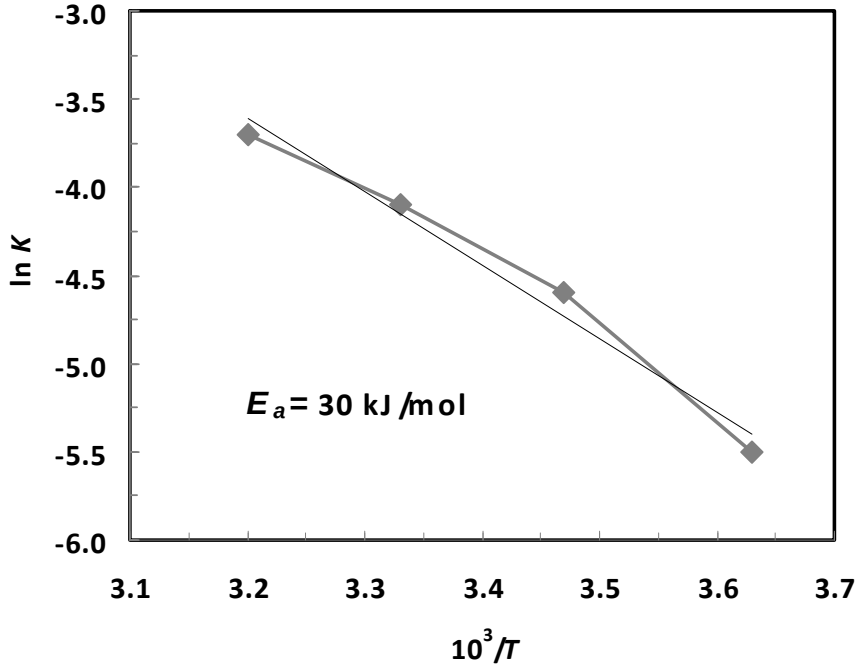

Fig. 6. Arrhenius plot for determining the activation energy

CONCLUSIONS

A selective leaching of magnesium from a low grade Halaib magnesite ore can be achieved by pressure leaching with carbon dioxide. It has been found that the dissolution of magnesium is enhanced by low reaction temperature (40 ^{0}C) and high carbon dioxide pressure (800 Pa) in the aqueous carbon dioxide during the leaching process. The kinetic data were analysed in terms of the modified chemical reaction rate equation and the apparent energy of activation of 30 kJ/mol suggests that the rate controlling step is controlled chemically at the surface of the $Mg(OH)_2$ particles.

REFERENCES

AMER A.M. (1996). A *contribution to hydrometallurgical processing of low-grade Egyptian dolomite deposits*. Hydrometallurgy 42, 343-356.

AMER A.M. and IBRAHIM, I.A. (1997). *Leaching of a low grade Egyptian chromite ore*. Hydrometallurgy 43, 307-16.

EKMEKYAPAR, A. (1989). *Dissolution of magnesite in H_2SO_4 solutions*. Ph. D. Thesis, Alaturk Univ. Erzurum.

KRIK-OTHMER (1995). *Encyclopedia of Chemical Technology*. 4th ed. Vol. 15.

LI, C. (1991). *Method for purifying magnesia oxide*. Chinese Pat. CN 1, 057, 247.

SAID, R. (1991*). Geology of Egypt*, Ed. Balkema, Rotterdam.

SHEILA, D., Sankaran, C. and Khangaonkar, P.K. (1991). *Studies on the extraction of magnesia from low grade magnesites by carbon-dioxide pressure leaching of hydrated magnesia*. Minerals Eng. U. 4, No. 1, pp. 79-88.

TREUSHCHENKO, N.N., Dmitrevsku, B.A., Rumyantseu, A.Y. and Belyakov, V.A. (1991). *Manufacture of magnesium oxide*. USSR Pat 1,6423, 463.

TUNLEY, T.H. (1992). *Magnesia manufacture from dolomite*. S. Afr. Pat. ZA 9, 103, 939.

VAN STADEN, J.F. 1994). The *industrial significance of magnesium compounds*. Spectrum 32(2), 20-22.

WHALEY, T.P. (1981). *Magnesium compounds of industrial significance*. Ind. Miner. Tech., 10, 733-39.

Amer A.M., *Hydrometalurgiczna przeróbka ubogiej egipskiej rudy magnezytowej*, Physicochemical Problems of Mineral Processing, 44 (2010) 5-12, (w jęz. ang), http://www.minproc.pwr.wroc.pl/journal

Badano zastosowanie ługowania ciśnieniowego ditlenkiem węgla do produkcji wysokiej czystości magnezytu z ubogiego magnezytu pochodzącego z obszaru Halaiba na Pustyni Wschodniej. Osiągnięto ponad 90-cio procentowy uzysk magnezu stosując następujące warunki: temperatura kalcynacji 700 ^{o}C, temperatura ługowania 50 ^{o}C, ciśnienie ditlenku węgla 600 kPa oraz czas ługowania 120 min. Badano także kinetykę procesu karbonatyzacji.

słowa kluczowe: magnezyt, ługowanie, kalcynacja, kinetyka

Physicochem. Probl. Miner. Process. 44(2010) 13-22

journal homepage
www.minproc.pwr.wroc.pl/journal/

Physicochemical Problems of Mineral Processing

Index No. 32213X ISSN 1643-1049

R. Aranowski*, J. Hupka*, Ch. Jungnickel*

CHANGES IN RHEOLOGICAL PROPERTIES DURING ANAEROBIC DIGESTION OF ACTIVATED SLUDGE

Received July 1; reviewed; accepted July 27, 2009

The measurements of rheological properties of activated sludge suspension after mechanical disintegration indicate a substantial decrease in viscosity of up to 60%. Together with the decrease of viscosity pseudoplastic properties increased and the flow limit dropped. Similarly, significant changes of rheological properties occurred in the sludge, subjected to methane fermentation. One can observe that the length of fermentation period influences the decrease in viscosity of the sewage sludge. It is postulated to use the measurement of viscosity for the estimation of excessive sludge disintegration ratio as this method is much faster than determination of COD.

key words: rheological properties, activated sludge, anaerobic digestion, rheology, sludge disintegration

INTRODUCTION

Due to substantial deviations from Newtonian properties occurring during the flow of sewage sludge, hydraulic transport ought to take place only for well defined rheological properties. Lack, or insufficient amount of information can lead to too fast damage of plumbing fittings and pipes and in particular cases resulting in dangerous accidents. Also, of utmost importance is the information on rheological properties of sludge at the stage of designing new sewage treatment systems.

Currently, numerous sewage treatment plants apply systems decreasing the amount of formed sludge through methane fermentation. With regard to a substantial

* Department of Chemical Technology, Gdansk University of Technology, ul. Narutowicza 11/12, 80-952 Gdansk, Poland, e-mail: aran@chem.pg.gda.pl

concentration of dry matter in condensed sludge fed to fermentation chambers, the transport process at this stage is of crucial importance for the whole sewage treatment process.

With respect to complex composition of sewage sludge its properties undergo continuous changes during treatment as well as methane fermentation process. Hence, the knowledge of rheological properties changes that occur during transport and fermentation process allows for optimization of the choice of pumps and mixers. These elements are of crucial importance for correct working of closed fermentation chambers (Baudez, 2006) and dewatering process (Gilles et al., 2005, Örmeci, 2007).

Activated sludge has pseudoplastic properties indicating the presence of thixotrophic behavior (Moeller, Torres, 1997, Mori et al., 2006, Pham et al., 2009). One can also find numerous contradictory opinions proving that activated sludge has both Newtonian and non Newtonian properties. The presence of hysteresis on flow curves is most frequently explained by disintegration of internal structure of liquid suspension as a result of the operation of shear stress. As a consequence there is an assumption that the higher the initial peak, the bigger force must be applied to overcome the internal structure and the bigger the hysteresis loop the longer must be the deformation of the liquid in order to achieve the steady state. When the forces acting on the liquid are removed, the structure of the liquid should be restored, however, there is documentation which does not confirm the occurrence of this phenomenon. Thus, irreversible disintegration of internal structure of the liquid must be explained differently. As it was proved by Magnin and Piau (1990) as well as Greener and Connely (1986) the viscoelastic effect can produce a substantial hysteresis on flow curves. In the research of rheology of polymers one can find information explaining the presence of initial peak. It is the transition from elastic to viscous phase. As proved by Mujumdar and coauthors (Mujumdar et al., 2002), sewage sludge exhibit a non-Newtonian behaviour characterized by three domains: a linear viscoelastic part below a first critical shear stress, then an intermediate regime and beyond a second critical stress, a purely viscous part.

MATERIALS AND METHODS

FERMENTATION AND DIGESTION PROCEDURE

The process of mesophylic methane fermentation was carried out in a mobile installation. For the tests two 600 dm^3 containers filled with 300 dm^3 of biomass were used. The installation diagram is presented in Fig.1.

The process of fermentation was initiated by filling fermentation chambers with 300 dm^3 of biomass composed of 60% of primary sludge and 40% of thickened excessive sludge from municipal waste water treatment plant in such a way that the

content of dry matter in the mix was 3%. The method of periodical feeding of biomass to fermentation chambers (once every 24 hours) in the amount of 5% of the volume of the fermentation chamber (15 dm^3) has been applied. Prior to feeding the new portion of sludge 15 dm^3 of fermented biomass was removed from the lower part of reactors.

The mix was fed via circulating pumps to the upper part of the reactor flowing through the heater and mixing with the content of the reactor. The recirculation pump sucked in the biomass from the lower part of the reactor and after heating in the heat exchanger it was fed to the upper part of the reactor. The average number of exchanges varied between 100 and 150 per 24 hours.

The fermentation process temperature was regulated by heating system with total power of 12 kW with the accuracy of ±1.0°C. The heating system was integrated with the mixing system of circulating pump.

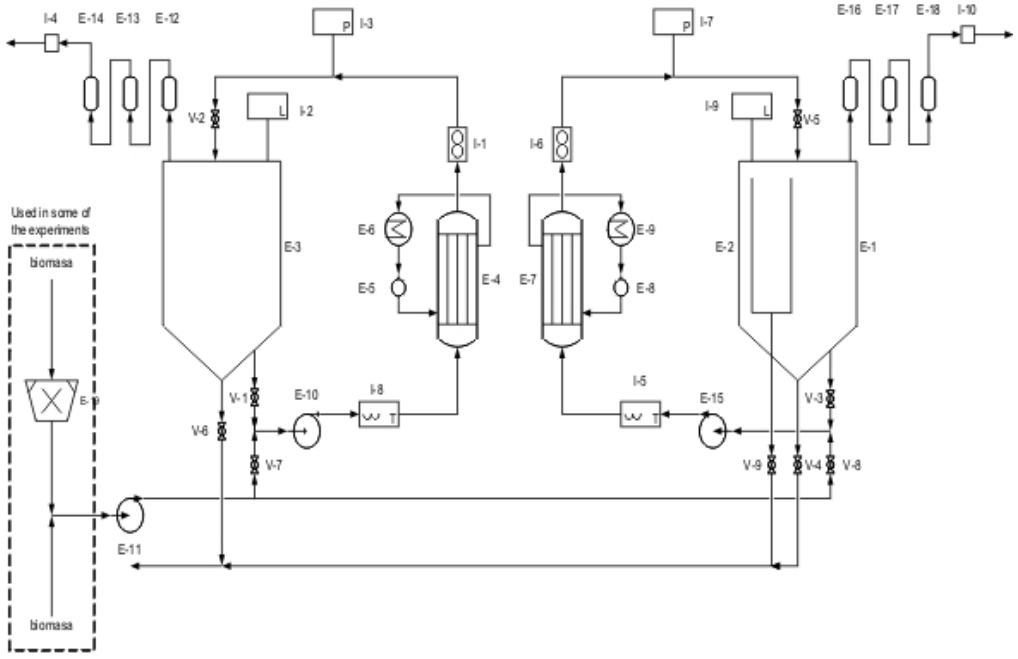

Fig. 1. Anaerobic digestion process flowsheet; E-1 - bioreactor Z2; E-2 internal tank; E-3 - bioreactor Z1; E-10, E-11, E-15 - centrifugal pump; E-12, 14, 16, 17, 18 – washer; E-4,5,7 - heat exchanger; E-5,8 - recirculation pump; E-6,9 - electric heater; E-19 – pump with fragmentize; V-1÷9 – valve; I-1,6 - flow meter; I-2,9 level meter; I-3,7 - manometer, I-5,8 - temperature sensor; I-4,10 - volume meter

Another series of experiments performed to fermentation of sludge with underwent mechanical disintegration in a centrifugal pump equipped with fragmentize. The power of the pump was 500 W. Only the excessive sludge was subject to disintegration. 30 dm^3 of excessive sludge was subject to one pass disintegration. The estimation of disintegration ratio was performed with by means of (DD_{COD}) method (Eq. 1.).

$$DD_{COD} = \frac{COD_D - COD_0}{COD_{NaOH} - COD_0} \cdot 100\% \quad (1)$$

where:
COD_0 - COD of supernatant before dezintegration
COD_D - COD of supernatant after dezintegration
COD_{NaOH} - COD of supernatant after dezintegration with 0.5 molar NaOH (22 hours at 20 ^oC).

RHEOLOGICAL MEASUREMENTS

Rheological measurements of sludge were performed using rotation rheometers Broekfield LVDV II+ and Rheotest II fitted with measuring system of coaxial cylinders. Prior to measurements, viscometers were calibrated with the Broekfield standards of viscosity. The rheological measurements were carried out in the temperature of 25 ^oC, and the examined samples were thermostated over 20 min before measuring with the accuracy of ±0.1 ^oC. The flow curves were made by the increase of shear rate to the maximum value for which the measurement of shearing stress was still possible, subsequently the shear rate was decreased. For each rate the sample was stressed for 1 min.

Among numerous rheological models the involutive model is broadly applied (Eq. 2.).

$$\tau = k\dot{\gamma}^n \quad (2)$$

where dynamic viscosity can be derived at from the following equation (3)

$$\eta = \frac{\tau}{\dot{\gamma}} = k\left(\dot{\gamma}\right)^{n-1} \quad (3)$$

where: η - apparent viscosity [Pas], τ - shear stress [Pa], $\dot{\gamma}$ - shear rate [s^{-1}], k consistency coefficient of fluid [$Pa \cdot s^{-1}$] (greater value of k the more viscous the fluid), and n is the flow behavior index, which is a measure of the degree of deviation from the Newtonian fluid behavior.

Depending on the value of n, the power low describes three flow behaviors. These behaviors include pseudoplastic (n<1.0) – effective viscosity decreases with shear rate, Newtonian (n=1.0) – the viscosity does not change with the shear rate and dilatants (n>1.0) - the viscosity increases with the shear rate. However, due to visible flow limit for the description of rheological properties Herschel-Bulkley model (Tixier et al., 2003, Gilles et al., 2005) has been applied (Eq. 4)

$$\tau = \tau_0 + K_h\left(\dot{\gamma}\right)^n \quad (4)$$

where: τ_0 - yield strength [Pa].

RESULTS AND DISCUSSIONS

RHEOLOGICAL BEHAVIOR OF ACTIVATED SLUDGE

Rheological properties of sludge are complex and dependent on numerous factors. Sewage sludge apart from mineral constituents also contains a substantial part of organic substances with majority of microorganisms. The complexity of biological structures poses significant difficulties in description of rheological properties of sewage sludge. As demonstrated by Baudez (2006), the application of traditional parameters, such as flow curves and departure cycles are not sufficient for characterization of thixotropic properties of sludge. Rheograms of mixture of excessive and primary sludge (Fig. 2) have peak at low shear speed and hysteresis loop, which indicates the thixotropic characteristics of sludge and the presence of strong internal structure of the suspension. Table 1 shows basic physical and chemical data of sludge subjected to fermentation.

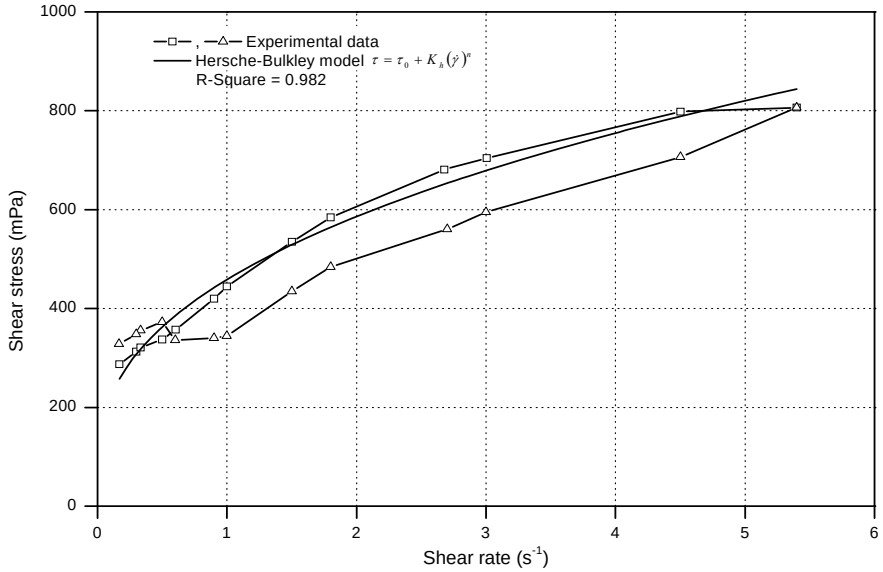

Fig. 2. Flow curve of mixture of activated sludge fed to bioreactors

Table 1. Physical and chemical parameters of sludge fed to bioreactors

Determination	Unit	Value
Alkalinity	pH	6.38
Volatile fatty acids	mval/dm^3	13.6
COD	mgO_2/dm^3	1684
COD	mgO_2/g d.m.	795.968
Dry mass	%	5.01
Calcination loss	%	76.5

EFFECT OF MINERAL PARTICLES CONTENT ON RHEOLOGICAL PROPERTIES OF SLUDGE

During anaerobic fermentation a series of biochemical processes occur in which organic matter yields mainly methane and carbon dioxide. As a result of these processes there occurs the decrease in the amount of solids in the sludge especially those of organic mature. It has decisive influence on changes of rheological properties of fermenting sludge. As presented in Fig. 3 viscosity and pseudoplasticity of sludge decreases as fermentation proceeds, which is most frequently explained by the significant influence of the content of solids. In Fig. 4 the expotential relationship of viscosity and the content of solid particles are clearly visible. In the literature one can encounter other methods of presenting the relationship between rheological properties and the content of solids, however, all unequivocally indicate that Einstain's equation ought not to be applied (Pevere et al., 2007; Seyssiecq et al., 2008). According to assumptions of Einstain's theory this equation describes mixtures of solid particles content above 10% v/v for systems without intermolecular interaction. Table 1 presents the changes of physical and chemical parameters of sludge during fermentation process. According to Sanin (2002), rheological properties of sludge can be influenced by reaction, however, in this case pH changes are minimal.

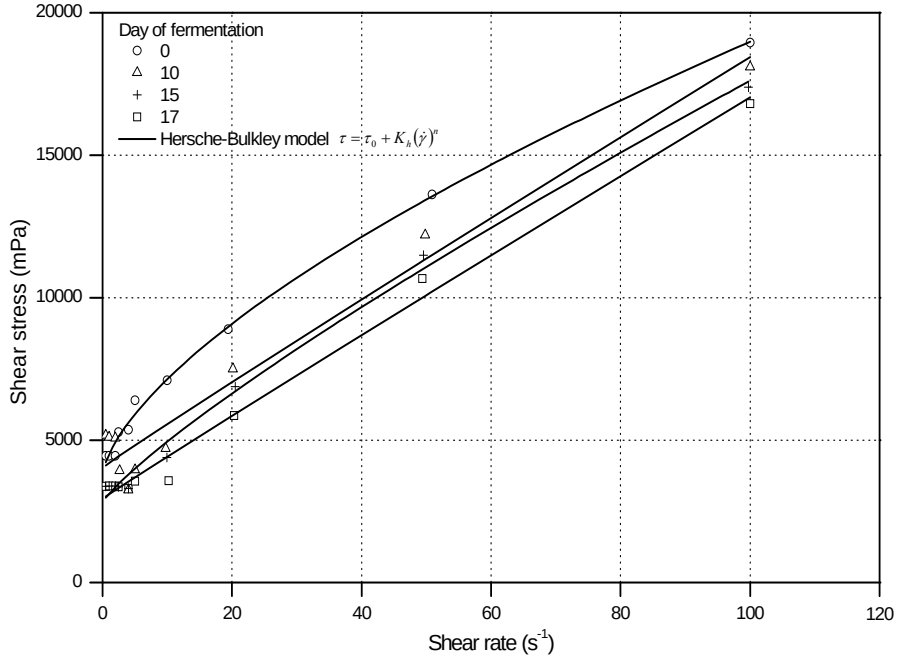

Fig. 3. Rheological character of fermented sludge vs the content of solids

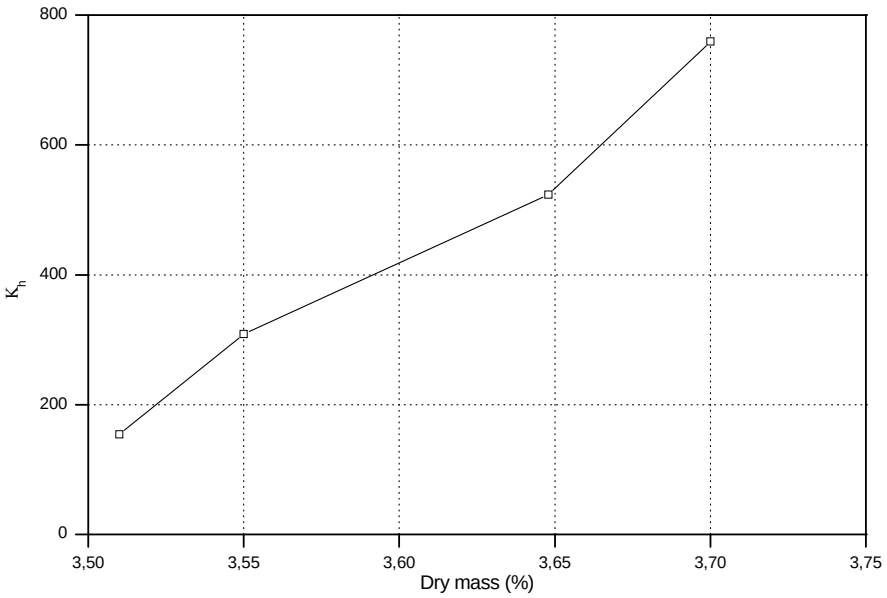

Fig. 4. Consistency ratio vs. content of solids

Table 2. Changes of physical and chemical properties of sludge during fermentation process

Determination	Unit	Day of anaerobic digestion			
		0	10	15	17
Alkalinity	pH	6.75	6.92	7.13	7.06
Volatile fatty acids	mval/dm^3	32.0	39.2	48/6	45.2
COD	mgO_2/dm^3	25333	19200	22266	24933
COD	mgO_2/g d.m.	790.41	648.97	592.11	1379.30
Dry mass (d.m.)	%	3,70	3,66	3,55	3,51
Calcination loss	%	70.45	69.12	71.42	71.04

EFFECT OF SLUDGE DISINTEGRATION ON RHEOLOGICAL PROPERTIES

Disintegration of sewage sludge is an increasingly frequently used operation in connection with anaerobic fermentation. As a result of lysis of cells it is possible to achieve a significant increase of fermentation speed and decrease of content of organic matter. In the pilot tests mechanical disintegration carried out in the pump with a fragmentizer was applied. Figure 5 presents the dependence of disintegration degree (DD) on the time of the pump operation.

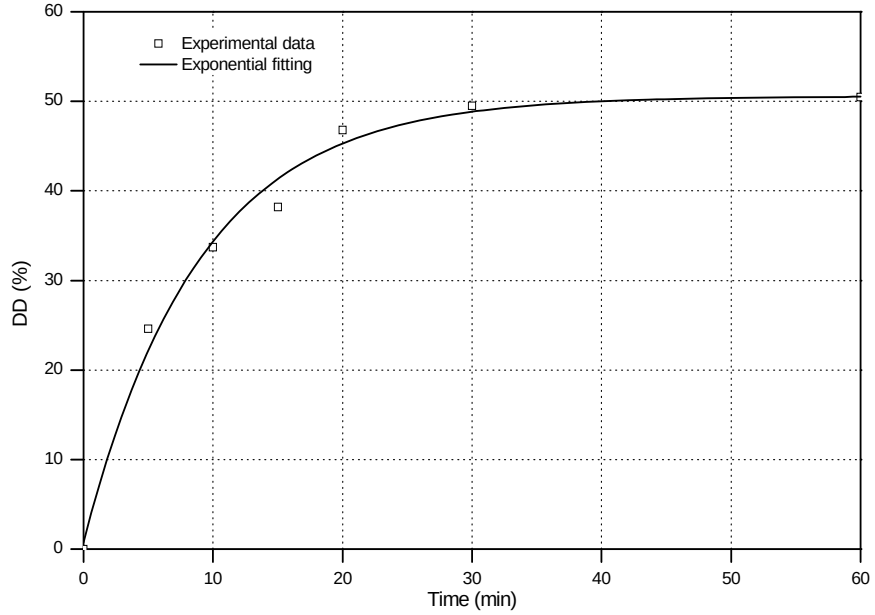

Fig. 5. Degree of disintegration of activated sludge vs. time of disintegration

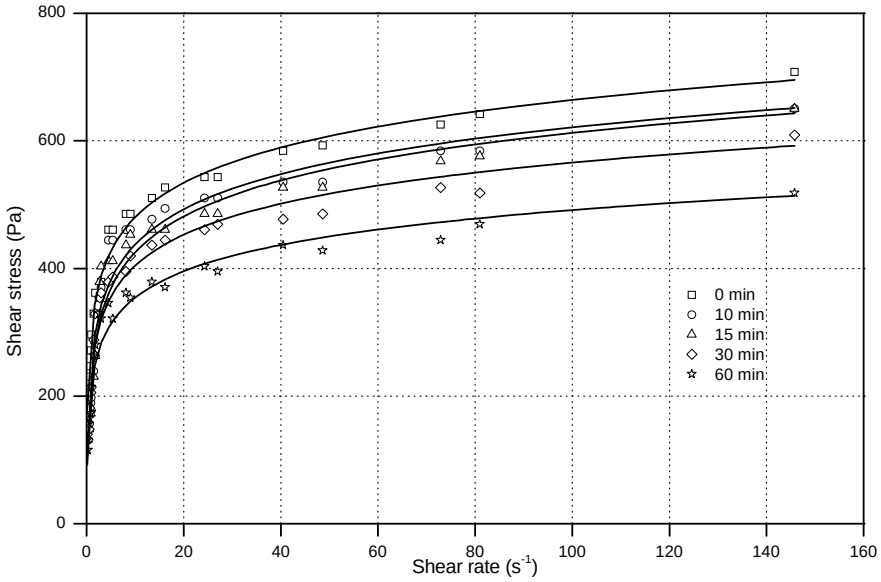

Fig. 6. Sludge flow curves subject to mechanical disintegration

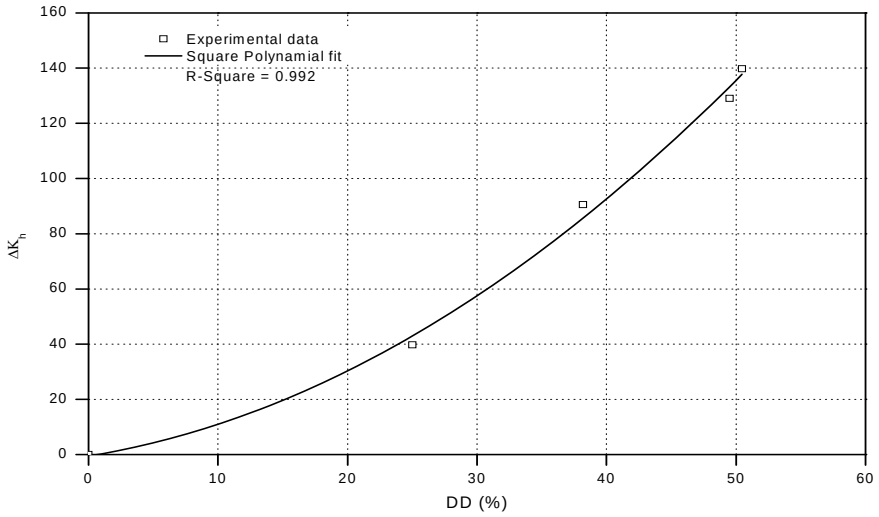

Fig. 7. Relative changes of consistence ratio to sludge disintegration degree

During disintegration the sludge samples were collected and they had rheological properties determined. As one can seen in the Fig. 6 rheological parameters changed significantly during time of disintegration. Viscosity of sludge decreased and both pseudoplasticity and consistency ratio increased. The changes were so significant that they can be applied for a quick identification of disintegration degree on the basis of rheological properties measurements. Figure 7 shows a relative increase of consistency ratio due to disintegration degree.

CONCLUSIONS

As it results from the achieved rheograms, sewage sludge has flow limit and exhibits pseudoplasticity, which most often results from thixotropy of the system. Among numerous parameters influencing rheological properties, most significant is the content of solids. Pseudoplasticity of sludge increases together with the increase of solids content. Consequently, in the process of fermentation, as a result of decrease in the content of organic matter even by 60%, pseudoplasticity and consistence ratio increases.

Rheological parameters changes during disintegration of excessive sludge enable a quick estimation of disintegration degree. In comparison with the DD_{COD} method, viscosity measurement is considerably more environmentally friendly (no chemicals needed), cheaper and faster. In order to compare disintegration degree using viscosity measurement preparation of the calibration curve is necessary.

ACKNOWLEDGEMENTS

This research was supported by the Gdansk University of Technology, contract DS No. 014668/003.

REFERENCES

BAUDEZ J-Ch., (2006) *About peak and loop in sludge rheograms*. Journal of Environmental Management 78: 232-239.

DILEK SANIN F., (2002). *Effect of solution physical chemistry on the rheological properties of activated sludge.* Water SA 28 (2): 207-211.

GREENER J., CONNELY R.W., (1986). *The response of viscoelasticliquids to complex strain histories: the thixotropic loop*. Journal of Rheology 30 (2): 285-300.

GUIBAUD G., TIXIER N., et al. (2005). Hysteresis area, a rheological parameter used as a tool to assess the ability of filamentous sludges to settle. Process Biochemistry 40: 2671–2676.

MAGNIN A., PIAU J.M. (1990). *Cone and plate rheometry of yield stress fluids: study of an aqueous gel.* Journal of Non-Newtonian Fluid Mechanic 36: 85-108.

MOELLER G., TORRES L.G., (1997). *Rheological Haracterization of Primary and Secondory Sludge Treated by Aerobic and Anaerobic Digestion*. Bioresource Technology 61: 207-211.

MORI M., SEYSSIECQ I., et al. (2006). *Rheological measurements of sewage sludge for various solids concentrations and geometry.* Process Biochemistry 41: 1656–1662.

MUJUMDAR A., BERIS A.N., et al. (2002). *Transient phenomena in thixotropic systems*. Journal Non-Newtonian Fluid Mechanics 102: 157-178.

ÖRMECI B., (2007). *Optimization of a full-scale dewatering operation based on the rheological characteristics of wastewater sludge*. WATER RESEARCH 41: 1243-1252.

PEVERE P., GUIBAUD G., et al. (2007). *Identification of rheological parameters describing the physico-chemical properties of anaerobic sulphidogenic sludge suspensions.* Enzyme and Microbial Technology 40: 547–554.

PHAM T.T.H., BRAR S.K., et al. (2009). *Influence of ultrasonication and Fenton oxidation pre-treatment on rheological characteristics of wastewater sludge.* Ultrasonics Sonochemistry In press.

SEYSSIECQ I., MARROT B., et al. (2008). *In situ triphasic rheological characterisation of activated sludge, in an aerated bioreactor.* Chemical Engineering Journal 142: 40-47.

TIXIER N., GUIBAUD G., et al. (2003). *Determination of some rheological parameters for the characterization of activated sludge*. Bioresource Technology 90: 215-220.

Aranowski R., Hupka R., Jungnickel Ch., *Zmiany właściwości reologicznych podczas fermentacji metanowej osadu czynnego,* Physicochemical Problems of Mineral Processing, 44 (2010), 13-22, (w jęz. ang), http://www.minproc.pwr.wroc.pl/journal

Wykonane pomiary właściwości reologicznych osadów nadmiernych poddawanych procesowi dezintegracji mechanicznej wskazują na znaczny spadek lepkości sięgający 60%. Wraz ze stopniem dezintegracji rosły również właściwości pseudoplastyczne oraz malała granica płynięcia. Podobnie istotne zmiany właściwości reologicznych następowały w osadach poddawanych fermentacji metanowej. Z analiz pobieranych próbek po różnym okresie trwania procesu wynika, że czas fermentacji wpływa na zmniejszenie lepkości osadów ściekowych. Pomiar lepkości może być stosowany do oceny stopnia dezintegracji osadu nadmiernego, ponieważ metoda ta jest znacznie szybsza niż oznaczenie ChZT (analiza zalecana przez ATV).

słowa kluczowe: właściwości reologiczne, osad czynny, fermentacja metanowa, reologia, dezintegracja osadów

Physicochem. Probl. Miner. Process. 44(2010) 23-34

journal homepage
www.minproc.pwr.wroc.pl/journal/

Physicochemical Problems of Mineral Processing

Index No. 32213X ISSN 1643-1049

M. Brożek*, A. Młynarczykowska*

PROBABILITY OF DETACHMENT OF PARTICLE DETERMINED ACCORDING TO THE STOCHASTIC MODEL OF FLOTATION KINETICS

Received December 30, 2008; reviewed; accepted May 13, 2009

Due to the random character of elementary processes (collisions, adhesion, detachment) flotation can be considered as a stochastic process of birth and death. The probability of detachment of a particle from a bubble is one of the parameters of the equation of flotation kinetics, obtained on the grounds of the stochastic model. Applying this fact, the paper presents the results of investigations according to which the authors determined the dependence of probability of detachment on particle size and ash content during flotation in the laboratory flotation machine with mechanical agitation of the flotation pulp. Interpreting the probability of detachment as the partition number, the authors determined the parameters of a division particle (particle size and ash content) for certain physicochemical state of the flotation medium. Such an approach enables the theoretical models of probability of detachment and the stability of flotation aggregates to be verified for industrial flotation machines.

key words: flotation, stochastic model, process of birth and dead, probability of detachment

INTRODUCTION

Detachment of a particle from a bubble surface is the least known microprocess of flotation. It is a result of action of external forces acting upon the flotation aggregates which are generated by turbulent motions in the flotation chamber and concerns especially large and heavy particles with relatively low hydrophobic properties. The probability of occurrence of this event, apart from the above mentioned factors, depends

* AGH, Al. Mickiewicza 30, 30-059 Krakow, Poland, email: brozek@agh.edu.pl

upon the intensity of turbulence of the medium, characterized quantitatively by the turbulent energy dissipation. Turbulence can be generated by the motion of flotation aggregates, for example in the flotation column, and also by the motion of a rotor in the flotation chamber with mechanical pulp agitation (Maksimov and Emalianov, 1983). Vortices formed in the chamber can be of different values (Schubert, 1999). They can be several times smaller or larger than flotation aggregates, and be of the same order of values as flotation aggregates. In the first case their energy is so small that they do not affect the aggregate durability. In the second case the aggregate gets taken by the vortex and due to the liquid thrust forces it rotates round the central vortex axis. In this case the centrifugal force acts upon aggregate particles and is responsible for tearing off the particles from the bubbles. In the third case the action of aggregate and liquid vortex is the source of oscillatory motion of particles upon the bubble surface.

PROBABILITY OF DETACHMENT OF PARTICLE FROM A BUBBLE SURFACE

Detachment of the particles and disintegration of the flotation aggregate depends on the balance of forces, i.e. internal - the particle-bubble interaction, i.e. adhesion forces and external, acting upon the particle from the medium. The relation of the detaching forces to the adhesion forces is a modified Bond B_o^* number and characterizes the aggregate durability (Schulze, 1993):

$$B_o^* = \frac{F_{\text{det}}}{F_{ad}}. \tag{1}$$

In the flotation chamber with the mechanical pulp agitation, the dissipation of energy close to the rotor axis is from 10 to 100-fold larger than average energy dissipation in the flotation chamber. In this zone, the flotation aggregates, built of large particles, are not durable. Yet, the average energy dissipation is responsible for the average aggregate durability in the flotation chamber (Schulze, 1977). If the probability of detachment has an exponential distribution, it can be then expressed by the following formula (Schulze, 1993):

$$P_d = \exp\left(1 - \frac{F_{ad}}{F_{\text{det}}}\right) = \exp\left(1 - \frac{1}{B_o^*}\right). \tag{2}$$

Bloom and Handel (2003), according to the empirical investigations, modified this model introducing the empirical constant $A_s = 0.5$ into formula (2):

$$P_d = \exp\left[A_s\left(1 - \frac{1}{B_o^*}\right)\right]. \tag{3}$$

As it results from formula (2), the probability of detachment increases with the increase of the detaching forces. The effect of physicochemical conditions in the flotation chamber upon the probability of detachment is contained in the adhesion forces.

The empirical investigations carried out by Cheng and Holtham (1995) indicate that a bubble agitated by external forces present in the flotation chamber with mechanical pulp agitation behaves like an elastic mass, performing vibrational movements. Those vibrations, transmitted onto particles attached to the bubble surface, constitute a source of force F_f, proportional to the amplitude and frequency of vibrations.

Despite the vibrational movement, the particles perform circular movement upon the bubble surface which constitute a source of centrifugal force F_c.
Therefore, the maximum value of detaching force is equal to:

$$F_{detmax} = F_f + F_c + F_g \tag{4}$$

where: F_g – effective force of gravity.

Woodburn et al. (1971) studied the model of tearing off a particle from a bubble, treating the bubble surface as an elastic body, which cracks under the influence of the tension exceeding the permissible value and the particle placed on it is shed. It is assumed that in the initial moment the bubble and particle (flotation aggregate) move with velocity u_a. If under the effect of the rotational motion of the liquid the aggregate accelerates suddenly, the force of inertia, acting upon the particle, will cause a slight shift in the direction opposite to the bubble movement and it will result in an elastic linear deformation of the bubble surface (elongation towards the action of the force of inertia), equal to the particle shift, which is the source of bubble tension force T_N.

$$T_N = k_b\left[u_a - \overline{u}_p(t)\right]t = \frac{\pi\, d_p^3}{6}\rho_p \frac{\mathrm{d}u_p(t)}{\mathrm{d}\,t} \tag{5}$$

where: k_b – coefficient of elasticity of the bubble surface, $u_p(t)$ – change of momentary velocity of the particle versus the bubble, u_a – velocity of the flotation aggregate,

$\overline{u}_p(t) = \dfrac{u_p(t) - u_p(0)}{2}$ - average change of the momentary velocity of particle in the time range $(0,t)$, while $u_p(0) = 0$.

The expression on the left side of Eq. 5 describes the force of elasticity (tension), acting upon the bubble surface while, on the right side, the force of inertia acting upon the particle.

The maximum value of force T_{Nmax} is (Woodburn et al, 1971):

$$T_{N\max} = u_a k_b \left(\frac{\pi\rho_p\, \mathrm{d}_p^3}{3k_b}\right)^{\frac{1}{2}} \exp\left(-0.5\right). \tag{6}$$

As it is shown in Eq. 6, the maximum value of bubble tension force is proportional to $d_p^{1.5}$. It is possible then to assume that $P_d \sim d_p^{1,5}$. So, the maximum value of particle size d_{pmax} exists, above which they will detach from bubbles. That is why for the particle detachment probability, the following equation may be applied (Woodburn et al., 1971):

$$P_d = \left(\frac{d_p}{d_{p\max}} \right)^{1.5} \qquad \text{for } d_p \le d_{p\max} \tag{7a}$$

$$P_d = 1 \qquad \text{for } d_p > d_{p\max}. \tag{7b}$$

Yoon and Mao (1996) for probability of detachment applied a formula analogical to the formula for adhesion probability. Consequently:

$$P_d = \exp\left(-\frac{W_a + E_1}{E_k^{'}} \right) \tag{8}$$

where: W_a - adhesion work, E_1- flotation

$$W_a = \pi r_p^2 \, \sigma (1 - \cos\theta)^2. \tag{9}$$

Thus, probability of detachment is:

$$P_d = \exp\left(-\frac{\pi r_p^2 \, \sigma (1 - \cos\theta)^2 + E_1}{E_k^{'}} \right). \tag{10}$$

PROBABILITY OF DETACHMENT IN THE STOCHASTIC MODEL OF KINETICS

Recovery of particles risen to the froth layer, calculated according to the stochastic model of flotation, is expressed by the formula (Brozek and Mlynarczykowska, 2006):

$$R(t) = \frac{\lambda_o}{\lambda_o + \mu_o} \left[1 - e^{-(\lambda_o + \mu_o)t} \right] \tag{11}$$

while constants λ_o and μ_o respectively are the constants of the permanent adhesion and detachment of particles from air bubbles, whereas $k = \lambda_o + \mu_o$ is the flotation rate constant or constant of flotational adhesion.

It results from formula given in Eq. 11 that:

$$\lim_{t \to \infty} R(t) = \frac{\lambda_o}{\lambda_o + \mu_o} = R_\infty \tag{12}$$

$$\left.\frac{\partial R(t)}{\partial t}\right|_{t\to 0} = \lambda_o \tag{13}$$

where: R_∞ - value of ultimate recovery.

Fitting the model dependence to the empirical one, it is possible to estimate of processes of adhesion and detachment under the given physicochemical and hydrodynamic conditions of the flotation chamber.

From theEq. 11, the recovery of useful mineral in to the froth product $R_\infty = 1$, which means that after long enough time the floatable mineral will be completely transferred to the froth product (all particle attached to the bubbles will report go to the froth product). The flotation rate constant is:

$$\frac{dR}{dt}\left(t=0\right) = k. \tag{14}$$

When this formula is compared to Eq. (11), it can be concluded that in the case of flotation without detachment the flotation rate constant is equivalent to the total adhesion rate constant. All the particles attached to the air bubbles will pass to the froth product and none will be detached from the flotation aggregate.

From Eq. (11) for $R_\infty = 1$ the flotation rate constant and, at the same time, the total adhesion rate constant is:

$$k = \frac{1}{1-R}\frac{dR}{dt} \cong \frac{1}{1-R}\frac{\Delta R}{\Delta t}. \tag{15}$$

Since

$$R = \frac{l}{n_o} \qquad \text{and} \qquad \Delta R = \frac{\Delta l}{n_o} \tag{16}$$

flotation rate constant is equal to:

$$k = \frac{\Delta l}{\Delta t\left(n_o - l\right)} = \frac{\frac{1}{4}S_b\, l_c}{\Delta t\left(n_o - l\right)}\,\frac{\Delta l}{\frac{1}{4}S_b\, l_c} = \frac{1}{4}S_b P_c\, P_a \tag{17}$$

where: n_o – initial number of floatable particles in the flotation chamber, l –number of particles attached to the air bubbles up to the time t, Δl - number of particles attached to the bubbles in the time Δt , l_c – number of particles colliding with the bubbles in the unit of time, P_c and P_a – respectively, probabilities of collision and adhesion, equal to:

$$P_c = \frac{l_c}{\Delta t\left(n_o - l\right)} \qquad P_a = \frac{\Delta l}{\frac{1}{4}S_b\, l_c}. \tag{18}$$

The occurrence of adhesion is conditional to a prior particle-bubble collision. Thus, the total adhesion rate constant is the product of the probability of collision and the probability of adhesion to the surface of air bubbles flowing through a unit of

transverse cross-section surface of the flotation chamber in the unit of time. In the case of the flotation model which considers the process of detachment of particles from the bubbles surfaces, the following schema of the adhesion process can be assumed, in the sense of the balance of the number of particles:

$$\text{total adhesion} = \text{permanent adhesion} + \text{detachment} \tag{19}$$

If the fact, that the flotation rate constant equals the total of adhesion rate is taken into consideration, the above scheme results from the fact that the flotation rate constant is equal to:

$$k = \lambda_o + \mu_o . \tag{20}$$

It is obvious that the particles which were already attached to the bubbles are subjected to detachment. Consequently, the detachment rate constant will be the product of the total adhesion rate constant and the probability of detachment:

$$\mu_o = k\, P_d = \frac{1}{4} S_b P_c P_a P_d . \tag{21}$$

According to Eq. (20) the permanent adhesion rate constant is:

$$\lambda_o = k - \mu_o = \frac{1}{4} S_b P_c P_a - \frac{1}{4} S_b P_c P_a P_d = \frac{1}{4} S_b P_c P_a (1 - P_d) . \tag{22}$$

Applying Eqs 17 and 22 the value of ultimate recovery can be calculated:

$$R_\infty = \frac{\lambda_o}{\lambda_o + \mu_o} = \frac{0.25\, S_b\, P_c\, P_a (1 - P_d)}{0{,}25\, S_b\, P_c\, P_a} = 1 - P_d . \tag{23}$$

Therefore, from the empirical dependence R(t) it is possible to determine the probability of detachment. This fact gives a tool to investigate the basis of the process of air bubble mineralization in the large scale process. In this paper the dependence of probability of detachment of coal particles as a function of ash content and particle size in a laboratory mechanical flotation machine is presented.

EXPERIMENTAL

METHOD OF SAMPLES PREPARATION

Coal (type 33, Polish classification), originating from a coal mine, crushed to -0.5 mm, was used. Particle size and density analyses were performed. Narrow size and density fractions, according to the Polish standard, were analyzed for ash content. To study the kinetics as a function of particle size the density fraction 1.3 – 1.4 Mg/m^3 was selected, whereas as a function of ash content the size fraction 0.2–0.315 mm and the density fractions of -1.35 Mg/m^3 and + 1.35 Mg/m^3 were used.

Narrow size and density fractions were stored under vacuum and they were used for analyses during a possible short period of time in order to limit possible oxidation of coal surface. This material was used as the flotation feed.

DETERMINING THE FLOTATION KINETICS

Flotation experiments for coal were carried out at room temperature in a Denver type laboratory machine of 1 dm^3 chamber capacity at a constant 2020 number of rotor rotations per minute (rpm) and fixed air flow rate. The content of solids was the same in all experiments, i.e. 80 g/dm^3. Such conditions provided a constant size of air bubbles in the chamber with limited pulp turbulence caused by the rotor. A low solids concentration in the flotation pulp was due to practical reasons to provide favorable coal flotation results which can be achieved at low pulp density (Sablik, 1998).

An aqueous solution of n-butanol was used as a collecting and froth making reagent. It does not change pulp's pH but only reduces the surface tension on gas-liquid interfaces, increasing at the same time air dispersion in the suspension. Also the adsorption of alcohol occurs on the surface of air bubbles which ensures their stabilization and prevents coalescence (Malysa, 2000; Krzan and Malysa, 2002).

On the basis of initial investigations, appropriate reagent concentrations were chosen which guaranteed froth of appropriate structure and durability. The fractioned flotation was performed and concentrates were collected during the following time intervals: 15, 15, 30, 30, 30 i 60 s. The time of flotation depended up the particle size and fraction density. Usually the last froth product was collected after 6 minutes of flotation. After drying the samples were weighed and their ash content determined. The investigations of flotation kinetics of respective density fractions of 0.2–0.315 mm were performed at the butanol concentration which corresponded to the surface tension of 68.5 mN/m of the solution. Subsequent flotations were performed at the surface tension of the flotation solution equal to 70 mN/m for size fractions of 0.1–0.2, 0.2–0.315, 0.315–0.4, 0.4–0.5 mm and density 1.3–1.4 Mg/m^3. The ash contents of the tested samples were close to each other.

RESULTS AND DISCUSSION

Figures 1 and 2 present the flotation kinetics, respectively for narrow density fractions of coal particles 0.2-0.315 mm in size (Brozek and Mlynarczykowska, 2006) and narrow size fractions of 1.3-1.4 Mg/m^3 density. The model relationship based on Eq. 11 were in agreement with the empirical relationship of recovery of combustible and volatile matter upon time.

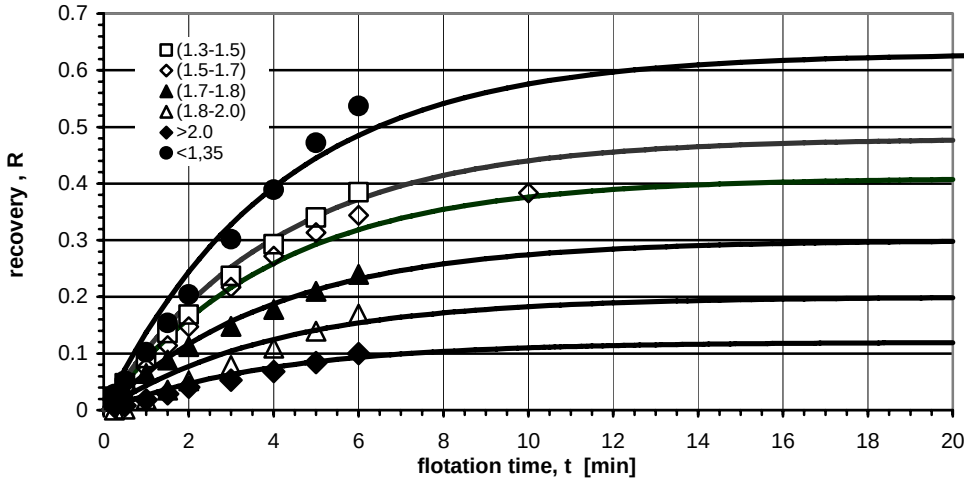

Fig. 1. Curves of flotation kinetics of narrow density fractions of coal. Numbers indicate density in Mg/m^3

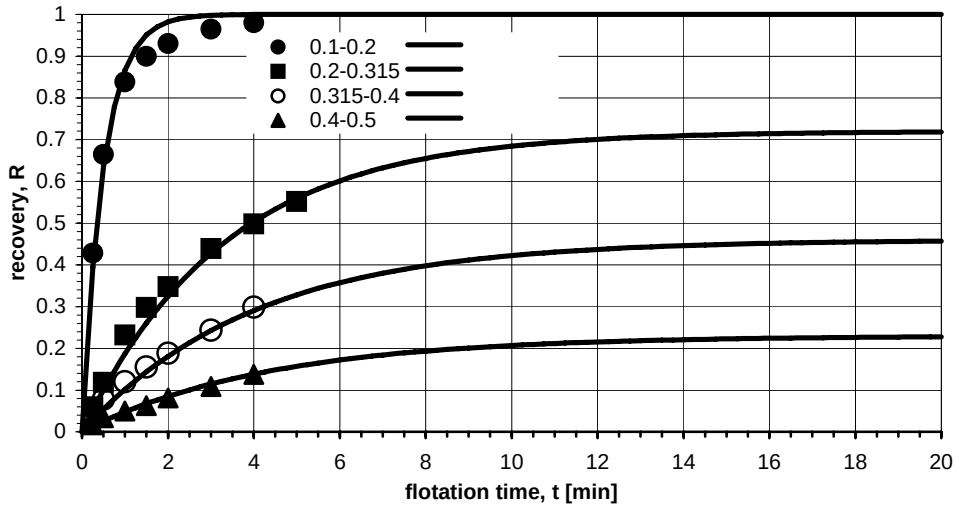

Fig. 2. Curves of flotation kinetics of narrow size fractions. Numbers indicate particle size in mm

Model curves shown in Fig.1 are based on the following formulas:

$R(t) = 0.63\ (1 - e^{-0.245\ t})$ for $\rho < 1.35$ Mg/m^3 $A_v = 1.06$ % (24a)

$R(t) = 0.48\ (1 - e^{-0.249\ t})$ for $\rho = 1.35 - 1.5$ Mg/m^3 $A_v = 7.91$ % (24b)

$R(t) = 0.41\ (1 - e^{-0.250\ t})$ for $\rho = 1.5 - 1.7$ Mg/m^3 $A_v = 23.18$ % (24c)

$R(t) = 0.30\ (1 - e^{-0.246\ t})$ for $\rho = 1.7 - 1.8$ Mg/m^3 $A_v = 36.32$ % (24d)

$R(t) = 0.20\ (1 - e^{-0.245\ t})$ for $\rho = 1.8 - 2.0$ Mg/m^3 $A_v = 48.71$ % (24e)

$R(t) = 0.12\ (1 - e^{-0.249\ t})$ for $\rho > 2.0$ Mg/m^3 $A_v = 77.63$ % (24f)

On the basis of the Eqs 23 and 24 it is possible to determine the dependence of probability of detachment upon the ash content. This dependence is presented in Fig.3. The probability of detachment as a function of ash content is expressed by the following formula:

$$P_d(A_v) = 1 - 0.65 \exp(-2.23A_v). \tag{25}$$

It results from formulas (24) that the value of the flotation rate constant k , i.e. the total adhesion rate constant, does not depend upon the ash content. On the other hand, product kR_∞ i.e. λ_o, depends upon the ash content (Brozek and Mlynarczykowska, 2006). If the classical model of flotation kinetics is applied to the analysis of flotation kinetics (in which k and R_∞ are parameters), only the information about the change of the value of maximum recovery (without the information about the rate of the process) could be obtained at the change of hydrophobic properties of particles, resulting from the change of ash content. Analogical situation occurs when a change of addition of the reagent causes a change of R_∞ value without causing any change of k value (Xu, 1998). In such cases the application of the stochastic model enables us to obtain full information about the kinetic and thermodynamic side of the flotation process.

The following equations (Fig. 2) were obtained for flotation kinetics for different size fractions:

$R(t) = 1.0(1 - e^{-2.01\,t})$ for $d_p = 0.1 - 0.2$ mm $P_d = 0$ (26a)

$R(t) = 0.72(1 - e^{-0.3\,t})$ for $d_p = 0.2 - 0.315$ mm $P_d = 0.28$ (26b)

$R(t) = 0.46(1 - e^{-0.25\,t})$ for $d_p = 0.315 - 0.4$ mm $P_d = 0.54$ (26c)

$R(t) = 0.23(1 - e^{-0.23\,t})$ for $d_p = 0.4 - 0.5$ mm $P_d = 0.77$ (26d)

From formula 7a it can be concluded that $P_d = 0$ for $d_p = 0$ which has no physical interpretation. The authors propose the following modification of this formula:

$$P_d = \left(\frac{d_p - d_{p\min}}{d_{p\max} - d_{p\min}} \right)^n \tag{27}$$

where: d_{pmin} – the size of floating particles below which $P_d = 0$, d_{pmax} – the size of particle above which $P_d = 1$, n – empirical constant.

In the flotation machines with mechanical agitations of the flotation pulp it is possible to calculate the minimum particle size below which there is no detachment of particles and the maximum size of floating particles from fitting dependence (27) to the empirical data. Figure 4 presents the dependence of probability of detachment on the coal particle size.

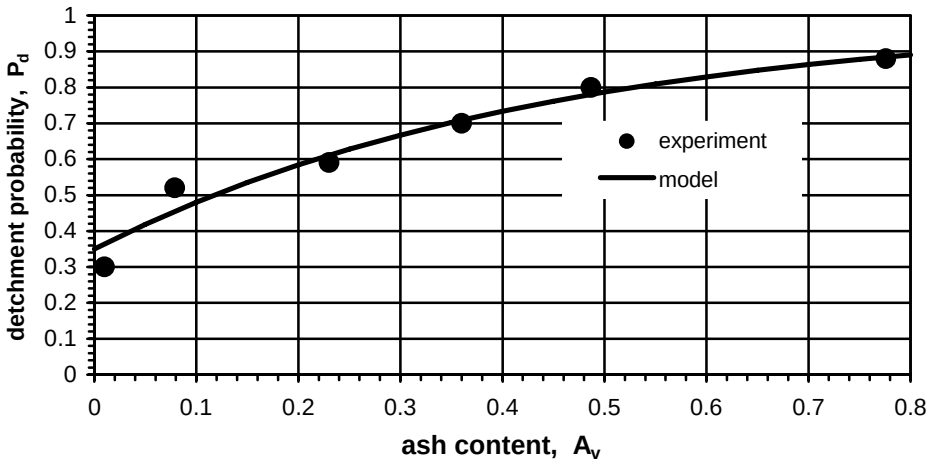

Fig. 3. Dependence of detachment probability upon ash content

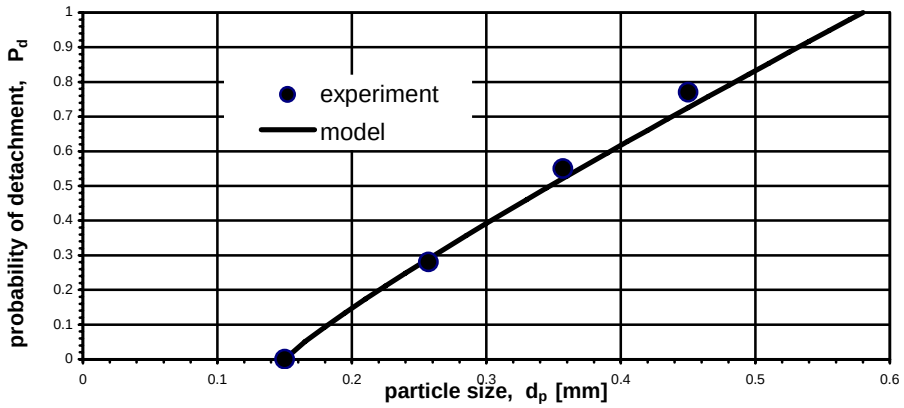

Fig. 4. Dependence of probability of detachment upon the particle size

Denoting d_{pmax} - d_{pmin} = Δd , Eq. 27 takes the form:

$$P_d = \left(\frac{d_p - d_{p\min}}{\Delta d} \right)^n \tag{28}$$

The best consistency of expression (28) with the empirical data was achieved by means of the least square method (after finding the logarithm) for d_{min} = 0.15 mm:

$$P_d = \left(\frac{d_p - 0.15}{0.43} \right)^{0.89} \tag{29}$$

From the above formula it is possible to calculate the maximum size of floatable particles under given physicochemical conditions in the flotation chamber and fixed pa-

rameters of the flotation machine (number of rotor rotations, air flow-rate): $d_{pmax} = \Delta d + d_{min} = 0.58$ mm.

The probability of detachment can be also considered as a measure of probability of transfer of particle to the lower (chamber) product. Then, the value of this probability will be equivalent to the partition number and the curves of the dependence $P_d(d_p)$ or $P_d(A_v)$ to partition curves. This approach to the interpretation of probability of detachment was applied by Drzymala (1994). The size of the particle for which $P_d = 0.5$ denotes the maximum size of floatable particles because they can or cannot undergo flotation with the same probability. With such an interpretation, the maximum size of floatable particles, according to formula (29) is equal to $d_{pmax} = 0.35$ mm.

Dependence $P_d(A_v)$ can be interpreted analogically. Particles of such an ash content for which $P_d(A_v) = 0.5$ are the border line particles. If the contact angle depend on ash content by means of, for example, the flotometry method (Drzymala, 1994), it may be possible to try verifying the theoretical relationship probability of detachment and hydrophobic properties, particle size, type of raw material (coal type), etc. in a given type of a flotation machine.

CONCLUSION

1. The application of the stochastic model of flotation kinetics enable us, on the basis of empirical dependences obtained in a particular flotation machine, to calculate probability of detachment of a particle under given physicochemical conditions and, on this basis to determine the maximum size of floatable particles.
2. Interpreting the probability of detachment as a partition number and the dependence of detachment upon the particle size or ash content as partition curves in the case of coal, an attempt could be made to verify the theoretical models of probability of detachment and stability of flotation aggregates in industrial flotation machines.

ACKNOWLEDGEMENTS

The paper has been supported by a grant of the National Research Committee no 4 T12A 035 30

REFERENCES

BLOOM F., HEIDEL T.J., (2003), *Modeling of flotation separation in a semi-batch process*. Chemical Engineering Science, 58, 353-365.

BROZEK M., MLYNARCZYKOWSKA A., (2006), *Application of the stochastic model for analysis of flotation kinetics with coal as an example*. Physicochemical Problems of Mineral Processing, 40, 31-44.

CHENG T.W., HOLTHAM P.N.,(1995), *The particle detachment process in flotation.* Minerals Engineering, 8, 883-891.
DRZYMALA J., (1994), *Characterization of materials by Hallimond tube flotation. Part 2: maximum size of floating particles and contact angle*. Int. J. Miner. Process., 42, 153-167.
KRZAN M., MALYSA K.,(2002), *Profiles of local velocities of bubbles in n-butanol, n-hexanol, n-nonanol solution*. Coll. Surfaces. A: Physicochemical and Engineering Aspects, 207, 279-291.
MAKSIMOV I.I., EMELJANOV I.I., (1983), *The effect of turbulence on detachment process in the flotation pulp.* Obogascenie rud, no 2, 16-19, (in Russian)
MALYSA E., (2000), *Floatability of coals as a function of surfach activity of the alcohols*. Gospodarka Surowcami Mineralnymi, 16, 45-54.
SABLIK J., (1998), *Flotacja węgli kamiennych*. Główny Instytut Górnictwa. Katowice, Poland
SCHUBERT H., (1999), *On the turbulence – controlled microprocesses in flotation machines*. Int. J. Miner. Process., 56, 257-276.
SCHULZE H.J., (1977), *New theoretical and experimental investigations on stability of bubble particle aggregates in flotation: a theory on the upper particle size of floatability*. Int. J. Miner. Process., 4, 241-259.
SCHULZE H.J., (1993), *Flotation as a heterocoagulation process: possibilities of calculating the probability of flotation. In: Coagulation and flocculation. Theory and applications*, Marcel Dekker Inc., New York.
WOODBURN E.T., KING R.P.,COLBORN R.P., (1971), *The effect of particle size distribution on the performance of a phosphate flotation process.* Metall. Trans., 2, 3163-3174.
XU MANQUI, (1998*), Modified flotation rate constant and selectivity index*. Minerals Engineering, 11, 271-278.
YOON R.H., MAO L., (1996), Application of extended DLVO theory, IV. Derivation of flotation rate equation from first principles. J. Coll. Int. Sci. 181, 613 – 626.

Brożek M., Młynarczykowska A., *Prawdopodobieństwo oderwania ziarna określane na podstawie stochastycznego modeli kinetyki flotacji,* Physicochemical Problems of Mineral Processing, 44 (2010) 23-34, (w jęz. ang), http://www.minproc.pwr.wroc.pl/journal

Ze względu na losowy charakter procesów elementarnych (zderzenia, adhezji, oderwania) flotację można rozpatrywać jako proces stochastyczny narodzin i ginięcia. Jednym z parametrów równania kinetyki flotacji uzyskanego na gruncie modelu stochastycznego jest prawdopodobieństwo oderwania ziarna od pęcherzyka. Wykorzystując ten fakt w artykule przedstawiono wyniki badań, na podstawie których określono zależność prawdopodobieństwa oderwania od wielkości ziarna oraz od zawartości popiołu przy flotacji w laboratoryjnej maszynce flotacyjnej z mechaniczną agitacją zawiesiny flotacyjnej. Interpretując prawdopodobieństwo oderwania jako liczbę rozdziału wyznaczono parametry ziarna podziałowego (wielkość ziarna i zawartość popiołu) dla określonych warunków fizykochemicznych ośrodka flotacyjnego. Ten sposób postępowania stwarza możliwość weryfikacji teoretycznych modeli prawdopodobieństwa oderwania i trwałości agregatów flotacyjnych w przemysłowych maszynach flotacyjnych.

słowa kluczowe: flotacja model stochastyczny, prawdopodobieństwo odrywu

Physicochem. Probl. Miner. Process. 44(2010) 35-40

journal homepage
www.minproc.pwr.wroc.pl/journal/

Physicochemical Problems of Mineral Processing

Index No. 32213X ISSN 1643-1049

J. Grodzka*, A. Pomianowski**

HYDROGEN-BOND PUZZLE

Received February 10, 2009; reviewed; accepted May 8, 2009

A scientist creating the models of material structures works in a way similar to the artist painting from the nature. Various models, similarly as different images may describe the *same* reality in a better or worse way. We think that it is the time to admit that the models of the percolating lattice and dynamic clusters are two images of the same structure of water, viewed from different perspectives. We believe that the most important will be such improvement of the basic model of the structure of water molecule that both ways of its modeling would give practically the same consistency with experimental results.

key words: hydrogen bond, percolating lattice, connectivity of bonds, water clusters

The molecule of water is one of the smallest in the Nature. Prof. Kamieński has even used to say that it is an atom of a double negative oxygen, that has hidden in its orbitals two protons of not fully compensated charges. This results in huge electric moments of the molecules that are the source of hydrogen bonds. To describe the interactions of charges located at atomic distances in each water molecule a modification of the coulomb potential rather than the „diameter" of these molecules is needed.

Such necessity clearly results from Prof. Adamczyk's statement, that „everything" is determined by charges. In the newest works much attention is paid to the Yukawa potential, (Blum et al. (1999) and to the experiments that combine the power of the hydrogen bond with the local charge densities in the anti-bonding orbitals σ_{OH}* (Kumar et al. (2007)).

* Medical Center of HCP Poznań, janina.grodzka@wp.pl

** prof. em. PAN Kraków, ncpomian@cyf-kr.edu.pl

Maybe this year is the last one, when we can call the hydrogen bond a mysterious one. Although in one of the recent papers, Gilli et al. (2009), concerning the structure of liquid water the statement '*H-bond puzzle'* appears, several other papers indicate that in reviews published in Chemical Review 2010 this puzzle should practically disappear.

It is therefore reasonable to summarize the long period of the development of various competing descriptions of the hydrogen bond with the expectation that the *present generation of our PhD graduates* will develop a homogeneous and generally accepted theory of this bond. Why do we think so? After a long period of the competition of various basic assumptions concerning different models of the water molecule, the ideas of their combination have appeared. Two theories of the structure of liquid water that apply *the same* models of water molecule lead to the results equally close to experimental results.

Somewhat older theory, known as the theory of the *percolating lattice* of the liquid water was developed in the late 70-ties, by Stanley and Teixeira (1980) and 10 years later come up the theory of *water clusters* (Chaplin, 2008). The first one describes water as the dynamic lattice of locally variable structures, while the second one treats it as the equilibrium mixture of dynamic aggregates of water molecules, differing in size and structure.

In some more recent works there has appeared the proposal of creating the model of water molecules, based on the known parameters of all studied structures of ice, including those anisotropic ones, starting from the experimentally confirmed fact that the *average* strength of hydrogen bonding is the function of both, temperature and pressure (Dougherty, 1998; Dougherty and Howard, 1998). In such a virtual molecule, whose construction uses both the model lengths of bonds and their angles between the hydrogen bonds, might take the values remaining within the regions *known from the experiments* carried out in the wide range of pressure and temperature values. The modeling is usually performed in the NTV system that takes into account also the structures present in the equilibrium interface regions. The laws of the statistical thermodynamics make possible the transfer of the results of the calculations onto the *pVT* system.

The experimental works prove that water is not a „van der Waals" liquid because it does not meet the assumptions of this model. No single molecules but their aggregates, „clusters", are the objects of translational movements. The condition required that the vdW equation describes the behavior of water to a good approximation is that the dynamic *clusters* of water should be sufficiently large and „stable" so as to interact with the *neighboring clusters* only by the London dispersive forces, due to the saturation of their *internal* hydrogen bonds (depending on the value of the parameters of state, the strength of a hydrogen bond may be of the order of kT). It is assumed that large, symetric clusters contain the tetrahedrally combined

molecules of water but the *strength of a local* hydrogen bond within the cluster, within the range of the whole order of values, depends on its location

Particularly important seems to be the fact that water, in addition to the „classical" triple point has two additional breaks on the density – temperature curve. („Light" water – at about 4°C and about 45°C, and the „heavy" one – at about 11°C and about 60°C). The first *kink* corresponds to the temperature of maximum density, while the second one – to the minimum solubility of hydrophobic compounds.

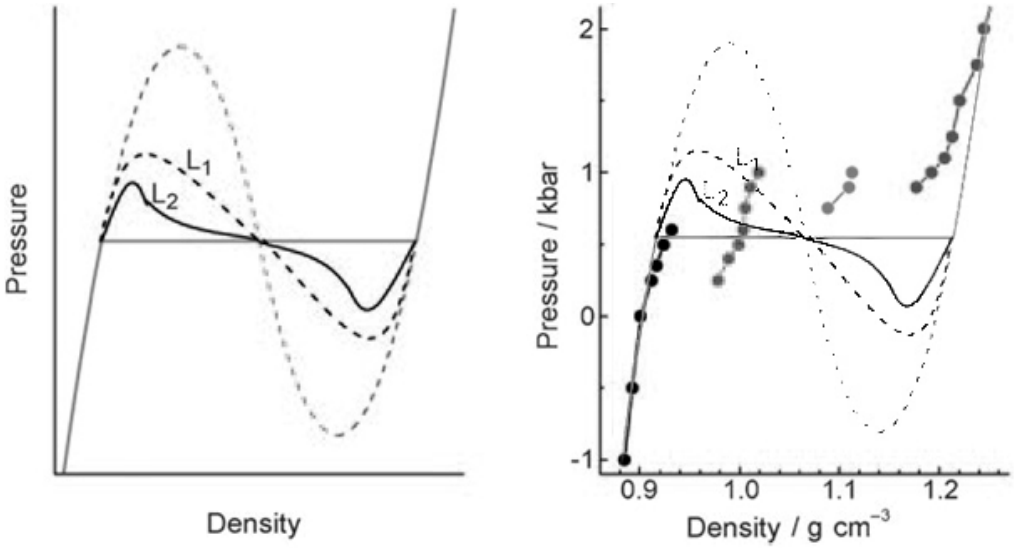

a b

Fig. 1. a) Isotherm of a fluid at subcritical temperature. Meta-stable and unstable parts of the Van der Waals loop are shown by different lines. Respectively. L1 and L2 show isotherms of finite systems of different sizes, with L1<L2. b) Isotherm of a macroscopic fluid. Model isotherm of supercooled ST2 water at T=235 K, simulated in the restricted NPT ensemble. Four branches of this isotherm, (given by points, on separate lines) correspond to the four phases of supercooled liquid water.

Such behavior is typical for mixed solvents, and in the case of water – for the *mixture* of its structures. (This reminds rather the „resonance of structures" than the *homogeneous* mixture with its local fluctuations. It causes the necessity of considering at equilibrium the simultaneous run of several processes of different relaxation times.

The condition necessary for the system to create the lattice of percolating hydrogen bonds during reduction of volume (*V*), containing (*N*) particles, at fixed temperature (*T)* is that the system must reach the so called "*percolation threshold"* , Blumberg et al. (1984). In the work of Bernabei et al. (2008), it has been shown that the probability of the increase of the number of these bonds may be higher in the lattice points neighboring with oxygen atoms of four bonds. Hydrogen bonds are formed even in the gaseous phase, in water vapor. But the condition required for their

„*connectivity*" is the threshold value of the average number of bonds n_{HB}, per one oxygen atom in the lattice point. For the three-dimensional lattice the critical percolation threshold takes the value of: $n_c = 1.55$ per one water molecule in the system considered. It is rather commonly accepted that after the melting of ice there remain on average 3.6 hydrogen bonds from each 4 bonds, and at the boiling point there remain still 3.2 bonds, per each oxygen atom. At present, the possibility of the existence of the percolation lattices even in the supercritical states of water (Bernabei et al., 2008) has become the subject of interest.

The tetrahedral system with four water molecules at the corners, characteristic for the crystals of hexagonal ice (Ih) is generally accepted for hydrogen bonds. Oxygen atoms of five molecules are bound with hydrogen bridges: ─O••••H──O , and each of them is both a donor and an acceptor of electric charges[ii]. In this idealized system the length of a hydrogen bond is equal to about 2.82Å, and the angle between the bonds of the hydrogen bridge and the covalently bound hydrogen atom (O─H) takes about 109.5°. In various places of the percolation lattice the local and temporary locations of water molecules cause a significant deformation of both the above given distances and angles, as well as the local electron density of the σ_{OH}* orbitals.

The graphs shown above are taken from a most recent work of Brovchenko and Oleinikova (2008). They illustrate the trend in such application of the experimental data on the influence of temperature and pressure on the radial distributions of oxygen and hydrogen atoms, and on the electric densities of liquid water and ice, that it would make possible the use of this information for improving the models of water molecule. The final goal is an equation of state for liquid water, showing clearly inadequacy of the van der Waals equation.

Under the imposed *NTV* conditions the model calculations should give the dependence of the average energy of hydrogen bond upon temperature and pressure for liquid water consistent with experiments. This labor-consuming way has been confirmed by the early work by Berendsen et al. (1987), in which the theory of percolating bonds has been applied. It has been shown that the results of calculations carried out using the SPC model of water are clearly approaching the experimental ones, when in addition to the stable dipole moment (in the SPC/E model) also the existence of induced moments is taken into account.

The more complex attempt to describe the structure of liquid water, using the information on the defined lattice elements has been presented in the already cited work of Brovchenko and Oleinikova (2008). The authors have assumed that liquid water formed after melting ice has the structure of a percolating lattice, where in addition to the structures of the parameters characteristic for the hexagonal lattice of ice appear also increasing numbers of groups of molecules in the pentagonal system. In the latter case, the angle between hydrogen bonds and hydroxide bonds is reduced to 108°. The number of pentagonal structures increases up to about 4°C. At this temperature the tetrahedral structures (Ih ice) are transformed into the plane hexagonal

groups of the bond angle equal to 120°. This last structure is the most numerous at about 45° C when large hydrophobic molecules are the least soluble in water. Starting from this temperature, in the percolating lattice, the systems of pentagonal symmetry are replaced by the groups of molecules characteristic for the simple cubic lattice of the overheated water and critical regions. The authors have simulated radial distributions of water molecules for each of the assumed models of its particles and have obtained the results similar to the results of experiments carried out for water at varying temperature.

Summing up, we may state that the scientist creating the models of material structures works in a way similar to the artist painting from the nature. Various models, just as different images, may describe the *same* reality in a better or worse way. We think that it is the time to admit that the models of the percolating lattice and dynamic clusters are two images of the same structure of water, viewed from different perspectives. We believe that the most important will be such improvement of the basic model of the structure of water molecule that both ways of its modeling would give practically the same consistency with experimental results.

REFERENCES

BERENDSEN H.J.C., GRIGERA J.R., STRAATSMA T.P., (1987), *The missing term in effective pair potentials*, J.Phys.Chem., vol 91, pp 6269-6271

BERNABEI M., BOTTI A., BRUNI F., RICCI M.A., SOPER A.K., *Percolation and three-dimensional structure of supercritical water*, Physical Review E (2008), vol 78, pp 021505-1 -021505-8

BLUM L., VERICAT F., DEGREVE L., (1999), *The Yukagua model of water*, Physica A, vol 265, pp 396 – 409

BLUMBERG R.L., STANLEY H.E., GEIGER A., MAUSBACH P., (1984), *Connectivity of hydrogen bonds in liquid water*, J.Chem.Phys., vol 80,pp 5230 – 5240

BROVCHENKO I., OLINIKOVA A., (2008), *Multiple phases of liquid water*, ChemPhysChem, vol 9, pp 2660-2675

CHAPLIN M., modyf. (2008), *Water Cluster History*, <http://www.lsbu. ac .uk /water>

DOUGHERTY R.C., (1998), *Temperature and pressure dependence of hydrogen bond strength: A perturbation molecular orbital approach*, J.Chem.Phys., vol 109, pp 7372 – 7378

DOUGHERTY R.C., HOWARD L.N., (1998), *Equilibrium structural model of liquid water: Evidence from heat capacity, spectra, density, and other properties*, J.Chem.Phys., vol 109, pp 7379 – 7393

GILLI P., PRETTO L., BERTOLASI V., GILLI G., (2009), *Predicting hydrogen-bond strengths from acid-base molecular properties. The pK_a slide rule: Toward the solution of a long-lasting problem*, Accounts of Chemical Research, (2009), vol 42, pp 33 – 44

KUMAR R., SCHMIDT J.R., SKINNER J.L., (2007), *Hydrogen bonding definitions and dynamics in liquid water*, The Journal of Chemical Physics vol 126, pp 204107-1 – 204107-12

STANLEY H.E., TEIXEIRA J., (1980), *Interpretation of the unusual behavior of H_2O and D_2O at low temperatures: Tests of of a percolation model,* J.Chem.Phys., vol 73, pp 3704-3422

Grodzka J., Pomianowski A., *Tajemnica wiązania wodorowego*, Physicochemical Problems of Mineral Processing, 44 (2010), 35-40 (w jęz. ang), http://www.minproc.pwr.wroc.pl/journal

Uczony – tworząc modele struktur materialnych – postępuje jak artysta malujący obrazy *z natury*. Podobnie jak różne obrazy, tak też różne modele mogą lepiej lub gorzej opisywać *tę samą* rzeczywistość. Sądzimy, że nadszedł czas aby uznać, że modele, zarówno perkolującej sieci, jak też dynamicznych klasterów to dwa obrazy tej samej struktury wody, lecz oglądanej z innych perspektyw. Odnosimy wrażenie, że *środek ciężkości* zagadnienia przenosi się wyraźnie na *takie* udoskonalenie *podstawowego* modelu *molekuły wody*, aby obie *drogi* modelowania jej struktury, dawały praktycznie taką samą zgodność z wynikami prac doświadczalnych.

słowa kluczowe: wiązania wodorowe, klastery wody, łączność wiązań

Physicochem. Probl. Miner. Process. 44(2010) 41-52

journal homepage
www.minproc.pwr.wroc.pl/journal/

Physicochemical Problems of Mineral Processing

Index No. 32213X ISSN 1643-1049

Y. S. Haroun*, M. F. Raslan *

OCCURRENCE OF BARITE MINERALIZATION IN BAHARIYA DEPRESSION, WESTERN DESERT, EGYPT

Received December 20, 2008; reviewed; accepted May 15, 2009

Barite vein mineralization has been recorded South of Gebel El Haufhuf in the ground surface of El Bahariya depression, Western Desert of Egypt. The barite veins that trend in different directions are actually associated with major fold and fault structures that are retricted to the oldest sandstone rock of the Sabaya Formation. Some of these veins attain more than 7m length and a width ranging between 0.5 and up to 4m. The discovered barite veins are exclusively composed of barite and quartz with barite attaining 56% by weight. Besides the genetic aspects of the studied mineralization, the degree of liberation have been discussed.

key words: barite mineralization, genetic aspects, liberation degree, Bahariya depression, Western Desert of Egypt

INTRODUCTION

Barite ($BaSO_4$) is the only commercial source of barium except for minor sources of witherite ($BaCO_3$), which is generally restricted to China. By virtue of its relatively high specific gravity (4.5), over 70% of barite demand is used primarily as a weighting agent in drilling muds in the oil and gas industry as well as to cap oil and gas wells. Barite for drilling purposes must be free of soluble salts, contain a minimum of 92% $BaSO_4$ and have a specific gravity of 4.2, several percent iron oxide is not objectionable and 90-95% of the ground materials must pass a -325 mesh screen. Due

* Nuclear Materials Authority, P.O. Box 530, EL Maadi, Cairo, Egypt
Corresponding author: raslangaines@hotmail.com

to its physical attribute and/or chemical inertness, barite is also used in construction and as functional filler in paints, plastics, rubber, printing inks and papers industries.

Barite is widely distributed in several districts of the USA (Carterville, Georgia) (Bate, 1996) and in western Ouachita mountaines, Arkansas (Mitchell, 1984). Barite deposits are also known in several other countries; namely Canada, Southern America (Peru, Argentina, Brazil, Chile and Colombia), Germany, former USSR, Italy besides Algeria, Morocco, Zimbabwe, China and Australia.

In Egypt barite is widely distributed in the North Eastern Desert such as Um Monqul area besides the veins in the pink granite at east of Aswan and at Gebel El Hudi near Aswan. Also, it occurs as sediments and veins in El Shieh El Shazly area in South Eastern Desert. Additionally, barite is present as a cementing material for sandstones in Kharga Oasis, Western Desert. Several modes of formation of barite deposits have been identified with most commercial sources belonging to replacement deposits in limestone, dolomite sandstone and shales or residual deposits in which lumps of barite are enclosed in clay caused by differential weathering. Barite sometimes occur in veins and as a gangue mineral in metallic ores such as lead, zinc and silver and is frequently associated with fluorspar.

High grade barite mineralization has actually been recorded for the first time in the Cretaceous Sabaya Formation occurring in El Bahariya Oasis, Northwestern Desert. Field investigation and mineralogical studies were carried out in order to define its characteristics and to elucidate its origin as well as its economic significance.

SAMPLING AND TECHNIQUES

A representative bulk composite sample of the defined barite veins was collected (weighing about 12 kg) from the different mineralized zones in the study area. For a proper mineralogical and chemical characterization of the discovered mineralization, a portion of the collected sample was subjected to both XRD and XRF analyses. On the other hand, for the liberation investigation, the representative bulk sample was subjected to proper crushing, grinding and sieving using screens: 0.80, 0.63, 0.40, 0.20, and 0.045mm. The obtained size fractions were subjected to heavy minerals separation using bromoform (sp. gr. = 2.85 gm/cm^3). The obtained heavy and light fractions were then microscopically examined under the binocular microscope to determine the degree of barite liberation. In addition, picked composite and pure grains were subjected to examination by the Environmental Scanning Electron Microscope (ESEM). The latter is supported by energy dispersive spectrometer unit (EDS), model Philips XL 30. The analytical conditions included 30 kV accelerating voltages, 1-2 mm beam diameter and 60-120 second counting time, and minimum detectable weight concentration from 0.1 to 1 wt%. All of the mentioned analyses

were carried out at the laboratories of the Egyptian Nuclear Materials Authority (NMA).

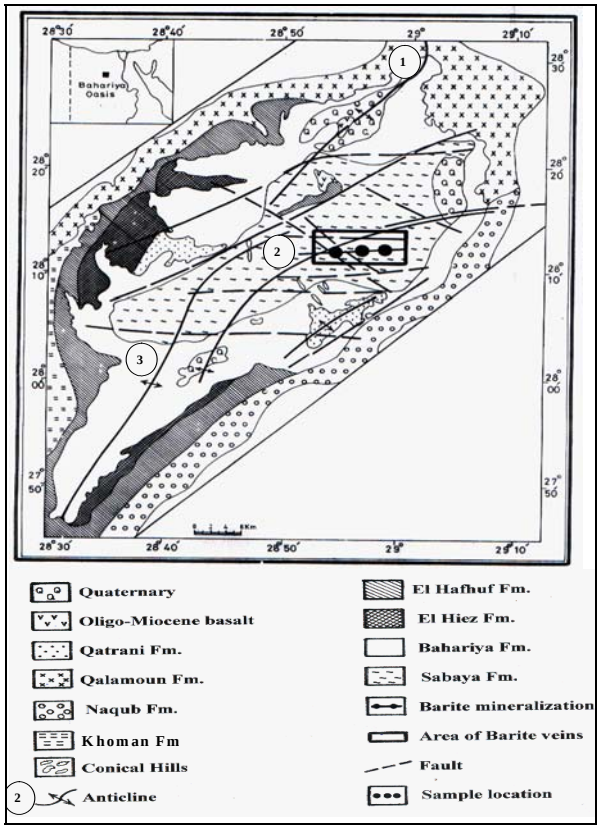

Fig.1. Geologic map of Bahariya Oasis showing barite occurrence, after Morsy (1987) with slight modification

FIELD INVESTIGATION

GENERAL STRATIGRAPHY OF THE EL BAHARIYA OASIS

The El Bahariya Oasis is an oval shaped depression (Fig. 1) trending in a NE-SW direction. Within the depression, the Cretaceous rocks outcrop at its base as well as at the base of the conical hills and the scarp. The Cretaceous rock succession (Sabaya, Bahariya, El Heiz and El Hafhuf Formations) comprises fluvialite to fluviomarine clastics of sandstone, claystone and shale. The Sabaya Formation of Lower Cenomanian age (Morsy, 1987) is coverd by Bahariya Formation which also belongs

to the Lower Cenomanian (Soliman and El Badry, 1980). The Bahariya Formation is unconformably overlain by the Upper Cenomanian fluviomarine marly shale, sandy dolomitic limestone and calcareous sandstone of El Heiz Formation as well as by the Campanian cherty cavernous dolostone, crossbedded sandstone and phosphatic limestone of El Haufhuf Formation (Morsy, 1987).

The succeeding maeastrichtian Khoman Formation is mainly represented by chalk and chalkly limestone. It overlies conformably El Haufhuf Formation on both sides of the depression and extends southward with increasing thickness (Fig. 1). The Eocene rocks are represented by the Naqb Formation which belongs to the Middle Eocene (Said, 1962) and comprises gray and pink limestone and by the Qalamoun Formation which belongs to the Lower Eocene (El Shazly, 1962). The Qalamoun Formation is deposited on the Bahariya Formation and El Haufhuf Formation to the North of El Bahariya depression (Fig.1). The succeeding Oligocene Qatrani Formation (Morsy, 1987) covers El Bahariya Formation at the top of the conical hills besides occurring as small outcrops within the depression. This formation consists of quartizitic sandstone, quarzite, shale and silt.

At the northern part of Gebel El Haufhuf, Oligo-Miocene basaltic and doleritic extrusions (sheets, sills and dikes) are recorded (Morsy, 1987; Meneisy and El Kaleubi, 1975).

MODE OF OCCURRENCE OF EL BAHARIYA BARITE

High grade barite mineralization is found mainly in the form of different veins restricted to the ground surface of El Bahariya depression (Fig. 1). The barite veins trend in different directions and are actually associated with the major folds and faults that are restricted to the oldest rocks of Sabaya Formation which form the floor of the depression. In order to study the barite veins, the structure configuration of the El Bahariya Oasis depression must first be studied. The latter occurs within a major northeast trending belt of considerable extension about 100 km long and 40 km wide. Several other folds of the same or later tectonic phase but of lesser extension occur parallel to or perpendicular to the main anticlinal trend i.e. trending either NE or NW. Morsy (1987) discussed the structure of the Bahariya Oasis and concluded that more than two folding generations can be identified. The trends of these folds are chronologically arranged from the younger to the older according to the following sequence; viz, NW-SE, NE-SW and E-W.

The following is a brief description of the major fold trends restricted to the northern part of the El Bahariya Oasis.

i- Anticline No.1 is a NE trending fold. Its axis has NE-SW direction and plunges 5º due North. The length of the anticline is about 30 km.

ii- Anticline No.2 has the same NE trend of anticline No.1 and its axis plunges 4º due North. Many small to medium size synclines occur parallel to the axis of this anticline.

iii- Anticline No.3 is a major fold restricted in southern part (Fig. 1).

On the other hand, several faults of different directions and magnitudes are also observed in the El Bahariya Oasis (Fig. 1). These faults include E-W faults that dip due South with more than 30 m vertical displacement as well as NE-SW faults that dip to the north or south and extend for a length reaching 100 km with 10-40 m vertical displacement.

The discovered barite mineralization veins are hosted in the sandstone beds of the Sabaya Formation. This Formation is composed of channel sediments of tabular cross-stratification, medium to coarse grained sandstone and of flood plain deposits of clayey sandstone (Fig. 2A).

The lithological features suggest the sandstone beds were deposited in a fluviatile environment. The barite veins are widely distributed to the south of Gebel El Hafhuf which is composed of a rock sequence including sandstone, shale, limestone, phosphatic limestone and phosphatic calcareous sandstone. This succession is capped by the Oligo-Miocene basaltic sheet which takes the form of open circle of about 20 m thickness (Fig. 2B).

The barite veins are restricted to the fractures that are parallel to the main E-W or NW-SE striking faults in the Sabaya Formation (Fig. 1). These veins occur subparallel sets with more than 7 m length and ranging in width between 0.5 to 4 m. They dip 50º towards N, S or NE directions. The barite veins are hard, massive, siliceous and white to gray in color (Fig. 2C). These veins are numerous and distributed in association with tectonically formed fractures and fissures.

GENETIC ASPECTS OF EL BAHARIYA BARITE MINERALIZATION

From the field investigation and the geologic setting of the barite veins host rocks, it has been possible to elucidate the origin of the studied barite mineralization. Accordingly, the following genetic model and succession has been proposed:

i- The Cretaceous shallow marine to fluvial siliciclastic strata have been first deformed by both folding and faulting.

ii- Barium was leached from the basaltic extrusion during high temperature circulation (Von Damn et al, 1985). Tertiary Oligocene basalt at Gebel El Haufhuf, Bahariya Oasis is related to continental intraplate volcanism, which is contiemporaneous with the opining of the red sea and uplift of Afro-arabian mountain. Fumarolic and geyser activities belong to Oligocene period were consider as gas maar resulting from a phreatic explosion (El-Kammar, 2000).

iii- Release of sulphate fluids from the sulphate-rich minerals involved in the Brine deposits distributed within El Bahariya Depression at the Qaternary (Haroun, 1990) ; namely polyhalite, kieserite and kyanite.

iv- Migration of these fluids through the deformed strata followed by barite mineralization as a result of a rapid primary precipitation at or above the sediment / fluid interfaces.

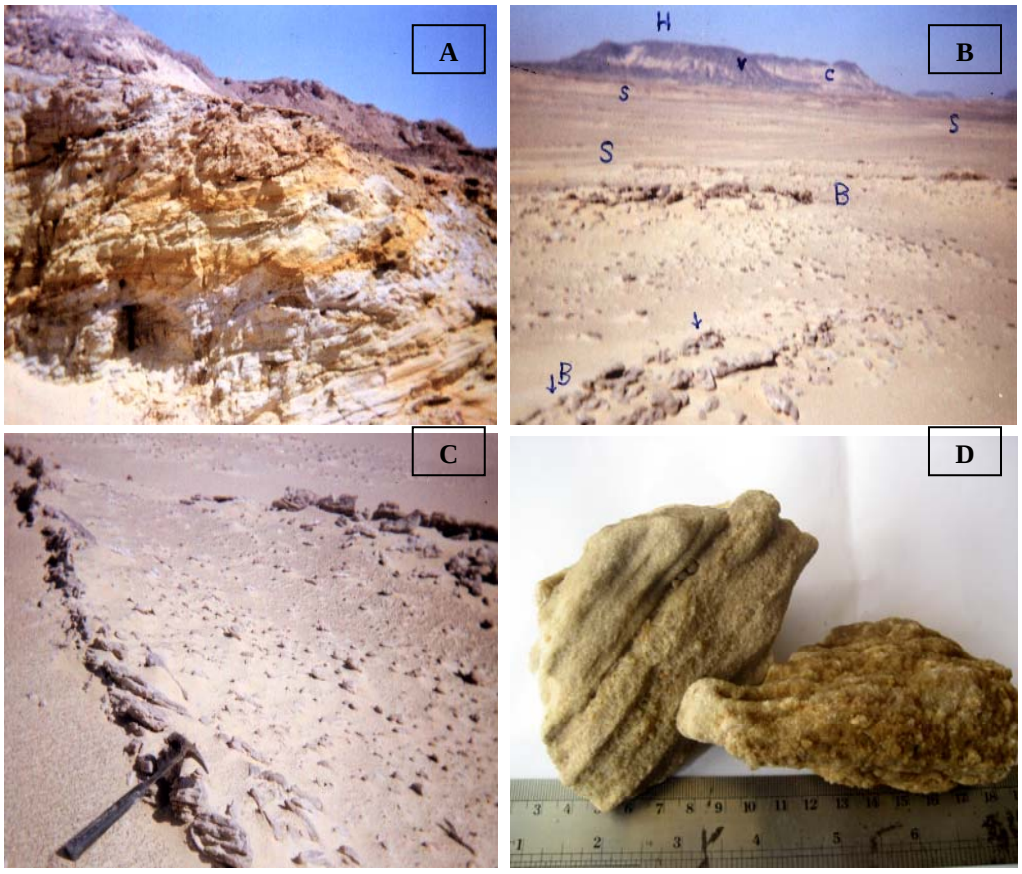

Fig. 2.
A- Outcrop of Sabaya sandstone (Lower Creataceous) hosting barite mineralization. Crossbedded sandstone represent the channel deposits of fluvial environment. B- Photograph showing the area of barite veins. Subparallel barite veins (B) are hosted in sandstone of the Sabaya Formation (S). Barite mineralization restricted south Gebel El Hafhuf (H) which is composed of Creataceous rocks (Campanian) (C) caped by Oligomiocene Basaltic sheets (V). Barite veins trending NE-SW. Looking North West. C- Closed up view of barite vein dipping 50 toward NW direction with length more than 7 m. (Hammar = 20 cm).D- Closed up view of barite samples characterized by well developed quartz granules. Barite occur as aggregates and tabular forms with white to grey coloration.

MINERALOGICAL AND LIBERATION CHARACTERISTICS

MINERALOGICAL INVESTIGATION

As mentioned above, the collected samples of the barite -bearing veins are hard, compact, heavy and siliceous. The barite veins are almost exclusively composed of barite cementing quartz sand grains. The barite mineral itself occurs as aggregates of tabular form crystals and is characterized by a white to grey coloration**.** The sand grains in the veins are of coarser grain size and are ill sorted indicating a low degree of maturity (Fig. 2 D).

Table 1. XRD pattern for barite veins bulk sample

Sample		Barite ASTM 5-0448		Quartz ASTM 5-0490	
dA°	I/I_0	dA°	I/I_0	dA°	I/I_0
4.44	5	4.44	17		
4.33	13	4.34	36		
4.25	17			4.26	35
3.90	16	3.90	57		
3.77	4	3.77	12		
3.57	35	3.576	31		
3.44	100	3.442	100		
3.34	75			3.343	100
3.32	31	3.317	67		
3.10	37	3.101	97		
2.83	16	2.834	53		
2.72	15	2.726	47		
2.48	5	2.481	14		
2.46	6	2.444	2	2.458	12
2.32	5	2.322	15		
2.28	3	2.281	7	2.282	12
2.21	8	2.209	27		
2.12	24	2.120	80		
2.10	25	2.104	76		
2.05	6	2.056	23		
1.98	4			1.980	6
1.93	3	1.930	7		
1.86	5	1.857	16		
1.81	13			1.817	17
1.79	5	1.787	3		
1.76	3	1.760	9		
1.67	9	1.673	14	1.672	7
1.63	1.8	1.636	8		
1.59	2	1.593	8		
1.54	7	1.534	18	1.541	15
1.53	4	1.536	11		
1.47	2	1.474	10		

Table 2. Trace elements concentration in barite veins

Elements (ppm)	Cr	Cu	Ni	Zn	Zr	Y	Pb	Sr	V	Nb	U*
Sample	20	8	4	11	u.d	2	14	49	134	3	u.d

u.d Under limit of detection
* Gamma-ray spectrometry

As previously mentioned, the barite veins are associated with El Haufhuf major fault and although various radiometric anomalies have been recorded in the altered sediments affected by this fault (Morsy, 1987 and El Agami et al, 2005), however, radioactivity is not associated with the studied barite mineralization. The lack of radioactive elements in the discovered barite mineralization is greatly advantageous in increasing its economic significance.

On the other hand, to define the mineral composition of the studied barite veins, the representative collected bulk composite sample was subjected to the XRD analysis. From the obtained results shown in Table 1, it was verified that the barite veins are only composed of barite and quartz.

In the meantime, to elucidate the purity of the studied mineralization a representative portion of the collected bulk composite sample was subjected to the XRF analysis to determine the presence of trace elements and their concentration (Table 2).

From the obtained data, it was revealed that the studied barite sample is almost pure where V and Sr assay 134 and 49 ppm respectively while the assay of Cr, Cu, Ni, Zn, Y, Pb and Nb ranges between only 2 and 20 ppm. In the meantime, Zr is under its limit of detection. In this regard, it is interesting to mention that a laboratory gamma-ray spectrometry has indicated that uranium is also under its limit of detection. These results indicate that except for Cr, the barite of Bahariya is almost not contaminated with harmful metallic elements; a matter which is greatly beneficial in reducing environmental hazards associated with the disposal of spent drilling mud.

LIBERATION INVESTIGATION

Wills (1979) noted that a correct degree of liberation is the key to the success in mineral processing, especially when the economic mineral is soft and the accompanied gangue mineral is hard. Although, some degree of separation is possible between locked particles by crushing , it should be evident that production of a reasonable degree of liberation is a pre-requisite to make a fair separation (Gaudin, 1980). As a mattar of fact, liberation is increased by comminution through two means; namely liberation by size reduction and liberation by detachment.

Due to the softness of barite and the the hardness of the accompanied gangue mineral (quartz), comminution must be carfully performed to avoid the possibility of overgrinding and excessive slime production. Accordingly, for the liberation investigation a controlled crushing was carried out on the representative bulk sample

of the study barite vein in order to reduce the size of the head sample to pass 0.800 mm screen. The comminution process involved indeed a combination of jaw and roll mill crushers in a closed circuit. The crushed product was then deslimed using a desliming cone, dried and screened using a suitable set of screens; viz 0.800, 0.630, 0.400, 0.200, and 0.045 mm. The obtained size fractions were collected and a representative portion from each fraction was subjected to heavy liquid separation by bromoform. The obtained heavy and light fractions were then weighed and microscopically investigated under the binocular microscope to check mineral liberation. The microscopic examination for the various heavy fractions has actually indicated that barite represents almost exclusively the main constituent together with some scattered quartz crystals in some composite barite grains. The barite grains occur indeed as coarse massive crystals of vitreous luster and range in color from white to yellowish white. The crystals are transparent to translucent and are generally present in the form of angular to subangular shape. On the other hand, the heavy liquid separation of the bulk representative barite sample revealed that the average content of barite assays 56 % by weight of the original bulk rock sample and the rest is almost exclusively represented by quartz. It is quite clear that the weight percentages of the size fractions and their barite content increase with the decreasing of grain size (Fig. 3).

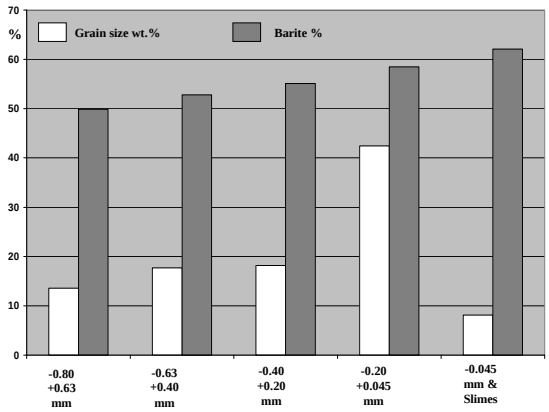

Fig. 3. Histogram show grain size distribution of the studied barite bulk sample and distribution of barite among various size fractions

Due to the variation in the friability between barite (a relatively soft mineral) and quartz, the degree of liberation of barite is relatively low in the two coarser size fractions i.e. -0.800+0.630 mm and -0.630 + 0.400mm; a matter which reflected in the presence of most barite grains as locked or composite crystals with quartz. However, microscopic investigation for the various size fractions indicated that both the degree of liberation and the percentage of barite increase with decreasing grain size.

Several liberated and composite barite crystals were hand picked and subjected to elemental analysis using the Environmental Scanning Electron Microscope (ESEM).

The SEM microphotograph (Fig. 4A) for a locked barite crystal (bright) together with quartz (dark) reflects the degree of liberation of barite in the coarser size. On the other hand, the back scattered images (Figs 4D and F) represent liberated barite and quartz

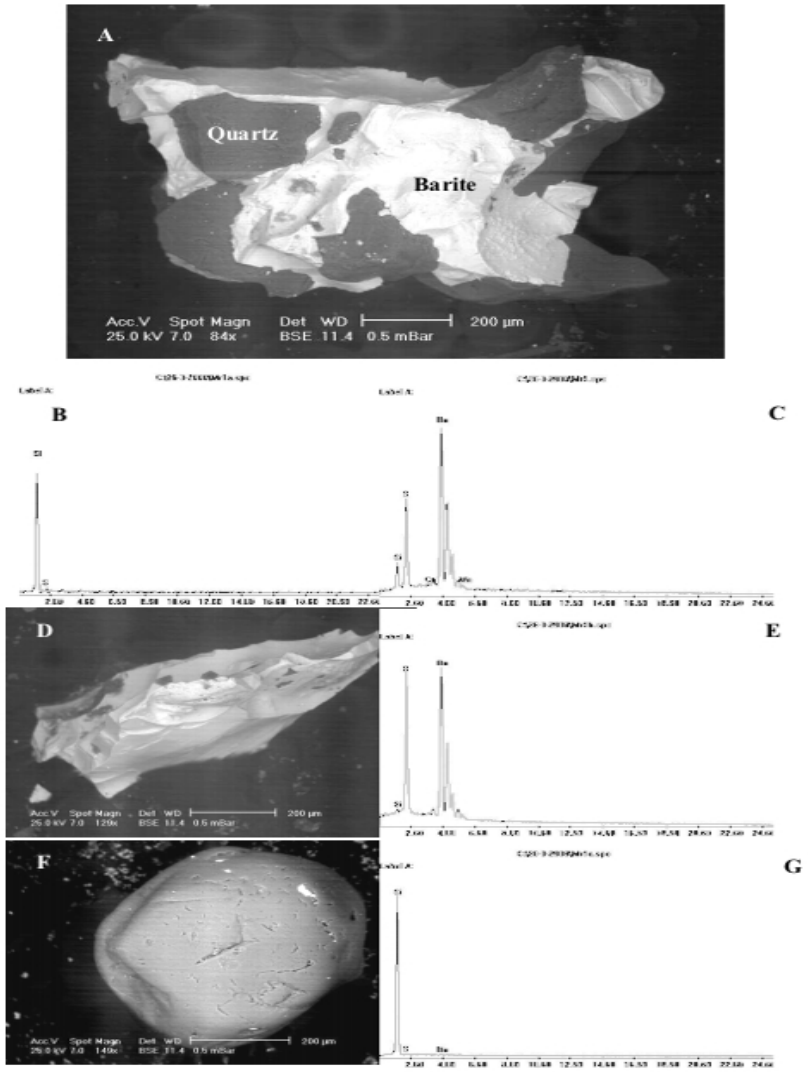

Fig. 4. A- backscattered image of composite grain consisting of barite (bright) and quartz (dark). B&C- chemical analyses spectra for barite and quartz respectively. D&E- BSE image for barite crystal and crossponding analyses. F&G- back scattered image of quartz grain and its chemical analyses.

crystals respectively. The corresponding EDAX analyses (Figs. 4 B, C, E and G) reflect the chemical composition of barite and quartz either in the locked or free grains. These analyses indicate that the major elements in barite are Ba (75.90%) and S (23.50%) together with a minor amount of silica.

Finally, it is interesting to mention that the quartz crystals were found to be present in two main habits in the studied barite samples. The first is represented by liberated rounded to subrounded crystals and have most probably attained their liberation by detachement rather than size reduction (Fig. 4F). The second habit is represented by angular to subangular crystals that are mainly present as locked crystals within barite (Fig.4A) and would thus attain their liberation by size reduction (Fig. 4D). The first type has been most probably brought to the already formed barite veins by mechanical weathering through wind and water currents. These rounded to subrounded quartz granules must have filled any cracks and fissures that have been formed after the formation of the barite veins. The second type is the silica that has been leached from the Tertiary basalt together with barium. The leaching fluids have subsequently filled the cracks and fissures to form the mineralization by rapid precipitation.

CONCLUSIONS

A high grade barite vein mineralization has been recorded for the first time in the ground surface of the El Bahariya Depression, Western Desert of Egypt. This mineralization is usually hosted in the sandstone beds of the lower Cretaceous Sabaya Formation and covers a great area south Gebel El Haufhuf. The barite veins occupy indeed the fractures that have been set up parallel to the main faults that are restricted in the Sabaya Formation. These fractures have actually been well developed along the fault zone trending E-W and NW-SE with more than 7m in length, a width ranging between 0.5 to 4m and a dipping angle attaining 50º towards NE direction.

A genetic model of the discovered barite mineralization has been proposed depending on barium leaching from the existing basaltic extrusion. On the other hand, it was mineralogically revealed that the discovered mineralization assays 56% by weight, associated with quartz as the sole gangue mineral. Liberation investigation indicated that a high liberation degree could be obtained in mesh size below 0.40 mm. Trace elements analyses has shown a very low assay where apart from V (134 ppm) and Sr (49 ppm), the other elements were found to range from only 2 to 20 ppm.

ACKNOWLEDGEMENTS

The authors sincerely thanks Prof. Dr. N. T. El Hazek, Egyptian Nuclear Materials Authority, for his interest, reading the manuscript and fruitful discussions.

REFERENCES

BATE, L.R. (1969) *Geology of industrial rocks and minerals*. Dover publications, Inc, New York.

EL-AGAMI, N. L. ABDEL WAHAB, A.A., HAROUN, Y.S. (2005) *Apatite alteration and its relation to REE fractionation and U-mineralization: A Case study of Western Desert and Sinai*, Egypt. The fourth international Conference on the geology of Africa.

EL- KAMMAR, A. EL- KAMMAR, M.,EL- GAMAL, I. (2000): *Rare earth elements and uranium geochemistry of terrestrial Tertiary bones from Fayium*, Egypt. 5th International Conference on the Geology of the Arab World, pp. 213-238.

EL SHAZLY E. M. (1962) *The results of drilling in iron ore deposits of Gharabi, Bahariya Oasis*, *Western Desert and report on the mineralogy of the low grade iron of El Heiz area, Bahriya Oasis*, Western Desert, Geol. Surv. Egypt.

GAUDIN, A. M. (1980) *Principles of mineral dressing*, TATA McGraw Hill publishing Co. Ltd, New Delhi.

HAROUN, Y. S. M. (1990) *Geological and geochemical studies on some radioactive deposits, Bahariya Oasis*, Western Desert, Egypt. M.Sc. Thesis, Ain Shams University, 184 p.

MENEISY, M. Y., B. A. EL KALIUOBI (1975*) Isotopic ages of the volcanic rocks of Bahariya Oasis.* Annals Geol. Surv. Egypt, V.119-122.

MITCHELL, A W. (1984) *Barite in the western Ouachita mountaines*, Arkansas. In Stone, C.G. and Haley, B. R. eds. Guidbook to the gology of the central and southern Ouachita mountaines, Arkansas: Arkansas, Geological commission, Guidbook 84-2, p. 124-131.

MORSY, M. A. (1987) *Geology and radioactivity of late Cretaceous – Tertiary sediments in the Northern Western Desert*, Egypt. Ph.D. Thesis, Fac. Sci, Mansoura Uni., Egypt, 351 p.

SAID, R. (1962) *The geology of Egypt*. Elsevier, Amesterdam.

SOLIMAN, S. M., EL BADRY, O. A. (1980) *Petrology and tectonic framework of Cretaceous*, *Bahariya Oasis*, Egypt, J. Geol. Soc. U. AR., V. 27 No. 1-2 P.1153.

WILLS, B. A. (1979) *Mineral processing technology*, Pergamon Press, Oxford, New York, Toronto, Sydney, Paris, Frankfurt.

VON DAMN, K.L., EDMOND, J.M., GRANT, B., MEASURES, C.L., WAKLEN, B., WEISS, R.F. (1985) *Chemistry of submarine hydrothermal solutions at 2°/N East Pacific*. Geochim Cosmochim Acta, 49, 2197-2220.

Haroun, Y.S., Raslan, M.F., *Występowanie mineralizacji barytowej na Obniżeniu Bahariya, Pustynia Zachodnia, Egipt,* Physicochemical Problems of Mineral Processing, 44 (2010), 41-52 (w jęz. ang), http://www.minproc.pwr.wroc.pl/journal

Odnotowano występowanie mineralizacji barytowej na południe od Gebel El Haufhuf na powierzchni ziemi Obniżenia El Bahariya (Pustynia Zachodnia, Egipt). Żyły barytowe wiją się w różnych kierunkach i są związane z załamaniami i uskokami ograniczonymi do najstarszych skał piaskowcowych formacji Sabaya. Niektóre żyły mają 7m długości i od 0.5 do 4m szerokości. Żyły te zawierają do 65% wagowych barytu oraz kwarc. Omówiono mieneralizację i uwolnienie ziarn.

słowa kluczowe: mineralizacja barytowa, genetyka, uwolnienie, żyły barytowe

Physicochem. Probl. Miner. Process. 44(2010) 53-62

journal homepage
www.minproc.pwr.wroc.pl/journal/

Physicochemical Problems of Mineral Processing

Index No. 32213X ISSN 1643-1049

A. Heim*, A. Obraniak*, T. Gluba*

CHANGE IN THE PROPERTIES OF BEDS GRANULATED IN DISC GRANULATORS

Received January 21, 2009; reviewed; accepted March 19, 2009

During tumbling of a powder bed wetted with liquid, material particles are agglomerated. Both the formation of granules and increase of the bed moisture content cause changes in bulk density and the coefficient of material friction against the granulator surface. They in turn determine energy transfer to the granulated material.

In the present study, a change of the above mentioned parameters during batch granulation was investigated by comparing results obtained with a change in granulation degree and torque on the granulator shaft. Experiments were made in three disc granulators of diameters 0.5, 0.7 and 1 m, with rotational speeds equal to 0.2 of critical velocity. Variable parameters were the degree of disc filling and the angle of inclination of the disc axis to the level. The experimental material was bentonite with particles from 0 to 0.16 mm in diameter (d_m = 0.056 mm), specific density 2420 kg/m^3 and bulk density 790 kg/m^3. The material was wetted drop-wise with water during the granulation at constant liquid flow rate Q = 0.7 ml/s.

The angle of disc axis inclination in the applied range of its changes had no effect on the process and layer properties.

In all cases, bulk density of the bed during granulation decreased. When observing change of the coefficient of friction between the bed and disc surface during granulation, three ranges of this parameter change were found. In the first, the coefficient was growing. In the second, short period, the coefficient decreased slightly. In the third, it increased again.

Changing the in torque on the granulator shaft was also analysed. Three ranges could be distinguished here as well. In the first, unit moment increased to up to 50%. In the second, it dropped. In the third, it remained constant.

key words: agglomeration, bulk density, friction coefficient, energy of granulation

* Faculty of Process and Environmental Engineering, Technical University of Lodz, Wolczanska 213, 90-094 Lodz, Poland

INTRODUCTION

In drum or disk batch granulators, agglomeration of particles and formation of granules are induced by material layers mutually dislocating in the bed. The bed is elevated to a certain level due to the friction between it and moving surface of the apparatus. It then goes downward due to gravity force. At the beginning of the process, the primary material layer slides down the free bed surface and it is wetted with liquid. Granules formed after a certain time do not slide down but roll down, and relevant mechanisms cause an increase in mean diameter and strength (Rumpf, 1977). The intensity of granulated bed tumbling is determined among the others by the coefficient of bed friction against the granulator surface. At higher values the material is elevated to a higher level. It slides or rolls down a more inclined surface and tumbling is more intense. This is related to a higher torque value on the granulator shaft. A change of the inner bed structure during wetting and agglomeration (an increase of moisture content and granulation degree) causes a change in its bulk density and coefficients of inner friction and material friction against the apparatus surface. These, in turn, determine energy transfer onto the granulated material and its tumbling intensity (Gluba, 2000; Chadwick, 1997).

The aim of the present study was to investigate how the above parameters change over time during granulation, and how they are related to moisture content of the bed and particle size distribution. Another parameter which was measured for comparison during the granulation was changing torque on the granulator shaft over time.

EXPERIMENTAL

Granulation was carried out on a properly equipped experimental rig with an exchangeable disc whose angle of inclination to the level α could range from 45° to 53°. Tests were made for three disc diameters: 0.5, 0.7 and 1 m. In all cases, rotations frequency of the disc was $n = 0.2\ n_{cr}$, where n_{cr} represents the critical value of rotations frequency at which the bed started swirling with the disc. This enabled proper bed dynamics and prevented the feed from getting outside the disc. On the other hand, this made it possible for the results of all disc diameters to be compared. Tests were made for five different degrees of disc filling: 3%, 4%, 5%, 6% and 7%. The granulated material was bentonite with particle size ranging from 0 do 0.16 mm. The mean particle diameter was 0.056 mm. Specific density of dry bentonite was 2420 kg/m^3, its bulk density was 790 kg/m^3, and tangent of the angle of natural repose was 1.15.

The material was wetted drop-wise with distilled water during granulation at constant liquid flow rate of 0.7 ml/s. At time intervals, samples were taken to determine the particle size composition of granulated material, the bulk density, and

the coefficient of material friction against the disc surface. Instantaneous values of the torque on the disc shaft were also measured. The values were used to calculate the unit moment varying in time using the following formula:

$$M^*(t) = \frac{M(t) - M_0}{m_s + Q \cdot \rho_l \cdot t} \tag{1}$$

where:

$M(t)$ – instantaneous value of measured moment,
M_0 – moment at the empty disc rotation,
m_s – mass of loose material (feed) on the disc,
Q – wetting water flow rate,
ρ_l – wetting water density,
t – time of water dosing (granulation time).

RESULTS

There have been many stadies on the change of material particle size distribution over time (Kapur, 1972) (Sastry, 1973) (Kapur, 1981) (Pataki, 1987). Most of these studies were conducted on a small scale in the laboratory. The present study was conducted on a large scale. Basing on particle size analysis of the agglomerated material, mean particle diameter d_m for subsequent granulation times, was calculated from the formula:

$$d_m = \sum_{i=1}^{n} x_i \, d_{mi} \tag{2}$$

where: x_i–mass fraction i,
d_{mi}–mean particle diameter in fraction i.

The change in particle diameter over in time at different filling degrees and disc diameters is shown in Fig. 1 and 2, respectively. Significant differences result mainly from the fact that, in subsequent trials, the mass of raw material to be granulated was different, while wetting intensity was constant.
The mean moisture content of the bed in particular trials for the same wetting time was different.

If we compare the change of mean diameter d with the change of bed moisture content, this relationship will be similar for all trials, regardless of the disc diameter, the filling, and the angle of inclination of the disc axis. Fig. 3 shows this for random points taken from the whole data set.

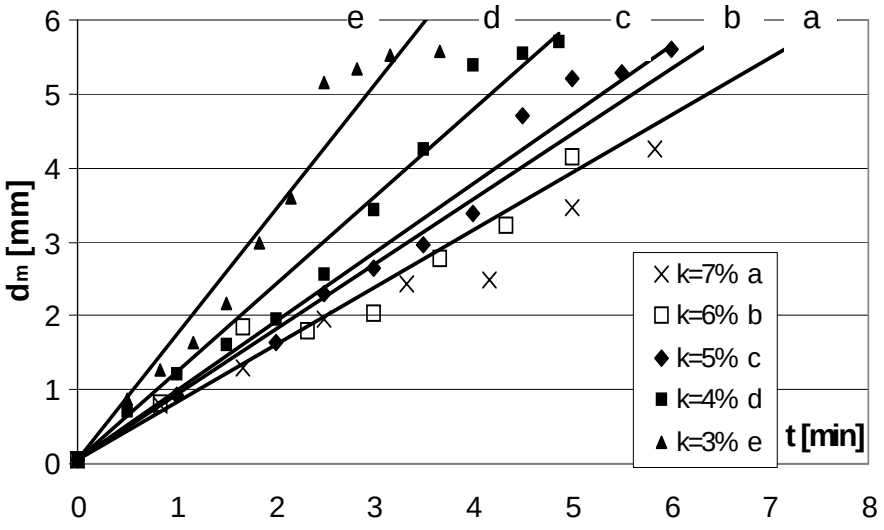

Fig. 1. The effect of wetting time (process duration) on mean particle diameter of the granulated material, for different disc filling degrees
(D = 0.5 m, α = 45°)

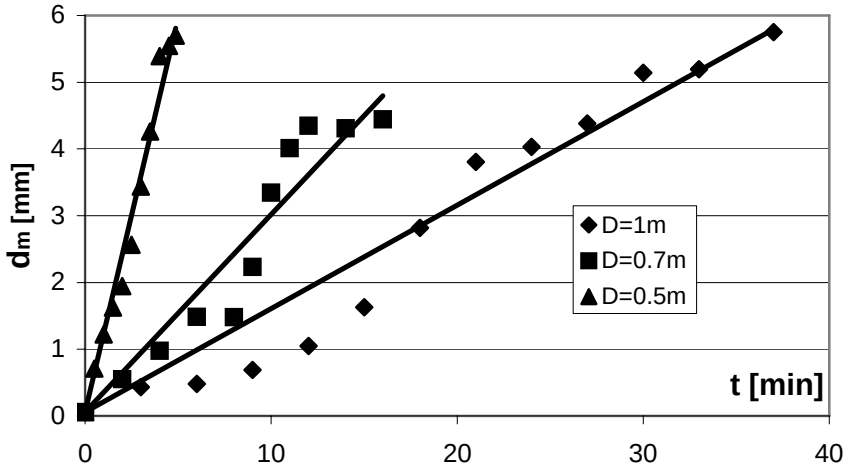

Fig. 2. The effect of granulation time on mean particle diameter of granulated material at different disc diameters D (α = 45° and k = 4%)

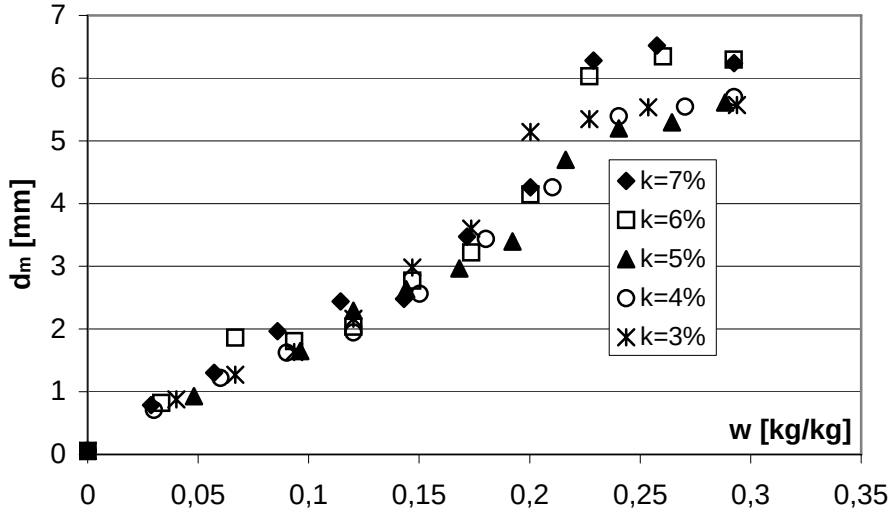

Fig. 3. The effect of mean moisture content of the bed on mean particle diameter of the granulated

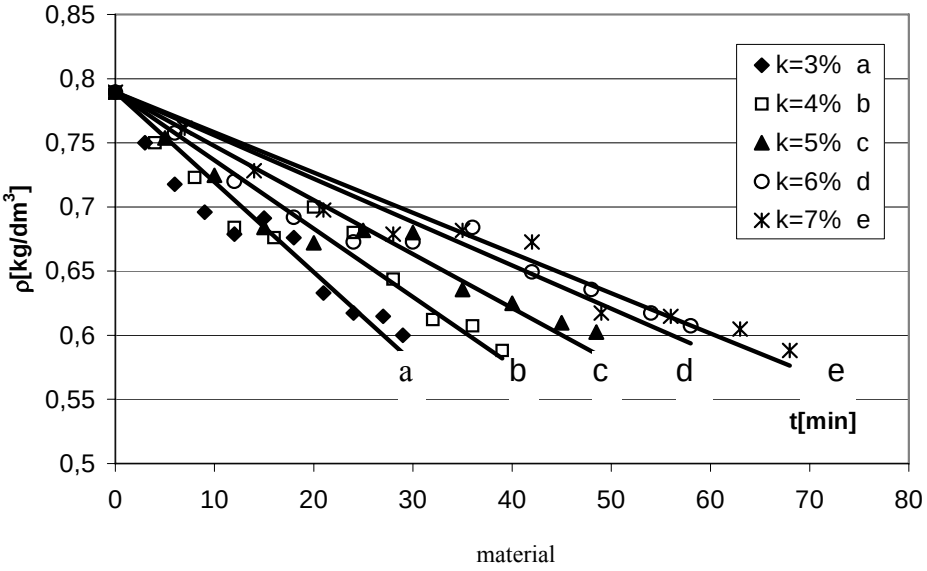

material

Fig. 4. Change in bulk density of granulated material for different degrees of disc filling (D = 1 m, α = 47°)

Similar conclusions follow from the analysis of data which describe a change of bulk density of the material during granulation. Opposite relationship are obtained for

subsequent disc filling degrees and diameters when this density change is observed over time (Fig. 4 and 5).

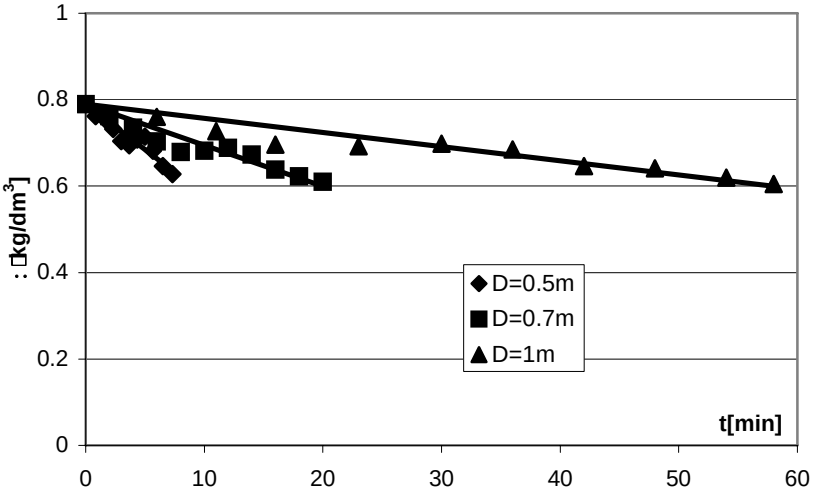

Fig. 5. The effect of wetting time (granulation time) on bulk density for different disc diameters (k = 6%, α = 49°)

When bed moisture content is the independent variable, then the measuring points are located on a single straight line (Fig. 6 and 7).

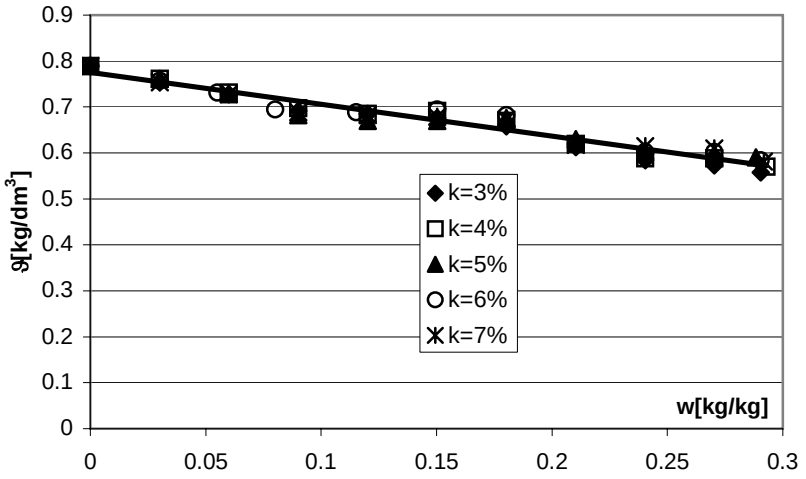

Fig. 6. Change of bulk density as a function of bed moisture content for different disc filling degrees (D = 1 m, α = 51°)

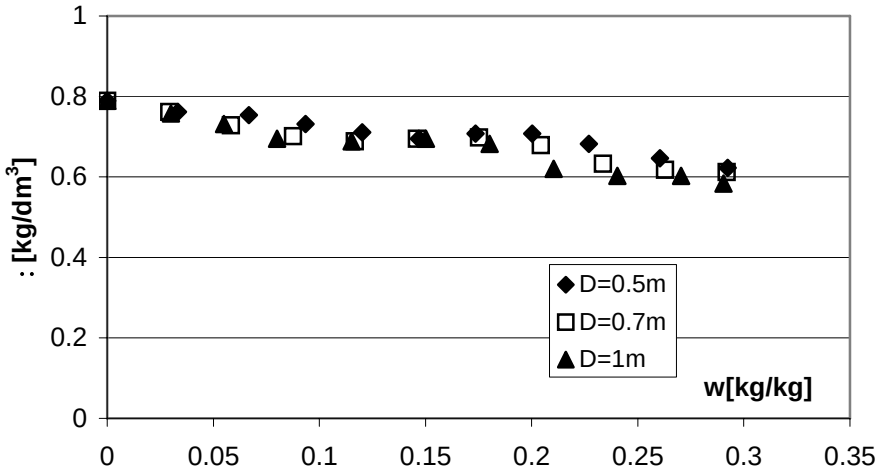

Fig.7. Change of bulk density with an increase of bed moisture content for different disc diameters (k = 6%, α = 51°)

Analogously, disc inclination angle had no effect on this relationship. In the tested range of disc filling, diameter and inclination angle, these parameters have no effect on the relationships between bulk density and granulated material moisture content.

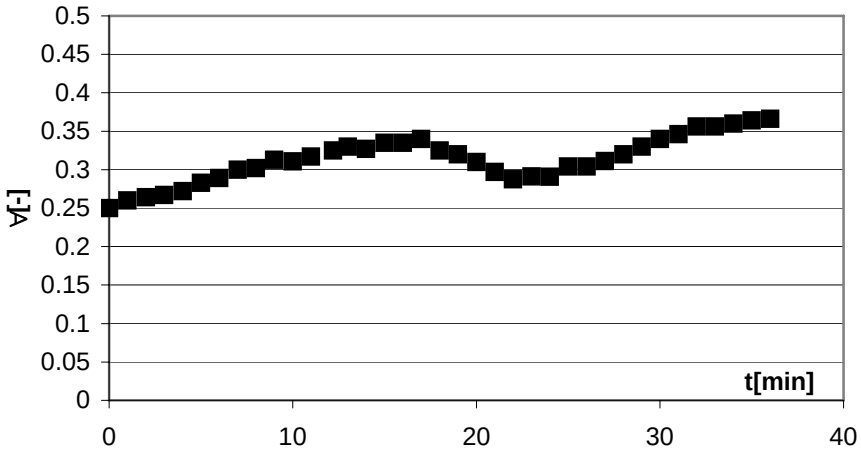

Fig. 8. An example of change in the coefficient of friction between granulated material and disc surface during the process

Energy input for granulation is related to the coefficient of friction between the bed and disc surface, because the energy is transmitted from the disc to the bed

because of the friction. The coefficient change during granulation is therefore important. For all granulation tests, this relationship was the same (Fig. 8).

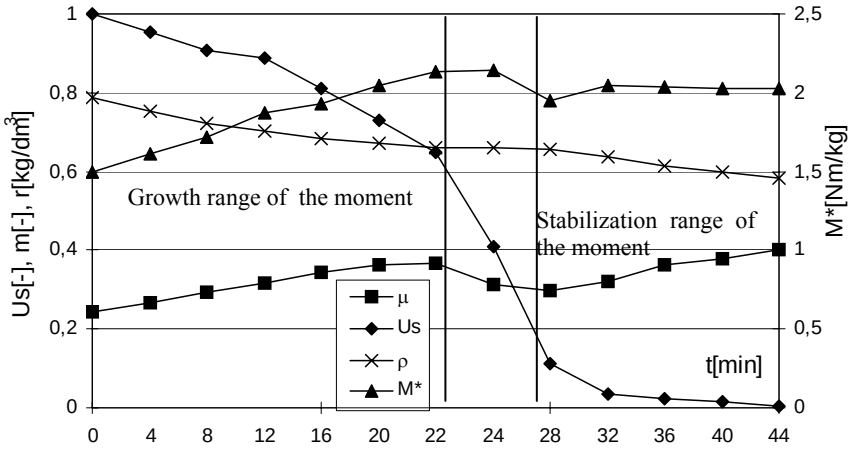

Fig. 9. A comparison of friction coefficient μ, bulk density ρ, non-granulated material U_s and unit moment M* during granulation (D = 1 m, k = 5%, α = 53°)

Three periods can be observed when changes in friction coefficient in the granulation process proceed differently. At the beginning, there is an increase caused by the growth of bed moisture content and partial sticking of material to the disc surface. As a result, the bed is elevated to a higher level and tumbling is more intense. At a certain point, the friction coefficient decreases. In the second stage, the amount of non-granulated material decreases quickly. This is illustrated in Fig. 9, where U_s is the amount of non-granulated material calculated on the basis of sieve analysis as a mass fraction smaller than 1 mm.

The second stage ends when practically the whole feed is transformed into granulated product with a relatively low moisture content mainly inside the granules. Further granulation and wetting causes an increase in the moisture content of the granules, which are additionally consolidated. Liquid from inside is pressed to their surface. This surface moisture causes that granules stick locally to the disc surface, and the coefficient of averaged friction on the whole bed-disc contact surface increases.

Figure 9 also shows the change over time of bulk density and unit moment calculated from equation (1) for the same granulation trial. The change over time of all measured values can be divided into three stages in the same time intervals. In the first stage non-granulated material appears and the fraction of granules increases. Bulk density of the bed decreases, the coefficient of material friction against the disc bottom grows and the unit turning moment on the disc shaft also increases significantly. In the second, transient period, an abrupt decrease of non-granulated material is observed,

granules are probably dry on the surface, friction coefficient decreases and the granules reveal a decreasing tendency to stick to the walls. In this time bulk density remains constant and the torque also decreases. In the third stage, there is no non-granulated material. A mean granule diameter continues to increase owing to the mechanisms of crushing weaker granules and combining them into more resistant granules (Fig. 2). Bulk density of the material decreases and friction coefficient grows due to an increase of surface moisture content of the granules. This moment on the granulator shaft is constant during this stage.

CONCLUSIONS

There are changes in the properties of the bed granulated in the disc granulator at continuous wetting. In the tested range of changes of the angle of disc inclination, filling, disc dimensions, the change of bulk density of the bed and the coefficient of bed friction against the granulator can be described only as a function of bed moisture content. There was a correlation between the change of bulk density and friction coefficient and the unit torque on the granulator shaft with the granulation degree (mass fraction of non-granulated material).

ACKNOWLEDGEMENTS

The research was carried out within basic research program of the Department of Process Equipment W-10/1/2009/Dz.St. 1

REFERENCES

CHADWICK P.C., BRIDGNATER I., (1997), *Solids Flow in Disc Granulators*, Chem. Eng. Sci. 54, 15, 2497-2509.

GLUBA T., HEIM A., OBRANIAK A., (2000), *Driving Torque in the Process of Drum Granulation*, CHISA 2000, Praha.

KAPUR P.C., SASTRY K.V.S., FUERSTENAU D.W., (1981) *Mathematical Models of Open-Circuit Balling or Granulating Devices.*, Chem. Process. Des. Dev., 20, 519-524.

KAPUR P.C., (1972)Kinetics of Granulation by Non-random Coalescence Mechanism, Chem. Eng. Sci., 27, 1863.

PATAKI K., HORVATH E., ORMOS Z., (1987) *The Effect of Rolling Time on the Physical Properties of Granules*, Hung. J. Ind. Chem., 15, 133-140.

RUMPF H., (1997) *Particle Adhesion, Some Fundamental Aspects of the Selective Agglomeration of Fine Coal*, Agglomeration 77 (K.V.S. Sastry ed.), AIME, New York 1977 pp. 97-129.

SASTRY K.V.S., FUERSTENAU D.W., (1973) *Mechanisms of Agglomerate Growth in Green Pelletization.*, Powder Tech., 7, 97-105.

Heim A., Obraniak A., Gluba T., *Zmiany właściwości złoża granulowanego w granulatorze talerzowym,* Physicochemical Problems of Mineral Processing, 44 (2010), 53-62, (w jęz. ang), http://www.minproc.pwr.wroc.pl/journal

Granulacja talerzowa to uniwersalna metoda aglomeracji pozwalająca prowadzić proces w sposób okresowy lub ciągły oraz sterować poprzez dobór parametrów procesowych rozmiarem i właściwościami uzyskanego produktu.

Celem pracy było zbadanie wpływu parametrach aparaturowo-procesowych (średnicy talerza, stopnia jego wypełnienia oraz kąta pochylenia) na zmiany wartości średniego rozmiaru granul, gęstości nasypowej granulatu, oraz kąta tarcia złoża podczas procesu granulacji talerzowej. Proces prowadzono w sposób okresowy dla następujących zakresów zmian parametrów:

- kąt pochylenia osi talerza w stosunku do poziomu α=45-53% co 2 stopnie
- stopień wypełnienia aparatu materiałem k=3-7% co 1%
- średnica talerza granulatora D=0.5, 0.7, 1m

Do badań jako materiał modelowy użyto drobnoziarnistego bentonitu odlewniczego o składzie granulometrycznym z zakresu 0-0.16mm. Badania granulacji przeprowadzono przy stałym natężeniu dopływu cieczy zwilżającej (woda) Q=0.7 g/s i ustalonej końcowej wilgotności granulowanego wsadu w=0.29. Uzyskane podczas trwania eksperymentów wartości badanych parametrów uzależniono od zmian wilgotności granulowanego złoża ziarnistego oraz czasu granulacji. Dokonano porównania szybkości zmian rozmiaru średniego oraz gęstości nasypowej dla szeregu granulatorów talerzowych różniących się średnicą talerza i kątem jego pochylenia, przy zmiennym stopniu wypełnienia surowcem.

słowa kluczowe: aglomeracja, gęstość, współczynnik poślizgu, energia, granulacja

Physicochem. Probl. Miner. Process. 44(2010) 63-78

journal homepage
www.minproc.pwr.wroc.pl/journal/

Physicochemical Problems of Mineral Processing

Index No. 32213X ISSN 1643-1049

S. S. Ibrahim*, A. A. El-Midany**, T. R. Boulos*

ECONOMIC PREFERENCES OF MECHANICAL ACTIVATION OVER MINERAL BENEFICIATION FOR PHOSPHATE ROCK DIRECT APPLICATIONS

Received February 5, 2009; reviewed; accepted May 13, 2009

The direct application of phosphate rock seems to offer a better alternative in terms of low cost, least energy-intensive and sophistication of processing of the phosphate ore to produce soluble fertilizers. On the other hand, lower sensitivity to the ore quality offers a big advantage and the presence of impurities, which may play a positive significant role in the process in addition to the technique flexibility in utilizing of some useful elements needed for plant growth. All these factors can be expressed in terms of the economic advantage of the mechanical activation technique. In this study, Red Sea phosphate ore was subjected to the mechanical activation treatment with and without the beneficiation. Various products before and after activation were compared in terms of solubility and the process economy. The results showed that the mechanical activation is economically preferable.

key words: mechanical activation, crystal lattice imperfection, phosphate fertilizer, surface reactivity

INTRODUCTION

Mineral fertilizers account for approximately 80% of phosphate use in the world, shared with detergents (12%), animal feeds (6%) and specialty applications (3%), e.g.

* Central Metallurgical R&D Institute, (CMRDI), P.O. Box 87, Helwan, Egypt

** Mining, Petroleum, and Metallurgical Engineering Dept, Faculty of Engineering, Cairo University, Egypt

food additives, metal treatment etc. More than 99% of all phosphate fertilizers are derived from phosphate rock, a relatively small quantity being supplied in the form of basic slag, a by-product of the steel industry (Maene, 1999).

World phosphate rock production capacity in 2006 is estimated at about 168 Mt. North America remains the world leader with 50 Mt, or nearly 33% of the world total. Africa accounts for 40 Mt, or about 25% of the total. With 26 Mt of capacity, Socialist Asia is the third largest producing area with about 17% of the world total capacity. Led by expansions in Morocco and China, world phosphate rock production is forecast to increase. Construction is under way on new mine capacity also in Canada and Australia (Maene, 1999). Table 1 shows the world fertilizer consumption by region and Figure 1 shows the world fertilizer consumption by type. About 2% of the rock is applied directly, without processing, most of the remainder being solubilized with mineral acids. Two thirds of the phosphate fertilizers are derived from rock treated with phosphoric acid; during the past 30 years, a large proportion of the net addition to phosphate fertilizer production has been in the form of phosphoric acid based products. About 90% of the world phosphoric acid output is used for fertilizer production (Fig. 1.).

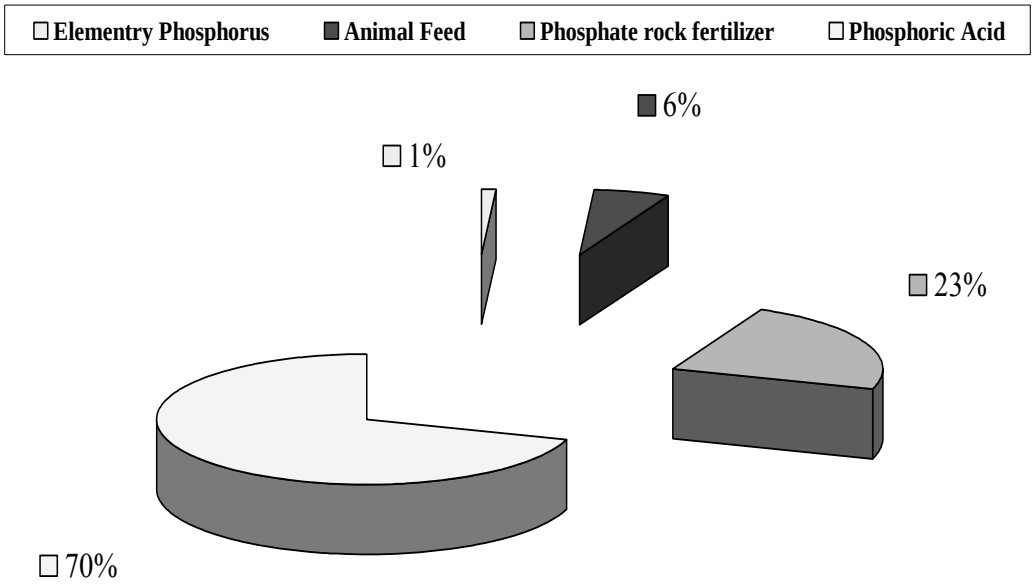

Fig. 1. Phosphate rock products

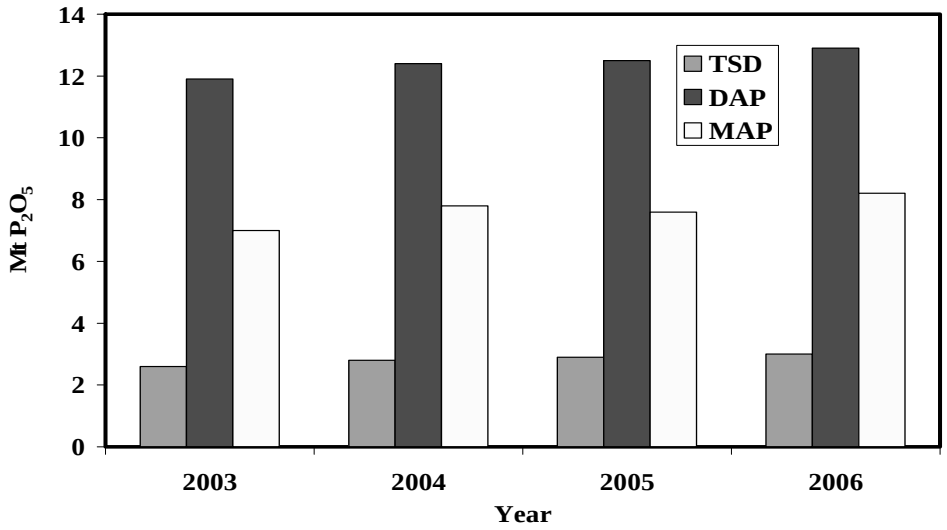

Fig. 2. World phosphate fertilizer production (IFA, 2006). DAP = diammonimum phosphate, MAP = monoammonium phosphate, TSP = triple super phosphate

Phosphoric acid is produced by either a dry or a wet process. In the dry process, phosphate rock is treated in an electric furnace to produce a very pure and more expensive phosphoric acid (frequently called white or furnace acid). In the wet process, the phosphate rock was treated with acid producing phosphoric acid (also called green or black acid) and gypsum, which is removed as a by-product (Maene, 1999).

Table 1. World phosphoric acid production

Country	Production, Mt	
	2003	2006
USA	11	11.5
China	4	4.5
Morocco	2.5	5
Russia	2.5	1.5
Tunisia	2	3
Others	8.9	9
Total	30.9	34.5

World processed phosphate trade has increased substantially. Total exports of phosphoric acid, ammonium phosphate and triple superphosphate increased from an average of 8 Mt P2O5 between 1984 and 1986 to 15 Mt P2O5 in 1998, despite a fall in total phosphate consumption during this period. Today, ammonium phosphate accounts for approximately 60% of the world processed phosphate trade and in 1998, the USA accounted for 60% of

world exports of ammonium phosphate, mostly as DAP. Asia is the biggest importing region, for ammonium phosphate, followed by West Europe and Latin America (Isherwood, 2000).

Table 2. World phosphoric acid, supply/demand, 2004 to 2007 (Alley and Spargo, 2007)

Item	Phosphoric acid (million tons P_2O_5)			
	2004	2005	2006	2007
Supply	28.5	29.1	30.4	30.4
Demand	27	27	29.1	30.2

These balances do not take into account the permanent closures in Western Europe and the USA and the temporary closures, which could be reactivated when market conditions permit. In addition, they do not take into account capacity that was under-utilized in 1995, for example in Russia. They explain the oversupply and pressure on prices, which developed especially in 1999 (Isherwood).

Because various phosphate (P) fertilizers differ widely in their solubility, it is commonly observed that crop response to P fertilizers varies under the same soil and crop conditions (Alley and Spargo, 2007; Chien et al., 1990). Furthermore, a major problem encountered in the methods for determination of the relative effectiveness (RE) of water-insoluble P fertilizer (e.g., phosphate rock) with respect to water-soluble P fertilizers, e.g., single superphosphate (SSP) and triple superphosphate (TSP), is that their growth response curves are usually nonlinear and often do not share a common maximum yield. In this paper, we review and discuss the advantages and disadvantages of the three most commonly used methods for calculating the RE of phosphate rock with respect to TSP (or SSP). The three methods are vertical comparison, horizontal (substitution rate) comparison, and linear-response comparison (Chien et al., 1990).

SUBSTITUTION RATES AS MEASURES OF THE RELATIVE EFFECTIVENESS OF ALTERNATIVE PHOSPHORUS FERTILIZERS

A procedure for representing the effectiveness of fertilizers relative to a standard fertilizer by the estimation of substitution rates is demonstrated with yield data from a fertilizer experiment with triple superphosphate and a partially acidulated rock phosphate. The substitution rate is estimated by an iterative regression procedure and the accuracy of the estimate indicated by a 5% confidence interval. The use of substitution rates to evaluate fertilizers depends on the assumption that the standard and alternative fertilizers differ in their effects on crop growth only because of differences in content of available

nutrient. This assumption is tested as a statistical hypothesis. Substitution rates calculated from experimental data with rates of application of the fertilizers represented in terms of chemical analysis of the fertilizers indicate the usefulness of the analyses as measures of the available nutrient content of the fertilizers (Colwell and Goedert, 1988).

A greenhouse study was conducted to determine if soil pH affects the requirement for water-soluble P and the tolerance of water-insoluble impurities in TSP fertilizers. Two commercial TSP fertilizers were selected to represent a range in phosphate rock sources and impurities. Phosphate fertilizer impurities were isolated as the water-washed fraction by washing whole fertilizers with deionized water. TSP fertilizers with various quantities of water-soluble P (1.2 to 99% water-soluble P) were simulated by mixing the water-washed fertilizer fractions or dicalcium phosphate (DCP) with reagent-grade monocalcium phosphate (MCP). The fertilizers were applied to supply 40 mg AOAC available P kg^{-1} to a Mountview silt loam (fine-silty, siliceous, thermic *Typic Paleudults*). Wheat (*Triticum aestivum* (*L.*)) was harvested at 49 and 84 days after planting. Soil pH values at the final forage harvest were 5.4±0.16 and 6.4±0.15. At a soil pH of 5.4, the TSP fertilizers required only 37% water-soluble P to reach maximum yields while at pH 6.4 the fertilizers required 63% water-soluble P. Results of this study show that higher levels of water -insoluble P can be tolerated in TSP fertilizers when applied to acidic soils. Phosphorus uptake was not affected by soil pH, but for the mixtures containing the fertilizer residues the source having the lowest level of Fe and Al had a higher relative agronomic effectiveness (Mullins and Sikora, 1994).

Table 3. Water-soluble & available phosphate % in common fertilizer sources

P_2O_5 Source		P_2O_5		
	N	Total	Available	Water Soluble*
	%			
Superphosphate (OSP)	0	21	20	85
Conc. superphosphate (CSP)	0	45	45	85
Monoammonium phosphate (MAP)	11	49	48	82
Diammonium phosphate (DAP)	18	47	46	90
Ammonium polyphosphate (APP)	10	34	34	100
Rock phosphate	0	34	3-8	0

*Water-soluble data are a percent of the total P_2O_5

Source: Ohio Agronomy Guide. Ohio Cooperative Extension Service Bull.472.

Elemental impurities in mono-ammonium phosphate (MAP) fertilizers, such as Fe, Al, Ca, Mg, and F, result in compounds other than $NH_4H_2PO_4$. The phosphorus availability of the impurity compounds was determined in 3 commercial MAP fertilizers produced from North Carolina, Florida, and Idaho phosphate rocks. Soluble compounds,

including $NH_4H_2PO_4$, were washed out of the fertilizers, and the water-insoluble fraction was collected. The North Carolina, Florida, and Idaho MAP fertilizers contained 13, 16, and 17% water-insoluble fractions, respectively. Availability of phosphorus in each MAP fertilizer and water-insoluble fraction was determined in a greenhouse pot study using sorghum-sudangrass (Sorghum bicolor) as the test crop. There were no differences in dry matter weights or phosphorus uptake between reagent grade MAP and each MAP fertilizer. Lower dry matter weights and phosphorus uptake were produced from the water-insoluble North Carolina, Florida, and Idaho fractions (NC greater than FL greater than ID). Chemical analysis and characterization with optical microscopy, infrared spectroscopy, and X-ray diffractometry indicated 77.3, 73.8, and 73.6% $NH_4H_2PO_4$ in the North Carolina, Florida, and Idaho MAP fertilizers, respectively. $MgAl(NH_4)_2H(PO_4)_2F_2$, $AlNH_4HPO_4F_2$, and $FeNH_4(HPO_4)_2$ were identified as water-insoluble phosphorus compounds. There was a significant negative correlation between the percent phosphorus present as $MgAl(NH_4)_2H(PO_4)_2F_2$ and the phosphorus (Sikora et al., 1989).

Based on historical trends of gross energy requirements, it was calculated that in 2001, that global energy embedded in fertilizer consumption amounted to 3660 PJ, which represents about 1% of the global energy demand. Total energy demand has increased at an average rate of 3.8% p.a. Drivers behind the trend are rising fertilizer consumption and a shift towards more energy intensive fertilizers. Our results show that despite significant energy efficiency improvements in fertilizer manufacture (with exception of phosphate fertilizer in the last 20 years), improvements in energy efficiency have not been sufficient to offset growing energy demand due to rising fertilizer consumption. Furthermore, it was found that specific energy consumption of ammonia and urea developed in close concordance with the learning curve model, showing progress ratios of 71% for ammonia production and 88% for urea. This suggests an alternative approach for including technological change in energy intensive industries in middle and long-term models dealing with energy consumption and CO_2 emissions, while few learning curves exist for energy efficiency of end use technologies (Ramírez and Worrell, 2005).

There have been several plant closures in Western Europe, where phosphoric acid production capacity and output have fallen by 60% since 1980, for economic and environmental reasons. The latest announced closure is that of the Norsk Hydro phosphoric acid plant at Vlaardingen in the Netherlands, due largely to problems related to the treatment of by-product phosphogypsum (Maene, 1999). The "reserves" of phosphate rock, i.e. deposits that are or could be profitably mined under prevailing costs, market prices and technology, are rather limited. However, the "resources" which are at present not economically exploitable, but which could potentially become so, are very large (Table 4).

Table 4. Phosphate rock reserve base in terms of cost (billion tones) (Maene, 1999)

Cost ($/tones)	Below $40	Below $100
North America	1.4	4.7
North and West Africa	7.2	22.1
Middle East	0.1	1.9

However, the trends move again towards using raw phosphate rock to reduce the cost. From one side this is due to the high expenses of the production of the fertilizers either by dry or wet processes. From the other side, it was found that the highly soluble fertilizers which have expensive manufacturing costs lead to the lack of micronutrients. The problem was found to be iron, zinc and manganese being tied up by phosphate.

In Zimbabwe, using phosphate rock appears to halve the cost of imported fertilizers. The main disadvantage of using the phosphate rock is its low solubility and consequently the low availability of the P for the plant growing. Therefore, the mixing of the rock phosphate with highly soluble fertilizers shows that the savings are impressive. In Kenya, a mixture of 90 percent local phosphate rock is blended with just 10 percent imported fertilizer (Morris, 1988).

Grinding of ordinary phosphorite powder of Central Kyzylkum with urea nitrate and ammonium carbonate salt to the particles size less than 0.16 mm leads to significant increase in content of P_2O_5 in the form consumable by plants (Seitnazarov et al., 2007).

Thermochemical synthesis offers possibility of getting effective compound fertilizers from low-grade poorly enrichable mineral raw materials. Agricultural field tests demonstrated that the compound fertilizers developed are much more effective than equivalent doses of the starting components equalized in terms of nitrogen and potassium. Consequently, apatite-based compound fertilizers can be used to radically improve soil fertility phosphoritization with simultaneous improvement of the nitrogen-potassium regime (Latkin and Samatova, 1998).

PHOSPHATE ROCK FOR DIRECT APPLICATION

It is clear from the abovementioned that if the solubility problem of the rock phosphate can be solved then the rock phosphate will be ready to be used for direct applications as a fertilizer. On the way to solve this problem and increase the rock phosphate solubility, highly intensive size reduction equipment like vibrating, centrifugal, jet and other types of mills were employed in the tribo-mechanical treatment of phosphate rocks (Heinike et al., 1977; Kolosov et al., 1979; Paudert et al., 1978; Kozlov and Kozyrev, 1982; Gock et al., 1986). However, many disadvantages in the comminution

process were recorded (Gock et al., 1986; Kurrer and Gock, 1986).Perhaps, that is why such grinding machines did not achieve economical advancement in the domain of phosphate activation under the mechanical forces (Gock et al., 1986).

To overcome the disadvantages of the tribo-mechanical treatment, the development of the principle of rotary-chamber vibrating mill is based upon the introduction of such freely moving chamber wheel in the milling tube. Caking of the ground product in such a mill is avoided by the paddle mixer. Beyond the surface expansion which occurs through the vibrating tube mill, the high collision energy conveyed by this method induces lattice defects through disintegration. These lattice defects, which deviate from the initial lattice structure, lead to a growth of free enthalpy (Kurrer and Gock, 1986). The decreasing activation energy related to this exerts a decisive influence on the reaction kinetics of rock dissolution (Kurrer and Gock, 1986).

Various investigations have already been done on the possibility of influences on the leaching–velocity of phosphorites, especially in connection to the aforesaid improvement of starting-effect by their direct application as fertilizer (Paudert et al., 1978). It has been thereby ascertained, that phosphorites of sedimentary origin are in comparison to the apatites of magmatic origin, fundamentally better suitable for a mechanical activation, because they show a high grade lattice distortion due to the partial substitution of the phosphate ions by carbonate ions in the initial ore. An economic processing of the Kola-apatites through mechanical activation has so far been considered impossible, because of the high expenditure of the necessary energy by applying vibration mill. The same method applied for the sedimentary phosphorites of Morocco, is, compared to the other commercial fertilizers like superphosphate as well as double-superphosphate, supposed to be more economical.

The technology of tribo-mechanical activation of phosphate rocks for direct application purposes may open the way, when thoroughly understood, for utilization of indigenous ores in so many developing countries and serve captive regional markets when arbitrary grade specifications do not apply.

MECHANICAL ACTIVATION OF PHOSPHATE AS A SOLUTION FOR THE DIRECT APPLICATION OF THE EGYPTIAN RED SEA PHOSPHATE, CASE STUDY

The mineralogical investigation of the worldwide phosphate deposits has shown that the general fluorapatite composition applies more closely to igneous and high grade metamorphic deposit types than to sedimentary phosphates (McClell and Gremillian,

1976). The composition, high crystallinity and low reactivity of such igneous apatites of Kola, former USSR and Phalaborwa, South Africa make them virtually useless for direct application (McClellan and Gremillian, 1976).

Sedimentary phosphate rocks contain apatitic phosphates of more complex chemical composition following, in general, the francolitic-type formula suggested by Lehr and McClellan (1973). The carbonate apatite in most sedimentary phosphate rocks is submicrocrystalline and occurs in several varieties of complex aggregates (McClellan and Gremillian, 1976).

Red sea phosphate grains are amorphous and cryptocrystalline cellophane. The ore is characterized by rounded, elongated and irregular grains of different sizes (50 to 200 μm). Biodetrital phosphate in the form of bone fragment, vertebrae and teeth are also identified in Red Sea phosphate cemented with calcareous siliceous matrices. The calcareous cement, most probable dolomite, is observed partially replacing the bone fragments and cellophane especially along the borders in the Red Sea sample.

Red sea phosphate was taken as an example on the possibility of the application of the mechanical activation to prepare the rock phosphate for direct application. Tables 5 and 6 depict the chemical analyses of both the raw and treated samples as well as their size distribution before activation. All the mechanical treatment tests were carried out using the pilot scale, circulating oil lubricated, three tube rotary chamber, type "Palla U 35", Humboldt Wedage AG vibrating mill of "Institut fur Aufbereitung, Technische Universitat", Berlin, Germany (Fig. 3.).

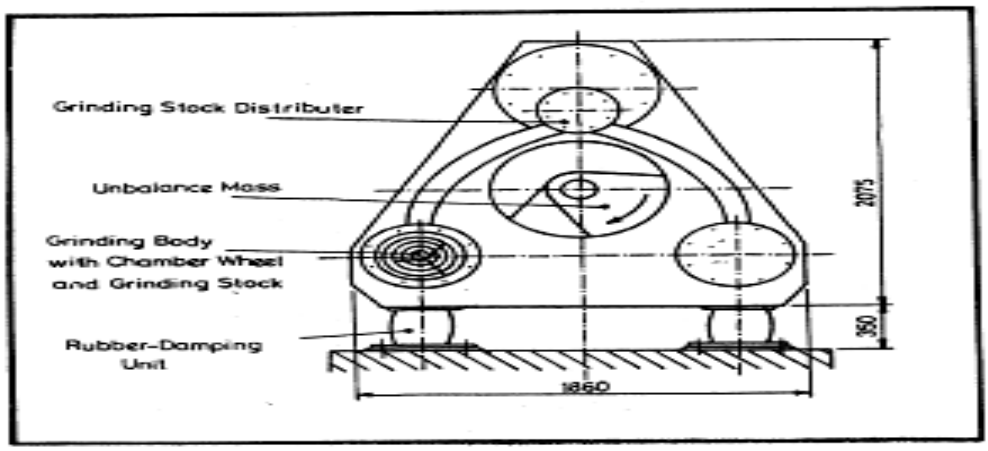

Fig. 3. Rotary-chamber vibrating mill

Mechanical activation of phosphate in highly intensive size reduction equipment, such as modified vibrating mill should result on an increase in degree of dispersion of the

milled product (Gock and Jacob, 1984). Figure 4 illustrates the size distribution of the ground end products (after 90 min). Gradual increase in the $\%D_{90}$ values with increasing milling time for raw and concentrate samples is indicating the limited advantage of increasing time.

Table 5. Chemical analysis of red sea phosphate samples

Constituents, %	Raw	Concentrate
P_2O_5	23.48	28.40
CaO	38.05	43.45
Fe_2O_3	1.61	1.12
Al_2O_3	2.38	1.05
MgO	2.64	1.72
SiO_2	10.14	5.61
CO_2	6.35	5.58
Humidity	3.83	3.88

Table 6. Size Analysis of Primarily Crushed Samples, (Mill Feed)

Size, mm	Wt.%, Raw	Wt.%, Concentrate
>2.00	8.09	12.42
-2.0+0.80	19.36	16.16
-0.80+0.50	8.96	10.34
-0.50+0.315	12.72	13.91
-0.315+0.20	8.96	10.78
-0.20+0.15	9.83	8.91
-0.15+0.10	8.67	7.15
-0.10+0.063	17.34	11.65
<0.063	6.07	8.69

Evidently, symptoms of agglomeration were recorded after 60 min. The progressive structural changes in the apatite lattice with time are proving that dispersion is not necessarily the main process affecting rock reactivity during mechanical activation.

The absolute solubility index (ASI) of Red Sea phosphate raw and beneficiated sample in 2 % citric acid, CA and neutral ammonium citrate (NAC) were measured, Figs 5 and 6.

A substantial increase in the dissolution rates of the activated products was recorded, indicating the efficiency of the mechanical activation process. Gradual improvement in the ASI values of the milled products with increasing milling time signifies the advantage of the grinding over longer time.

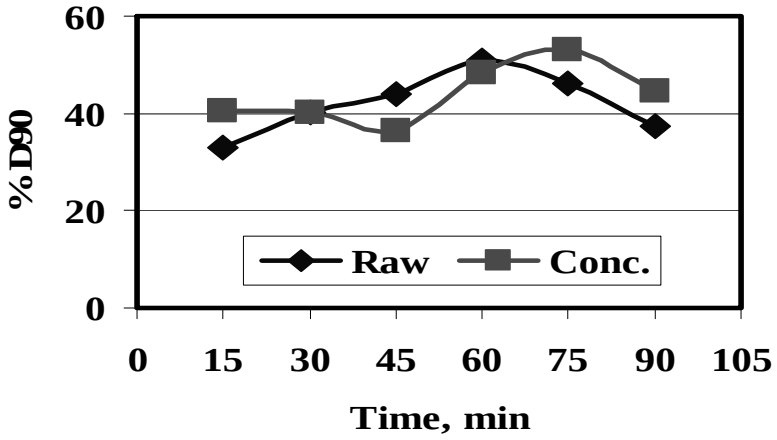

Fig. 4. Effect of milling time on % D_{90} of the ground products

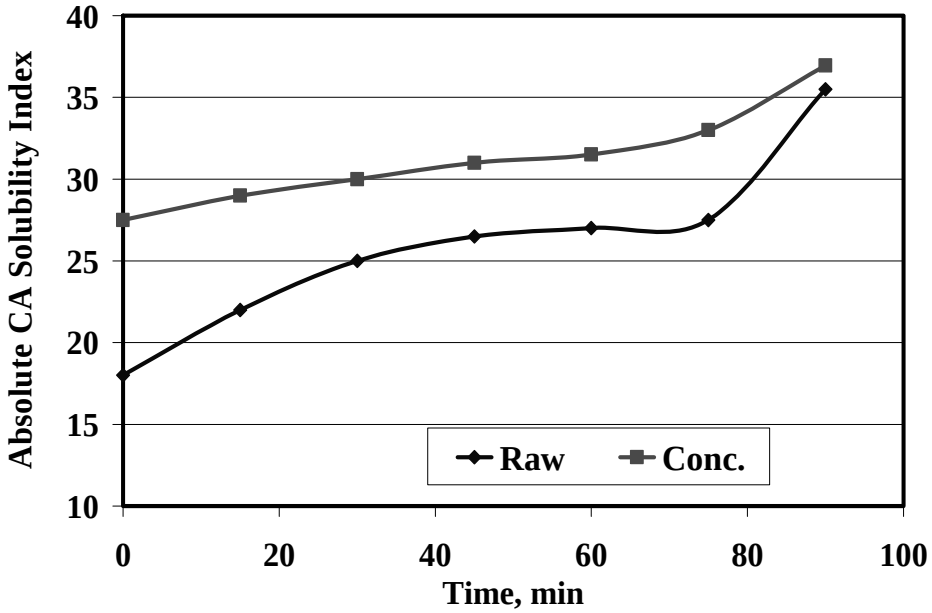

Fig. 5. Solubility index of phosphate samples in 2% citric acid at different milling times

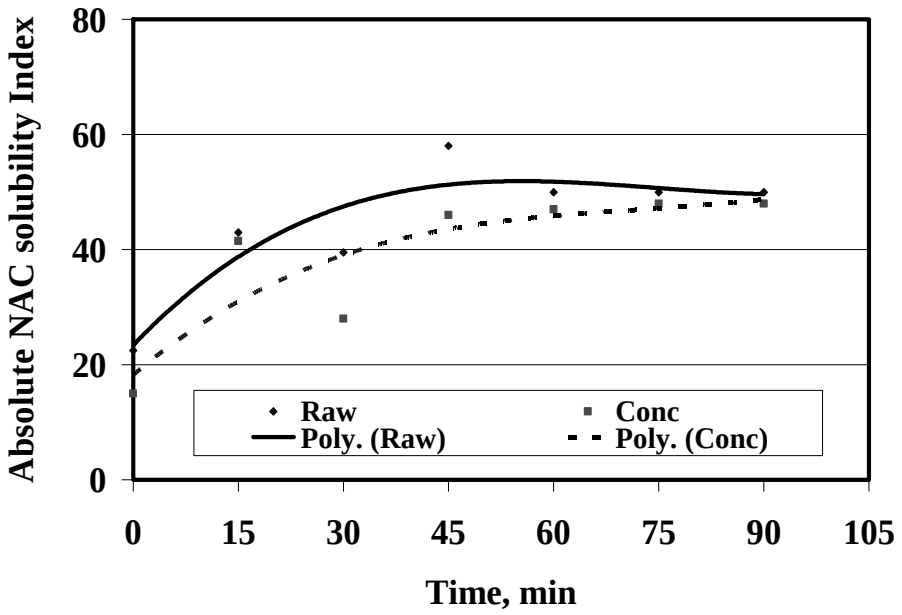

Fig. 6. Solubility index of phosphate samples in neutral ammonium citrate at different milling times

MECHANICAL ACTIVATION- ENERGY MEASUREMENTS

Table 7. The Solubility Tests of Different Phosphorites with the Mechanical Activation (kWh/t.) by using 2% Citric Acid

Phosphorite Types kWh/t	P_2O_5-content	0 kWh/t	25 kWh/t	50 kWh/t	100
Hyperphos (commercial prod.)	31.7%	33.5%	36.1%	45.3%	49.6%
Saphos (commercial Red Sea prod.)	28.6%	30.4%	34.6%	40.2%	43.8%
Abu Tartur (conc.)	30.0%	25.9%	33.5%	44.2%	49.4%
Sebayia (crude ore)	21.5%	29.2%	33.7%	37.1%	40.7%
Arad (conc.)	32.0%	34.9%	39.1%	40.9%	43.7%
Morocco (conc.)	31.0%	29.0%	33.2%	34.2%	35.7%
Togo (conc.)	34.2%	18.2%	23.6%	25.6%	28.9%

The solubility behavior of raw, either unactivated or activated samples in the alkaline medium was altered (Fig. 6.). Treated raw sample showed increase in the leaching efficiency in all the milling experiments.

The optimum solubility was found to be at milling time of 45 mins in NAC, Figure 7. This trend is identical with that of the change in $\%D_{90}$ of the phosphate samples by increasing in activation time which indicates the effect of the sample size on its solubility in NAC.

EFFECT OF PH ON MECHANICAL ACTIVATION

The influence of the mechanical activation was correlated to the pH-values (Gock and Jacob, 1984). It was shown that within a pH-range between 5 and 7, which is of great importance for the Egyptian cultivated lands, a good initial leaching velocity can be achieved, which, however, increases strongly with the progressive mechanical activation (Gock and Jacob, 1984). In addition to the leaching velocity, the phosphorous-equilibrium-concentration is also important for the fertilizing effect. Hence, further investigations are necessary to establish the existence of a relationship between the mechanically activated phosphorite and the phosphorous- equilibrium of the refined phosphate fertilizer (Gock, Jacob, 1984). A large proportion of potentially arable land in the tropics is strongly acidic and tends to be extremely deficient in phosphorus, a case which could be typical for natural phosphate application

IMPURITIES EFFECT

Most of the phosphate ores contain impurities, which may affect the mechanical activation process either positively or negatively. The prevailing impurity, in most of the phosphate ores, is silica. In case of adding the raw phosphate as a fertilizer, the silica impurities does not harm the soil because of it represents one of the soil components.

In regard to mechanical activation process, the effect of tribomechanical activation of Red Sea phosphor-concentrate, after such a change in its chemical and mineralogical characteristics, should be interesting, where it showed lower tendency to the mechanical activation compared to the raw ore. Such behavior may be ascribed to its exo-gangue minerals contents, mainly silica and silicates. They seem to play an important role in the process. The same conclusion was reached by Malchikov et al. (1983) who got better activation results by adding silica to some phosphate ores (Malchikov et al., 1977).

ECONOMIC PREFERENCE OF MECHANICAL ACTIVATION

The comparison was carried out between the costs of mechanical activation of the phosphate ore with the running of different beneficiation steps to produce a concentrate suitable for the production of the phosphoric acid, which is an intermediate step of all the fertilizer manufacturing process. This comparison shows that the activation will lead to substantial savings. Initially, the saving is due to the reduction in the capital and operating costs of the beneficiation steps. Moreover, the same thing will happen to the wet process that cost much more than beneficiation processes due to dealing with acids (i.e., one ton of sulfuric acid costs about 700 $) and the corrosion problems, which increase the maintenance costs too.

Table 8. Costs of mechanically activated raw- and the processed phosphate fertilizers

Costs/ton	Processed phosphate fertilizer	Raw-phosphate fertilizer
Mining	70-80 $	70-80 $
Processing	50-60 $ Min. P_2O_5= 32%	------
H_2SO_4	700 $	-----
Energy	35$ (350 kWh/t)	2.50 $ (25kWh/t) 8.0 $ (80 kWh/t)
Market price/ton	1000-1200 $	400 $

- calculations based on 10 cents/ kWh

The 2006 price of residential electricity in the United States is 10 cents per kWh. In Egypt, under the new system, the price of electricity will also be from 5 to 7 cents per kWh for medium power consumers (Mixed Reactions to New Energy Pricing Strategy, Reem, 2007).

CONCLUSIONS

The paper revisited the phosphate fertilizers industry in terms of world consumptions and their energy constraints. It is noted that the raw phosphate rock is coming into the picture to be used as an alternative to the current phosphate fertilizers due to costs and energy limitations.

One of the reasons behind the rare use of the phosphate as direct application fertilizer is its solubility. To overcome this limitation, the mechanical activation was tried and has achieved a marked increase in the reactivity of the treated phosphate samples. The chemical reactivity of activated raw samples in 2% citric acid and neutral ammonium citrate showed improved leaching characteristics for all the milling times tested.

The comparison of the production costs of the current fertilizers at different stage from mining until marketplace with the phosphate rock shows the preference of the mechanical activation in terms of energy and economics.

Therefore, the technology of tribomechanical activation of phosphate rock for direct application may open the way for utilization of indigenous ores in many developing countries and serve capital regional markets when arbitrary grade specifications do not apply.

The simple technology of mechanical activation, for production of the fertilizer from domestic Egyptian phosphorites, will meet the local needs of the developing-country like Egypt, and would give the security to be independent of the international chemical concerns.

REFERENCES

ALLEY M., *John Spargo Fertilizers in 2007*, Crop and Soil Environmental News, February, 2007.

CHIEN S. H., SALE P. W. G., FRIESEN D. K., *A discussion of the methods for comparing the relative effectiveness of phosphate fertilizers varying in solubility Nutrient Cycling in Agro-eco systems*, Volume 24, Number 3, pp149-157, September, 1990

COLWELL J. D., GOEDERT W. J., *Substitution rates as measures of the relative effectiveness of alternative phosphorus fertilizers*, Nutrient Cycling in Agroecosystems, Volume 15, Number 2 / February, pp 163-172, 1988.

GOCK, E., JACOB, K.H. *Conceptions for processing the pyrite-bearing phosphorites of Abu-Tartur*, Berliner Geowissen Abh. (A) 50, 381-397, Berlin, 1984.

GOCK, E., KURRER, K, MICHEALIS, S., *Vibrating milling: progress in theory and industrial application*, 1st World Congress Fine Particle Technology, Part II, p. 653-666, 1986.

HEINIKE, G., PAUDERT, R, HARENX, H, STEINIKE, U, POETHIN, R, *Tribomechanical transfer of apatite to a soluble form*, Zhurnal Prikladnoi khimii, Vol.50, No.5, pp 969-974, 1977.

ISHERWOOD K. F., *The State of the Fertilizer Industry Past, Present and Future*, Annual General Meeting, 68th IFA Annual Conference, Oslo, Norway, 22-25 May 2000

KOLOSOV, A.S., BOLDYREV, V.V., CHAIKINA, M.V., TRANZOVA, M.I., GORDEEWA, G.I., PAUDERT ,R.,HARENZ, "The Reactivity of Native Apatites Under Mechanical Activation", Proc. of the scientific academy of U.S.S.R. phy. Chemistry sec, 6, pp.148-55,(1979).

KOZLOV, V.I., KOZYREV, S.A., *Selection of apparatus in studies of mechanical activation of phosphate raw materials*, Proc. of the scientific academy of U.S.S.R. phy. chemistry sec, 6, pp.71-4,(1982).

KURRER, K, GOCK, E., *Effect of the operating conditions on motion and impact processes in viberatory tube mill*, Journal of preparation and processing, 10, 546-554, 27, 1986.

LATKIN A. S., SAMATOVA L. A., *Thermo-chemical methods of treatment of low-grade phosphatic raw materials*, Journal of Mining Science, Volume 34, Number 1 / January, 1998.

LEHR, J.R., MCCLELLAN, G.H., *A revised Labotatory reactivity scale for evaluating phosphate rocks for direct applications*, TVA Bull. Y-34, 36 p, NFDC, Muscle Shoals, Alabama, 1973.

MAENE L.M., *Phosphate Fertilizer Production, Consumption and Trade, The Present Situation and Outlook to 2010*, The Sulphur Institute's 17th Sulphur Phosphate Symposium, January 17-19, 1999, Boca Raton, Florida.

MALCHIKOV G.D., TERENTYENA, T.P., RUBAILO, , I.S., *Decomposition of mechanically activated phosphate by nitrogen dioxide*, Proc. of Scientific Academy of USSR (Phy. Chemistry Sec.) 233 (5), 892-5, 1977.

MCCLELLAN, G.H., GREMILLIAN, L.R., *Evalution of phosphatic raw materials,* Proceddings of a Symposium on the role of phosphorus in agriculture, NFDC, Muscle Shoals, Alabama, June 1976.

MORRIS L. *Economics of Fertilizer Application*, CYMMT Economics Working papers. 1988.

MULLINS G. L., SIKORA F. J., *Effect of soil pH on the requirement for water-soluble phosphorus in triple superphosphate fertilizers*, Nutrient Cycling in Agroecosystems, Volume 40, Number 3 / October, pp 207-214, 1994

PAUDERT ,R., HARENZ, H., POTHING, R, HEINIKE, G., KDT, DUNKEL, L., SCHUMANN, H., KDT, *Phosphate fertilizers through Tribomechanical Activation of apatitic phosphate*, chem. Techn.,30, jg., nr.9,470-475,(1978)

RAMÍREZ C. A., WORRELL E., *Feeding fossil fuels to the soil An analysis of energy embedded and technological learning in the fertilizer industry*, June 2005.

REEM NAFIE**,** *Mixed Reactions To New Energy Pricing Strategy*, August 22, 2007.

SEITNAZAROV A. R., MUSAEVA S. A., NAMAZOV SH. S., BEGLOV B. M., *Mechanochemical activation of ordinary phosphorite powder of Central Kyzylkum mixed with urea nitrate and ammobium carbonate salts,* Russian Journal of Applied Chemistry, Volume 80, Number 11 / November, 2007

SIKORA FJ, DILLARD EF, COPELAND JP, MULLINS GL *Chemical characterization and bioavailability of phosphorus in water-insoluble fractions of three mono-ammonium phosphate fertilizers***.,** J Assoc Off Anal Chem. 1989 Sep-Oct;72(5):852-6.

Ibrahim S.S, El-Midany A.A, Boulos T.R, *Ekonomiczne preferencje mechanicznej aktywacji dla pozyskania minerałów przy bezpośrednim stosowaniu rudy fosforanowej jako nawozu mineralnego*, Physicochemical Problems of Mineral Processing, 44 (2010), 63-78, (w jęz. ang), http://www.minproc.pwr.wroc.pl/journal

Bezpośrednie zastosowanie rudy fosforanowej wydaje się być lepszą alternatywą pod względem niższych kosztów, mniejszego zużycia energii niż skomplikowany proces produkcji nawozu mineralnego z rudy fosforanowej. Dodatkowo, mniejsze wymagania dotyczące jakości rudy przynoszą dodatkową korzyść dla samego procesu oraz wprowadzają zanieczyszczenia, które odgrywają pozytywna rolę w procesie, dostarczając użytecznych składników koniecznych dla wzrostu roślin. Wszystkie te cechy można przełożyć na korzyści ekonomiczne wynikające z procesu mechanicznej aktywacji. W relacjonowanych badaniach, ruda fosforanowa z morza Czerwonego była przedmiotem działania mechanicznej aktywacji z korzyścią lub przy jej braku. Szeroka gama produktów zarówno przed jak i po procesie aktywacji była testowana pod katem rozpuszczalności oraz rachunku ekonomicznego. Otrzymane wyniki wskazują, że aktywacja mechaniczna jest procesem ekonomicznie uzasadnionym.

słowa kluczowe: mechaniczna aktywacja, nawozy fosforowe, reaktywność powierzchniowa

Physicochem. Probl. Miner. Process. 44(2010) 79-92

journal homepage
www.minproc.pwr.wroc.pl/journal/

Physicochemical Problems of Mineral Processing

Index No. 32213X ISSN 1643-1049

S. S. Ibrahim*, A. A. El-Midany**, T. R. Boulos*

EFFECT OF INTENSIVE MECHANICAL STRESSES ON PHOSPHATE CHEMISTRY AS A WAY TO INCREASE ITS SOLUBILITY FOR FERTILIZER APPLICATION

Received December 20, 2008; reviewed; accepted March 15, 2009

Mechanical activation technique represents a unique process in which the mineral surface reactivity can be increased in addition to having new products. Phosphate is a one of the plant nutrients that can be produced from phosphate rock. However, direct usage of the phosphate rock has several limitations. In this study, the mechanical activation was used to modify the phosphate structure to be suitable for direct use as a natural fertilizer. It seems a better alternative for the highly sophisticated technology used worldwide to produce completely water-soluble fertilizers.

key words: mechanical activation, crystal lattice imperfection, phosphate fertilizer, solubility, reactivity

INTRODUCTION

The phosphate is one of the important nutrients for the plant growth. Because various phosphate fertilizers differ widely in their solubility (Table 1), it is commonly observed that crop response to phosphate fertilizers varies under the same soil and crop conditions (Maene, 1999; Chien et al., 1990).

The direct application of the phosphate as a fertilizer is limited due to its structure which results in low solubility. The improvement of phosphate structure, through mechanical activation, changes phosphate chemistry and increases its solubility

* Central Metallurgical R&D Institute (CMRDI), Helwan, Egypt

** Mining, Petroleum, and Metallurgical Engineering Dept, Faculty of Engineering, Cairo University, Egypt

(Ibrahim et al., 2010). Substitution rates as measures of the relative effectiveness of alternative phosphorus fertilizersTable 1. illustrates the water-soluble and available phosphate % in common fertilizer sources.

Table 1. Water-soluble and available phosphate % in common fertilizer sources

P_2O_5 Source	% P_2O_5		
	Total	Available	Water Soluble*
Superphosphate (OSP)	21	20	85
Conc. superphosphate (CSP)	45	45	85
Monoammonium phosphate (MAP)	49	48	82
Diammonium phosphate (DAP)	47	46	90
Ammonium polyphosphate (APP)	34	34	100
Phosphate rock	34	3-8	0

*Water-soluble data are a percent of the total P_2O_5

However, the energy needed for fertilizer application in 2001 amounted to 3660 PJ, which represents about 1% of the global energy demand. Total energy demand has increased at an average rate of 3.8% per year. Despite significant energy efficiency improvements in fertilizer manufacture, improvements in energy efficiency have not been sufficient to offset growing energy demand due to rising fertilizer consumption (Ramírez, 2003).

Therefore, the trends have moved again towards using raw phosphate rock to reduce the cost. The high costs of the production of the fertilizers either by dry or by wet processes as well as the lack of micronutrients in highly soluble fertilizers which have high manufacturing costs are the main drawback of the current fertilizer industry. It was found that iron, zinc and manganese were tied up by phosphate.

In Zimbabwe, using phosphate rock appears to halve the cost of imported fertilizers. The main disadvantage of using the phosphate rock is its low solubility and consequently the low availability of the P for the plant growing. Therefore, the mixing of the phosphate rock with highly soluble fertilizers shows that the savings are impressive. In Kenya, a mixture of 90 percent local phosphate rock is blended with just 10 percent imported fertilizer (Morris, 1988).

Grinding of ordinary phosphorite powder of Central Kyzylkum with urea nitrate and ammonium carbonate salt to the particles size less than 0.16 mm is shown to lead to significant increase in content of P_2O_5 in the form consumable by plants (Seitnazarov et al., 2007; Latkin and Samatova, 1998).

It is clear that if the solubility problem of the phosphate rock could be solved then it would be ready to be directly used as a fertilizer. On the way to solve this problem and increase the phosphate rock solubility, highly intensive size reduction equipment like vibrating, centrifugal, jet and other types of mills were employed in the tribo-mechanical treatment of phosphate rocks (Heinike et al., 1977; Kolosov et al., 1979; Paudert et al., 1978; Kozlov and Kozyrev, 1982; Gock et al., 1986). However, many disadvantages in the comminution process were recorded (Gock et al., 1986; Kurrer

and Gock, 1986). That could be reason why such grinding machines did not show economic advantage in the field of phosphate activation under the mechanical forces (Gock et al., 1986).

To overcome the disadvantages of the tribo-mechanical treatment, the development of the principle of rotary-chamber vibrating mill is based upon the introduction of freely moving chamber wheel in the milling tube. Caking of the ground product in such a mill is avoided by the effect of a paddle mixer. Beyond the surface expansion which occurs through the vibrating tube mill, the high collision energy conveyed by this method induces lattice break up through disintegration. This lattice destruction, which changes the initial lattice structure, leads to a growth of free enthalpy (Kurrer, Gock, 1986). The decreasing activation energy related to this has a decisive influence on the reaction kinetics of rock dissolution (Kurrer and Gock, 1986).

In this paper, the mechanical activation process using rotary chamber vibrating mill was tested to increase the solubility of the phosphate ore. The mechanically activated product was identified by XRD, FTIR, thermal analysis, and solubility tests. The comparison, from economic point of view, between the current fertilizer manufacturing and this process was presented.

EXPERIMENTAL

MATERIALS

Representative Red Sea phosphate sample of primary crushed ore was used. Chemical composition as well as size distribution of the crushed sample is given in Tables 2 and 3, respectively.

Table 2. Chemical analysis of Red Sea phosphate sample

Constituents	%
P_2O_5	23.48
CaO	38.05
Fe_2O_3	1.61
Al_2O_3	2.38
MgO	2.64
SiO_2	10.14
CO_2	6.35
Humidity	3.83

Table 3. Size Analysis of Primarily Crushed Red Sea Phosphate Sample, (Mill Feed)

Size, mm	Wt.%
>2.00	8.09
-2.0+0.80	19.36
-0.80+0.50	8.96
-0.50+0.315	12.72
-0.315+0.20	8.96
-0.20+0.15	9.83
-0.15+0.10	8.67
-0.10+0.063	17.34
<0.063	6.07

METHODS

THE ROTARY-CHAMBER VIBRATING MILL

All the mechanical activation tests involved in this study were carried out using the pilot scale, circulating oil lubricated, three tube rotary chamber, type "Palla U 35", Humboldt Wedag AG vibrating mill of "Institut fur Aufbereitung, Technische Universitat", Berlin, Germany, Figure 1. The mill was operated under the following predetermined optimum conditions:

- grinding tube capacity 13.4 liter, 300mm diameter, and 190mm height,
- grinding media: 50kg of steel balls, 30mm diameter ,
- machine working conditions: 150 A., 210 V., 95-100 kW, frequency was 1500min^{-1}, and amplitude 8mm.
- the initial weight of the feed material was 1200g each, grinding time 90 min; 40 g samples were withdrawn every 15min, for size and surface area as well as for the measurements of the structural changes in the apatite lattice by X-ray diffraction and infra red spectroscopy.

The two phosphate samples were separately directed to be ground for 90 mins. The Rotary –Chamber vibrating tube mill, type Palla U35, was used for grinding tests (McClellan, Gremillian, 1976). The machinery conditions were adjusted at the predetermined optimum working parameters (McClellan and Gremillian, 1976).

PHYSICAL CHARACTERIZATION OF MILLED SAMPLES

X-RAY DIFFRACTION ANALYSIS

X-ray diffraction (XRD) was adapted to follow up the physical changes in the major constituents of the ground samples using "Philips – PW1050/25" X-ray diffractometer (Seitnazarov et al., 2007; Latkin, Samatova, 1998). The operating conditions were CuK tube, 40 kV, 20 m Amp. 4X10^2 cps, and 1°/cm/10 sec scanning speed.

The relative intensities, I/I_o, of the X-ray impulses at a lattice plane of a material to be activated, were carried out, before (I_o) and after the mechanical stress. Every I/I_o can be assigned to a definite reaction behavior, e.g. the leaching behavior of definite

prescribed reaction conditions. This can be interpreted as a compaction of information resulting from the influence such as grain-size, lattice changes as well as one-or multi-phased solid state reactions.

INFRA -RED (IR) SPECTRA ANALYSIS

Similar to XRD, infra-red spectroscopy, IR using "PYE-Unicam Philips, SP 2000" IR spectrometer, were used under working conditions shown in the respective Figures. 1-2 gm of the finely ground sample was added to 200 mg KBr as an embedding medium and blended in an agate mortar for 10 minutes. The mixture was then pressed in an evacuated die for 4-5 minutes at about 10 t/cm^2 into a transparent pellet of 13 mm diameter and 1mm thickness. The pellets were then scanned 500-2000 cm^{-1} at a total scan time of 10 minutes.

PARTICLE SIZE ANALYSIS

Particle size measurements of the ground samples were carried out using "PABISCH" type 715 laser granulometer.

DIFFERENTIAL THERMAL ANALYSIS, DTA

Differential thermal analysis, DTA of the starting and end products were conducted using "Linseis" unit.

PROCESS KINETICS

Solubility tests according to the method of Stetter (1972) were carried out (Heinike et al., 1977). Other regulations prescribed by Gericke and Kurmies (1972) for earthy phosphates (Kolosov et al., 1979) were also taken into consideration. Accordingly, 2% citric acid (CA) and neutral ammonium citrate (NAC) at $65C^o$ solutions were the leaching media for the reactivity measurements tests. The following tests conditions have been maintained:

Weight of the ore sample	:	2.5g
Decomposition agent-initial concentration	:	250 ml of 2% citric acid
Duration of reaction	:	30 min
Temperature	:	20^oC
Separation solid/liquid	:	Centrifuged 2 min at 4000 rpm
Reproducibility	:	1%

RESULTS AND DISCUSSION

MINERALOGICAL CHARACTERIZATION

The mineralogical investigation of the worldwide phosphate deposits has shown that the general fluorapatite composition applies more closely to igneous and high grade metamorphic deposit types than to sedimentary phosphates (Paudert et al., 1978). The composition, high crystallinity and low reactivity of such igneous apatites of Kola, former USSR and Phalaborwa, South Africa make them virtually useless for direct application (Paudert et al., 1978).

Sedimentary phosphate rocks contain apatitic phosphates of more complex chemical composition following, in general, the francolitic-type formula suggested by Lehr and McClellan (1973) (Kozlov and Kozyrev, 1982). The carbonate apatite in most sedimentary phosphate rocks is submicrocrystalline and occurs in several varieties of complex aggregates (Paudert et al., 1978).

Red sea phosphate grains are amorphous and cryptocrystalline cellophane. The ore in characterized by rounded, elongated and irregular grains of different sizes (50 to 200 μm). Biodetrital phosphate in the form of bone fragment, vertebrae and teeth are also identified in Red Sea phosphate cemented with calcareous siliceous matrices. The calcareous cement, most probable dolomite, is observed partially replacing the bone fragments and cellophane especially along the borders in the Red Sea sample.

PHYSICAL CHARACTERIZATION

X-RAY DIFFRACTION PATTERN

The principle of using the tribomechanical treatment is based mainly upon the application of the aggressive mechanical energy on the solid phosphates which leads to destruction in the phosphatic crystal texture (Gock et al., 1986). Such lattice imperfection or distortion could be followed by XRD technique (Kolosov et al., 1979). Measurements of the changes in the relative intensities I/Io of the x-ray impulses before (I_o) and after (I) the mechanical stress could reflect the amount of lattice imperfection. Peaks covering the range of phosphatic mineral extended along 2θ = 30°-35°. XRD diagrams of such peaks, at different milling times are illustrated in Fig.1. Extraneous gradual decay in the XRD phosphatic peaks, with increasing milling time proving the validity of the grinding treatment, was clearly noticed in Fig. 1.

Measuring the integrated relative area under each diffracted curve for each milling period, could provide another mean to emulate how much the crystal lattice was distorted. Planometer was used to measure such areas (Kurrer and Gock, 1986). The rational amounts of lattice imperfection were found to increase with milling time. It reached 43.95% after 90 minutes, Table 4, and then variation in unit cell due to activation process is shown in Table 5.

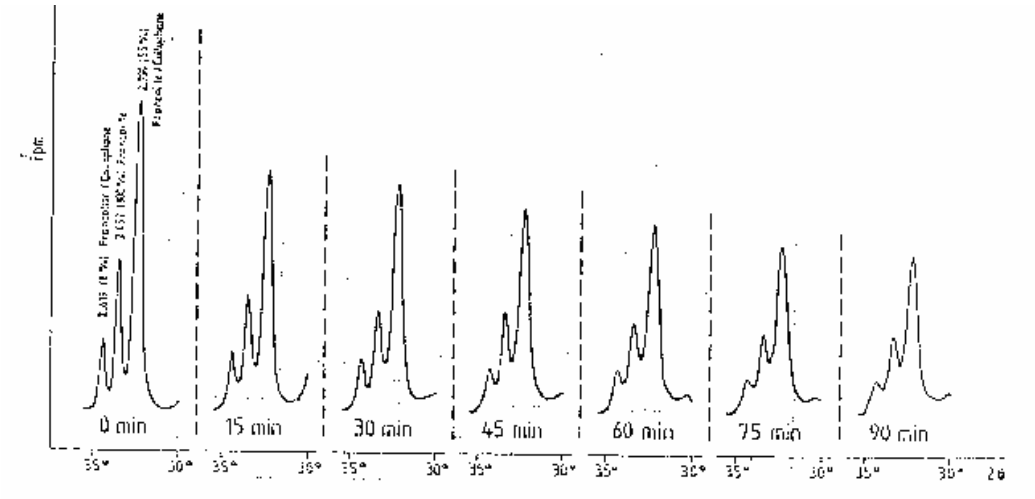

Fig. 1. The XRD analysis of raw Red Sea phosphate at different milling times

Table 4. The integrated relative area of XRD curves for each milling period

Milling Time, min	Peak Area, cm^2	Disorder %
0	223	-
15	188	15.69
30	166	25.56
45	140	37.22
60	137	38.56
75	130	41.70
90	125	43.95

Boldyrev et al (1976) proved the formation of different coordinate CaO_6F complexes, during the mechanical activation of some apatite minerals (Gock et al., 1986).

Gock and Jacob (1984) came to the conclusion that the destructions of the dolomite or calcite lattice plane causes the transformation of carbonate to oxide forms through CO_2 split off by the heat evolved during milling (McClellan, Gremillian, 1976).

Formation of a new compound, suggested to have the formula Ca_7 (CO_3) $(Si_6O_{18}).2H_2O$, as a result of the reaction between the highly activated carbonate and silica fragments, was also concluded (1990) (Gock et al., 1986).

Table 5. Unit cell dimensions of the raw and mechanically activated phosphate sample

Sample	2θ	θ	C(A^o)	a(A^o)	c/a
Crude	51.82	25.910	6.8929	9.3352	0.7383
	53.15	26.575	-	-	-
Activated	51.84	25.970	-	-	-
	53.32	26.660	6.8723	9.3151	0.7378

The effect of tribomechanical activation of Red Sea raw ore can be ascribed in view of its exogangue minerals contents, mainly silica and silicates. They seemed to play an important role in the process. The same conclusion was reached by Malchikov et al (1983) who got better activation results by adding silica to some phosphate ores (Kurrer, Gock, 1986).

INFRA-RED SPECTROSCOPY

It was interesting to record the effect of increasing mechanical treatment time through IR technique, Figure 2. The gradual corruption in the major P-O bands at V1 and V3 modes was obvious. They became identical after milling time of 90 minutes. Figures 2 shows the complete disappearance of the calcite peaks at the frequencies 878 and 1420 cm^{-1}. Remarkable decrease in the peak of quartz at 798 cm^{-1} frequency was also observed, Figure 2.

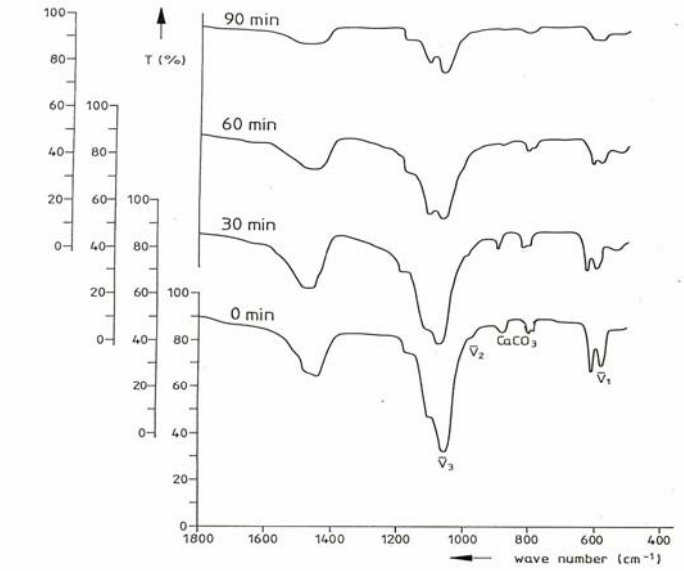

Fig. 2. IR spectra of phosphate samples at different milling times

However, the enhancing effect of the silica on tribo-mechanical activation of the ore is expected to diminish after 90 minutes, where due to over-grinding, the silica-related peaks began to disappear.

THERMAL BEHAVIOUR OF THE TREATED SAMPLES

Differential thermal analysis of mechanically activated Red Sea raw phosphate sample recorded broad exothermic peak in the temperature range 350-550°C. It may be due to the combustion of organic carbonate materials, which was not affected by mechanical activation. It seems probable that the closed system of milling is

responsible for the non-oxidation of such materials under that high temperature conditions.

The endo-exothermic peaks, appearing in the DTA of the original sample above 700° C, completely disappeared after the mechanical activation process, Fig.3. This may be explained by the decomposition of the inorganic carbonates, due to the excessive mechanical stress and free energy created by activation (McClellan and Gremillian, 1976).

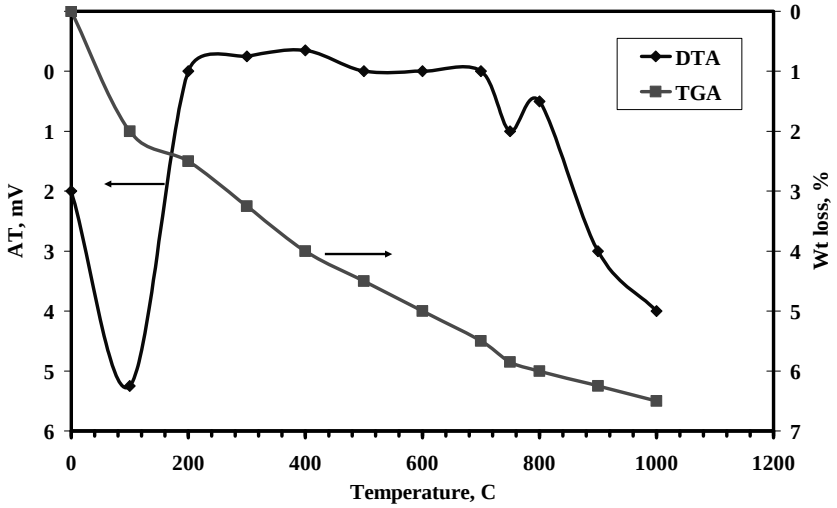

Fig. 3. Thermal analyses of Red Sea raw phosphate sample

The mechanism of activating phosphate rocks by the mechanical treatment does not mean structural distortion in the internal phosphatic composition only, but it may signify also a corresponding enhancement in lattice substitutions especially CO_3^{-2} for PO_4^{-3} (Sikora et al.,1989). It was also reported that the activation process increased in CO_2 milling atmosphere (Gock et al., 1986).

PROCESS KINETICS

CHEMICAL REACTIVITY AND SOLUBILITY

The absolute solubility index (ASI) is defined as `(Lehr, McClellan, 1973):
ASI= solvent –soluble P_2O_5 % / theoretical P_2O_5 concentration of apatite %

The absolute solubility index (ASI) of Red Sea phosphate in 2 % citric acid, CA and neutral ammonium citrate (NAC) were measured, Figs 4-5. A remarkable increase in the dissolution rates of the activated products was recorded, indicating the efficiency of the mechanical activation process. Gradual improvement in the ASI

values of the milled products with increasing milling time, signifies the advantage of the grinding of the extended time.

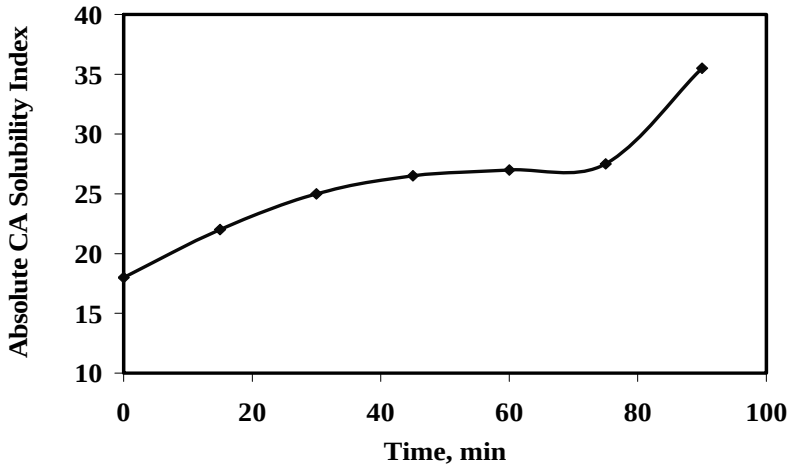

Fig. 4. Solubility Index of raw phosphate in 2% citric acid at different milling times

It is obvious from the curves that the solubility of the mechanically activated began to increase gradually for about 75 minutes after which a rapid increase in solubility took place. The absolute CA solubility Index values increased from 26 to 35.55 between 75 and 90 min.

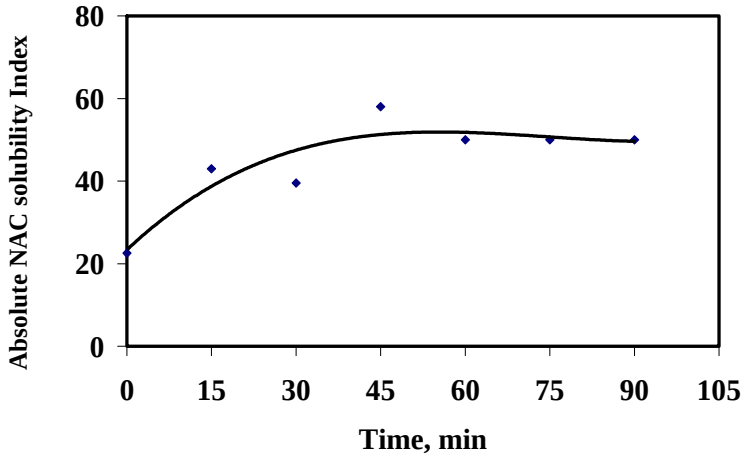

Fig. 5. Solubility Index of phosphate in neutral ammonium citrate at different milling times

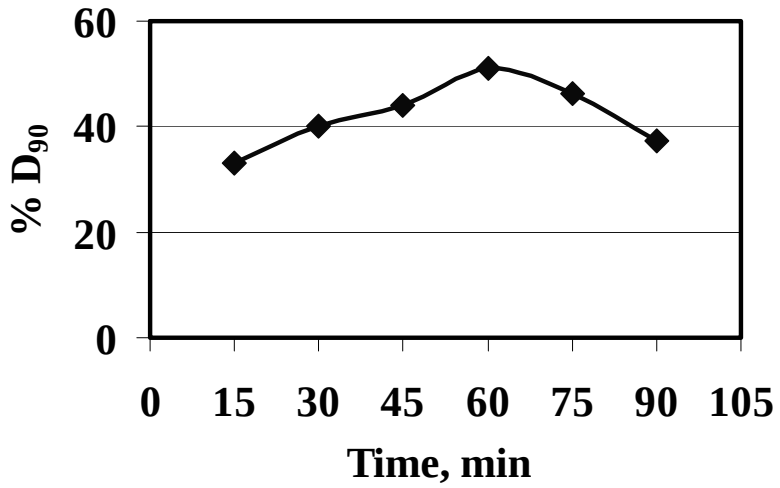

Fig. 6. Effect of milling time on $\%D_{90}$ of ground products

The solubility behaviour of either unactivated or activated samples in the alkaline medium was altered, Fig.5. Treated raw samples showed increase in the leaching efficiency till 60 min milling time. After that the absolute solubility index reaches asymptotic value. This trend is identical with that of both XRD pattern and IR spectra related to quartz, where it began to loose its frictional rubbing effect due to intensive size reduction after 60 min. Hard silica particles enhance the milling inside the mill by acting as small diameter grinding media, and accordingly increasing the internal lattice alteration of phosphate grains, which is leading to an increase in their the solubility character.

Therefore, the solubility optimum value at 45 min milling time in NAC was also observed (Fig. 5). This latter trend is identical with that of the change in $\%D_{90}$ of the phosphate by the increase in activation time (Fig. 6) which illustrates the effect of the particle size on its solubility in NAC.

Mechanical activation of phosphate in highly intensive size reduction equipment such as modified vibrating mill results in the dispersion of the milled product (Gock, Jacob, 1984). Gradual increase in the $\%D_{90}$ values with increasing milling time is shown in Fig. 6.

Evidently, symptoms of agglomeration were recorded after 60 min. The progressive structural changes in the apatite lattice with time are proving that dispersion is not necessarily the main process affecting rock reactivity during mechanical activation (compare Fig. 4 and 6).

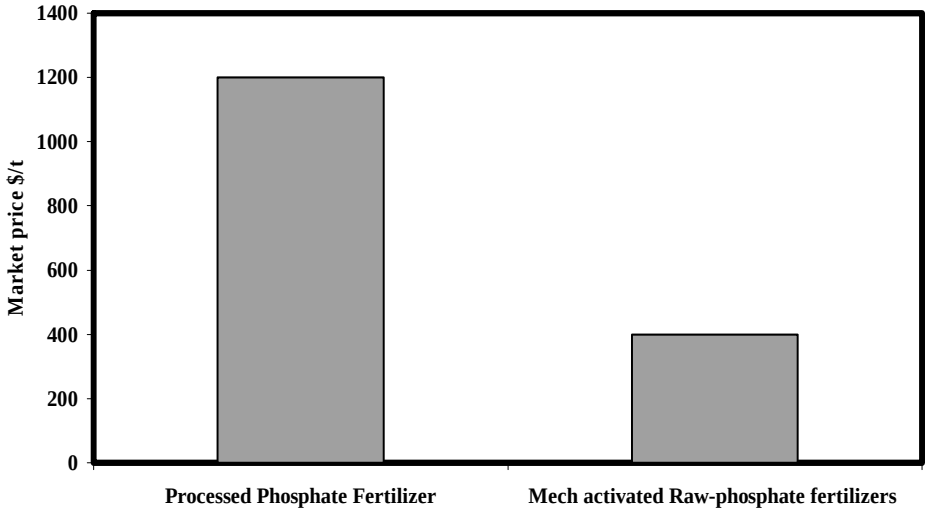

Fig. 7. Costs comparison of standard fertilizers to mechanically activated rock fertilizers

ASSOCIATED GANGUE MINERALS EFFECT

Most of the phosphate ores contain impurities, which may affect the mechanical activation process either positively or negatively. The prevailing impurity, in most of the phosphate ores, is silica. In case of adding the raw phosphate as a fertilizer, the silica impurities does not harm the soil because of it represents one of the soil components.

In regard to mechanical activation process, it was reported that the effect of tribo-mechanical activation of Red Sea phosphor-concentrate, after such a change in its chemical and mineralogical characteristics, should be interesting, where it showed lower tendency to the mechanical activation compared to the raw ore (Ibrahim, 1989). Such behavior may be ascribed to its exo-gangue minerals contents, mainly silica and silicates. They seem to play an important role in the process. The same conclusion was reached by Malchikov et al (1977) who got better activation results by adding silica to some phosphate ores (Malchikov et al., 1977).

ECONOMIC PREFERENCE OF MECHANICAL ACTIVATION

The comparison was carried out between the costs of mechanical activation of the phosphate ore with the running of different beneficiation steps to produce a concentrate suitable for the production of the phosphoric acid, which is an intermediate step of all the fertilizer manufacturing process. This comparison shows that the activation will lead to substantial savings, Fig.7. Initially, the saving is due to

the reduction in the capital and operating costs of the beneficiation steps. Moreover, the same thing will happen to the wet process that cost much more than beneficiation processes due to dealing with acids (i.e., one ton of sulfuric acid costs about $ 700) and the corrosion problems, which increase the maintenance costs as well.

CONCLUSIONS

Raw phosphate represents an alternative for currently used phosphate fertilizers due to costs and energy limitations. One of the reasons behind the rare use of the phosphate as a direct application fertilizer is its solubility. To overcome this limitation, the mechanical activation was tried and has achieved a marked increase in the reactivity of the treated phosphate samples. The chemical reactivity of activated raw samples in 2% citric acid and neutral ammonium citrate, showed improved leaching characteristics for all all the milling times tested.

Therefore, the technology of tribo-mechanical activation of phosphate rocks for direct application, due to its simplicity, may open the way for utilization of indigenous ores in many developing countries and serve regional markets when arbitrary grade specifications do not apply and would give the security to be independent of the international chemical concerns.

REFERENCES

CHIEN S.H., SALE, P.W.G., FRIESEN, D.K., *A discussion of the methods for comparing the relative effectiveness of phosphate fertilizers varying in solubility Nutrient Cycling in Agro-eco systems*, Volume 24, Number 3, pp149-157, September, 1990.

IBRAHIM S. S., EL-MIDANT A.A.,BOULOS T.R.; *Economic preferences of mechanical activation over mineral beneficiation for phosphate rock direct applications,* Physicochemical Problems of Mineral Processing, 44 ,2010.

IBRAHIM S. S. *Some tribochemical aspects for the treatment of indigenous Egyptian phosphates*, Ph.D Thesis, Faculty of Science, Cairo University, 1989.

GOCK E., KURRER K., MICHEALIS S., *Vibrating milling: progress in theory and industrial application*, 1st World Congress Fine Particle Technology, Part II, p. 653-666, 1986.

GOCK E.,JACOB, K.H. *Conceptions for processing the pyrite-bearing phosphorites of Abu-Tartur*, Berliner Geowissen Abh. (A) 50, 381-397, Berlin, 1984.

HEINIKE G., PAUDERT, R, HARENX, H, STEINIKE, U, AND POETHIN, R*, Tribomechanical transfer of apatite to a soluble form Zhurnal Prikladnoi khimii*, Vol.50, No.5, pp 969-974, 1977.

KOLOSOV, A.S., BOLDYREV, V.V., CHAIKINA, M.V., TRANZOVA, M.I., GORDEEWA, G.I., PAUDERT ,R.,HARENZ, *The Reactivity of Native Apatites Under Mechanical Activation*, Proc. of the scientific academy of U.S.S.R. phy. Chemistry sec, 6, pp.148-55, 1979.

KOZLOV V.I., KOZYREV, S.A., *Selection of apparatus in studies of mechanical activation of phosphate raw materials*, Proc. of the scientific academy of U.S.S.R. phy. Chemistry sec, 6, pp.71-4, 1982.

KURRER K., GOCK, E., *Effect of the operating conditions on motion and impact processes in viberatory tube mill*, Journal of preparation and processing, 10, 546-554, 27, 1986.

LATKIN A.S., SAMATOVA, L.A *Thermo-chemical methods of treatment of low-grade phosphatic raw materials*, Journal of Mining Science, Volume 34, Number 1 / January, 1998.

LEHR, J.R., MCCLELLAN, G.H*., A revised laboratory reactivity scale for evaluating phosphate rocks for direct applications*, TVA Bull. Y-34, 36 p, NFDC, Muscle Shoals, Alabama, 1973.

MAENE L.M. *Phosphate Fertilizer Production, Consumption and Trade, The Present Situation and Outlook to 2010*, The Sulphur Institute's 17th Sulphur Phosphate Symposium, January 17-19, 1999, Boca Raton, Florida.

MALCHIKOV G.D., TERENTYENA, T.P., RUBAILO, I.S., *Decomposition of mechanically activated phosphate by nitrogen dioxide*, Proc. of Scientific Academy of USSR (Phy. Chemistry Sec.) 233 (5), 892-5, 1977.

MCCLELLAN, G.H., GREMILLIAN, L.R., *Evalution of phosphatic raw materials, Proceddings of a Symposium on the role of phosphorus in agriculture*, NFDC, Muscle Shoals, Alabama, June 1976.

MORRIS L. *Economics of Fertilizer Application*, CYMMT Economics Working papers. 1988.

PAUDERT R., HARENZ, H., POTHING, R, HEINIKE, G., KDT, DUNKEL, L. AND SCHUMANN, H., DT, *Phosphate fertilizers through Tribomechanical Activation of apatitic phosphate chem. Techn*.,30, jg., nr.9,470-475, 1978.

RAMÍREZ C.A.,WORRELL, E. *Feeding fossil fuels to the soil An analysis of energy embedded and technological learning in the fertilizer industry*, June 2005.

SEITNAZAROV A.R., MUSAEVA S.A. NAMAZOV, SH. S., BEGLOV, B.M. *Mechanochemical activation of ordinary phosphorite powder of Central Kyzylkum mixed with urea nitrate and ammobium carbonate salts*, Russian Journal of Applied Chemistry, Vol.80, No.11/Nov., 2007.

SIKORA F.J., DILLARD E.F, COPELAND J.P., MULLINS G.L., *Chemical characterization and bioavailability of phosphorus in water-insoluble fractions of three mono-ammonium phosphate fertilizers*., J Assoc Off Anal Chem. 1989 Sep-Oct;72(5):852-6.

Ibrahim S.S, El-Midany A.A, Boulos T.R., *Wpływ intensywności stresów mechanicznych na właściwości chemiczne fosforanu, jako sposobu na wzrost jego rozpuszczalności przy wykorzystaniu jako nawóz mineralny*. Physicochemical Problems of Mineral Processing, 44 (2010), 79-92, (w jęz. ang), http://www.minproc.pwr.wroc.pl/journal

Technika aktywacji mechanicznej jest unikalnym procesem, w którym reaktywność powierzchni mineralnej może wzrastać dając w rezultacie nowy produkt. Fosforan jest jednym z ważnych składników odżywczych dla upraw roślinnych, który może być produkowany z rud fosforanowych. Jednakże, bezpośrednie zastosowanie rudy fosforanowej posiada szereg ograniczeń. W tych badaniach, aktywacja mechaniczna była zastosowana dla modyfikacji struktury wewnętrznej, w taki sposób by był on użyty bezpośrednio jako nawóz mineralny. Wydaje się, że dobrą alternatywą dla wysoce skomplikowanej technologii produkcji nawozu fosforowego jest użycie całkowicie rozpuszczalnego w wodzie nawozu otrzymanego po mechanicznej aktywacji rudy fosforanowej.

słowa kluczowe: aktywacja mechaniczna, zaburzenia sieci krystalicznej, nawozy fosforowe, reaktywność

Physicochem. Probl. Miner. Process. 44(2010) 93-102

journal homepage
www.minproc.pwr.wroc.pl/journal/

Physicochemical Problems of Mineral Processing

Index No. 32213X ISSN 1643-1049

A. Kołodziejczak-Radzimska*, T. Jesionowski*, A. Krysztafkiewicz*

OBTAINING ZINC OXIDE FROM AQUEOUS SOLUTIONS OF KOH AND $Zn(CH_3COO)_2$

Received February 2, 2009; reviewed; accepted May 4, 2009

Zinc oxide was obtained by precipitation from solutions of KOH and $Zn(CH_3COO)_2$. The effect of excessive presence of one of the reagents and temperature on the physico-chemical properties, structure and size of zinc oxide particles was analysed. The main aim of the study was to establish the optimum conditions of precipitation that would ensure getting the uniform particles of zinc oxide of the minimum diameter. The zinc oxide obtained had particles of nano- and micrometric size. The adsorption/desorption isotherms indicated the mesoporous character of the product. The wettability of ZnO obtained was determined first of all by the morphology and particle size.

key words: ZnO, precipitation, particle size distribution, surface morphology, wettability, adsorptive properties

INTRODUCTION

For the last decade, particular attention has been paid to the techniques for producing nanomaterials with interesting properties. Nanotechnology has been the subject of research at many corrorate and academic research centres (Zhong, 2008; Zhang, 2002; Schmidt-Mende, 2007).

* Poznan University of Technology, Institute of Chemical Technology and Engineering
Pl. M. Skłodowskiej-Curie 2, 60-965 Poznan
e-mail: teofil.jesionowski@put.poznan.pl, phone :+48(61)6653720, fax :+48(61)6653649

Besides clay nanomaterials like montmorillonite and carbon nanotubes, of great importance are nanometric metals and their oxides. Nanomolecular ultrafine zinc oxide of particles size from a few to a few ten nanometers are of particular interest. They are many times smaller than those of the standard zinc oxide particles used as an activator in synthetic rubber processing (Wang, 2003, Lu, 2000, Kahn, 2005).

In nature, zinc oxide occurs as the minerals zincite and franklinite in combination with iron oxides and magnesium oxides. It is mainly obtained from zinc ores such as calamine ($ZnCO_3$) or sphalerite (ZnS), and from the post-reaction sludge formed in the processes of reduction of organic compounds with zinc. Making use of the technique of sublimation at high temperature, with careful control of crystal growth and full analytical monitoring, it is possible to obtain ZnO nanocrystals in the shape of combs, rings, helices, spirals, arches, ribbons, strings and cages (Pyskło, 2007).

Particularly promising are ZnO nanopowders, which can be used in many technological processes. They have specific properties including semiconducting, piezoelectric and pyroelectric ones (Duan, 2007). That is why zinc oxide can be used in optoelectronics and laser technology, ceramics, as gas sensors and in production of paints (Wang, 2003; Gao, 2002; Paneva, 1998; Ristić, 2005). As a natural consequence of the progress in nanotechnology, interest in zinc oxide is groving.

EXPERIMENTAL

Precipitation was performed in a reactor 0.5 dm^3 in capacity equipped with a fast-rotating stirrer. The speed of the stirrer rotation was close to 1200 rev/min. A solution of potassium hydroxide was introduced in doses into a solution of zinc acetate (or the reverse) at different temperatures from 20 to 80^oC at a ratio of substrates of 1:1, with excess of KOH (POCh. S.A.), or with excess of $Zn(CH_3COO)_2$ (POCh. S.A). The substrates were dosed with the help of a peristaltic pump PB1B-05A at 1.1; 3.0, 11 and 15 cm^3/min. The zinc oxide obtained was filtered off under reduced pressure. The sediment was washed several times with water. After washing, the sample was dried in a stationary drier at 120°C. A schematic presentation of zinc oxide synthesis is shown in Figure 1.

Particle size distribution, surface morphology and wetability were recorded. Particle size distribution was measured with a Zetasizer Nano ZS using the light backscattering method (NIBS), and a Mastersizer 2000 using laser diffraction (both instruments made by Malvern Instruments Ltd.).

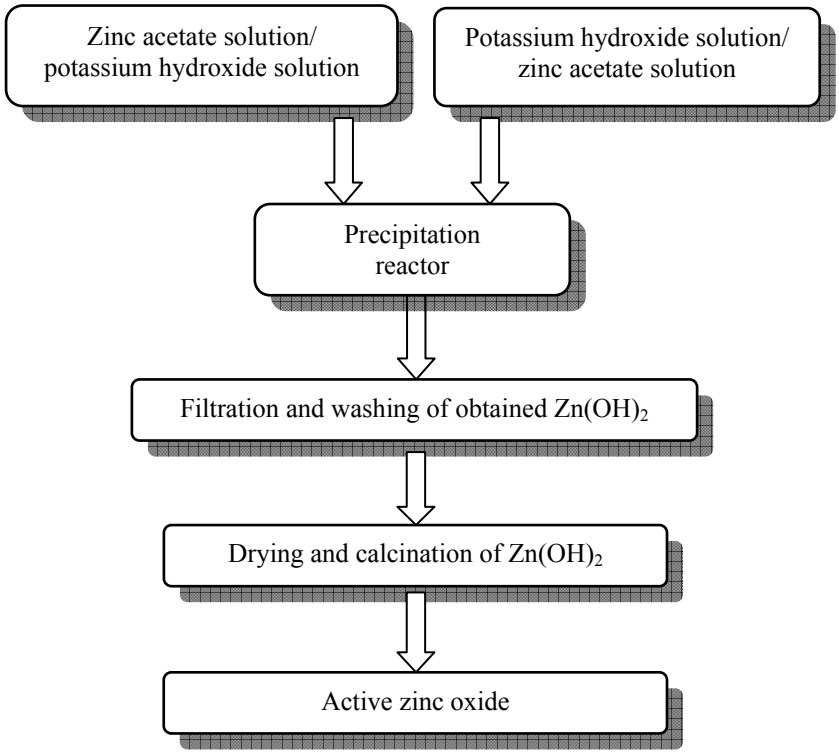

Fig. 1. Schematic presentation of zinc oxide synthesis by precipitation

The degree of dispersion, morphology of the zinc oxide particles and their tendency to agglomeration were assessed using a Zeiss VO40 microscope. Wettability was determined by a Krüss K100 tensiometer on the basis of capillary penetration of water in a sample of ZnO. Isotherms of nitrogen adsorption/desorption on the surface of zinc oxide and surface area were also determined. Measurements were made using Micromeritics ASAP 2020.

RESULTS AND DISCUSSION

At the first stage of the study, synthesis was carried out by introducing a 5% solution of KOH in doses to a 5% solution of $Zn(CH_3COO)_2$ (stoichiometric ratio of reagents). The zinc oxide obtained was characterised by the particle size distribution. The particle size distribution by volume (Fig. 2a) shows one band covering particles 190 to 531 nm in diameter. 27.5% of the total volume represented particles of 295 nm in diameter. The particle size distribution by intensity also shows one band covering the diameters in the range 220 to 459 nm (Fig. 2b). The maximum intensity of 31.4%

corresponds to the particles 295 nm in diameter. The polydispersity index of this sample is 0.682, which indicates a relatively low homogeneity of the particles. This conclusion is confirmed by the data presented in Fig. 3, which shows particle size distributions by volume for the samples of zinc oxide precipitated at the stoichiometric ratio of the reagents, with excess of potassium hydroxide, and with excess of zinc acetate. There was a significant effect of excess of one of the reagents on the sizes of particles of the ZnO solid. The smallest particles were obtained with a 20% excess of zinc acetate solution (Fig. 3).

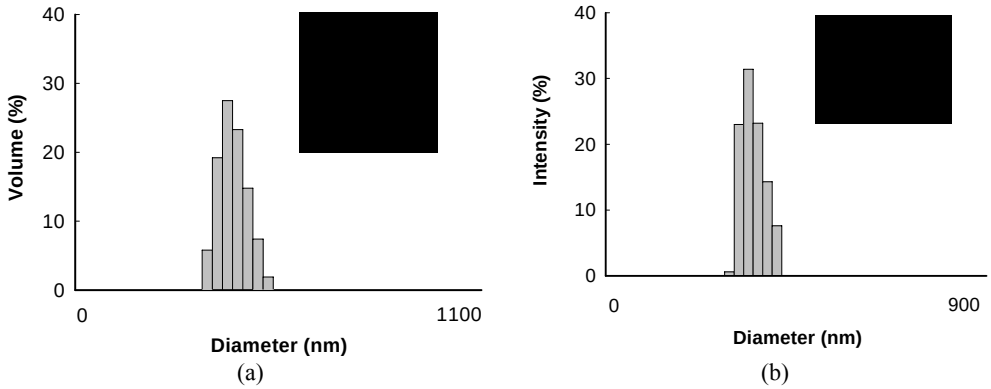

Fig. 2. Particle size distribution of ZnO precipitated by dosing a 5% solution of KOH to 5% solution of $Zn(CH_3COO)_2$ in stoichiometric conditions, by a) volume, b) intensity

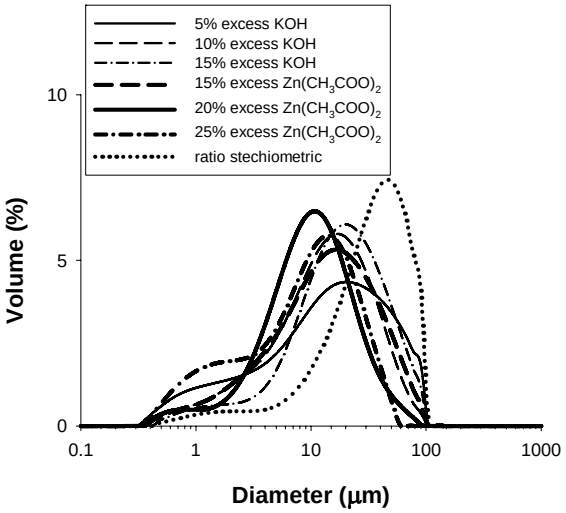

Fig. 3. Comparison of the micrometric particle size distributions versus the volume contribution for ZnO samples precipitated in the presence of excess of KOH or $Zn(CH_3COO)_2$

There were two bands in the particle size distribution by volume of the zinc oxide sample precipitated at the 20% excess of zinc acetate (Fig. 4a) The first was from 43.8 to 58.8 nm, with the maximum volume of 16.7% corresponding to the particles of 50.7 nm in diameter. The second was from 164 to 396 nm, with the maximum volume of 15.8% corresponding to the particles of 220 nm in diameter. There were also two bands in the particle size distribution by intensity for the same sample (Fig. 4b). The first corresponds to particles 50.7 nm in diameter, and the second corresponds to particles between 190 and 342 nm in diameter, with a maximum intensity at 190 nm. Fig. 4c confirms the undesirable contribution of micrometric size particles in the sample precipitated in the presence of 20% excess of zinc acetate. According to the micrometric particles size distribution (Fig. 4c), the sample contains 90% of particles smaller than 30.4 μm in diameter, 50% of particles of 9.61 μm in diameter, and 10% of particles not greater than 2.79 μm in diameter. Fig. 4d shows a SEM image of the sample obtained in the presence of 20% excess of zinc acetate solution confirming the occurrence of nano- and micrometric particles.

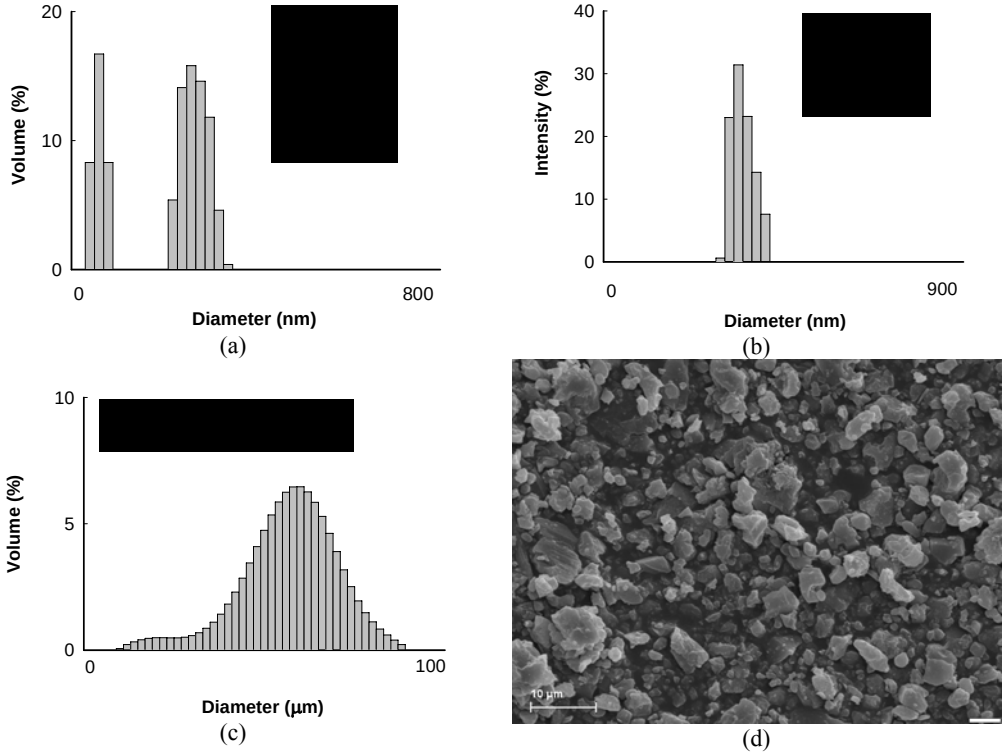

Fig. 4. Particle size distribution of ZnO samples precipitated in the presence of 20% excess of $Zn(CH_3COO)_2$ solution by (a) volume contribution for the particles of diameters from the range 0.6 – 6000 nm, (b) intensity, (c) volume contributions for the particles of diameters from the range 0.02 – 2000 μm, (d) SEM photograph

The effect of temperature on the particle size of zinc oxide precipitated was then analysed. Fig. 5 and Table 1 show the particle size distribution and particle diameters of the zinc oxide sample precipitated in the presence of 20% excess zinc acetate solution at different temperatures from 20 to 80°C. The higher the temperature of precipitation, the greater the size of zinc oxide particles.

Table 1. Analysis of the micrometric particles size of ZnO precipitated at different temperatures

Temperature	Diameter (μm)	Volume (%)	Diameter (μm)		
			d(0.1)	d(0.5)	d(0.9)
20°C	0.36	0.06	2.79	9.62	30.4
	11.5	6.46			
40°C	0.36	0.01	3.06	14.4	53.6
	15.7	5.75			
60°C	0.48	0.08	1.99	9.78	30.1
	15.1	5.49			
80°C	0.36	0.01	2.39	17.1	55.8
	15.1	5.08			

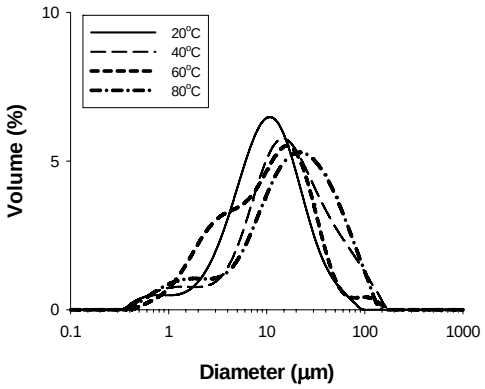

Fig. 5. Comparison of micrometric particle size distributions versus volume contribution for ZnO samples precipitated at different temperatures at a dosing rate of KOH solution to $Zn(CH_3COO)_2$ solution of 15 cm^3 and at the stoichiometric ratio of the reagents

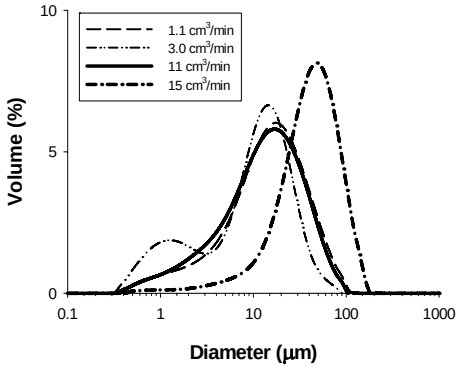

Fig. 6. Comparison of micrometric particles size distributions versus volume contribution for ZnO samples precipitated at different dosing rates of KOH solution to $Zn(CH_3COO)_2$ solution, at 20°C and at the stoichiometric ratio of the reagents

The effect of the rate of dosing on the particle size distribution was also studied. Micrometric particle size distributions obtained for the samples of ZnO synthesised at different rates of dosing of potassium hydroxide to zinc acetate are compared in Figure 6. The optimum rate was 11 cm^3/min. The SEM images presented in Fig. 7 support this conclusion. The ZnO sample precipitated at the rate of KOH dosing to

$Zn(CH_3COO)_2$ of 11 cm^3/min has small almost spherical particles (Fig. 7c) with little tendency to agglomerate. The ZnO samples obtained at the higher or lower rates of dosing show a considerable tendency to agglomerate (Fig. 7a and d).

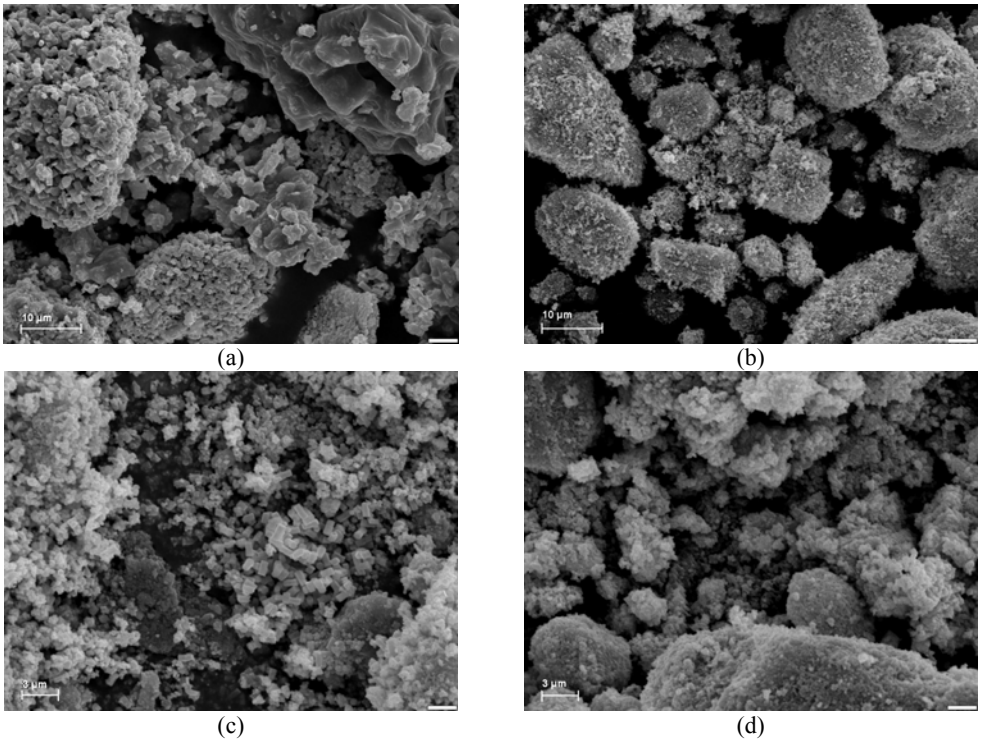

(a) (b)

(c) (d)

Fig. 7. SEM images of ZnO samples precipitated at different rates of dosing of KOH solution to $Zn(CH_3COO)_2$ solution of (a) 1.1 cm^3/min, (b) 3.0 cm^3/min, (c) 11 cm^3/min, (d) 15 cm^3/min, at 20°C, at the stoichiometric ratio of the reagents

Wettability was lowest in the sample precipitated in the presence of 5% excess of KOH (Fig. 8). For this sample, wetting was completed after 900 s. Wettability was highest in the samples precipitated in the presence of 10% and 15% excess of KOH solution. Wettability of the ZnO obtained is mainly determined by the size and morphology of particles.

Fig. 9 shows the isotherms of nitrogen adsorption/desorption on the surface of the ZnO samples obtained. The character of the curves indicates the mesoporous structure of the samples. The amount of nitrogen adsorbed on all samples increases slowly until the relative pressure reaches 0.9. Above this pressure, the amount of adsorbed nitrogen rapidly increases to reach the highest value of 45 cm^3/g for the samples precipitated at 20°C and 40°C at $p/p_0 = 1$. For zinc oxide precipitated at 60°C, the amount of nitrogen adsorbed is lowest at $p/p_0 = 1$ and reaches 35 cm^3/g. The surface area of the samples

obtained is small and does not exceed 20 m^2/g (Tab. 2). With increasing temperature, the BET surface area of the ZnO samples decreases.

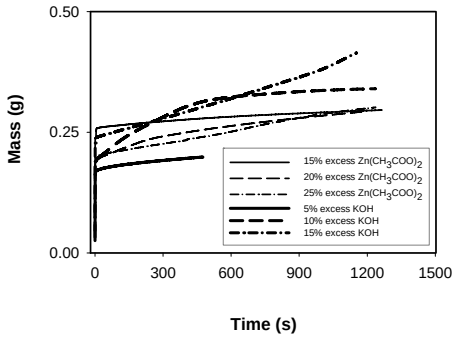

Fig. 8. The wettability curves of ZnO samples precipitated at different temperatures and the other parameters constant

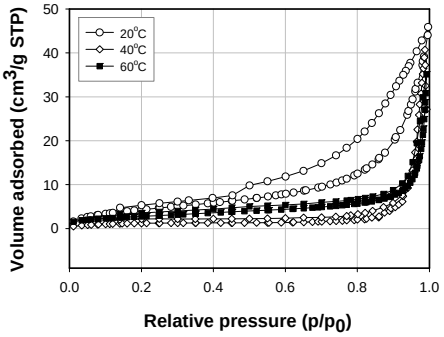

Fig. 9. Isotherms of nitrogen adsorption/desorption for selected samples of ZnO

Table 2. Basic parameters determining the adsorption properties of zinc oxide samples precipitated at different temperatures

Temperature	BET surface area (m^2/g)	Pore volume (cm^3/g)	Pore size (nm)
20°C	16.6	0.07	16.4
40°C	4.0	0.06	47.4
60°C	10.0	0.05	14.2

CONCLUSIONS

Zinc oxide obtained by precipitation from water solutions of potassium hydroxide and zinc acetate is characterised by small particles. The sample of the smallest particles was obtained by dosing a 5% solution of KOH to a 5% solution of $Zn(CH_3COO)_2$. The particle size of the samples was found to depend on the excess of the substrates. 20% of zinc acetate gave a sample with very small particles close to 50 nm in diameter. Unfortunately, this sample also contained micrometric size particles, as indicated by the particle size distribution plots and SEM photographs. Based on particle morphology, the optimum rate of dosing of KOH to $Zn(CH_3COOH)_2$ is 11 cm^3/min. Increasing the temperature of precipitation increases the diameters of the ZnO particles obtained. Wettability was lowest in the sample precipitated in the presence of 5% excess of KOH solution, and highest in the samples precipitated in the presence of 10% and 15% exceed of KOH solution. The isotherms of nitrogen adsorption desorption indicate the mesoporous character of ZnO samples obtained.

The sample of ZnO precipitated at 20°C had a BET surface area of 16.6 m^2/g. The higher the temperature of precipitation, the lower the surface area of the samples. This is probably related to the presence of particles of greater diameters.

REFERENCES

DUAN J., HUANG X., WANG H., ZHONG Q., SUN F., HE X., 2007, *Synthesis of porous ZnO micro-flakes via an integrated autoclave and pyrolysis process*, Mat. Chem. Phys., 106, 181-186.

GAO L., LI Q., LUAN W.L., 2002, *Preparation and electric properties of dense nanocrystalline zinc oxide ceramics*, J. of the American Ceramic Society, 85, 1016-1018.

KAHN M.L., MONGE M., COLLIÈRE V., SENOCQ F., MAISONNAT A., CHAUDRET B., 2005, *Size- and shape-control of crystalline zinc oxide nanoparticles: a new organometallic synthetic method*, Advanced Functional Materials, 15, 458-468.

LU CH.-H., YEH CH.-H., 2000, *Influence of hydrothermal conditions on the morphology and particle size of zinc oxide powder*, Ceramics International, 26, 351-357.

PANEVA R., GOTCHEV D., 1998, *Non-linear vibration behavior of thin multilayer diaphragms*, Sensor and Actuators, A: Physical, 72, 79-87.

PYSKŁO L., PARASIEWICZ W., PAWŁOWSKI P., NICIŃSKI K., Piastów 2007, *Tlenek cynku w mieszankach kauczukowych*, Instytut Przemysłu Gumowego „Stomil".

RISTIĆ M., MUSIĆ S., IVANDA M., POPOVIĆ S., 2005, *Sol–gel synthesis and characterization of nanocrystalline ZnO powders*, Journal of Alloys and Compounds, 397, L1-L4.

SCHMIDT-MENDE L., MACMANUS-DRISCOLL J.L., 2007, *ZnO – nanostructures, defects, and devices*, Materials Today, 10, 40-48.

WANG J., GAO L., 2003, *Synthesis and characterization of ZnO nanoparticles assembled in one-dimensional order*, Inorganic Chemistry Communications, 6, 877-881.

ZHANG J., SUN L.D., LIAO C.S., YAN C.H., 2002, *A simple route towards tubular ZnO*, Chemical Communication, 262-264.

ZHONG Q., HUANG X., DUAN J., LIU J., SUN F., HE X., 2008, *Preparation and characterization of ZnO porous plates*, Materials Letters, 62, 188-190.

ACKNOWLEDGEMENTS

This publication was prepared within the key project – PO IG no. 01.03.01-00-006/08 cofinanced from the funds of European Regional Development Fund within the framework of the Operational Programme Innovative Economy.

Kołodziejczak-Radzimska A., Jesionowski T., Krysztafkiewicz A., *Otrzymanie tlenku cynku wodnych roztworów KOH i $Zn(CH_3COO)_2$,* Physicochemical Problems of Mineral Processing, 44 (2010), 93-102, (w jęz. ang), http://www.minproc.pwr.wroc.pl/journal

Tlenek cynku został otrzymany w wyniku wytrącenia z roztworów KOH i $Zn(CH_3COO)_2$. Analizowano wpływ nadmiarowej objętości jednego z reagentów i temperatury na fizykochemiczne

właściwości otrzymanego materiału. Głównym celem badań było ustalenie optymalnych warunków prowadzenia procesu tak aby otrzymać jednakowe cząstki tlenku cynku o minimalnej średnicy. Otrzymany tlenek cynku miał wymiary cząstek w nano i mikrometrycznej skali. Izotermy adsorpcji i desorpcji wskazują, że produkt ma mesoporowaty charakter. W pierwszym rzędzie została określona zwilżalność otrzymanego tlenku cynku.

słowa kluczowe: ZnO, precypitacja, skład ziarnowy, morfologia powierzchniowa, zwilżalność, własności absorpcyjne

Physicochem. Probl. Miner. Process. 44(2010) 103-113

journal homepage
www.minproc.pwr.wroc.pl/journal/

Physicochemical Problems of Mineral Processing

Index No. 32213X ISSN 1643-1049

A. Korkosz*, M. Janczarek*, R. Aranowski*, J. Rzechuła*, J. Hupka*

EFFICIENCY OF DEEP BED FILTRATION IN TREATMENT OF SWIMMING POOL WATER

Received July 1, 2009; reviewed; accepted July 17, 2009

The effectiveness of water filtration in gravel-sand bed filters has been studied in the rehabilitating swimming pool treatment plant. Apart from instrumental analysis of the water the investigation considered additionally particle size distribution as well as thermal analysis of the sediment collected in the sand bed of depth filters and removed during the process of washing. Variable value of TOC in the washings for each filter indicates indirectly their non-uniform loading. It has been proved that the size of particles in the suspension easily changes as a result of operation of shear stress. Derivatographic research has indicated approximately 30 % presence of organic substances in the sediment. In neither of the investigated samples loss of mass over >460^{o}C has been observed.

key words: swimming pool, deep bed filtration, particle size distribution, thermal analysis

INTRODUCTION

The testing of swimming pool water presented in the literature refers mainly to the health of the users (Panyakapo, 2008; Lahl, 1981; Nemery, 2002; Judd, 2000; Judd, 2003). Swimming pools are enjoying increasing popularity not only among adults and the youth but also among children, even several months old. Therefore, the cleanness of the water is of crucial importance, especially as its users are often infants. The swimming pool water contains both dissolved and suspended contaminants. Among those suspended there are among others: bacteria, viruses, protozoa and fungi. Pool water is treated in two ways. Contaminants which settled at the bottom are removed

* Department of Chemical Technology, Gdansk University of Technology, 80-952 Gdansk, ul. Narutowicza 11/12, Poland, corresponding author, e-mail: jhupka@pg.gda.pl

by water vacuum cleaner, while the suspended contaminants are separated on filters. The selection of the filters as well as frequency and intensity of washing are of fundamental importance so that the dangerous microbiological contaminants are effectively removed.

Effective functioning of depth filter, with regard to particles of colloidal size is dependant on addition of coagulant agents. The model research in sand filter have shown that the addition of coagulants results in 90-99 % removal of polyester molecules, replacing bacteria of variety *Cryptosporidium* (Croll, 2007). There is a need to improve disinfection and cleaning procedures, with consideration given to the different uses and daily bather loads of each pool type. There is also a need to monitor water quality and to increase users' knowledge and awareness of the risks (Guida, 2009).

The most frequently used filter bed is sand-siliceous bed, which with proper operation can function at least several years without blocking. The main reason of filters being blocked is the poor quality of swimming pool waters, presence of algae (Saravia, 2007) and improper washing of the filter. There are also in use filters with the addition of anthracite. Application of too high backwash water flowrate to these filters can result in the uplift of antracite. The literature of the subject describe the possibilities of elimination of resting spores *Cryptosporidium* in the filter with the sand bed (Croll, 2007). Tests of swimming pool water have been performed with the application of ultra filtration in the pilot installation (Hobby, 2004). Also vacuum filters were used with cellulose fibers or diatomaceous earth as filter aid.

Recently research has been carried out on new ways of treatment and disinfection of swimming pool water, involving application of ultra filtration in connection with adsorption on activated carbon (Barbot, 2008), ultrafiltration followed by hyperfiltration (Resissmann, 2005), or the application of advanced methods of oxidation (Glauner, 2005). There is still in use a number of swimming pools of the old type in which the water from overflow is directed to sewage system. In the process of filter washing there have been observed substantial water losses which after consecutive treatment could be used again.

This paper discusses the results of water filtration alongside thermal analysis of flocks accumulated in the sand bed of depth filters and removed by washing. It is expected that the research will contribute for the implementation of the new technology of water treatment, whose main goal will be the increase of safety of the users of swimming pools and economy of water and energy.

RESEARCH SYSTEM

The object of the research was a normally operated water treatment and disinfection installation of rehabilitating indoor swimming pool, with lower water

overflow, with the basin capacity of 120 m^3. The water from the swimming pool flows through the hair separator and the pump directs it to the three layer gravel-sand filters. Ahead of the filters aluminum sulfate coagulant is dosed periodically at the amount of 3 g/m^3. After passing through the filters the water is heated in the counter current heat exchangers, aerated under pressure, disinfected with the solution of sodium hypochlorite and recirculated back to the pool basin.

Due to lack of equalizing tank, the pool water is used in the process of filters washing. In the first stage the filter is washed with water, next with water and compressed air. The time of washing depends on the level of contamination of the filter and can continue for the period from several minutes up to even one hour. The filter is considered washed up when no visual traces of suspended matter are present in the water.

For the prophylactic purposes against development of algae 0.2 kg copper sulfate in the solution is dosed for each filter. In the described swimming pool the filters are washed twice a week. There is neither automatic quality control of water nor automatic chemicals dosing.

The fundamental research has been carried out on gravel-sand filters with the measurements Ø800×2200 mm, with three filtration layers (from the top of the bed):

- I sand layer with granulation of 0.5-1 mm (the depth of the layer 900 mm),
- II sand layer with granulation of 1-2 mm (the depth of the layer 500 mm),
- III sand layer with granulation of 5-8 mm (the depth of the layer 300 mm).

RESEARCH METHODOLOGY

Sieve analysis of sand and gravel was performed for the three fresh granular media forming the increasing particle size layers. The first layer was sampled from the inside of the filter and for the sand that came into the aerator due to improper operation of the filters. For the sieve analysis a set of sieves with the opening sizes: 8; 6.3; 4; 2.5; 1.5; 0.85; 0.6; 0.5; 0.355; 0.212 mm was used. They were placed in the form of a stack on the shaker. The samples of 250 g of sand were dried to the constant mass at 105 ^oC and shaken over the period of 5 minutes. The residue on each sieve was manually shaken for the additional period of 1 minute and the minus mesh was added to the plus mesh on the sieve with smaller size openings and the mass of grain fraction was determined.

In order to determine the efficiency of filtration process the water samples were collected from the pool installation before and after the filters (after disinfection). Also the water from washing of each of the three filters was collected.

pH of the water samples was measured by means of multifunction device *Elmetron* with the application of combined electrode of the type ERH-111. The temperature was measured with the application of the sensor CT2S-121, and

conductivity with the application of conductometric sensor of type EC-60. Redox potential was determined by the use of platinum combined electrode of type ERPt-13. Concentration of available chlorine was determined by means of titration with N,N-diethyl-1,4-phenylenediamine in compliance with Polish Standard PN-ISO 7393-1.

The measurement of concentration of total organic carbon (TOC), total inorganic carbon(TIC) as well as total nitrogen (TN) was carried out with the application of LiquiTOC *Elementar* manufactured analyzer in the presence of oxygen as the carrier gas. The contaminants present in the water samples after oxidation at the temperature of 800°C were determined with analyzer integrated detectors: infrared IR (carbon) and electrochemical – EC (nitrogen).

Distribution of particle size in the backwash water was examined by means of Mastersizer X laser diffraction particle sizing instrument manufactured by *Malvern.* The applied system enabled the measurements of particle size in the range of 0.5-180 μm and 1.2-600 μm. 200 ml of examined suspension was circulated through measuring cell in the closed circuit.

Thermal analysis (TG/DTA) of the flocks from filter bed was performed by means of derivatograph Q-100 D, *Paupik, Paulik ERDEY,* MOM Budapest. First, the deposit was separated from the washing water in the centrifuge type MPW-2, and next dried in the dryer KBC G-100/250 manufactured by *Premed* to the constant mass. The weighed amount totaled up to 100 mg. The temperature increase rate was set at 10°C/min. TG sensitivity was 100 mg, while DTA sensitivity was 250 μV. The reference sample was α-Al_2O_3.

The photographs of the flocks were taken with the biological microscope type *L300* coupled with digital camera Canon PowerShot A650 IS.

RESULTS AND DISCUSSION

SAND PARTICLES SIZE DISTRIBUTION

The required effectiveness of filtration can be achieved in the sand-gravel bed maintaining the grain size in the particular layers. Analyzing the data obtained for investigated filters one can observe (Fig. 1) that particle size distribution in the particular layers of the filtration bed has changed during the operation of filter batteries.

The investigated fresh sand or gravel were characterized by the following particle diameters: I layer 0.4-1.0 mm; II layer 1.0-2.5 mm; III layer 3.0-8.0 mm. The sand collected during the inspection from the inside of the filter corresponds to the diameter of I layer of fresh bed 0.4-1.0 mm, whereas the sand with the particle diameter in the range of 0.7-4.0 mm collected from the aerator is composed of the mixture of the 3 layers of the bed. The data obtained from the sieve analysis correspond to the data

presented in the literature e.g. I layer 0.4-0.8 mm; II layer 1.0-2.0 mm; 2.0-3.15 mm; III layer 3.15-5.60 mm (Wyczarska-Kokot, 2002).

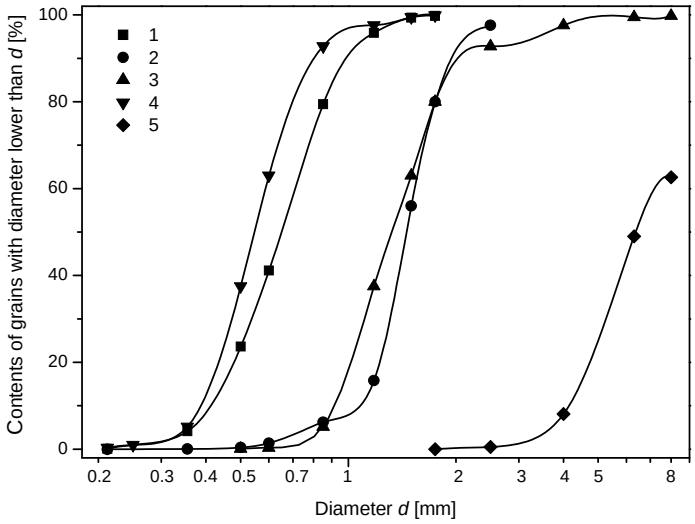

Fig. 1. Sieve analysis of 1- fresh fine sand; 2 - fresh medium-size sand; 3 - sand washed-out to aerator; 4 - fine sand bed in use, sampled during filter inspection; 5 - fresh gravel

As the sieve analysis curve indicates (Fig. 1. curve 4), the sample collected from the inside of the filter (layer I) is characterized by more fine particles than the fresh sand. The sieve analysis of fresh gravel for the II layer shows that 75% of particles belong to the size fraction 1.0-2.0 mm which can be explained by the fact that the beds undergo size reduction when washed, due to friction, especially in the fluidal state. Overturbulent conditions during washing of the filters caused by e.g. excess of the air forced, result in mixing layers I and II, which significantly increased the presence of the 0.355 – 1.0 mm size fraction in layer I. In the sample collected between the filter and the aerator the amount of the 1.0-2.0 mm size fraction present is characteristic to that of the II layer and confirms mixing of the layers during the process of filter washing. Due to the lack of possibility of collecting a representative sample from the layers II and III the current particle distribution in these layers has not been presented.

PHYSICAL AND CHEMICAL ANALYSIS OF WATER

Physical and chemical testing included swimming pool water before filters, water after filtration and washing water from 3 filters. The water samples were collected shortly before filter washing. The average tests results are presented in the table 1. The data indicates the proper functioning of the filters. TOC of water after passing through the filters decreases from 3.0 mg/dm^3 to 2.7 mg/dm^3.

The redox potential increases due to the increase of chlorine concentration to 0.6 mg/dm^3 which, after mixing with the water in the swimming pool, decreases to the acceptable level. Variable value of TOC in the washings for each of the filters indicates indirectly their non-uniform load. It is important to observe a similar tendency with regard to the general nitrogen content, as well as the total inorganic carbon (TIC).

The presence of fine sand particles in the layer I, has been observed in the filter 1, which translates into a better filtration effect. More suspended organic matter has been stopped in layer I than in the two remaining filters (see derivatographic results). In the filter 3 the thickness of the layer I was 25% lower than in the filter 1.

Table 1. Physical and chemical parameters for investigated indoor rehabilitating swimming pool

Water sampling location	Water temperature (°C)	Free chlorine level [mg/dm^3]	pH	Redox potential [mV]	TOC [mg/dm^3]	TIC [mg/dm^3]	TN mg/dm^3]
Tap water	18	0.0	7.8	-469	1.2	29.1	-
Before filters	32	0.1	6.9	-521	3.0	34.3	0.2
Washing water from filter 1	30	2	8.1	-864	8.3	40.9	0.4
Washing water from filter 2	28	2	8.3	-813	5.5	30.7	0.1
Washing water from filter 3	30	2	8.2	-750	4.8	40.7	0.3
After filters	33	0.6	7.8	-898	2.7	38.1	0.1

In filter 2. the sand level in layer I was similar to the level in filter 1, with aprox. 30% more of finer particles (in the range 0.7-1 mm). During the testing and sampling period, the users of the swimming pool were infants with their parents, therefore, the water temperature in the pool was high, at 32°C. With respect to swimming pool activities for infants the level of free chlorine was decreased to 0.1 mg/dm^3 while its concentration for the other age groups should be 0.5 mg/dm^3.

In tap water chlorine amount remained below the detection limit. Prior to washing the filters swimming pool water was subjected to chlorination up to the value of 2 mg/dm^3.

Swimming pool water pH was too low (according to the recommendation it should be 7.2-7.6), while filter washing water pH was 8.1-8.3 (due to the addition of carbonate with coagulant to raise the pH). The value of the redox potential correlates well with the level of water contamination. After filtration and chlorination redox potential level reached almost -900 mV.

THERMOGRAVIMETRY (TG) AND DIFFERENTIAL THERMAL ANALYSIS (DTA) OF FLOCKS

When heating deposit samples, loss of mass (TG curve) has been observed – whereas for the investigated system there was no increase of mass - and heat emission (exothermic reactions) or heat release (endothermic reactions) (DTA curve). The result of this measurements are presented as two curve pairs, see Fig. 3. The obtained TGA curves show that flocks are degraded thermally in three steps, which could be attributed to dehydration, fragmentation of the macromolecular structure which is probably the main thermal degradation step, and the carbonization of the product to ash. The investigation of the deposits from the washing of the filters 1 and 3 indicate similar content of organic suspended matter in both quantitative and qualitative respect.

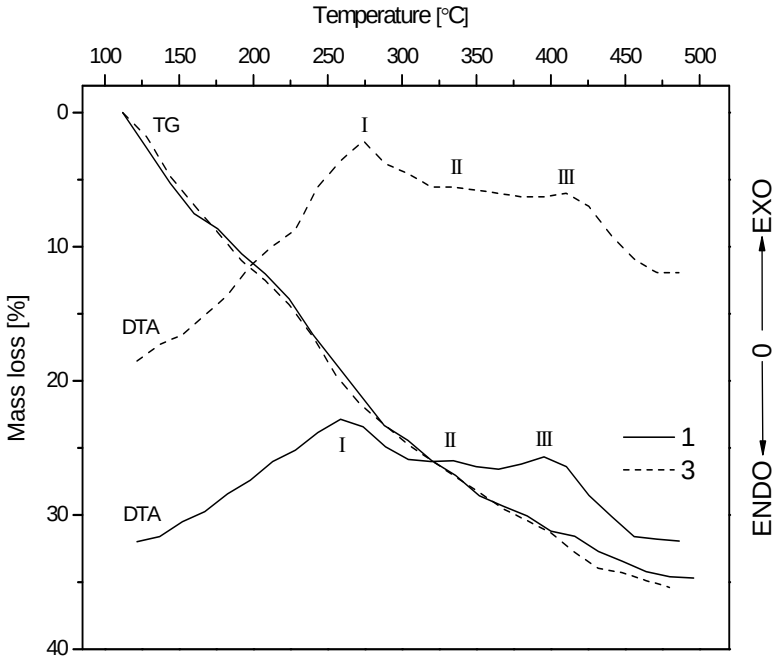

Fig. 2. TG and DTA curves of flocks washed from filter 1 and 3

As summarized in Table 2, water content of samples amounted from 7.4 to 11.7 weight %. The average loss of mass in the range of temperature 105-460°C amounted to 32.4 %. In none of the investigated samples the loss of mass over > 460°C has been observed. In the DTA curves 3 maxima are observed. In both sediment samples a strong maximum I has occurred – for filters 1 and 3 at 256°C i 272°C. Very weak maximum II corresponds to temperatures 344 and 365°C respectively. The third, more pronounced, maxima occurred at 400°C and 408°C.

From the course of DTA curves one can speculate that more fine particles including microorganisms have been captured by filter 1.

Table 2. Results of thermal analysis of flocks backwashed from filters

Flocks from	TG Curves			DTA Egzothermic Effects Maximum		
	Moisture 20-105°C	Mass Loss 105-460°C	Mass Loss > 460°C	I	II	III
Filter No. 1	10.1 %	32.9 %	0 %	256°C strong	344°C weak	400°C medium
Filter No. 3	7.4 %	31.4 %	0 %	272°C strong	365°C very weak	408°C weak

PARTICLE SIZE DISTRIBUTION OF FLOCKS

The investigation of particle size distribution of flocculated sediment washed from the filters indicates a significant range of flock size. Under the microscope it can be observed that there are numerous impurities trapped in the structure of the flocks among them bacteria and protozoa, but also fibrils and mineral particles. The adhesion forces of contaminants into the precipitated aluminum hydroxide flocks with positive surface charge result mainly from interaction with negatively charged particles. The interactions are weak which is clearly seen in Figure 3.

The plot in Figure 3 shows the size of particles analyzed by laser diffraction particle sizing instrument. The dashed line represents the particle size in sediment at the beginning of the measurement. The solid line represents the particle size after 85 minutes circulation through the measuring cell. Both lines show multimodal shape. Comparing both curves determined at the interval of several minutes one can observe that the size distribution of the particles varies as the suspension is the subjected to shear stress mainly in the pump. The measurement results indicate the need for the washing process of the sediments from the bed to be carried out by the rather low flowrate of water, which in fact, does not necessarily take place in practice, because of substantial turbulence of flow caused by the addition of compressed air.

On the curves 1 and 2 one can observe 3 maxima, corresponding to the medium size of particles in the size fractions 1.5-3 μm and 15-22 μm, 30 μm and 300-400 μm. The finest particles are bacteria, whereas the content of the particles 15-30 μm indicates the presence of fine flocks, resting spores, protozoa and even fragments of fibers (visible under the microscope, Fig. 4). The presence of stress in the suspension leads to both aggregation and degradation of already formed aggregates.

Figure 4 presents dried sediment, previously thickened in a centrifuge. The picture shows hair and synthetic fibrils, which also contribute to the presence of organic components in the sediment, see DTA curve in Figure 2.

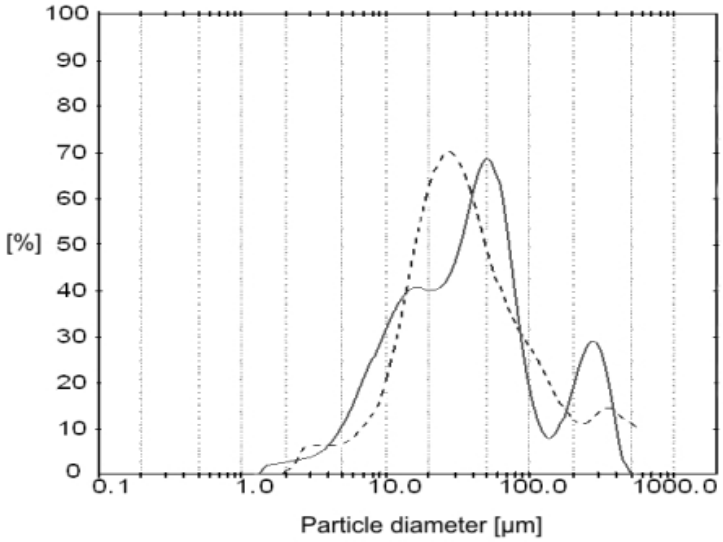

Fig. 3. Particle size distribution of flocks washed out from filter 1, Mastersizer X 1.2-600 µmlens; (dashed line – at the beginning, solid line – after 85 minutes of circulation)

Fig. 4. Sediment from backwashing filters – in the form of dried broken cake. Magnification 40x

FINAL COMMENTS

The quality of water in the swimming pool is controlled mainly by the effectiveness of the filtration process and by the intensity and frequency of back

washing the filters. Swimming pool water contains a number of both dissolved and suspended impurities which in the consequence of coagulation are captured within the bed and in the process of washing are removed. The choice of filtration bed is of crucial importance.

The content of total organic carbon varied depending on the location of the water sampling point. Variable value of TOC in the washings for each of the filters indicates indirectly their non-uniform loading. The important observation is a similar trend with regard to the content of total nitrogen, as well as total inorganic carbon (TIC).

The suspensions stopped in the bed have polydisperse particle size distributions. Despite electrical attraction of positively charged coagulant flockes and negatively charged impurities the particle size in the suspension changes easily as a result of shear stress.

The derivatographic investigation has indicated approximately 30 % participation of organic substances in the sediment washed out from the filters. From the DTA curves can be read the diversification of contamination content, stemming from the presence of microorganisms, including bacteria, protozoa, and minute organic impurities.

The performance of sieve analysis of sand collected from the functioning filter, and from the fresh bed (reserve) allows to estimate the correctness of operation of water treatment system and anticipate the effectiveness of the process of water treatment.

ACKNOWLEDGEMENTS

This research was partially supported by the Voivodeship Fund for Environmental Protection and Water Management, grant No. RX-10/2009, and the Gdansk University of Technology, contract DS No. 014668/03.

REFERENCES

BARBOT E., MOULIN P. (2008), *Swimming pool water treatment by ultrafiltration–adsorption process,* J. Membr. Sci., 314, 50–57.

CROLL B. T., HAYES C. R., MOSS S. (2007), *Simulated Cryptosporidium removal under swimming pool filtration conditions,* Water Environ. J., 21(2), 149-156.

DIN Standard 19643, 1997.

GLAUNER T., KUNZ F., ZWIENER C., FRIMMEL F.H. (2005), *Elimination of swimming pool water disinfection by-products with advanced oxidation processes (AOPs)*, Acta Hydroch. Hydrob., 33 (6), 585−594.

HAMEIRI Z., SPOONER T., SPROUL A.B. (2008), *High efficiency pool filtering systems utilising variable frequency drives*, Renew. Energ., 34(2), 450-455.

HOBBY R., HAGMEYER G., LANGE B., GIMBEL R. (2004), *Einsatz einer Ultrafiltrationsanlage im Pilotmaßstab zur Schwimmbadwasseraufbereitung*, GWF*, Wasser-Abwasser*, 145 (10), 700–705.

HUPKA J., KORKOSZ A. (2009), *Fizykochemiczne podstawy uzdatniania wody w basenach kąpielowych*, Proceedings of V Ogólnopolska Konferencja Szkoleniowa Baseny Polskie 2-3.04.2009 Warszawa, 87-94.

JUDD S.J., BLACK S.H. (2000), *Disinfection by-product formation in swimming pool waters: a simple mass balance,* Water Res., 34(5),1611-1619.

JUDD S.J., BULLOCK G. (2003), The *fate of chlorine and organic materials in swimming pools*, *Chemosphere*, 51 (9), 869-879.

NEMERY B., HOET P. H. M., NOWAK D. (2002), *Indoor swimming pools, water chlorination and respiratory health*, Eur. Resp. J., 19, 790-793.

LAHL U., BATJER K., DUSZELN J.V., GABEL B., STACHEL B. (1981), *Distribution and balance of volatile halogenated hydrocarbons in the water and air of covered swimming pools using chlorine for water disinfection,* Water Res., 15(7), 803-814.

PANYAKAPO M., SOONTORNCHAI S., PAOPUREE P. (2008), *Cancer risk assessment from exposure to trihalomethanes in tap water and swimming pool water,* J. Environ. Sci., 20(3), 372-378.

PIECHURSKI F.G., WYCZARSKA-KOKOT J., NIESŁAŃCZYK J., *Porównanie jakości wody z charakterystycznych punktów obiegów basenowych*. In: Kuś K., Piechurski F., Instalacje basenowe, Gliwice 2009, 135-156.

REIßMANN F.G., SCHULZE E., ALBRECHT V. (2005), *Application of a combined UF/RO system for the reuse of filter backwash water from treated swimming pool water*, *Desalination*, 178, 41-49.

SUGIMOTO A. (1997), *Ceramic filter filtration apparatus for purifying swimming pool water*, U.S. Pat. No. 5632890.

WYCZARSKA-KOKOT J., PIECHURSKI F. (2002), *Ocena skuteczności filtracji wody i jakości wód popłucznych w instalacjach basenowych,* Ochr. Środow., 1(84), 33-36.

Korkosz A., Janczarek M., Aranowski R., Rzechuła J, Hupka J., *Efektywność filtracji wgłębnej w oczyszczaniu wody basenowej,* Physicochemical Problems of Mineral Processing, 44 (2010), 103-113, (w jęz. ang), http://www.minproc.pwr.wroc.pl/journal

Przebadano efektywność filtracji wody w filtrach ze złożem żwirowo-piaskowym w instalacji basenu rehabilitacyjnego. Obok analizy instrumentalnej wody, w badaniach uwzględniono rozkład wielkości cząstek i analizę termiczną osadu zgromadzonego w złożu piaskowym filtrów wgłębnych i usuwanego podczas płukania. Zmienna wartość TOC w popłuczynach dla każdego z filtrów wskazuje pośrednio na nierównomierne ich obciążenie. Wykazano, że wielkość cząstek w zawiesinie łatwo zmienia się w wyniku działania naprężeń ścinających. Badania derywatograficzne wskazały na około 30% udział substancji organicznych w osadzie. W żadnej z badanych próbek, nie zanotowano ubytku masy powyżej >460°C.

słowa kluczowe: basen, filtracja wgłębna, rozkład wielkości cząstek, analiza termiczna

Physicochem. Probl. Miner. Process. 44(2010) 115-126

journal homepage
www.minproc.pwr.wroc.pl/journal/

Physicochemical Problems of Mineral Processing

Index No. 32213X ISSN 1643-1049

P. B. Kowalczuk*, T. Chmielewski**

CHANGES OF ELECTRODE POTENTIAL IN THE NON-OXIDATIVE LEACHING

Received May 16, 2009; reviewed; accepted July 30, 2009

Simultaneous measurements of pH and redox potential using a platinum electrode as well as potential of copper sulphide electrodes during non-oxidative leaching of Lubin shale middlings with sulfuric acid have been applied to determine leaching kinetics and to evaluate its electrochemical parameters as well as to assess the changes taking place at the mineral/solution interface during leaching process. Significant decrease in both redox potential of the solution (from +350 mV to +50 mV, Ag,AgCl) and potential of mineral electrodes were observed with increasing pH during carbonate decomposition with sulfuric acid. It is therefore concluded that the low value of red-ox potential is a parameter preventing oxidation of copper sulphide minerals present in leached material and prevents the transition of Cu and Fe to the solution. It was found that the non-oxidative leaching is a rapid and selective process, resulting in decomposition of calcium and magnesium carbonates and in saturation of the leaching slurry with carbon dioxide. It was recognized that with the increasing degree of carbonate decomposition from 50 to 100 % metals-bearing minerals liberation has remarkably improved, which beneficially facilitates and intensifies further upgrading or leaching processes.

key words: electrode potential, pH, leaching, sulphides

INTRODUCTION

Electrochemical monitoring of leaching process by means of redox potential using platinum and mineral electrodes prepared from copper sulfides is a

* Laboratory of Mineral Processing, Institute of Mining Engineering, Wroclaw University of Technology, 50-370 Wroclaw, Poland, e-mail: przemyslaw.kowalczuk@pwr.wroc.pl

** Division of Chemical Metallurgy, Faculty of Chemistry, Wroclaw University of Technology, 50-370 Wroclaw, Poland, e-mail: tomasz.chmielewski@pwr.wroc.pl

very important scientific and particle issue. This paper presents and discusses the use of pH and electrode potential measurements to monitor leaching kinetics of the Lubin shale middlings with H_2SO_4.

PRINCIPLES OF NON-OXIDATIVE LEACHING

Acidic non-oxidative leaching of the copper shale fraction is based on the chemical reactions of sulfuric acid with calcium and magnesium carbonates. The carbonate minerals are the main component of the hydrophilic gangue which forms intergrowths and impregnations with copper sulfides or creates hydrophilic ultra-fine slimes on the surface of metal sulfides. The small size of the leached solid particles enhances the rate of leaching. The following chemical reactions describe non-oxidative leaching:

$$CaCO_3 + H_2SO_4 + H_2O \rightarrow CaSO_4 \cdot 2H_2O \downarrow + CO_2 \uparrow \quad (1)$$

$$MgCO_3 + H_2SO_4 \rightarrow MgSO_4 + CO_2 \uparrow + H_2O\,. \quad (2)$$

Hydrated calcium sulfate (gypsum) is solid reaction product. Water-soluble magnesium sulfate and gaseous carbon dioxide are two other products. Due to fine particle distribution of middlings, the leaching of carbonate gangue with H_2SO_4 appeared to be very rapid and can be easily performed at ambient temperatures in reactors with mechanical stirring of a standard construction (Chmielewski, 2007a, 2007b).

The amount of H_2SO_4 applied in non-oxidative leaching directly corresponds to the content of carbonates and must be precisely controlled to maintain the final pH of the pulp at a level enabling its direct transfer either to the flotation circuit without pH correction or to the leaching and/or bioleaching. Therefore, for the further flotation, the amount of sulfuric acid introduced to the leaching operation should be always kept below the analytically determined maximum amount of acid required for total decomposition of carbonates ($z^{max}_{H_2SO_4}$). The maximum demand for acid ($z^{max}_{H_2SO_4}$) is the mass of pure H_2SO_4 necessary for the total decomposition of carbonates in 1 kg of a dry solid feed. $Z^{max}_{H_2SO_4}$ should be determined analytically in laboratory tests.

H_2SO_4 is frequently introduced to the reactor containing shale slurry at a rate that assures total acid utilization in leaching. Usually, 70-80 % of determined $z^{max}_{H_2SO_4}$ was applied in leaching, maintaining the final acidity of the slurry about at pH 5 or higher. This is the pH level that makes possible direct transfer of the slurry either to the flotation circuit without additional pH correction or to the leaching and/or bioleaching. If the residual solids are used for further atmospheric leaching, pressure leaching or bioleaching the amount of sulphuric acid exceeds the maximum demand to maintain pH at the required, acidic level.

Carbon dioxide, evolving in reactions (1) and (2), creates a favorable oxygen-free atmosphere in the leached slurry and prevents the undesirable digestion of sulphides of valuable metals (Cu, Pb, Zn, Ni, Fe). This remarkably minimizes the metal loses to the solution and simplifies the entire non-oxidative leaching process. Therefore, saturation of slurry with CO_2 assures the selectivity of carbonate leaching. This was confirmed by the chemical analyses of the wastewater during numerous laboratory tests.

Selectivity of carbonate leaching from a flotation feed is, according to the proposed method, particularly beneficial for the process and guarantees chemical stability of metal sulfide minerals. Noticeably beneficial effects of the leaching with H_2SO_4 on subsequent flotation of copper ores were already observed during comprehensive laboratory investigations and several pilot plant tests with various flotation feeds from Lubin and Polkowice concentrators (Łuszczkiewicz and Chmielewski, 1999, 2006, 2008; Chmielewski et al., 2007, 2008).

The acidic non-oxidative leaching of the carbonate-containing flotation feed resulted in the apparent decomposition of solid particles by means of selective, chemical process which precisely and economically liberated sulfide minerals. Under oxygen-free conditions all metal sulfides remain chemically stable and susceptible for flotation. This selective "chemical grinding" is very efficient particularly for fine intergrowths, which can not be broken up with typical mechanical grinding. High selectivity and low energy consumption are, therefore, additional beneficial factors of this process (Łuszczkiewicz and Chmielewski, 1999, 2006).

The purpose of this paper was to evaluate the effect of non-oxidative leaching on both the redox potential in the slurry measured by means of Pt electrode and potential of copper sulphide electrodes made of minerals contained in the leached Lubin middlings. These potentials were compared with potentials recorded in the presence of oxygen and iron(III) ions.

EXPERIMENTAL AND MATERIAL

The feed material used in laboratory experiments on non-oxidative leaching was shale containing middlings – tailings from 1st cleaning flotation 1st circuit at Lubin Concentrator (ZWR Lubin). Chemical composition of the solid is given in Table 1. The high content of organic carbon in middlings (~ 9 %) and observed close correlation between metals concentration and organic carbon content make the Lubin middlings a shale concentrate.

Table 1. Chemical composition of Lubin middlings (tailings of 1st cleaning)

CONTENT					
Cu, %	Fe, %	Ni, g/t	Co, g/t	Pb, %	As, %
2.72	1.76	374	572	1.51	0.09
CONTENT					
Ag, g/t	Zn, g/t	S_c, %	Sso_4, %	C_{total}, %	C_{org}, %
190	1 200	2.95	1.45	14.30	8.96

Very high content of carbonate matter in the middlings corresponds to utilization of 497 g H_2SO_4/kg of dry solid for total decomposition of carbonates. Any leaching or bioleaching unit operation taking place under acidic conditions requires previous non-oxidative leaching with acid in order to totally decompose of acid consuming components. Non oxidative leaching can also facilitate further upgrading by flotation or gravity methods as well as subsequent bioleaching or chemical leaching.

RESULTS AND DISCUSSION

Measurements of the potential, along with pH, during the sulfuric acid leaching under non-oxidative conditions were applied for identifying and evaluating possible changes taking place in the electrochemical parameters of the solid/solution interface during the process. It was expected that as a result of carbonate decomposition with sulfuric acid significant decrease of the potential of Pt and sulphide mineral electrodes in the leaching solution will be exhibited. The changes of electrode potential are mainly caused by the removal of oxygen from the solution and by the saturation with carbon dioxide. Non-oxidative leaching created in the course of the process can be monitored electrochemically.

Initially, the redox potential measurements with Pt electrode (versus Ag, AgCl reference electrode) were applied in order to assess changes in the magnitude of this potential as a result of saturation of leached suspension with carbon dioxide. The potential was recorded with time simultaneous with pH changes of leached solution (Fig. 1). Potential – time and pH – time relationships allow to determine the kinetic of reaction and to monitor the electrochemical conditions during the process of leaching.

Beginning of leaching was controlled after the introduction of sulfuric acid to the solution. In the leaching process the pH was observed to increase, while decrease of the potential of Pt and mineral electrodes was recorded. Both of these parameters characterized the rapid process of carbonate decomposition under non-oxidative conditions.

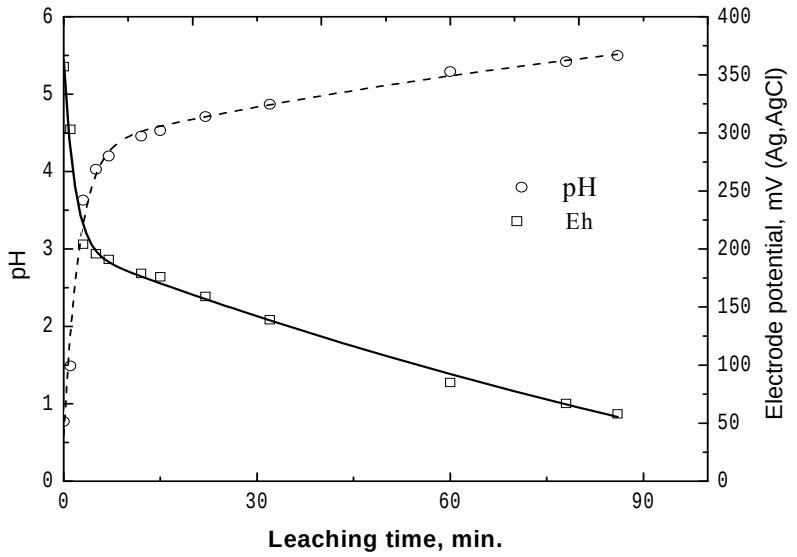

Fig. 1. pH and electrode potential vs. leaching time for non-oxidative leaching of Lubin middlings for 70 % of carbonate decomposition

Leaching process leads to significant changes in electrochemical properties in the solution. During the initial few minutes of leaching a sharp decrease in the potential of platinum electrode by about 150 mV took place with further decrease at the end of the experiment (Fig. 1). Over the whole testing period Pt electrode potential decreased markedly for different degrees of carbonate decomposition from +350 mV to +50 mV (Ag, AgCl).

Table 2. Chemical composition of Lubin shale middlings after non-oxidative leaching at different degree of carbonate decomposition (R_w) with H_2SO_4

Carbonates decomposition R_w, %	Cu, %	Fe, %	Ag, g/t	Ni, g/t	Co, g/t	Zn, g/t	C_{org}, %	As, %
0	2.60	1.890	168	328	613	740	6.30	0.085
30	2.50	1.760	165	325	605	690	6.52	0.080
50	2.52	1.789	162	315	603	660	6.52	0.086
70	2.30	1.648	157	326	588	660	6.54	0.073
90	2.52	1.717	168	327	606	720	6.49	0.088

After the consumption of all the available acid, subsequent changes in pH values resulted only from the saturation of the solution with carbon dioxide, and at this stage of tests, the process of non-oxidative leaching was considered to be complete. The observed low potential of red-ox electrode, prevented oxidation of sulphide minerals

present in leaching material and prevented the transfer of metal ions (mainly Cu and Fe) into the solution. This was also confirmed by chemical analysis of the material from non-oxidative leaching (Table 2).

The potential – pH curve in Fig. 2 shows the good correlation between the red-ox potential and pH of the solution during the 90 minutes of non-oxidative leaching. It may be found that with increasing pH, the potential for leaching decreases over the leaching time, which is the result of the saturation with carbon dioxide. A similar effect is obtained for all degrees of carbonate decomposition in the range of 30 – 90 %. The control of non-oxidative leaching can be therefore performed by monitoring two independent parameters – pH and redox potential.

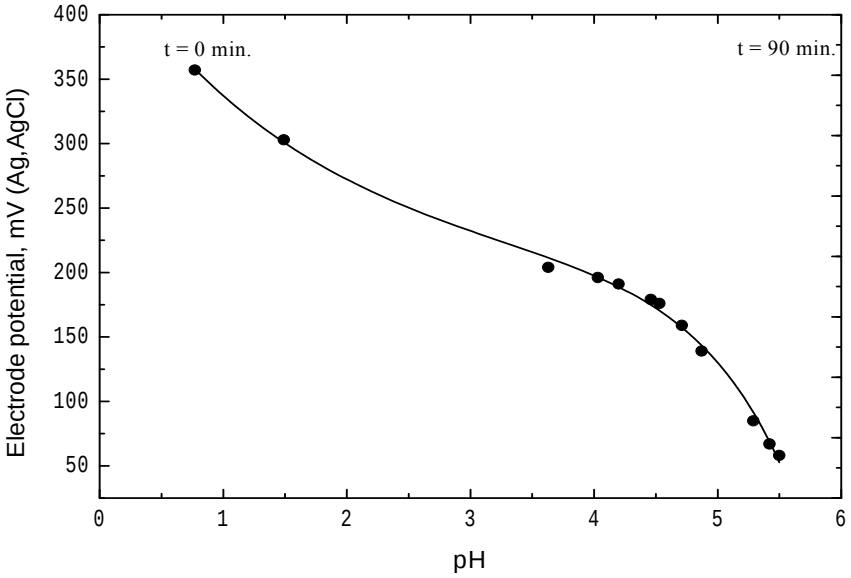

Fig. 2. Electrode potential vs. pH for non-oxidative leaching of Lubin shale middlings for 70 % of carbonate decomposition

It is possible that significant decrease of redox potential observed in non-oxidative leaching with sulfuric acid, may result in reductive decomposition of copper sulphide minerals, and in the evolution of hydrogen sulphide (H_2S). However, this unwanted reaction product was not detected, confirming the absence of the reaction (3) of cathodic reduction of chalcocite to metallic copper in the leaching process under non-oxidative condition

$$Cu_2S + 2H^+ + 2e^- = 2Cu^0 + H_2S\uparrow . \quad (3)$$

The presence of hydrogen sulfide in the leaching tests was not confirmed for any of the sulphide minerals contained in Lubin middlings leached with sulphuric acid.

From the E-pH diagram for the Cu-S-H_2O system (Fig.3) (Goodenough et al., 1988) it can be seen that the formation of hydrogen sulfide in a reduction reaction (3)

within the pH range of 0 - 2 is possible only below the potential of about - 250 mV (SHE), while the anodic movement of copper to the solution in the form of Cu^{2+} is possible above + 350 mV. In the course of our study of non-oxidative leaching of Lubin middlings neither the top nor the bottom of the potential range was reached. Therefore, no danger of chemical decomposition of copper sulphides can be expected in this selective process.

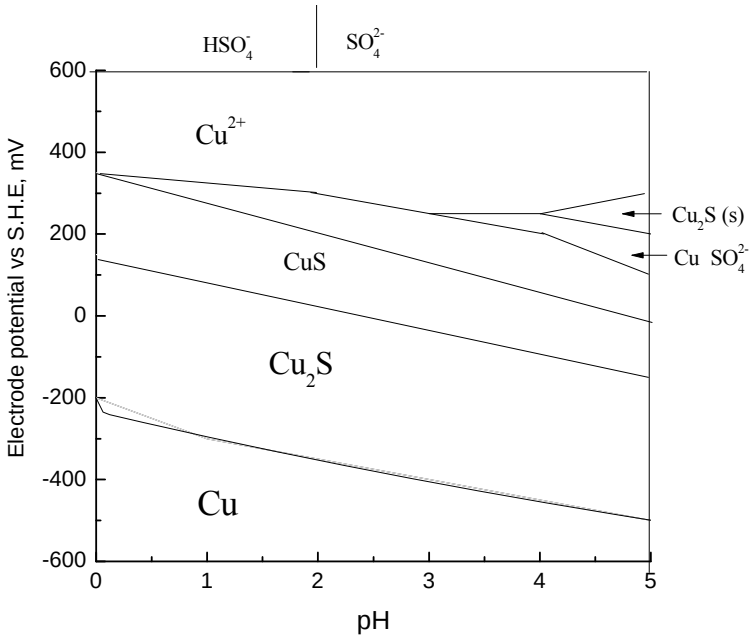

Fig. 3. E-pH diagram of Cu-S-H_2O system at 25 ^oC based on Goodenough et al., 1988

The behavior of sulphide minerals changes markedly in terms of their stability when oxidation agent (air, oxygen, iron(III) ions) is introduced to the solution. Copper ions are liberated into the solution as the process of anodic oxidation of sulphide minerals and cathodic reduction Fe(III) ions to Fe(II) takes place simultaneously, according to the following reaction:

$$MS + 2Fe^{3+} \rightarrow M^{2+} + 2Fe^{2+} + S^0 . \quad (4)$$

The effect of increase of Pt redox electrode potential and sulphide minerals electrodes is expected to be significant in the presence of oxidation agent. Consequently, metal ions concentration in the solution starts to increase as sulphides are subjected to leaching.

In our experiments, we have initially changed the conditions of leaching process, from non-oxidative to oxidative, by the introduction of gaseous oxygen into the leached slurry. Two types of reaction take place in the presence of oxygen. First is the leaching of copper sulphides according to reaction:

$$Cu_2S + O_2 + 4H^+ = 2Cu^{2+} + S^0 + 2H_2O. \quad (5)$$

The presence of oxygen initiates also the reaction of oxidation of Fe(II) ions to Fe(III):

$$2Fe^{2+} + \tfrac{1}{2}O_2 + 2H^+ = 3Fe^{3+} + H_2O, \quad (6)$$

and increase of the rest potential of electrodes was recorded. Changes in potential of electrodes (Pt red-ox electrode and mineral: bornite, chalcopyrite) are shown in Figs 4, 5, and 6 during the leaching process performed initially as non-oxidative (about 130 minutes) and then as oxidative , in presence of O_2 and Fe(III) ions.

As it was already shown (Figs 1 and 2), the electrode potential during non-oxidative leaching decreases rapidly with increasing pH. When non-oxidative conditions at total decomposition of carbonates were achieved, gaseous oxygen was introduced to the solution and increase of electrode potential (red-ox and minerals) occurred (Figs 4, 5, and 6). The observed increase in potential of the mineral electrode is a measure of changes in the conditions of the digestion of the mineral in the aqueous environment. The introduction of oxygen to the solution raises the value of bornite and chalcopyrite electrodes potential slightly above +300 mV, which corresponds to the area of sulphides digestion, even at small solubility of oxygen under examined acidic conditions.

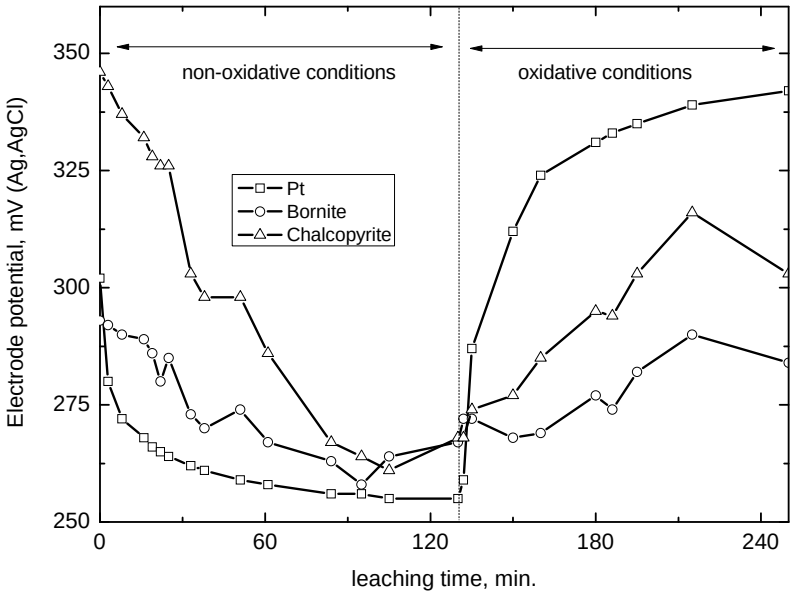

Fig. 4. Potential of electrodes vs. leaching time under non-oxidative and oxidative conditions (oxygen was introduced after 130 minutes) for total carbonate decomposition

More profound effect of potential raise was observed when Fe(III) ions were added to the leaching slurry (Fig. 5). Iron(III) is apparently the most efficient leaching agent in terms of reaction rate. Its presence evidently increases the potential of both Pt and chalcopyrite electrodes. Chalcopyrite exhibits the potential value slightly above + 400 mV, which is considerably higher when compared to that observed in the presence of oxygen. Similar effect was observed when bornite electrode was applied for electrochemical examinations (Fig. 6). The observed potential changes for Pt, chalcopyrite and bornite electrodes confirm that the iron(III) ions are significantly more effective leaching agent for copper sulphides than the oxygen. The presence of oxygen in leaching system together with Fe ions is necessary to regenerate Fe(II) to Fe(III) according to reaction (6).

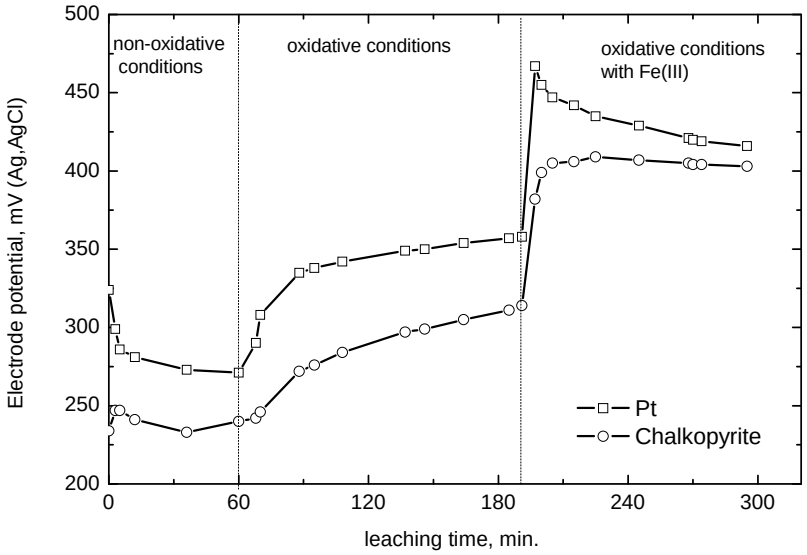

Fig. 5. Potential of Pt and chalcopyrite electrodes vs. leaching time in non-oxidative leaching and under oxidative conditions after introduction of oxygen (60 minutes) and in the presence of Fe(III) (20 g/dm^3). Total carbonate decomposition

Digestion of metal sulphide minerals in hydrometallurgical leaching processes follows the mechanism similar to corrosion and can be initially evaluated and compared using the E – pH diagrams. This electrochemical mechanism of leaching was previously studied for sulphides from Polish copper deposits (Chmielewski, 1982). Chalcocite and bornite were recognized as a easy-leached copper sulphides, whereas chalcopyrite – as the most refractory in terms of leaching rate. Therefore, sulphides exhibiting the highest rest potential in leaching media are more stable in terms of both thermodynamics and kinetics (FeS_2, FeAsS, $CuFeS_2$). Sulphides with lower rest potentials are much more easily leached (PbS, Cu_2S) (Ahonen, 2006).

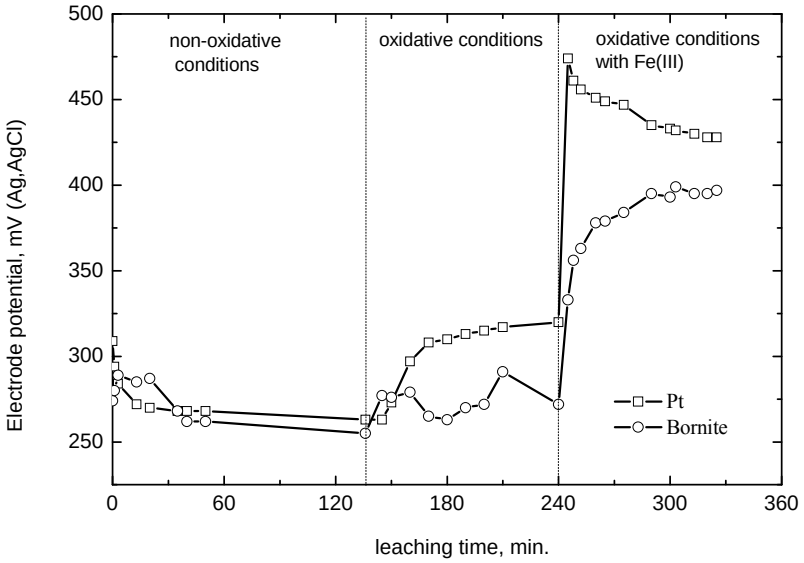

Fig. 6. Potential of Pt and bornite electrodes vs. leaching time in non-oxidative leaching and under oxidative conditions after introduction of oxygen (~ 130 minutes) and in the presence of Fe(III) (Initial concentration of Fe(III) – 20 g/dm^3). Total carbonate decomposition

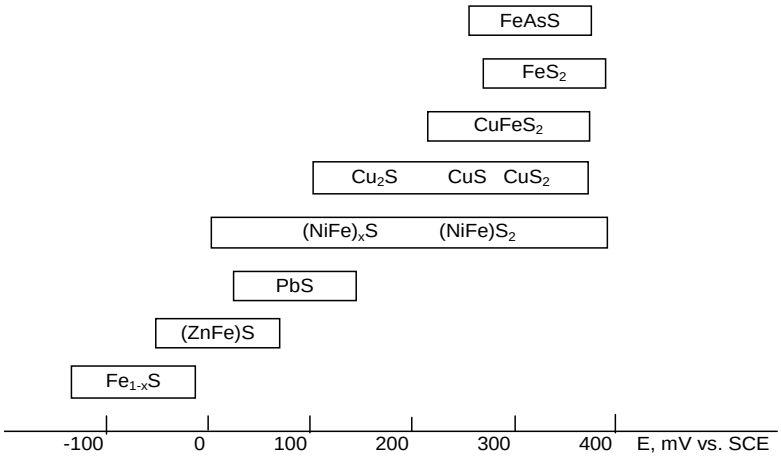

Fig. 7. The rest potentials of electrodes made of different sulphide minerals (Ahonen, 2006)

The ability of sulphides to dissolution under acidic conditions can also be characterized on the basis of a series of solubility discussed by Łętowski (1975):

increase the solubility of sulphides

Ag_2S, PbS, $CuFeS_2$, NiS, CuS, Ni_3S_2, FeS_2, Cu_5FeS_4, Cu_2S, ZnS

Therefore, from our leaching experiments and simultaneous measurements of electrode potentials it can be seen that the magnitude of sulphide rest potential is the measure of leaching susceptibility in acidic environment. Redox potential and potential of sulphide electrode can be also utilized as a way of monitoring of leaching conditions. This was confirmed by electrochemical tests presented in this paper (Figs 4 and 6).

CONCLUSIONS

Measurements of the redox potential by means of Pt electrode and the rest potential of natural copper sulphide electrodes is a good method of evaluation of copper leaching conditions, both non-oxidative and oxidative. The observed magnitudes of potential changes in non-oxidative acidic leaching, along with thermodynamic evaluation with E- pH diagrams indicate, that the leaching process is very selective and copper sulphides remain stable in terms of metals digestion. Introduction of oxygen leads to essential increase of electrodes potential to the region where metals dissolution starts. Most remarkable increase of electrodes potential can be observed when iron(III) ions are the leaching agent.

REFERENCES

AHONEN, L., 2006, *Biohydrometallurgy – electrochemical and thermochemical aspects, In: Perspectives for applying boleaching technology to process shale-bearing copper ores*, BIOPROCOP'06, Lubin 2006, KGHM Cuprum, Wroclaw 2006.

CHMIELEWSKI, T., 1982. *Intensification of leaching of copper sulphide concentrates In the light of electrochemical investigations*. PhD thesis, Wrocław University of Technology, 1982 (in Polish).

CHMIELEWSKI T., 2007a, Non-*oxidative leaching of black shale copper ore from Lubin Mine*, Physicochemical Problems of Mineral Processing, 41, 323-348.

CHMIELEWSKI T., 2007b, Atmospheric *leaching of shale by-product from Lubin concentrator*, Physicochemical Problems of Mineral Processing, 41, 337-348.

CHMIELEWSKI T., ŁUSZCZKIEWICZ A., KONOPACKA Ż., 2007, *Separation and concept of processing of black shale copper ore from Lubin mine*, Proc. VIII International Conference on Nonferrous Ore Processing, Wojcieszyce (Poland), May 21-23, KGHM Cuprum, Wroclaw 2007, 171-184 (in Polish).

CHMIELEWSKI T., LUSZCZKIEWICZ A. AND KONOPACKA Z., 2008, *Acidic pretreatment of hard-to-tread copper ore flotation middlings to facilitate flotation efficiency*, Proc. XXIV International Mineral Processing Congress, Beijing – China, Sept. 24-28 2008, vol.1, (Wan Dianzuo et al., Eds.), Science Press Beijng 2008, 1189-1200.

GOODENOUGH, M.R., KELSALL, G.H., LIANG, Z., 1988. *Electrochemical decomposition of covellite (CuS) particles in a bipolar packed bed electrode*. Electrochemistry in mineral and metal processing II.

LETOWSKI, F., 1975, *Principles of Hydrometallurgy* (Handbook), PWN Warszawa, (in Polish).

LUSZCZKIEWICZ A., CHMIELEWSKI T., 1999, *Acid treatment of copper sulfide concentrate in the flotation circuit*. Proceedings V International Conference of Nonferrous Ore Processing, Szklarska Poręba, 25-27.10.1999, Publ. CBPM Cuprum, IMN, 59-66.
LUSZCZKIEWICZ A., CHMIELEWSKI T., 2006, *Technology of chemical modification of by-products in copper sulphidic ore flotation systems.,* Rudy i Metale Niezelazne, R-51, Nr.1, pp. 2-10 (in Polish).
LUSZCZKIEWICZ A., CHMIELEWSKI T., 2008, *Acid treatment of copper sulfide middlings and rougher concentrates in the flotation circuit of carbonate ores*, Int.J.Min.Process 88 (2008) 45-52.

Kowalczuk P., Chmielewski T., *Zmiany potencjału elektrod podczas ługowania nieutleniającego*, Physicochemical Problems of Mineral Processing, 44 (2010), 115-126 (w j. ang)
http://www.minproc.pwr.wroc.pl/journal

Pomiary pH i potencjału redox (za pomocą elektrody platynowej) podczas nieutleniającego ługowania kwasem siarkowym pozwalają równocześnie określić kinetykę oraz zmiany parametrów elektrochemicznych zachodzących w roztworze podczas prowadzonego procesu. W czasie rozkładu węglanów za pomocą kwasu siarkowego zaobserwowano w roztworze ługującym znaczny spadek potencjału redox roztworu (od +350 mV do +50 mV, względem elektrody Ag,AgCl) przy jednoczesnym wzroście pH. Tak niskie wartości potencjału red-ox uniemożliwiają utlenianie siarczkowych minerałów miedzi obecnych w ługowanym materiale i przechodzenie metali do roztworu. Stwierdzono, że ługowanie nieutleniające jest procesem szybkim i selektywnym, powodując wyłącznie rozkład węglanów wapnia i magnezu. Uznano, że w miarę zwiększenia stopnia rozkładu węglanów wzrasta udział uwolnionych ziaren minerałów użytecznych, co ułatwia i intensyfikuje dalsze procesy wzbogacania lub ługowania.

słowa kluczowe: potencjał elektrody, pH, ługowanie, siarczki

Physicochem. Probl. Miner. Process. 44(2010) 127-142

journal homepage
www.minproc.pwr.wroc.pl/journal/

Physicochemical Problems of Mineral Processing

Index No. 32213X ISSN 1643-1049

I. Kursun*

DETERMINATION OF FLOCCULATION AND ADSORPTION-DESORPTION CHARACTERISTICS OF Na-FELDSPAR CONCENTRATE IN THE PRESENCE OF DIFFERENT POLYMERS

Received March 15, 2009; reviewed; accepted July 1, 2009

Feldspars are among the most important mineral groups on the earth. Although the group of feldspar has 20 minerals, only nine of them are well known. These minerals make up the largest percentage of minerals in nature. Esan albite beneficiation plant faces serious disposal problems in dewatering the minus 20 μm albite concentrate. Flocculation studies conducted with albite in the presence of various charged and nonionic polymers indicate that nonionic polymers exhibit the best performance. Electrokinetic studies on pure albite shows that it is negatively charged throughout the entire pH and the isoelectric point of the mineral is below pH 2. Adsorption of the nonionic polymer (N-300) is found to increase with increasing pH and concentration of the polymer. A hydrogen bonding mechanism between the polymer carbonyl (-C=O) or the amide ($-NH_2$) groups and the surface oxygen species is proposed to be responsible for the adsorption of nonionic polymer onto albite.

key words: albite, flocculation, zeta potential, adsorption, nonionic polymer

INTRODUCTION

For several decades, inorganic electrolytes, natural polymers and synthetic, high molecular weight polymers have been used as coagulants or flocculants for clarification of effluents, acid mine drainage and treatment of paper, textile, sugar and

* Istanbul University Mining Eng Depart, Avcılar-Istanbul-Tukey, e-mail: ilginkur@istanbul.edu.tr

other industrial waste water processing applications. Research has shown that interactions between the functional groups on particulate surfaces and those on polymers are responsible for adsorption and subsequent flocculation, and can be appropriately controlled by tailoring polymers with specific functional groups suitable for particular applications. The effectiveness of a polymer for a given flocculation system depends on several parameters, e.g. the polymer dosage, amount adsorbed on the solid surfaces, molecular weight of the polymer, particle size, shape, porosity, ionic strength of the system, electrokinetic properties and more importantly, conformation of the polymer at the solid-liquid interface. According to desorption tests, no significant change was observed for the albite-non-ionic polymer system.

Polymer molecules can be made to selectively adsorb onto particles by a) adjusting the chemical composition of the suspending media, b) introducing into polymer, active functional groups that will form complexes or salts with the metal atoms on the surfaces of the desired minerals, and c) using depressants, such as sodium silicate, that would adsorb on the undesired mineral surface, thereby preventing adsorption of the polymers by using activators that induce adsorption of polymers on desired minerals (Akers, 1975). Adsorption of polymers on solid surfaces is dependent on polymer properties, such as molecular weight and configuration, distribution of functional groups, solid properties, such as surface charge and oxidation states, and solution properties such as ionic strength, temperature and solvent power for the polymer. The various forces responsible for the adsorption of the polymers on the mineral surfaces result primarily from three types of bonding, namely electrostatic, hydrogen and covalent bonding. The solution-chemistry conditions, the rheology of the solid suspension and the polymer properties dictate the nature of interactions (Chou and Wollast. 1985).

Often several mechanisms may be operating at the same time controlling the adsorption/flocculation behaviour system. Long chained polymers can be adsorbed onto the grains from several locations along the chain in a single polymer molecule and can also be adsorbed onto more than one grain. in such cases, the grains are bridged by the adsorbed polymers. This mechanism plays an important role in a number of applications. In order for the bridging flocculation to form, the polymer should be of large molecular weight, and a large part of the polymer chain should be adsorbed without interaction with the grain surface. Moreover, the adsorbed amount should not be high, so that a larger part of the grain surface remains free (Çelik et al., 1991). Only in such a case, the free part of the grain surface and extended part of the polymer that is adsorbed onto another grain come into mutual contact. When over-adsorption of a polymer occurs, there remains no free surface for bridging to take place, and bridging is further prevented because of steric impulsion. Therefore, in order for bridging flocculation to occur, there is an optimum polymer dosage, the value of which depends generally on grain concentration.

Albite ($NaAlSi_3O_8$), one of the minerals in the plagioclase feldspars series, is characterized by a lustre appearance with white and grey colours, less frequently greenish and yellowish (Potter, 1985). Albite is usually found together with quartz, mica, and sometimes iron oxides, rutile, and tourmaline. Feldspars is principally used in the manufacture of glass and ceramics as a flux or source of alumina. Beneficiation of albite is primarily accomplished by a number of separation methods including magnetic, electrostatic and flotation. Although the concentration scheme is usually dependent on the quality of the end product, flotation is almost invariably the most popular beneficiation method. While anionic collectors such as oleic acid is used to collect colored impurities, e.g., iron oxides and rutile, cationic collectors are used to float feldspar at pH 2 while depressing quartz with HF (Hill et al., 1969; Warren, Kitchener, 1972). Important reserves of feldspar ores are available in western Turkey. Turkish feldspars, especially albite, contain relatively high levels of TiO_2 and Fe_2O_3 as their main impurities. Mineralogical investigations on the main ores show mainly albite and quartz, mica and microcline with secondary minerals such as anatase, rutile, ilmenite, sphene, magnetite, hematite, limonite, epidote, grona, biotite, phlogopite, pyrite and zirconium minerals (Kangal et.al.1998, 2001)The largest feldspar reserves of Turkey are located in the Çine-Milas district. Çine-Milas has significant quantities of albite with much as 400 million tons of reserves represented with average qualities (Kangal et al. 2001) Esan-Eczacıbaşı Milas Albite concentrator produces glass and ceramic quality albite with a production capacity of 150,000 Mg/g. The ore is reduced to -0.5 mm in size and a fatty acid type collector is used to float the color impurities at pH 8-10. The minus 0.5 mm flotation concentrate is then passed through a combination of hydrocyclone/spiral c1assificator to obtain three products, i.e. 0.5x0.1 mm,0.lx0.02 mm and -0.02 mm. The latter two products are fed into the settling cones where the solids is densified with the aid of flocculants followed by dewatering by di sc filters. The overt1ow is recirculated back to the plant after it is clarified.

Investigations in the plant have revealed that the flocculation regime used in the dewatering circuit is not appropriate and thus leads to slow settling rates and in turn to inefficiencies in the plant operation. No literature of relevance was found on the subject of albite flocculation. It is therefore the objective of this study to test the performance of various acrylamide based polymers in settling the minus 20 μm albite concentrate and find out the optimum operating conditions. Towards this aim, a systematic study has been also initiated to understand the way albite interacts with nonionic polymer (Kursun, 2000).

EXPERIMENTAL

MATERIALS

The sample used in the flocculation tests was collected from the fine (-20 μm) settling cone product in the Esan-Eczacibaşı Albite concentrator. The chemical composition of the sample is presented in Table 1. Ultrapure albite crystals received from the same deposit was ground in an agate mortar to obtain a sample of -74 μm in size. This sample was used for both adsorption and zeta potential measurements. While experiments associated with pure albite were conducted in distilled water, the actual plant water was used in the flocculation tests.

Table 1. Analysis of -20μm albite concentrate

Item	Weight %
SiO_2	71.9
Al_2O_3	17.6
Na_2O	9.8
K_2O	0.3
TiO_2	0.07
Fe_2O_3	0.14
CaO	0.10
MgO	0.20

The anionic (A-120, A-95, and A-130), cationic (C521), and nonionic (N-I00, N-200 and N-300) flocculants were all received from Cytec Industries Inc. and specified to have molecular weights of $3\text{-}15x10^6$, $3\text{-}4x10^5$, and $3\text{-}4x10^6$, respectively. Tannic acid, NaCl, NaOH and HCl were all Fluka made certified chemicals.

METHODS

The flocculation tests were performed in a one dm^3 graduated cylinder. The settling tests, apart from studies on solids concentration, were done by adding 200 g of -20 μm material into the cylinder, mixed thoroughly and falling of the interface height was recorded as a function of time. Zeta potential measurements were conducted by means of Zeta Meter 3.0 which is equipped with a microprocessor unit capable of directly measuring the average zeta potential and its standard deviation. 100 mg - 20 μm pure albite was added into 100 ml of distilled water and conditioned for 10 min. The suspension was kept stationary for 3 min and the average of ten particles was taken as the zeta potential. Details of the measurement procedure is given elsewhere (Celik and Yasar, 1995; Kursun et al., 1996). Adsorption tests were carried out in 20 ml-glass scintillation vials. A sample of 1 g pure albite was added to 15 ml of polymer solution

of desired concentration. The supernatant was subjected to polymer analysis described below. Polymer analysis was made by a nephelometric method developed by Attia and Rubio (1975) for low concentrations of polyethylene oxide and polyacrylamide flocculants. A series of nonionic polymer solutions of known concentrations (5 ml) in the range of 0-3 parts/10^6 (ppm) were treated with 40 ml of 0.1 M NaCl solution and 5 ml of 0.1% tannic acid solution in 50 ml volumetric flask. The mixture was shaken for 1 h and the turbidity of the resultant solution was measured by a Shimadzu UV/Vis spectrophotometer at 625 nm wavelength. The linear portion of the calibration curve in the range of 0.5-2.5 mg/kg was used for calculating the residual polymer concentrations.

RESULTS AND DISCUSSION

FLOCCULATION STUDIES

Figure 1 presents the height of the interface in the absence of polymer as a function of time at different pulp densities as defined by percent solids by weight. The plant water was used as the medium at its natural pH. It is apparent that as the pulp density increases the settling rate, as defined by the initial slope in the sedimentation curve, and also the interface height decrease. Despite higher sedimentation rates at low pulp densities, considering both conditions at the plant and economic capacity of the operation, 20 % pulp density was considered suitable for performing the subsequent flocculation tests. It is also evident in Figure 1 that most of the sedimentation occurs during the first 15 min of the settling for all pulp densities. However, it is interesting to note that, in the absence of any polymer addition, the upper portion of the suspension appeared to be rather hazy indicating that under natural conditions a long retention time is required to achieve a clear supernatant.

Figures 2-5 illustrate the effect of various type of flocculants on the elapsed settling time as determined by the interface height. The amount of polymer is 5 g/Mg for all polymers used. Compared to the anionic and cationic polymers, the nonionic polymers yields the best settling condition. The settling rate further increases with increasing the degree of nonionicity, Figures 2-5 also further show that the settling time is drastically reduced in the presence of polymer. Settling is almost over in less than five min. The same improvement was observed in the supernatant as the cloudiness was substantially reduced in the order of effectiveness shown in Figures 2. A similar enhancement was also noted upon increasing the amount of polymer up to a certain concentration above which destabilisation of the suspension was observed as reported in most flocculation studies.

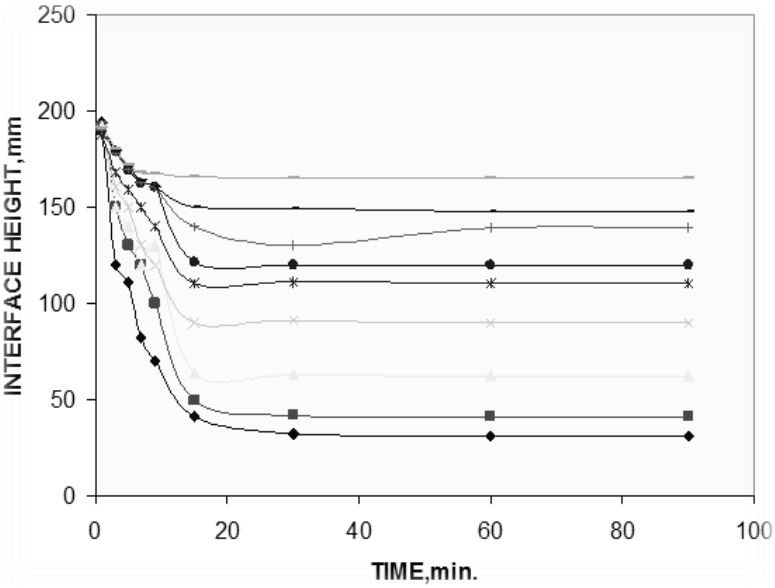

Fig. 1. Settling behaviour of -20μm albite concentrate against time in the absence of flocculant at different pulp densities

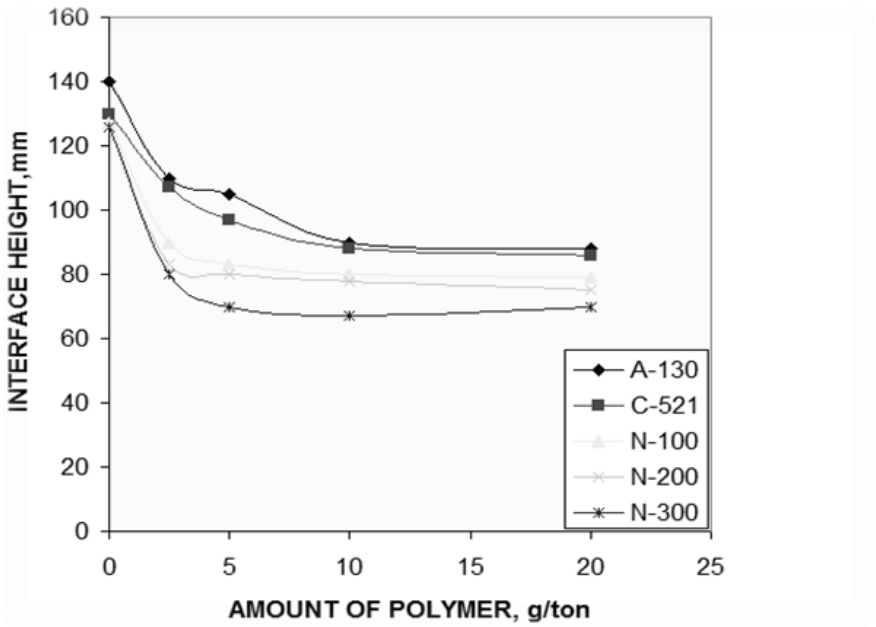

Fig. 2. Variation of interface height with the amount of polymer for 20μm albite concentrate up on 5 in of settling time

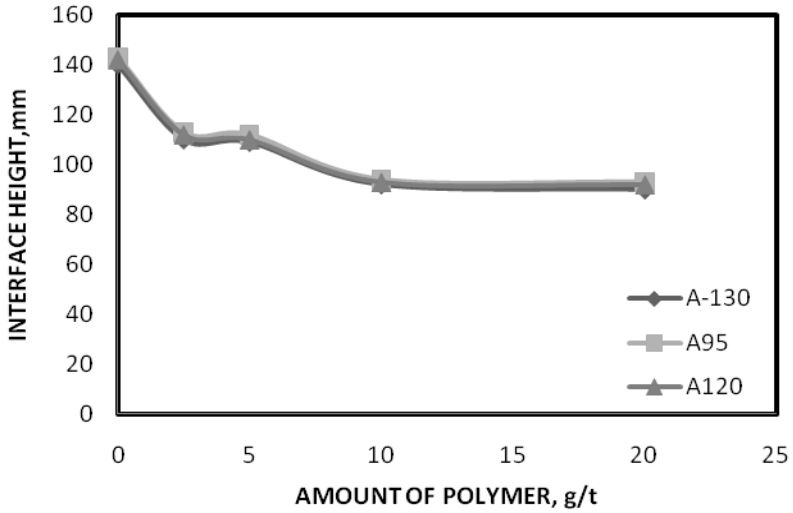

Fig. 3.Variation of interface height with the amount of anionic polymer for 20 µm albite concentrate up on 5 min of settling time

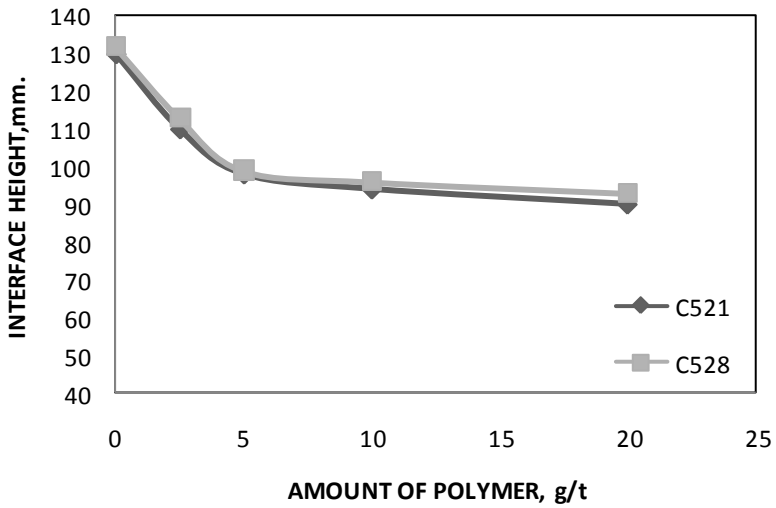

Fig. 4.Variation of interface height with the amount of cationic polymer for 20 µm albite concentrate up on 5 min of settling time

Figure 5 exhibits the settling behaviour of albite in the absence and presence of polymer as a function of pH. it is clear that, due to scattering, no significant effect of pH is apparent both in the presence and absence of polymer.

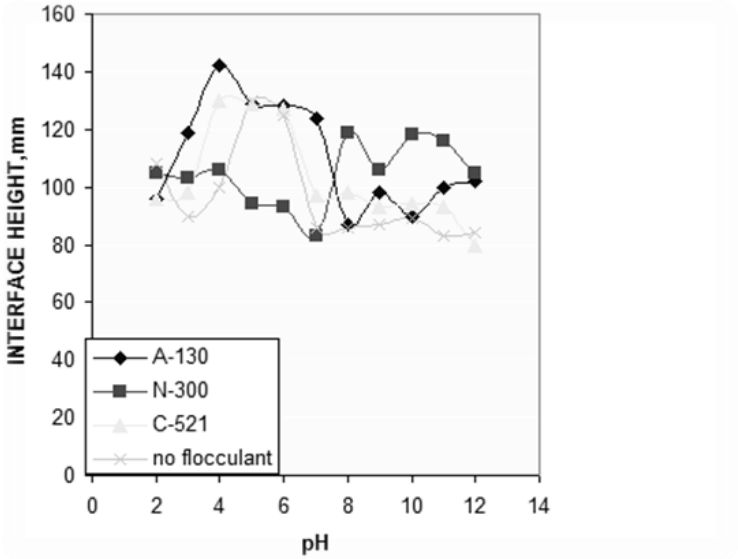

Fig. 5. Settling behaviour of -20 μm albite concentrate versus pH with different flocculant (settling time 5 min, polymer concentration 5 g/Mg)

EQUILIBRATION OF ALBITE IN WATER

The plagioclase feldspars form a complete solid solution series from pure albite ($NaAlSi_3O_8$) to pure anorthite ($CaAl_2Si_2O_8$). Considerable potassium may be present toward the albite end of the series (Hurlbut, 1971).Therefore, it is more likely that albite should be written as $(Na,K)AlSi_3O_8$. The dissolution behaviour of albite has been systematically studied by Chou and Wollast (1985). Helgeson et al. (1984) suggest that the rate of hydrolysis of feldspar is highly pH dependent and results from the following reactions:

at low pH < 2.9

$$(H_3O)AlSi_3O_8 + H^+ = (H_3O)AlSi_3O_7(OH)^+ \quad (1)$$

at intermediate pH (2.9-8.0)

$$(Na,K)AlSi_3O_8 + nH_2O = (Na,K)AlSi_3O_8\,(H_2O)n \quad (2)$$

at high pH > 8.0

$$(Na,K)AlSi_3O_7 + 0.4\ OH^- = (Na,K)AI(OH)_{0.4}Si_3O_8^{\ 0.4-}. \quad (3)$$

Stumm and Morgan (1981), based on coordination chemistry, suggest that the factoral orders on H^+ and ligands given in Eq. 3 are compatible with a direct dependence on the degree of surface protonation or on the concentration of ligand surface complexes. Stumm et al. (1983) also propose the existence of charged

complexes at mineral surfaces. In both Eqs. 1 and 2 hydronium ($H_3O^{+)}$ ions can replace Na^+ or K^+ Wikby (1972) has demonstrated that the alkali ions are replaced by H^+ rather than H_3O^+. This hypothesis is further supported by the fact that the volume occupied by alkali ions in albite is rather small compared to the large H_3O^+ (Chou, Wollast, 1985). The most important factors affecting the rate of dissolution of albite are pH and the concentration of dissolved Al. The rate dependence on pH exhibited remarkable similarities to the solubility curves of Al compounds and also Al showed the largest inhibiting effect on the dissolution rate. Chou and Wollast (1985) thus suggest the formation of surface complexes involving both H^+ and Al.

DISSOLUTION BEHAVIOR OF ALBITE

Figure 6 presents the dissolution kinetics of albite in water as a function time at initial pH values of 3, 11, and natural. The natural pH of albite was found to be 8.1. When the suspension is mixed with distilled water of about pH 6, it takes approximately 15 min for albite mineral to reach its equilibrium pH of 8.1. When the initial pH is adjusted to 3 or 11 it takes about 15 min to approach one pH unit to the natural pH but several additional hours to reach its equilibrium pH. In other words, albite suspensions are buffered relatively strongly in both acidic and alkali media. This feature becomes important in the interpretation of adsorption results.

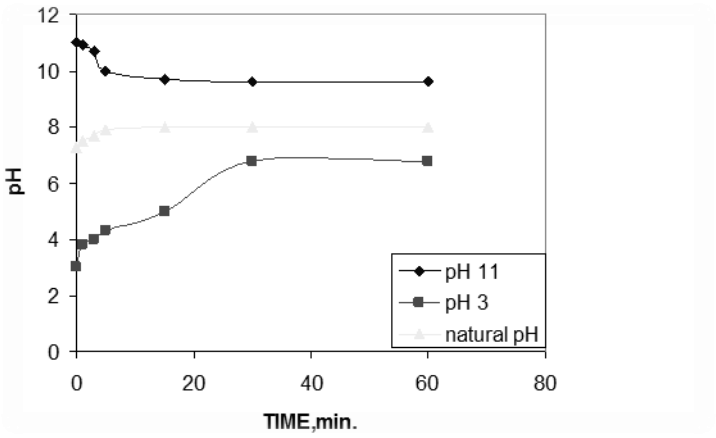

Fig. 6. Dissolution kinetics of pure albite in water at different initial pH values

ELECTROKINETIC BEHAVIOR OF ALBITE

Albite, as most other silicate minerals, exhibit negative zeta potentials throughout the practical pH range of 2 to 12. The zero point charge (zpc) of albite is below pH 2,

as shown in Figure 7. This is in line with the zpc of many silicate minerals including quartz (Fuerstenau and Palmer, 1976). However, no electrokinetic data on albite was found in the literature.

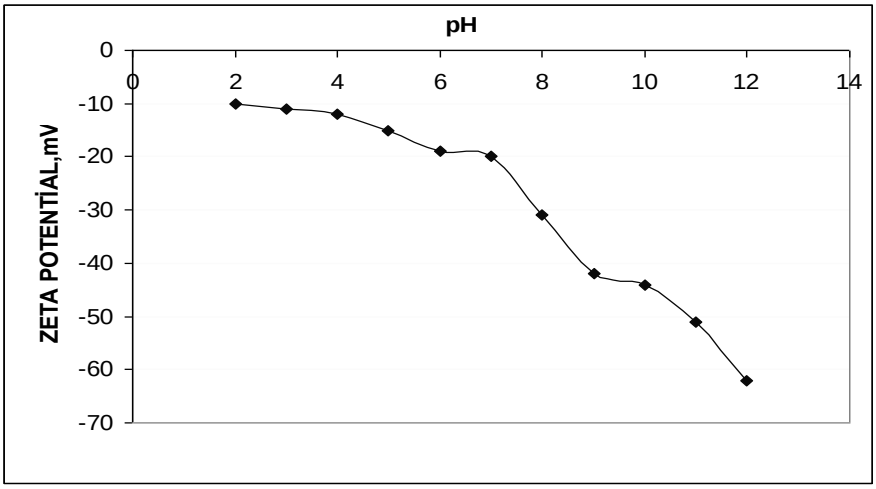

Fig. 7. Zeta potential of albite as a function of pH in water

The zeta potential of albite as a function of N-300 nonionic polymer concentration is given in Figure 8. The zeta potential gradually decreases with increasing N-300 concentration, i.e. it becomes less negative. The albite suspension was found to flocculate at 1 mg/kg N-300 concentration and measurements became increasingly difficult above this value.

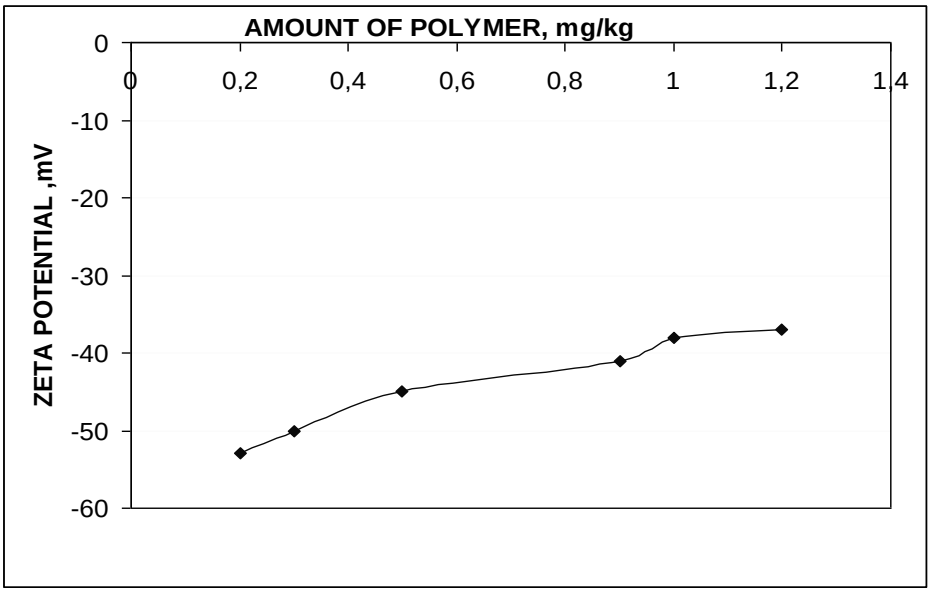

Fig. 8. Variation of zeta potential with N-300 concentration

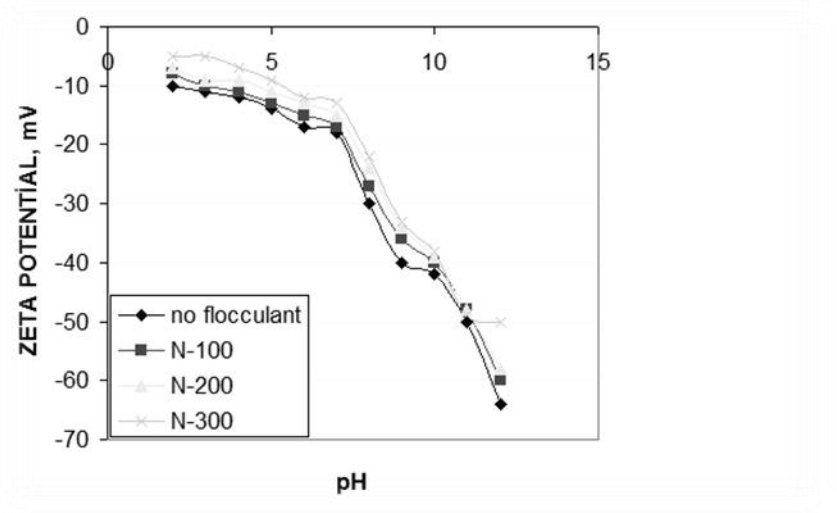

Fig. 9. Zeta potential versus pH profile for albite with 1 mg/kg and without polymer addition

The dependence of pH on zeta potential of albite in the presence and absence of different nonionic polymers is presented in Figure 9. It is clear that the addition of polymer makes the surface of albite less negative at all pH values with N-300 being the most effective. This indicates that as the nonionicity increases more of negative charges on the albite surface are tied up with the polymer.

ADSORPTION OF POLYMER ON ALBITE

Adsorption is a rate dependent phenomenon. Polymers, unlike law molecular weight compounds, are made up of thousands of units. Adsorption kinetics is therefore not only dependent on the conducted at surface properties of minerals but also on those of chemicals as well. For a polymer to adsorb it is sufficient to attach its one or more of segments to the solid. The dependence of adsorption on conditioning time is given in Figure 10 at natural pH of albite. The equilibrium is practically attained after about one hour and this is maintained with only a slight drift. One hour of equilibrium time was used in the subsequent adsorption experiments.

Flocculation and adsorption are both dependent on the solids concentration. In Figure 1, flocculation was shown to drastically change with the amounts of solid in solution. Similarly, adsorption also changes with solids concentration, as shown in Figure 11. It is seen that adsorption decreases with increasing the solids concentration and the curve flattens out at above about 5g/100 dm^3. For the sake of convenience all adsorption tests were thus conducted at 1g/15 ml solids concentration. It should be noted that flocculation is generally preceded by polymer uptake but not all polymer

adsorption leads to flocculation (Yarar, 1982).Polymer conformation whether straight or coiled plays a significant role in the magnitude of final flocculation. High molecular weight polymers are more akin to coiling particularly under high salinity and temperature conditions (Celik et al.,1991).

Since pH was pointed out as an important parameter in the dissolution of albite, the dependence of adsorption of N-300 was studied as a function of pH. This is shown in Figure 12. Evidently, the adsorption density increases with increasing pH and it reaches a constant value above pH 9 where it becomes difficult to adjust pH. Adjusting the initial pH of the solution to pH 12 resulted in a pH value of 9.3. High adsorption density at neutral and high pH correlates well with the flocculation and settling tests discussed previously.

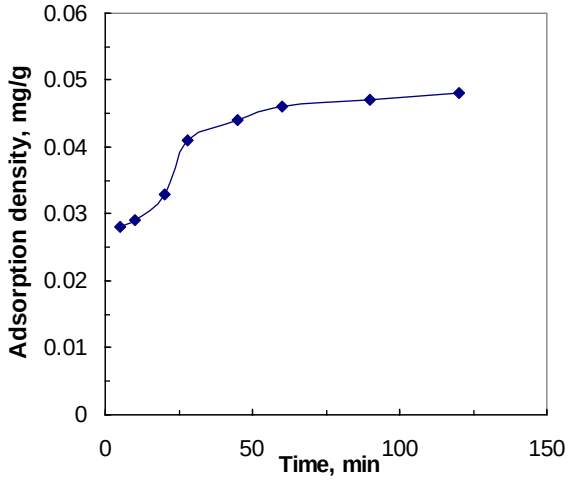

Fig. 10. Dependence of adsorption of 10 mg/kg N-300 on albite against conditioning time at natural pH

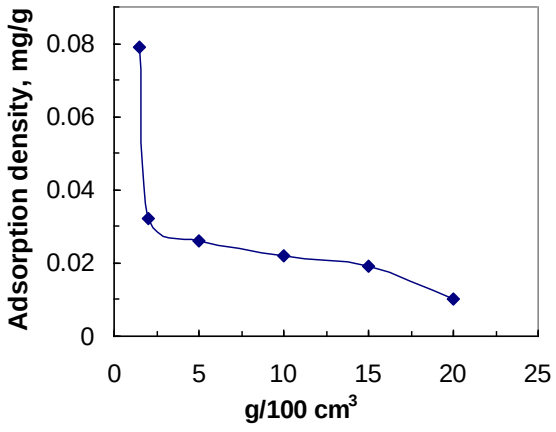

Fig. 11. Adsorption density as a function of solid concentration at 10 mg/kg N-300 concentration

Adsorption isotherm of N-300 onto albite is presented in Figure 13 where the adsorption density is plotted against the residual polymer concentration. Adsorption is found to increase with an increase in polymer concentration and reaches a plateau value at about 10 mg/kg N-300 concentration. The adsorption isotherms appears to be of a typical Langmuir type.

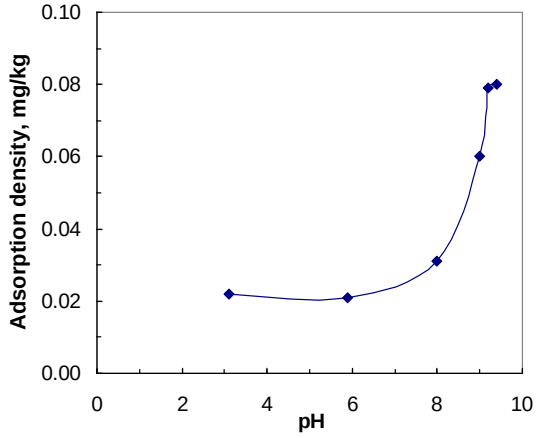

Fig. 12. Effect of pH on the adsorption of 10 mg/kg N-300 onto albite

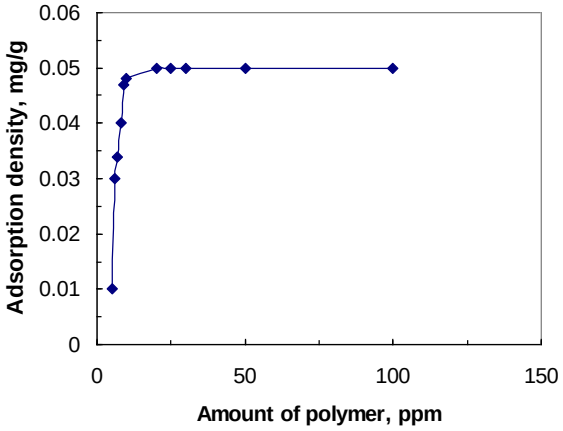

Fig. 13. Adsorption of N-300 onto albite at natural pH

DESORPTION EXPERIMENTS

Desorption tests were carried out by replacing the removed portion of the supernatant (2/4 ml) with a supernatant solution of the same salinity and adjusted pH to match the original supernatant. The desorption cycle was continued until the

polymer concentration was below detection limit of the polymer analyses technique. As a result of the desorption tests, no significant change was observed fort he albite-nonionic polymer system.

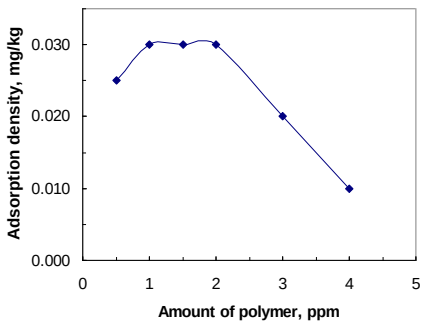

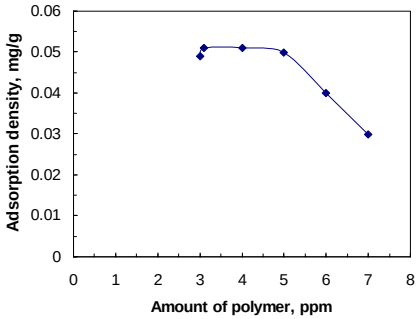

Fig. 14. Desorption of 5 ppm polymer concentration Fig. 15. Desorption of 10 ppm polymer concentration

ADSORPTION MECHANISM OF NONIONIC POTLYMER ON ALBITE

Several mechanisms of polymer adsorption have been suggested including electrostatic interaction, hydrogen bonding, chemical interactions and hydrophobic bonding (Slater and Kitchener, 1966). Since the polymer under discussion is of nonionic in nature, the electrostatic mechanism can be ruled out. Hydrophobic bonding requires that the surface of mineral be modified by a non-polymeric surfactant and thus can be excluded as well. The latter two mechanisms are therefore possible candidates. Hydrogen bonding occurs through binding of hydrogen to an electronegative element such as F, N, S and O. This is a widely accepted mechanism for freshly ground natural silica (Griot and Kitchener, 1965) and clays (Hollander et al., 1981) with nonionic polymers. Hydrogen bonding can occur between the polymer carbonyl (-C=O) or the amide ($-NH_2$) groups and the hydrogen bonding with surface oxygen species. The sharing of the hydrogen bonding between the two electronegative oxygen species induces the adsorption. Flocculation then follows by interparticle bridging if the electrostatic repulsion between the particles is not strong. Since albite is a sodium form of silicate mineral and the polymer is nonionic, it appears that hydrogen bonding is the only plausible mechanism in the system. As shown in Equations 1 through 3, albite acquires a positive charge below pH 2.9 and thus is not as much amenable to adsorption of N-300. This is clearly seen in Figure 12 where adsorption remains at its lowest level above pH 3, adsorption progressively increases due to formation of silanol groups and reaches its highest level above pH 8 where additional negatively charged surface complexes form. The decrease in the zeta potential of surface with the addition of polymer shown in Figures 8 and 9 is in

agreement with the above explanation. It appears that positive sites are depleted upon addition of the polymer.

CONCLUSIONS

Experimental studies are apparent that as the pulp density increases the settling rate, as defined by the initial slope in the sedimentation curve, and also the interface height decrease. Despite higher sedimentation rates at low pulp densities, considering both conditions at the plant and economic capacity of the operation, 20 % pulp density was considered suitable for performing the subsequent flocculation tests.Flocculation studies conducted with albite in the presence of various charged and nonionic polymers indicate that nonionic polymers exhibit the best performance. Increasing the degree of nonionicity improves the degree of settling. Electrokinetic studies conducted with pure albite shows that albite is negatively charged throughout the entire pH and the isoelectric point of the mineral is below pH. Adsorption of the nonionic polymer is found to increase with increasing the pH and concentration of the polymer. A hydrogen bonding mechanism between the polymer carbonyl (-C=O) or the amide (-NH_2) groups and the surface oxygen species is proposed to be responsible for the adsorption nonionic polymer onto albite. According to desorption tests, no significant was change system.

ACKNOWLEDGMENT

The author would like to sincerely thank the late Prof.Dr.Bedri İpekoğlu, retired Prof.Dr. Yalçın Kaytaz and Prof.Dr.M.Sabri ÇELİK for their valuable comments on the research.

REFERENCES

AKERS, R.J. 1975.Flocculation. I Chem Services, London.

ATTIA, YA, RUBIO, 1975. Determination of Very Low Concentrations of Polyacrylamide and Polyethylene Flocculants by Nephelometry. *Polymer*, 1. (7):135-138.

CELIK, M.S., AHMAD, S., A1-HASHIM, H.S. 1991. Adsorption/Desorption of Polymers from Saudi Arabian Limestone. *J. Petroleum Sci and Engineering*, 6:213-223.

CELIK, M.S., YASAR, E. 1995. Electrokinetic Properties of Some Hydrated Boron Minerals. 1. *Colloid Interface Sci.* 173:181-185.

CHOU, L., WOLLAS, R. 1985. Steady-State Kinetics and Dissolution Mechanism of Albite. *Arner. 1. Sci*. 285:963-993.

FUERSTENAU, M.E., PALMER, B.R. 1976. Anionic Flotation of Oxides and Silicates. İn Flotation: AM. Gaudin Memorial Volume, VoL 1 , *AIME PubL*, New York, p. 148-196.

GRIOT, O., KITCHENER, JA 1965. Role of Surface Silanol Groups in the Flocculation of Silica Suspensions by Polyacrylamide. *Trans. Faraday Soc*. 61: 1 026-1038.
HELGESON, H.E., MURPHY, W.M., AAGAARD, P. 1984. Thermodynamic and Kinetic Constraints on Reaction Rates among Minerals and Aqueous solution. *Geochim. et Cosmochim. Acta*, 48:2405-2432.
HILL, TE, KENWORTHY, H., RITHCEY, RA., GERARD, JA 1969. Separation ofFeldspar, Quartz, and Mica from Granite, *U.S. Bureau of Mines Research and Investigations* 7245.
HOLLANDER, AF., SOMASUNDARAN, P., GRYTE, E.E. 1981. Adsorption Characteristics of Polyacrylamide and Sulfonate-Containing Polyacrylamide Copolymers on Sodium Kaolinite. 1. *Applied Polymer Sci*. 26:2123-2138.
HURLBUT, E.S., 1971. Dana's Manual of Mineralogy, 18th, Wiley, p.467.
POTTER, MJ. 1985. Mineral Facts and Problems, *U.S Bureau of Mines Bulletin.* 675:255-263.
SLATER, R.W., KITCHENER, JA 1966. Characteristics of Flocculation of Mineral Suspensions by Polymers. *Discussion Faraday Soc*. 42:267-275.
KANGAL, O., EROĞLU, B., GÜNEY, A., 2001, "Treatment of Low Grade Albites by Jet Flotation", New Developments in Mineral Processing, Önal, et. al. (eds), IXth Balkan Mineral Processing Congress, 11-13 September 2001, Istanbul-Turkey, p. 253-258.
KANGAL O., GÜNEY, A., GÜRKAN, V., 1998, "Evaluation of Feldspar Ores with High Titanium Contents" Innovations in Mineral and Coal Processing, Proceeding of the 7th International Mineral Processing Symposium, Istanbul, Turkey, 15-17 September 1998, eds. Atak et al, Balkema, Rotterdam, ISBN 90 5809 013 2, pp. 333-338.
KANGAL, O., GÜNEY, A., 2001, "Comparison of HIWMS and MGS in the Evaluation of Low Grade Feldspar Ores", New Developments in Mineral Processing, Önal, et. al. (eds), IXth Balkan Mineral Processing Congress, 11-13 September 2001, Istanbul-Turkey, p. 331-336
KURSUN, I., KAYTAZ, Y., IPEKOGLU, B., CELIK, M.S., 1996 . Flocculation Behaviour of Fine Albite Concentrate with Various Polymers, In Changing Scopes in Mineral Processing, Eds. M. Kemal et al., Proceedings of 6th International Processing Symposium, Kuşadası, Turkey, pp. 661-666.
KURSUN,I., IPEKOGLU,B., CELİK.,MS., KAYTAZ,Y.,2000.Flocculation and Adsorption Mechanism of Polymers on Albite, Proceedings of the XXI International Min. Proc. Cong. Italy, p.25-31.
STUMM, W., MORGAN, 1.1. 1981. Aquation Chemistry, 2nd ed. New York, John Wiley&Sons p.780.
STUMM, W., FURRER, G., KUNZ, B. 1983. The Role of Surface Coordination in Precipitation an Dissolution of Mineral Phase. *Croat. Acta*. 58:593-611.
WARREN, LJ., KITCHENER, 1.A 1972. Role o Fluoride in the Flotation of Feldspar. *Inst. Minin and Metal. Trans. Sect*. C 81:137-147.
WIKBY, A 1972. The surface Resistance of Glass Electrodes in Neutral Solutions, *J. Electro Chem*.33:145-159.
YARAR, B. 1982. Polymeric Flocculants and Selectiv Flocculation. in Solution Behavior of Surfactan, K.L. Mittal and EJ. Fendler (ed), Plenum Pres New York, p. 1333-1364.

Kursun I., *Określenie flokulacji, adsorpcji – desorpcji dla koncentratu skalenia sodowego w obecności różnych polimerów*, Physicochemical Problems of Mineral Processing, 44 (2010), 127-142, (w jęz. ang), http://www.min/proc.pwr.wroc.pl/journal

Zakład Wzbogacania Albitu Esan boryka się z poważnym problemem, jakim jest odwodnienie koncentratu zawierającego ziarna albitu poniżej 20 μm. Badania nad flokulacja zawiesiny albitu z udziałem różnych polielektrolitów i niejonowych polimerów wykazały, ze niejonowe polimery wykazują najlepsze działanie flokulujące. Badania elektroforetyczne przeprowadzono na czystym albicie wykazały, że cząstki tego minerału są ujemnie naładowane w całym badanym zakresie pH, a punkt izoelektryczny jest położony poniżej pH =2. Adsorpcja niejonowego polimeru N-300 wzrastała wraz ze wzrostem pH oraz wraz ze wzrostem stężenia polimeru. Zaproponowano mechanizm wiązania oparty na wiązaniu

wodorowym między grupami –C=O lub $–NH_4$ polimeru i tlenowymi grupami na powierzchni ziaren albitu. Mechanizm ten jest odpowiedzialny za adsorpcję niejonowego polimeru na albicie.

słowa kluczowe: albit, flokulacja, potencjał dzeta, adsorpcja, polimery niejonowe

Physicochem. Probl. Miner. Process. 44(2010) 143-150

journal homepage
www.minproc.pwr.wroc.pl/journal/

Physicochemical Problems of Mineral Processing

Index No. 32213X ISSN 1643-1049

W. Malewski*, T. Jesionowski*, F. Ciesielczyk*, A. Krysztafkiewicz*

DISPERSION CHARACTERISATION OF COLLOIDAL SILICA AT SUBSEQUENT STAGES OF SILICA SOL PREPARATION

Received February 2, 2009; reviewed; accepted May 5, 2009

Dispersion properties of colloidal silica were studied at subsequent stages of silica sols preparation. Dilute sols were obtained from solutions of sodium silicate by ion exchange method. In them SiO_2 particles were built up and next the sols were concentrated. The concentrations of the sols in which SiO_2 particles were built-up ranged from 5.89 to 6.44 wt. % SiO_2, while the mean concentrations of the sols which were added into the heel sols were 3.28 and 6.20 wt. % SiO_2. The particle size distributions were measured by DLS, while the contribution of the ionic form of silica was determined by the colorimetric method on the basis of the intensity of the yellow colour coming from the heteropolycomplexes of silicomolybdic acid.

key words: silicic acid sol, colloidal silica, sodium silicate, water solutions of silicates

INTRODUCTION

Colloidal silica refers to stable dispersions of discrete particles or sols of amorphous silica. This arbitrary definition excludes solutions of polysilicic acids in which the polymer or silica particles are too small to be stable. In most sols of silicic acids, silica particles range from 4 to 100 nm. The most common methods of obtaining the sols of silicic acid are electrodialysis, sol peptisation, ion-exchange, and neutralization of silica solutions with acids. The first attempts at removal of sodium

* Poznan University of Technology, Institute of Chemical Technology and Engineering
M. Sklodowskiej-Curie 2 Sq, 60-965 Poznan, Poland
e-mail: Teofil.Jesionowski@put.poznan.pl, phone:+48(61)6653720, fax:+48(61)6653649

from sodium silicate solution by the method of ion-exchange were made by Bird (1941). Iler and Wolter obtained silica sols in periodical and flow-through reactors in which ion-exchange was conducted in the pH range from 8 to 10 and at a temperature above 60^{o}C (Iler, 1953).

The sols obtained were free from dissolved salts. The silica particles ranged from 5 to 8 nm, and the silica specific surface area ranged from 350 to 600 m^2/g. Dirnberger (1955) passed sodium silicate solutions through a fluidal bed of ionite at a rate adjusted so that the individual ionite grains were suspended in the solution flowing up the column. This solution ensured better contact of the solution with the grains, which permitted the use of sodium silicate solutions of the SiO_2 concentrations up to 6 wt. %. Alexander (1956) obtained a sol of water-like clarity, free from dilute salts, with the silica particles from 5 to 8 nm in diameter and silica specific surface area from 350 to 600 m^2/g. The process proposed by Alexander included the following steps: (a) removal of metal cations from a dilute solution of sodium silicate by ion exchange, (b) alkalization of dilute sol with sodium hydroxide or a solution of sodium silicate until stabilisation of the molar ratio of SiO_2/Na_2O from 30:1 to 150:1, (c) heating of the sol at temperatures from 50 to 120^{o}C to promote silica particle growth to reach the surface area from 350 to 600 m^2/g, (d) purification of the sol with cationite and anionite to remove the salt residues, (e) final stabilization of the molar ratio of SiO_2/Na_2O in the range from 20:1 to 300:1 by using sodium hydroxide, and (f) water evaporation to get a SiO_2 concentration in the sol of at least 15 wt. %.

Dirnberger and Nelson (1961) obtained a silica sol of minimum turbidity by adding to the periodical reactor a solution of sodium silicate and ionite in the hydrogen form simultaneously so that the pH of the sol in the reactor was always between 8.3 and 8.7. The content of the reactor was stirred and heated to 88 to 90^{o}C. The silica sol obtained had surface area from 200 to 250 m^2/g, and the SiO_2 concentration was 10 to 20 wt. %.

Mindick and Reven (1969) patented a method overcoming problems with gelation and blockage of the ionite bed in production of acidic silica sols of pH from 2.5 to 4.0 and the content of SiO_2 from 6 to 12 wt. %. Gelation was reduced to 2 wt. % of SiO_2 of maintaining the total amount of silica introduced onto the column. This was achieved by maintaining low temperatures in the bed and increasing the volume flow rate of sodium silicate solution. The minimum flow rate at a lowered temperature should be 245 dm^3/m^2 of the bed cross-section area. For higher temperature, it should be 695 dm^3/m^2 of the bed cross-section area.

Bechtold and Snyder (1951) patented a method for obtaining silica sols of particles of controlled size. The method is known as the process of built-up particles. A dilute solution of silica sol with a pH over 7 is divided into two parts. One part is heated to over 60^{o}C so that the diameters of the nuclei of the dispersed phase reach the size of a few nanometers. This part is called the heel sol. The other part of the dilute silica sol solution is introduced into the heel at a rate slow enough to make sure that the introduced silica would deposit on the nuclei of the dispersed phase. At the same tame,

water can be evaporated at a rate ensuring maintenance of a constant concentration of SiO_2 in a unit volume of the solution. The mechanism of particle build-up is explained in terms of the Ostwald ripening process. The driving force of the ripening process can be described by the variance of the particle size distribution. Iler (1979) proposed a quantitative description of particle build-up by defining the particles build-up index $\boldsymbol{B_r}$ related to the particle size using equations 1 and 2.

$$B_r = \frac{W_a}{W_n} \quad (1), \qquad \left(\frac{d_f}{d_t}\right)^3 = 1 + B_r \quad (2)$$

where:

W_a represents the amount of silica added to the system; W_n represents the amount of silica in the initial heel sol; d_t represents the initial diameter of the silica particles; d_f represents the final diameter of the silica particles.

The aim of this study was to determine particle size distribution at subsequent stages of production of silica sols. Mutual influence of different sols on the particle size distribution after the build-up process and sol concentration were analyzed.

EXPERIMENTAL

MATERIALS

The sodium silicate solution used in the study had the following properties: density at 20°C of 1.252 g/cm^3; Na_2O content of 6.380 wt. %; SiO_2 content of 20.311 wt. % and silicate modulus of 3.28. This solution was obtained by dilution and filtration of the sodium silicate solution made by Vitrosilicon S.A. For ion exchange, a strong acid ion exchange macroporous resin *Amberlyst® 15* made by ROHM and HASS was used in the hydrogen form with a grain size from 0.3 to 1.2 mm and a guaranteed exchange capacity of 1.7 mmol/cm^3.

METHODS OF STUDIES

The silicic acid sol was obtained at three stages. In the first stage, a dilute sol was prepared. In the second stage, silica particles were built-up. In the third stage, the sol was concentrated. The parameters of the sols in which SiO_2 particles were built-up were similar. The silica concentration in these sols ranged from 5.89 to 6.44 wt. %, and pH ranged from 8.08 to 8.93. The sols introduced into the heel can be divided into two groups. The first group comprises sols with a silica concentration of 3.50, 3.02, 3.49 and 3.10 wt. % and a pH of 10.24, 9.84, 9.00 and 11.33. The second group comprises sols with a silica concentration of 6.02 and 6.21 wt. % and a pH of 9.30 and 8.50. Sols were produced in a periodic reactor using ion exchange. The process of

silica particle build-up was carried out in accordance with the method described by Bechtold and Snydera (Bechtold, 1951). Details of the particle build-up processes in particular series of experiments are given in Table 1. Build-up indices were calculated using Equation 2 on the basis of the SiO_2 concentrations and the densities of the sols. During the process of particle build-up, water was evaporated. The sols in which the silica particles were built-up were subjected to concentration in a vacuum evaporator at 94°C.

Table 1. Operational data of the processes of silica particle build-up

Series no. of experiment	Temp. (°C)	Volume of the heel sol in which the build-up process took place (cm^3)	Volume of the sol which was added into the heel (cm^3)	Dosing rate (cm^3/min)	Dosing time (min)	Build-up index
I	92	100	1000	3.31	302	5.54
II		100	1000	3.31	302	4.75
III		100	1000	3.31	302	5.31
IV		340	850	3.31	257	1.30
V		100	1000	3.31	302	9.33
VI		100	1000	3.31	302	10.21

RESULTS AND DISCUSSION

Table 2 presents results collected from six series of experiment. In these series the sols which were added into the heel had the following SiO_2 concentrations: 3.50, 3.02, 3.49, 3.10, 6.02 and 6.21 wt. %. Selected results of particle diameters for the first series are compared in Fig. 1. For sols with a mean SiO_2 concentration of 3.28 and 6.00 wt. %, the correlation curves of the relative content of the ionic form of SiO_2 vs. pH were drawn (Fig. 2). SiO_2 particles of greater size were obtained when the processes were carried out using sols added into the heel at lower SiO_2 concentrations. The SiO_2 particle sizes obtained in series V and VI at subsequent stages of silica sol preparation were practically the same. Results of the first four series point to the positive effect of increasing pH of the sols added into the heel and the sols received as a result of build-up process on the growth of the SiO_2 particles.

As the build-up process is an effect of polymerization of silicic acid monomers, the results in Table 2 can be explained using the correlation curves given in Figure 1. Particle build-up took place when the pH was between 9.5 and 11.0. Sols with a mean SiO_2 concentration of 3.38 wt. % had much more ionic silica than similar sols with a mean SiO_2 concentration of 6.00 wt. %. The predicted diameters of the built-up particles were calculated from Equations 1 and 2 of and compared with the experimental data (Table 3).

Table 2. The particle diameters, pH, sol densities and total content of SiO_2 in the sols at subsequent stages of their preparation

Series no.	Parameter measured	Heel sol	Sol added into the heel	Sol after the build-up process	Sol after evaporation
I	Density at 20°C (g/dm^3)	1.041	1.023	1.039	1.112
	SiO_2 (wt. %)	6.21	3.50	5.63	19.31
	pH	8.33	10.24	10.90	10.74
	Diameter of dominant particles (nm)	1.46	2.06	6.27	9.02
	Volume of dominant particles (%)	99.8	99.3	100	100
II	Density at 20°C (g/dm^3)	1.041	1.017	1.033	1.160
	SiO_2 (wt. %)	6.21	3.02	5.68	23.81
	pH	8.33	9.84	10.69	10.62
	Diameter of dominant particles (nm)	1.46	1.20	6.67	3.51
	Volume of dominant particles (%)	99.8	99.7	100	99.3
III	Density at 20°C (g/dm^3)	1.038	1.018	1.040	1.110
	SiO_2 (wt. %)	6.44	3.49	5.81	17.12
	pH	8.08	9.00	9.46	9.34
	Diameter of dominant particles (nm)	1.66	1.43	2.15	1.61
	Volume of dominant particles (%)	99.8	99.6	99.0	99.9
IV	Density at 20°C (g/dm^3)	1.029	1.019	1.033	1.061
	SiO_2 (wt. %)	5.89	3.10	6.10	12.04
	pH	8.93	11.33	11.15	11.11
	Diameter of dominant particles (nm)	1.36	3.43	7.29	7.19
	Volume of dominant particles (%)	99.8	99.9	100	100
V	Density at 20°C (g/dm^3)	1.038	1.036	1.059	1.156
	SiO_2 (wt. %)	6.44	6.02	8.80	22.36
	pH	8.08	9.30	9.50	9.42
	Diameter of dominant particles (nm)	1.66	1.25	1.41	1.43
	Volume of dominant particles (%)	99.8	99.8	99.7	100
VI	Density at 20°C (g/dm^3)	1.041	1.036	1.047	1.110
	SiO_2 (wt. %)	6.05	6.21	7.96	17.69
	pH	8.74	8.50	9.31	9.12
	Diameter of dominant particles (nm)	1.21	1.63	1.49	1.16
	Volume of dominant particles (%)	99.9	100	99.8	100

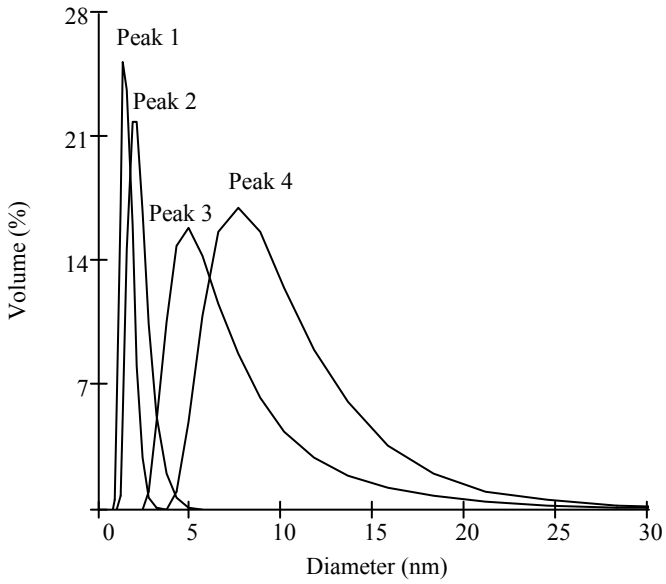

Fig. 1. Comparison of particle size distributions at subsequent stages of silica sol preparation: Peak 1. size distribution of particles in the heel sol, by volume – 1,46 nm (Series I); Peak 2. size distribution of particles in the sol which was added to the heel sol, by volume – 2,06 nm (Series I); Peak 3. size distribution of particles in the result sol after build-up process, by volume – 6,27 nm (Series I); Peak 4. size distribution of particles in the result sol after evaporation process, by volume – 9,02 nm (Series I)

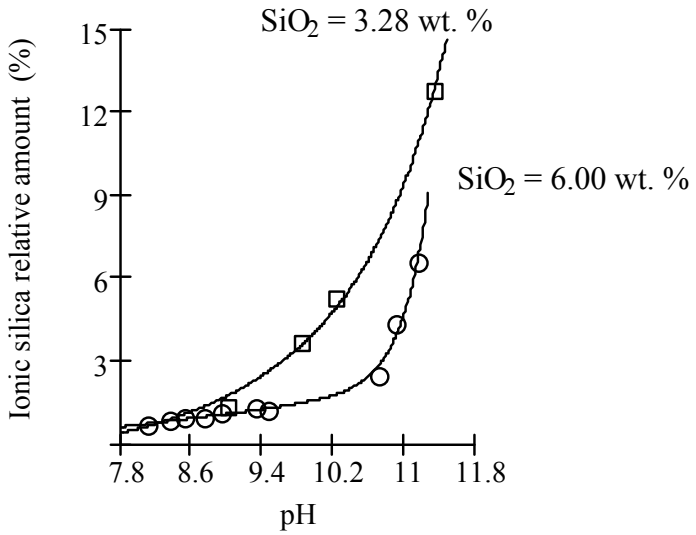

Fig. 2. The influence of pH on ionic silica contents in sols with a mean silica concentrations of 6.00 and 3.28 wt. %

Table 3. Comparison of SiO_2 particle diameters calculated theoretically with results of experiments

Series no.	Diameter of dominant particles in the heel sol (nm)	Calculated diameter of particles in sol after the build–up process (nm)	Determined diameter of dominant particles in sol after the build–up process (nm)	Build-up index
I	1.46	2.73	6.27	5.54
II	1.46	2.61	6.67	4.75
III	1.66	3.07	2.15	5.31
IV	1.36	1.79	7.29	1.30
V	1.66	3.61	1.41	9.33
VI	1.21	2.71	1.49	10.21

According to the results collected in Table 3, all SiO_2 particles in the solution took part in the process of the particle build-up, not only those introduced with the sols added into the heel. The sols added into the heel in series I and IV were obtained at 25°C, while those used in series II and III were obtained at 40°C. The size of the SiO_2 built-up particles obtained after concentration was the same or greater for series I, IV but smaller for series II, III. A probable explanation is that, in sols from series II and III, the process of particle agglomeration was more effective during the build up stage and in the process of concentration the agglomerates underwent redispersion.

CONCLUSIONS

It was expected that an increase in the silica concentration of the sols which were added into the heel to 6.02 and 6.21 wt. % would increase build-up indices and make the process of sol preparation more economic, especially at the evaporation stage. Unfortunately, the expected improvement was not achieved in the pH range of 9.5 to 11. The sol with a SiO_2 concentration of 6 wt. % contained much less silica in the ionic form than the sol with a mean SiO_2 concentration of 3.28 wt. %. The increase in silica particle size was a result of the build-up of monomeric silica ions on the surface of particles. Sols added into the heel at room temperature were more able to elicit stable build-up of colloidal silica particles.

ACKNOWLEDGEMENTS

This work was supported by the Ministry of Science and Higher Education research grant no. N N205 109735 (2008-2010).

REFERENCES

ALEXANDER G.B., 1956, *Process For Producing Sols Of 5 – 8 Milimicrons Silica Particles, And Product*, U.S. Pat. 2,750,345 (Du Pont).
BIRD P.G., 1941, *Colloidal Solutions Of Inorganic Oxides*, U.S. Pat. 2,244,325 (National Aluminate Co.).
BECHTOLD M.F. and SNYDER O.E., 1951, *Chemical Processes And Composition*, U.S. Pat. 2,574,902 (Du Pont).
DIRNBERGER L.A., 1955, *Process Of Preparing An Aqueous Silica Sol*, U.S. Pat. 2,703,314 (Du Pont).
DIRNBERGER L.A. and NELSON R.T., 1961, *Preparation Of Silica Sols Of Minimum Turbidity*, U.S. Pat. 2,974,109 (Du Pont).
ILER R.K., 1979, *The Chemistry of Silica,* J. Wiley & Sons, New York, p. 315.
ILER R.K. and WOLTER F.J., 1953, *Silica Sol Process*, U.S. pat. 2,631,134 (Du Pont).
MINDICK M. and REVEN L.E., 1969, *Method Of Producing Acid Silica Sols*, U.S. Pat. 3,468,813 (Nalco Chemical Co.).

Malewski W., Jesionowski T., Ciesielczyk F., Krysztafkiewicz A., *Charakterystyka dyspersyjna krzemionki koloidalnej w kolejnych etapach otrzymywania zolu kwasu krzemowego,* Physicochemical Problems of Mineral Processing, 44 (2010), 143-150 (w jęz. ang), http://www.minproc.pwr.wroc.pl/journal

W pracy badano charakterystykę dyspersyjną krzemionki koloidalnej w kolejnych etapach otrzymywania zolu kwasu krzemowego. Rozcieńczone zole otrzymywano z roztworów krzemianu sodu metodą wymiany jonowej, nabudowywano w nich cząstki SiO_2 i następnie zatężano. Stężenia zoli, w których nabudowywano cząstki zawierały się w przedziale 5,89÷6,44 % wag. SiO_2, a zole stosowane do nabudowania miały średnie stężenia 3,28 i 6,20 % wag. SiO_2. Rozkłady wielkości cząstek mierzono techniką DLS, a udział formy jonowej krzemionki oznaczano kolorymetrycznie mierząc intensywność żółtego zabarwienia heteropolikompleksu kwasu molibdenowo–krzemowego.

słowa kluczowe: zol kwasu krzemowego, krzemionka koloidalna, krzemian sodu

Physicochem. Probl. Miner. Process. 44(2010) 151-156

journal homepage
www.minproc.pwr.wroc.pl/journal/

Physicochemical Problems of Mineral Processing

Index No. 32213X ISSN 1643-1049

A. Malicka-Soczka*, L. Domka**, A. Kozak***

KAOLIN MODIFIED WITH SILANE COMPOUNDS AS A FILLER USED IN RUBBER INDUSTRY

Received March 9, 2009; reviewed; accepted July 1, 2009

Kaolin unmodified and modified with the following silanes: 3-aminopropyltriethoxysilane, N-2-aminoethyl-3-aminopropyltriethoxysilane and 3-metacryloxypropyltrimethoxysilane has been characterised as to its physico-chemical properties (DTA and SEM methods) and mechanical performance. The course of vulcanisation of rubber blends and physical properties of butadiene–styrene rubber (KER 1500) vulcanisates containing unmodified and modified kaolin have been determined. The vulcanisates filled with kaolin modified with silane compounds containing amine groups have been found to show better mechanical performance than those with kaolin modified with 3 metacryloxypropyltrimethoxysilane and unmodified kaolin.

key words: kaolin, surface chemical modification, rubber (KER 1500)

INTRODUCTION

One of the methods for obtaining polymer materials of improved physico-chemical properties, leading at the same time to reduction of the cost of their production is the introduction of mineral fillers into the polymer matrix. The most often used white fillers are kaolin and chalk (Alexandre, Dubois, 2000, Lebaron et al., 1999). The

* Department of Metalorganic Chemistry, Adam Mickiewicz University, Grunwaldzka 6, 60-780 Poznan, Poland

** Department of Macromolecular Physics, Adam Mickiewicz University, Umultowska 85, 61-614 Poznan

*** Department of Water Protection, Faculty of Biology, Adam Mickiewicz University, Umultowska 89, 61-614 Poznan, Poland

mechanism of polymer reinforcement by the fillers has been the subject of interest of many authors. It has been established that of the greatest importance is the activity of the fillers that depends on many parameters such as the surface area, degree of dispersion in the polymer system, polymer-filler and filler-filler interactions (Zaborski et al., 1993, Domka, 1990, 2008). The free hydroxyl groups on the surface of the filler molecules hinder a direct introduction of the filler into the hydrophobic polymer matrix, leading most often to the formation of agglomerations in the matrix. To minimise these tendencies the surface of the filler should be chemically modified with the use of the so-called promoters of adhesion and reinforcement (Domka, 2005, 2006). Such promoters are organic acids and their derivatives, surfactants, polyoxyethylene glycols, organic proadhesive compounds of zirconium and titanium and silane coupling agents, playing a particularly important role in the systems kaolin-polymers. Chemical modification of the fillers considerably changes the morphology of the filler molecule surface and affects the filler influence on the properties of the composite. Kaolin is used as a filler in numerous cheap blends that have to be resistant to wear, and used for shoe soles, shoes, floor covering, bicycle tyres and conveyer belts (Domka, 1983). The stiffening effect of kaolin in rubber blends is used in production of hoses, inner tubes, extruded cords and rings. As kaolin is neutral to human health, it is used for production of sanitary products, household appliances, toys and others. The kaolin resistance to acids permits its use in production of elasto- and plastomers (ebonite blends) used as anticorrosion covers and protective clothing.

EXPERIMENTAL

Kaolin KOG from the bed Surmin near Bolesławiec was studied. Modification of kaolin was performed with the following silane compounds : 3-aminopropyltriethoxysilane, N-2-aminoethyl-3-aminopropyltriethoxysilane and 3-metacryloxypropyltrimethoxysilane. The modification was made using 3 wt parts of the modifying agent per 100 wt parts of kaolin. To ensure homogeneous cover of kaolin surface, the modification was performed in a mixture of water and ethanol using different amounts of the solvent for different silane agents, see Table 1.

Table 1. Silane compounds used for kaolin surface modification and the composition of the solvent used

Silane agent	H_2O [cm^3]	EtOH [cm^3]
3-aminopropyltriethoxysilane	70	50
N-2-aminoethyl-3-aminopropyltriethoxysilane	80	50
3-metacryloxypropyltrimethoxysilane	50	50

Modification with the three silane agents was performed under the same conditions. Appropriate amounts of kaolin, modifying agent and solvent were placed in a glass vessel and stirred for 60 minutes by a homogenizer Universal Laboratory Aid

type MPW-309. The modified kaolin was dried at room temperature, and filtered through the mesh size 75 μm.

The unmodified and modified kaolin samples were subjected to physico-chemical examination. Analysis of the morphology and microstructure of the samples studied were based on SEM images Fig.1. DTA measurements were performed in helium atmosphere; the results are presented in Fig. 2. Moreover, the rubber blends of the composition according to the Polish Norm PN-87/C-04258, containing unmodified and modified kaolin were studied (Table 2).

Table 2. Composition of the rubber blends studied

Components	Weight parts
Butadiene-styrene rubber (KER 1500)	100
Stearin	1
Titanium white	3
Kaolin unmodified	6.5
or modified with 3-aminopropyltriethoxysilane	6.5
or with N-2-aminoethyl-3-aminopropyltriethoxysilane	6.5
and with 3-metacryloxypropyltrimethoxysilane	6.5
Accelerator – Vulkacit	1
Sulphur	1.75

The course of vulcanisation of rubber blends was characterised by a vulcameter with oscillating rotor at 150 ºC according to PN-ISO 3417. The following physico-mechanical parameters of the vulcanisates were determined.

Shore hardness according to PN-80/C-04238

- Elasticity according to PN-88/C-04255
- Tearing strength - PN-ISO 34-1, method B, procedure (a)
- Tensile strength - PN-ISO 37, ore type 1
- Stress on elongation by 300 % and 500 %
- Grindability - PN-75/C-04235.
- Permanent deformation on compression at 30 Hz measured on Goodrich apparatus, according to PN-81/C-04292.

RESULTS AND DISCUSSION

Modification of the kaolin surface with the silanes used has insignificantly changed the agglomeration of particles; SEM photographs of the unmodified and modified kaolin samples show relatively large crystal structures. The most effective for disintegration of the agglomerations is the modification with 3-aminopropyltriethoxysilane, less effective is the modification with 3-metacryloxypropyltrimethoxysilane.

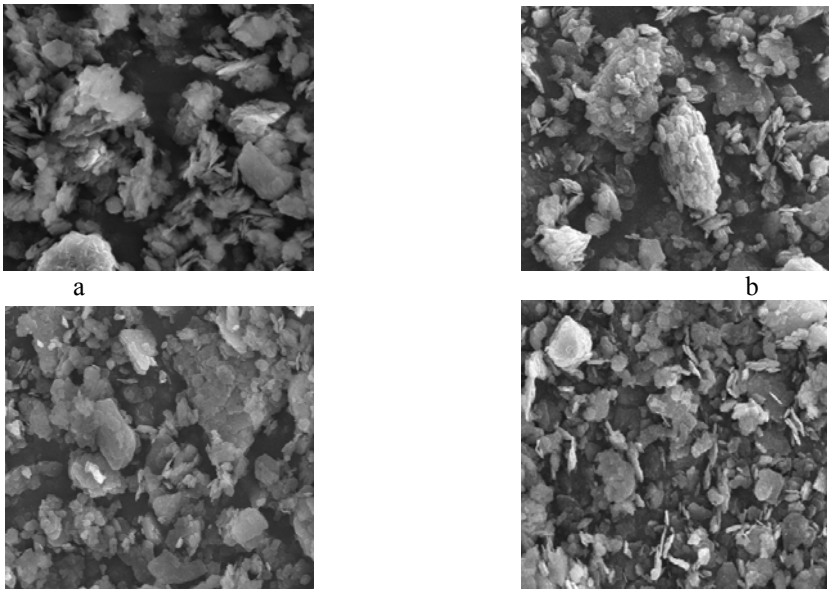

Fig. 1. SEM images of a) unmodified kaolin, b) kaolin modified with N-2-aminoethyl-3-aminopropyltriethoxysilane, c) kaolin modified with 3-metacryloxypropyltrimethoxysilane, d) kaolin modified with 3-aminopropyltriethoxysilane .

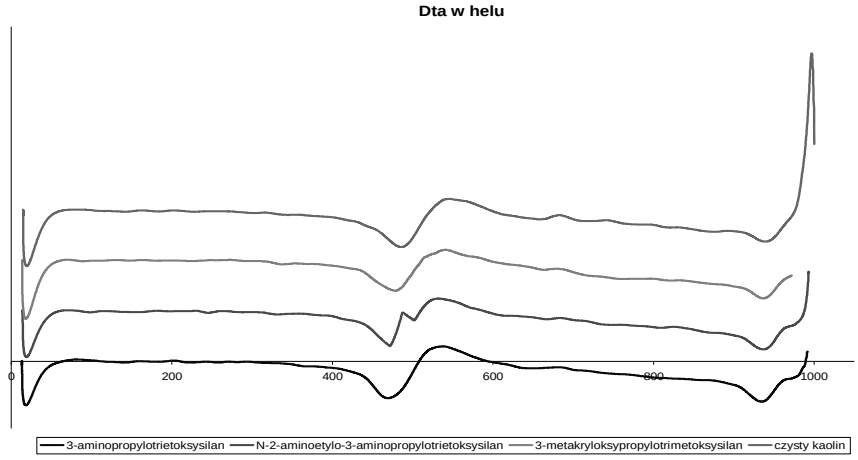

.

Fig. 2. DTA curves recorded for kaolin unmodified and modified with the silanes studied

Figure 2 presents the DTA curves for the kaolin samples studied. The endothermic peaks at 470 ºC and 500 ºC are much sharper for the kaolin sample modified with N-2-aminoethyl-3-aminopropyltriethoxysilane than for unmodified kaolin. For the unmodified kaolin the endothermic peak occurs at 490 ºC, whereas for the samples of modified kaolin this peak is shifted to lower temperatures by 10 or 20 ºC. For kaolin modi-

fied with 3-metacryloxypropyltrimethoxysilane it is shifted by 10 ºC, while for kaolin modified with silane containing amine groups by 20ºC (Lebaron P.C., 1999)

Table 3. Physico-mechanical characterisation of vulcanizates filled with kaolin unmodified or modified with the silanes studied

Parameter	unit	Sample number			
		1	2	3	4
Conditions of vulcanisation	min	50	20	15	50
Shore hardness	ShA	54	58	60	56
Elasticity	%	44	50	50	46
Tearing strength	kN/m	28.3	49.0	63.6	43.9
Tensile strength	MPa	5.9	10.9	14.2	8.4
Stress on elongation by					
300%	MPa	2.1	8.3	8.2	4.6
500%	MPa	2.7	10.6	12.3	5.8
Grindability	cm^3	0.169	0.199	0.097	0.131
Permanent deformation	%	13.0	1.63	1.86	2.70

Table 3 presents results of the physico-mechanical tests of vulcanisates filled with modified and unmodified kaolin. According to the results of these tests, samples studied can be divided into 2 groups. Grup 1 includes tests involving blends and vulcanisates containing unmodified kaolin (Alexandre, Dubois 2000) and kaolin modified with 3-metacryloxypropyltrimethoxysilane (Domka, 1990), while grup 2 includes tests involving blends and vulcanisates containing kaolin modified with 3-aminopropyltriethoxysilane (Lebaron, 1999) and N-2-aminoethyl-3-aminopropyltriethoxysilane (Zaborski et al., 1993). The most important mechanical parameters are shown in Fig. 3.

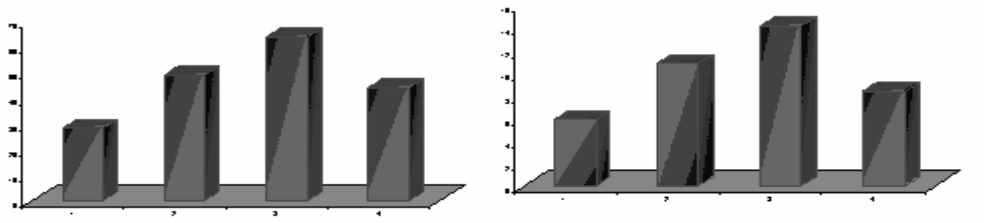

a b

Fig. 3. Diagrams illustrating the tearing strength (a) and tensile strength (b) of the vulcanizates obtained

The blends filled with kaolin modified with silanes containing amine groups (Lebaron et al., 1999, Zaborski et al., 1993) are characterised by higher elasticity, hardness and stress on elongation by 300 % and 500 %, greater grindability and tensile strength than those with kaolin unmodified or modified with 3-metacryloxypropyltrimethoxysilane silane. High tensile strength was obtained for the rubber filled with kaolin modified with silanes containing amine groups (Lebaron et al., 1999, Zaborski et al., 1993). The results have shown that the use of kaolin modi-

fied with silanes with amine groups as filler improves the tensile strength and grindability of the material filled. The parameters characterising vulcanizate 1 were much poorer then those obtained for the other samples (Zaborski et al., 1993).

CONCLUSIONS

The modification of kaolin with silane agents was found to reduce the agglomeration of particles and change the positions of the peaks on the DTA curves towards lower temperature. The use of kaolin modified with silane agents containing amine groups as filler of rubber blends has permitted a considerable shortening of the time of vulcanisation and has improved the tensile strength and tearing strength of the vulcanisates. Particularly beneficial was the influence of 3-aminopropyltriethoxysilane and N-2-aminoethyl-3-aminopropyltriethoxysilane on the grindability of the vulcanisates

REFERENCES

ALEXANDRE M., DUBOIS P., 2000, Mat. Sci. Eng, 28,1
LEBARON P.C., WANG Z., PINNAVALA T.J., 1999, Appl. Clay Sci., 15,11
ZABORSKI M., ŚLUSARSKI L., VIDAL A., 1993, *Wpływ budowy osrodka elastomerowego na aktywnosc napełniaczy*, Polimery-tworzywa wielkoczasteczkowe, 38,114
DOMKA L., 1990, J.ADHESION SCI. TECHNOL., 4, 1-6.
DOMKA L., MALICKA A., STACHOWIAK N., 2008, Acta Physica Polonica A, 114 (2) 413-421
DOMKA L., URBANIAK W., MORAWSKA A., 2005 Pat. PL – 190802
DOMKA L., MORAWSKA A., URBANIAK W., 2006, Pat. PL – 191851
DOMKA L., 1983, Chemik, 36, 65-69

Malicka-Soczka A., Domka L., Kozak A., *Kaolin modyfikowany silanem jako wypełniacz dla przemysłu gumowego*, Physicochemical Problems of Mineral Processing, 44 (2010), 151-156, (w jęz. ang), http://www.minproc.pwr.wroc.pl/journal

Próby kaolinu niemodyfikowanego jak również kaolinu modyfikowanego za pomocą następujących silanów: 3-aminopropylotrioksysilan, N-2-aminoetylo-3-aminopropylotrioksysilan i 3 metakrylooksypropylotrioksysilan, zostały scharakteryzowane pod katem właściwości fizykochemicznych (analiza DTA i SEM) oraz właściwości mechanicznych. Przeprowadzono procesy wulkanizacji mieszanek gumowych oraz określono fizykochemiczne właściwości wulkanizatów z gumy butadienowo-styrenowej, które zawierały modyfikowany lub niemodyfikowany kaolin. Wulaknizaty z wypełnieniem kaolinowym, który to kaolin był modyfikowany związkami zawierającymi grupy aminowe wykazywały lepsze właściwości mechaniczne niż wulkanizaty zawierające kaolin niemodyfikowany lub kaolin modyfikowany 3-metakryloksypropylotrioksysilanem.

słowa kluczowe: kaolin, powierzchniowa modyfikacja, guma KER 1500

Physicochem. Probl. Miner. Process. 44(2010) 157-168

journal homepage
www.minproc.pwr.wroc.pl/journal/

Physicochemical Problems of Mineral Processing

Index No. 32213X ISSN 1643-1049

A. Modrzejewska-Sikorska*, F. Ciesielczyk*, A. Krysztafkiewicz*, T. Jesionowski*

SYNTHESIS AND CHARACTERISATION OF PRECIPITATED COPPER(II) SILICATES

Received February 6, 2009; reviewed; accepted June 19, 2009

The study was undertaken to obtain a blue inorganic pigment of copper(II) silicate of high degree of dispersion. The process of precipitation of synthetic copper(II) silicates was optimised. The effect of the direction of dosing, percent concentration and volume ratio of the reagents, temperature and type of copper salt used on the physico-chemical properties of the products was studied. The copper(II) silicate obtained was characterised by satisfactory parameters; bulk density of 198 g/dm³, water absorbing capacity of 225 cm³/100g and paraffin oil absorbing capacity of 300 cm³/100g. The diameters of the precipitated silicates varied from 0.955 – 120.2 μm, with a dominant presence of larger particles making secondary agglomerates.

key words: copper silicate, precipitation process, particle size distribution, wettability, colorimetric data

INTRODUCTION

Pigments are colouring inorganic or rarely organic substances in the form of fine powder, insoluble in water, oil, resins or organic solvents. Pigments added to carrier or matrix, acting as a binder, make the fundamental component of coating materials; paints and enamels (Erfutrh 1998, Xuening 2000, Yuan 2005).

Highly dispersed pigments should be characterised by low bulk density to minimise sedimentation of pigments in dispersive media. Low water absorbing

* Poznan University of Technology, Institute of Chemical Technology and Engineering
M. Sklodowskiej-Curie 2 Sq, 60-965 Poznan, Poland
e-mail: Teofil.Jesionowski@put.poznan.pl, phone:+48(61)6653626, fax:+48(61)6653649

capacity at elevated level of paraffin oil absorbing capacity is desired to permit the use of pigment in lyophilic systems, while the reverse relation of these parameters the pigments can be used in lyophobic (hydrophilic) systems (Krysztafkiewicz 1997, 1999).

Inorganic pigments, divided into natural and synthetic (Wieczorek 2003, Johnston 2004) are resistant to chemical compounds and to extreme pH values and have higher covering power than organic ones. Besides they are highly resistant to light (Werner 1985).

Highly dispersed silicates of calcium, aluminium, magnesium, zinc and aluminium-sodium are used as insoluble components of rubber blends and other organic polymers, e.g. as fillers of polyvinyl chloride (Rothe 2009, Anastasiadis 2008, Lee 2008) or rubber (Krysztafkiewicz 1998, Wang 2005, Varghese 2003). The use of silicates as fillers brings improvement in mechanical properties of the filled polymers and do not change the colour of the substance to which they are added (they belong to the so-called bright fillers).

Inorganic pigments are used in paints, varnishes and resins (El-Nahhal 2005) and they often have colour other than white: e.g. chromium silicates are green (Krysztafkiewicz 2008, Klapiszewska 2003), nickel silicates are blue-green (Klapiszewska 2005).

Recent development in production of synthetic silicates has promoted their use in many fields. Interestingly, the synthesis of silicates permits formation of more types of silicate bonds than met in nature. Synthetic silicates can have crystalline structure (as natural ones) or amorphous structure. Many of them are obtained in the form of inter-oxide systems.

EXPERIMENTAL

MATERIALS

The substances used included: 5% and 10% solution of sodium silicate (VITROSILICON S.A.); 5%, 10% and 20% solutions of copper(II) sulphate(VI) and 5% solution of copper(II) nitrate(V) or copper(II) chloride (Chempur Piekary Śląskie).

METHODS OF STUDIES

Precipitation reaction was carried out by introducing doses of sodium silicate solution by a peristaltic pump into a reactor of the capacity of 0.5 dm^3 with copper(II) sulphate(VI). The reaction was also conducted in the reverse direction and by dosing the reagents into water environment. Precipitation of highly dispersed copper(II)

silicate was performed with additional use of copper(II) nitrate(V) and copper(II) chloride solutions. The conditions of precipitation were the same as for the sample characterised by the best parameters and precipitated by copper(II) sulphate(VI).

For precipitation the solutions of Na_2SiO_3 and $CuSO_4$ of the following volume ratios were used 1:1, 1:2, 1:3 and 2:1, 3:1. The process was carried out at temperatures 20÷85°C. Copper silicate obtained was separated from the post-reaction mixture on a filter with the use of vacuum pump. The samples were dried at 105°C for 2h. The bulk density, absorbing capacity of water and paraffin oil were measured. In order to determine the brightness, contribution of colours, saturation and hue of colour, the colorimetric analysis was made with the CIE *L*a*b** system (SPECBOS 4000 colorimeter made by Carl Zeiss Jena). With the use of a Tensiometer K100 made by Krüss, on the basis of the mass of water absorbed by the sample, the sample wettability was estimated. The size of particles was determined by Mastersizer 2000 made by Malvern Instruments Ltd. Morphology of the surface of the precipitated samples of copper silicate was analysed by the scanning electron microscopy (SEM), with a scanning microscope VO40 made by Zeiss.

RESULTS AND DISCUSSION

The blue inorganic pigment of copper(II) silicate of high degree of dispersion was obtained. The probable mechanism of its synthesis is presented in Fig. 1.

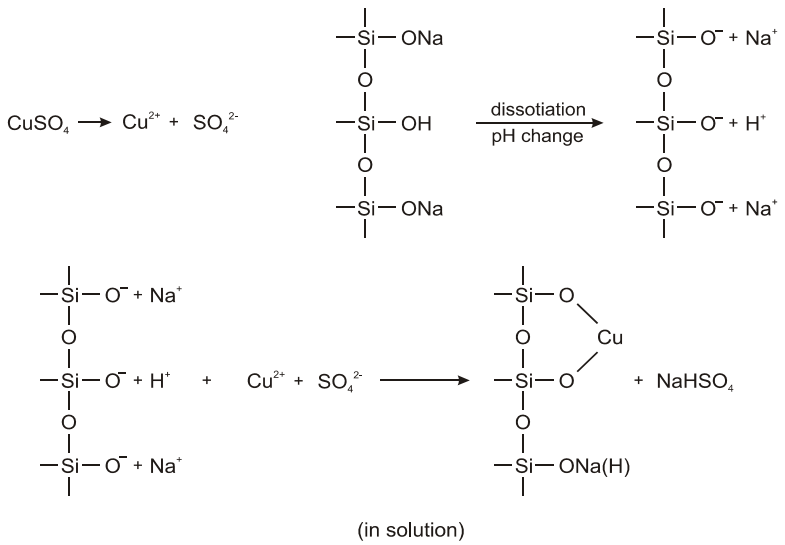

Fig. 1. Mechanism of copper silicates synteshis

Table 1 presents the method of obtaining copper silicates, while Table 2 gives their basic physico-chemical parameters and specifies the reaction systems in which they were precipitated.

Table 1. Characteristic of precipitation process

Sample No.	Precipitation direction	Solution concentration (%)		Reagents volume ratio	Temperature (°C)
		sodium silicate	cooper salts		
1	Na_2SiO_3 to $CuSO_4$	5	5	1:1	20
2	$CuSO_4$ to Na_2SiO_3				
3	Na_2SiO_3 and $CuSO_4$ to H_2O				
4	Na_2SiO_3 to $CuSO_4$	5	10		
5			20		
6		10	5		
7			10		
8			20		
9		5	5	1:2	
10				1:3	
11				2:1	
12				3:1	
13				1:1	40
14					60
15					85
16	Na_2SiO_3 to $Cu(NO_3)_2$				20
17	Na_2SiO_3 to $CuCl_2$				

The lowest bulk density of 198 g/dm³ was obtained for sample 1 that is copper silicate precipitated at the 1: 1 volume ratio of the reagents, at 20°C, by dosing a 5% solution of sodium silicate into the reactor containing a 5% solution of copper(II) sulphate(VI). The highest bulk density of 562 g/dm³ was obtained for sample 5, that is copper silicate precipitated in the same conditions as sample 1 but with the use of a 20% solution of copper(II) sulphate(VI).

The use of another copper salt in the process of precipitation leads to an increase in the bulk density of copper(II) silicate to 220 g/dm^3 when copper(II) nitrate(V) is applied and to 456 g/dm^3 when copper(II) chloride is applied.

The values of absorbing capacity of water and paraffin oil were similar for all samples. The exceptions are samples 9 and 10 precipitated at the 1:3 and 3:1 volume ratio of the reagents, whose absorbing capacities are much different.

Table 2. Physicochemical parameters of precipitated cooper silicates

Sample No.	Bulk density (g/dm^3)	Water absorbing capacity ($cm^3/100g$)	Paraffin oil absorbing capacity ($cm^3/100g$)
1	198	225	300
2	447	150	250
3	508	200	300
4	399	150	250
5	562	185	250
6	413	185	250
7	376	200	250
8	553	150	200
9	365	150	185
10	440	100	150
11	307	235	300
12	537	150	200
13	247	200	350
14	330	225	250
15	238	200	350
16	220	200	300
17	456	150	250

As shown from Table 3 and on Fig. 2, the direction of dosing, concentration and temperature of the process have significant effect on the particle size of copper(II) silicate. In fact the primary particles accumulate forming aggregates and agglomerates.

Samples 4 and 11 contain the finest particles. Ninety percent of the volume of sample 4 (precipitated at the 1:1 volume ratio of reagents, at 20°C, from a 5% solution of sodium silicate and a 10% solution of copper(II) sulphate) is taken by particles of diameter smaller than 28.4 μm, 50% of sample 4 volume is taken by particles of diameter smaller than 7.1 μm, and 10% of sample 4 volume is taken by particles of diameter smaller than 2.3 μm. As to sample 11 (precipitated at the 2:1 volume ratio of reagents, at 20°C, from a 5% solution of sodium silicate and a 20% solution of copper(II) sulphate) particles of diameter smaller than 31.6 μm take 90% of its

volume, those of diameters below 9.1 μm take 50% of its volume and those of diameters below 3.0 μm occupy 10% of its volume.

According to the results, the particle size of the samples obtained depends strongly on the type of copper salt used in precipitation, Fig. 2e. In sample 16 obtained from copper(II) nitrate(V) 90% of its volume is occupied by particles of diameters smaller than 39.3 μm. In sample 17 obtained from copper(II) chloride 90% of its volume is taken by particles of diameter smaller than 32.5 μm.

Table 3. Dispersive characteristic of precipitated cooper silicates

Sample No.	Diameter (μm)		
	d(0.1)	d(0.5)	d(0.9)
1	3.6	10.9	40.3
2	3.5	16.3	45.4
3	3.5	13.9	51.7
4	2.3	7.1	28.4
5	3.3	13.2	48.3
6	3.3	10.9	41.3
7	3.9	17.3	49.3
8	3.0	9.0	36.5
9	4.1	18.9	53.5
10	3.5	25.7	68.9
11	3.0	9.1	31.6
12	2.5	8.7	36.1
13	4.6	13.8	40.6
14	4.2	14.7	43.6
15	4.7	14.8	47.3
16	3.3	11.7	39.3
17	2.9	11.2	32.5

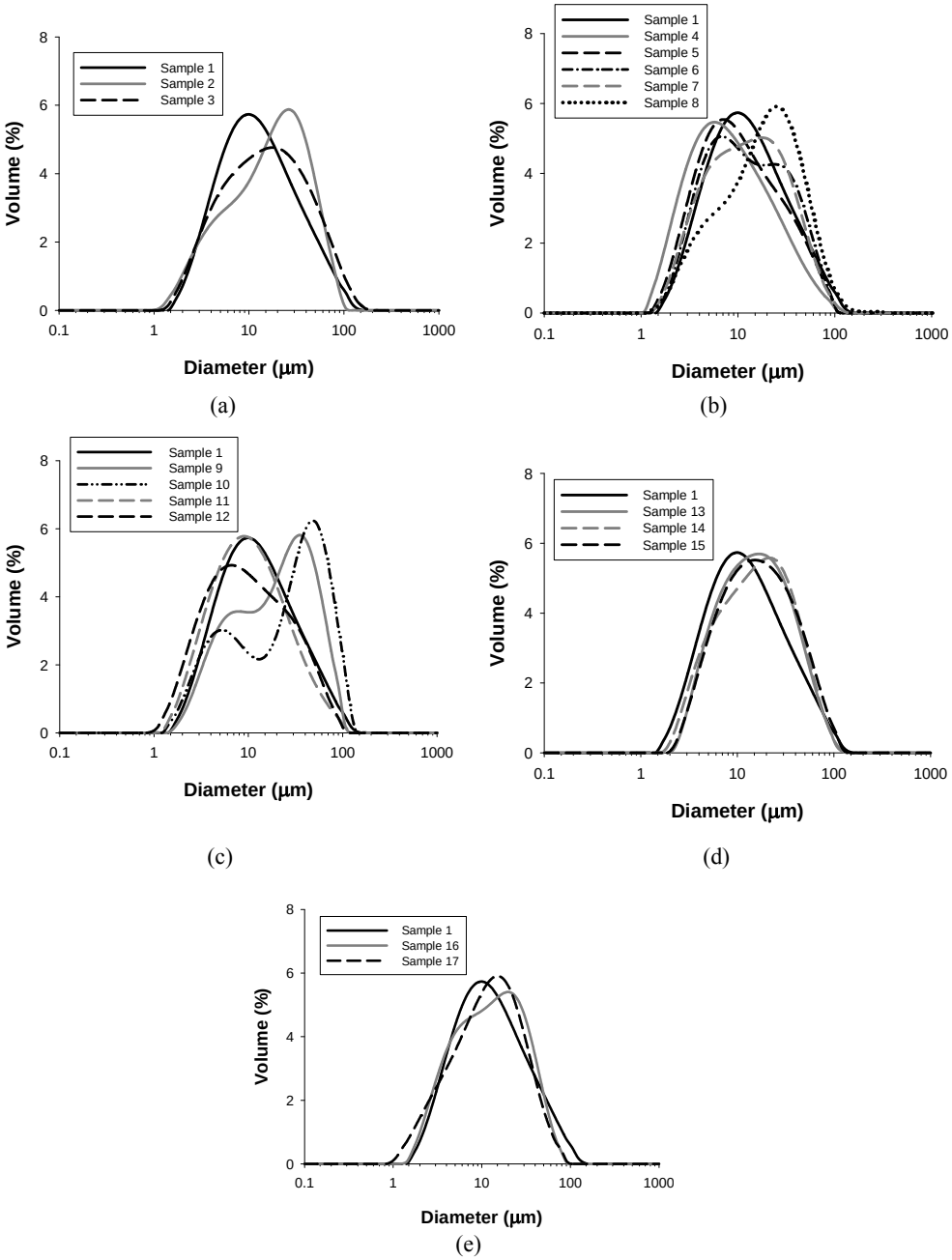

Fig. 2. PSD of copper silicates precipitated (a) at different precipitation direction (b) at different reagents concentration (c) at different reagents volume ratio (d) at different temperatures (e) using different copper salts

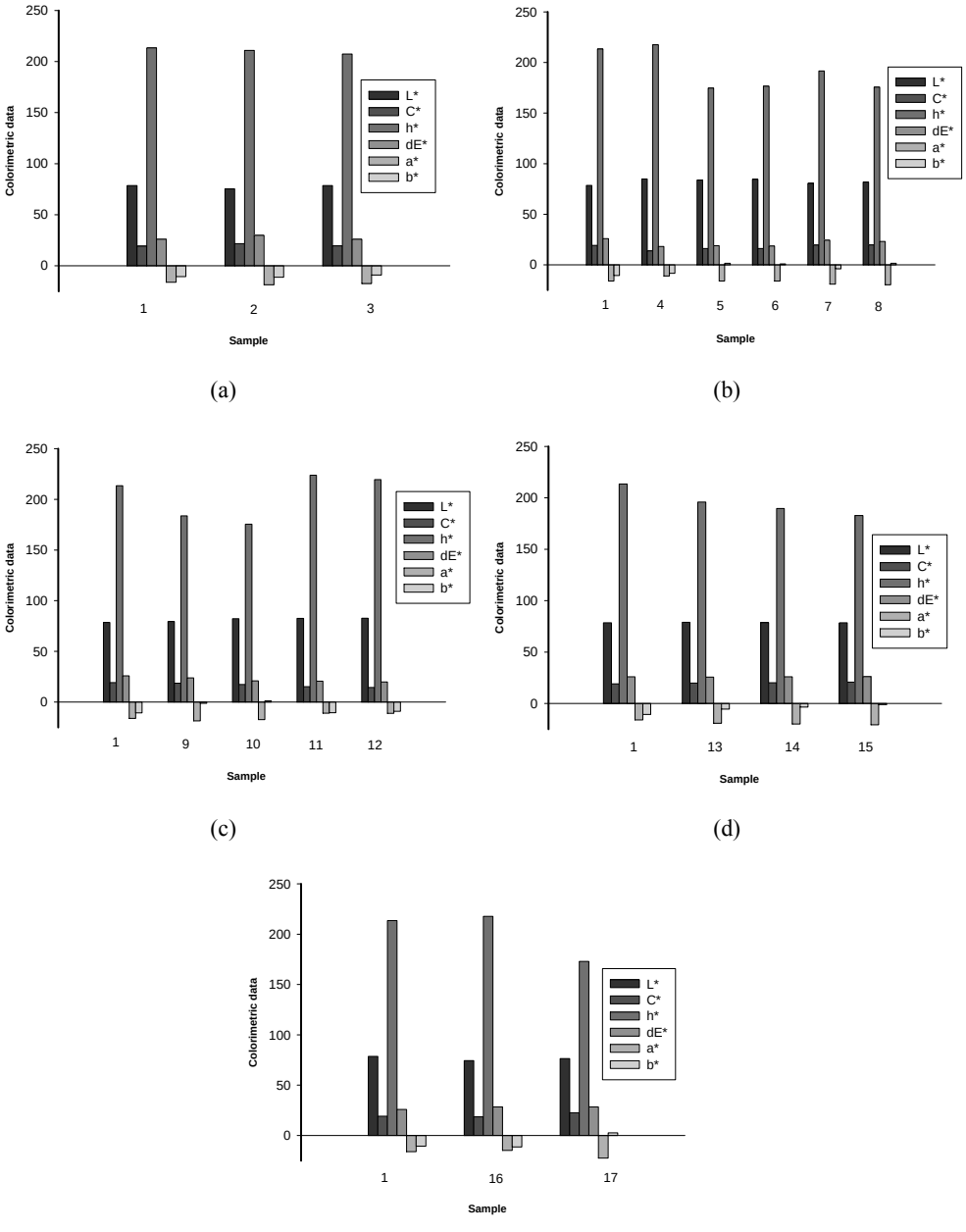

Fig. 3. Colorimetric parameters of copper silicates precipitated (a) at different precipitation direction (b) at different reagents concentration (c) at different reagents volume ratio (d) at different temperatures (e) using different copper salts

Colorimetric analysis in the CIE *L*a*b** system provides the information on the pigment colour, Fig. 3. The greatest contribution of blue colour (-*b**) was found for samples 1 and 2, their blue contributions were similar; of -10.57 and -11.12, respectively. The contribution of green (-*a**) in these samples was also similar of -16.02 and -18.59, respectively.

As follows from Fig. 3e, the type of copper salt used in precipitation of copper silicate also influenced the colour of the pigment. When copper(II) sulphate(VI) (sample 1) or copper(II) nitrate(V) (sample 16) were used, the contributions of blue (-*b**) and green (-*a**) were comparable and equalled -10.57 and -11.38 (blue) and -16.02 and -14.73 (green). When copper(II) chloride was used (sample 17), no contribution of blue was observed, while the contribution of green (-*a**) was -22.40.

Fig.4 presents the SEM photograph of copper(II) silicate precipitated from copper(II) sulphate(VI), sample 1. The material has complex structure of particles showing relatively high tendency towards formation of aggregates and agglomerates. The structure of this type has been earlier described when determining the sizes of particles. The particle diameters in micrometers indicate that the particles in this sample of copper silicate form agglomerate structures.

The wettability curves of the copper silicates studied are presented in Fig. 5. The greatest mass increase in time was found for sample 1, precipitated from copper(II) sulphate(VI). The mass increase in sample 16 – precipitated with the use of copper(II) nitrate(V) - and in sample 17 – precipitated with the use of copper(II) chloride – is much smaller.

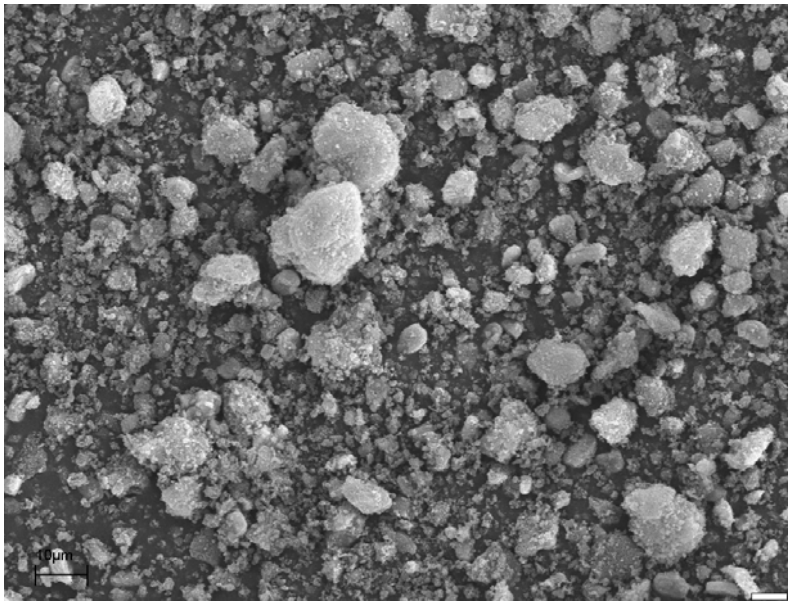

Fig. 4. SEM photograph of copper silicate – sample no. 1

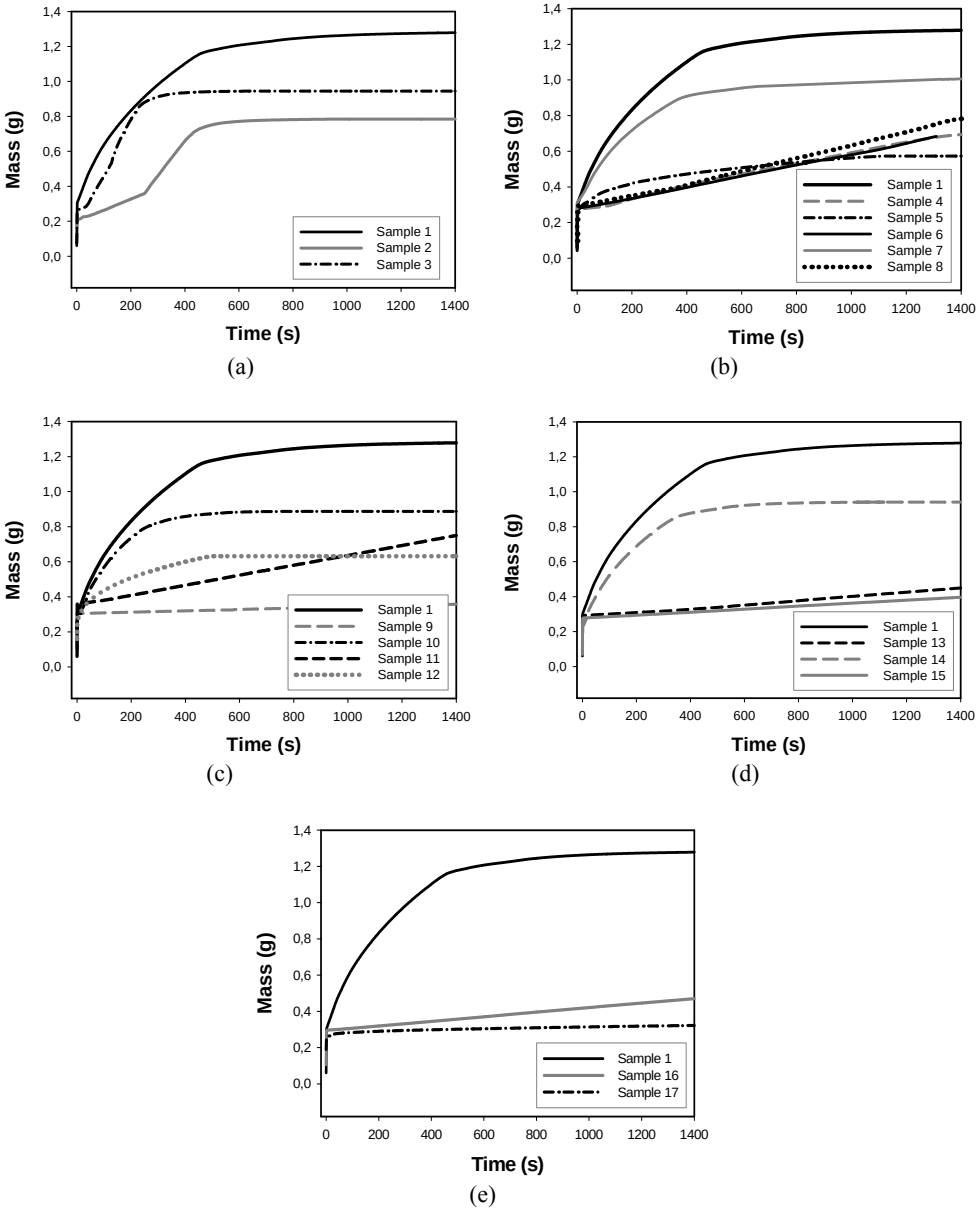

Fig. 5. Wettability of synthetic copper silicates samples precipitated (a) at different precipitation direction (b) at different reagents concentration (c) at different reagents volume ratio (d) at different temperatures (e) using different copper salts

CONCLUSIONS

As follows from the above presented and discussed results, the direction of dosing, concentration and volume ratio of the reagents, temperature of the process and type of the copper salt applied have significant effect on the physico-chemical properties of the final products.

The physico-chemical parameters most beneficial from the point of view of the desired applications were obtained when the copper silicates were precipitated with the use of copper(II) sulphate (VI) (sample 1) and copper(II) nitrate(V) (sample 16). The parameters of these two samples are similar, although sample 1 has lower bulk density.

ACKNOWLEDGEMENTS

This work was supported by the Poznan University of Technology research grant no. 32-117/09-BW

REFERENCES

ANASTASIADIS S., CHRISSOPOULOUA K., FRICKC B., 2008, *Structure and dynamics in polymer/layered silicate nanocomposites*, Materials Science and Engineering B, 152, 33–39.

EL-NAHHAL Y.Z., LAGALY G., 2005, *Salt effects on the adsorption of a pesticide on modified bentonites,* Colloid Polym. Sci., 283, 968–974.

ERFURTH U., 1998*, Farby na bazie żywic silikonowych – mity i rzeczywistość*, Renowacje, 3, 17–23.

JOHNSTON J., MCFARLANE A., BORRMANN T., MORAES J., 2004, *Nano–structured silicas and silicates – new materials and their applications in paper,* Current Applied Physics, 4, 411–414.

KLAPISZEWSKA B., KRYSZTAFKIEWICZ A., JESIONOWSKI T., 2003, *Highly dispersed green silicate and oxide pigments precipitated from model systems of postgalvanic waste***,** Environ. Sci. Technol., 37, 4811–4818.

KLAPISZEWSKA B., KRYSZTAFKIEWICZ A., JESIONOWSKI T., 2005, *Nickel(II) silicates and oxides–highly dispersed green pigments***,** Pigment Resin Technol., 34, 139–147.

KRYSZTAFKIEWICZ A., RAGER B., JESIONOWSKI T., 1997, *Otrzymywanie barwnych krzemianów–pigmentów o dużym stopniu rozdrobnienia,* Fizykochemiczne Problemy Mineralurgii, 31, 165–173.

KRYSZTAFKIEWICZ A., MICHALSKA I., JESIONOWSKI T., BOGACKI M., 1999, *Highly dispersed synthetic zinc silicates as future pigments for ecological silicate paints,* Physicochemical Problems of Mineral Processing, 33, 83–92.

KRYSZTAFKIEWICZ A., MICHALSKA I., JESIONOWSKI T., WIECZOREK W., 1998, *Odpady chromowe i żelazowe – potencjalne źródło do otrzymywania pigmentów,* Fizykochemiczne Problemy Mineralurgii, 32, 77–85.

KRYSZTAFKIEWICZ A., KLAPISZEWSKA B., JESIONOWSKI T., 2008, *Precipitated green pigments: Products of chromate postgalvanic waste utilization,* Environ. Sci. Technol., 42, 7482–7488.

LEE S., YOUN J., 2008, *Properties of polypropylene/layered-silicate nanocomposites and melt-spun fibers,* Journal of Applied Polymer Science, 109, 1221–1231.
ROTHE B., ELAS A., MICHAELI W., 2009, *In situ polymerisation of polyamide-6 nanocompounds from caprolactam and layered silicate,* Macromol. Mater. Eng., 294, 54–58.
VARGHESE S., KARGER-KOCSIS J., GATOS K.G., 2003, *Melt compounded epoxidized natural rubber/layered silicate nanocomposites: Structure-properties relationships,* Polymer, 44, 3977–3983.
WANG Z., WANG B., QI N., ZHANG H., ZHANG L., 2005, *Influence of fillers on free volume and gas barrier properties in styrene-butadiene rubber studied by positrons,* Polymer, 46, 719–724.
WERNER J., *Podstawy technologii malarstwa i grafiki,* 1985, PWN, Warszawa
WIECZOREK M., KRYSZTAFKIEWICZ A., JESIONOWSKI T., 2003, *Comparative characteristics of local and foreign bentonites,* Macromolecular Symposium, 194, 345–350.
XUENING F., TIANYONG Z., CHUNLONG Z., 2000, *Modification study involving a naphthol as red pigment*, Dyes and Pigments, 44, 75–80.
YUAN J., ZHOU S., GU G., 2005, *Encapsulation of organic pigment particles with silica via sol-gel process,* Journal of Sol-Gel Science and Technology, 36, 265–274.

Modrzejewska-Sikorska A., Ciesielczyk F., Krysztafkiewicz A., Jesionowski T., *Synteza i charakterystyka wytrąconych krzemianów miedzi(II)*, Physicochemical Problems of Mineral Processing, 44 (2010), 157-168, (w jęz. ang), http://www.minproc.pwr.wroc.pl/journal

Przeprowadzone badania miały na celu otrzymanie niebieskiego nieorganicznego pigmentu krzemianu miedzi(II). Badano wpływ sposobu dozowania, stężenia procentowego, stosunku objętości reagentów, temperatury procesu oraz rodzaju użytej soli miedzi na fizykochemiczne właściwości otrzymywanych produktów końcowych. Otrzymany krzemian miedzi charakteryzował się zadawalającymi parametrami, takimi jak: gęstość 198/dm^3, pojemność absorbowanej wody 225 cm^3/100g, pojemność absorbowanego oleju parafinowego 300cm^3/100g. Średnice wytrąconych cząstek krzemianów zmieniały się od 0,55 do 120,2 μm, z dominacją dużych cząstek tworzących wtórne agregaty.

słowa kluczowe: krzemian miedzi, precypitacja, skład ziarnowy, zwilżalność, dane alorymetryczne

Physicochem. Probl. Miner. Process. 44(2010) 169-178

journal homepage
www.minproc.pwr.wroc.pl/journal/

Physicochemical Problems of Mineral Processing

Index No. 32213X ISSN 1643-1049

R. Modrzewski*, P. Wodziński*

THE RESULTS OF PROCESS INVESTIGATIONS OF A DOUBLE-FREQUENCY SCREEN

Received December 17, 2008; reviewed; accepted March 15, 2009

In the present study the preliminary results of process investigations, being part of the research programme which has been carried out at the Department of Process Equipment, Technical University of Lodz, have been presented. The investigations are aimed at the process examinations of a new double-frequency screen in respect of its usefulness for screening of finely grained loose materials. The main objective of the present study is to demonstrate the results of the process investigations of this screen for various drive configurations in the form of the graphical efficiency – and capacity dependencies.

key words: classification, double-frequency screen, vibrator, rotational frequencies

INTRODUCTION

In the industry of rock raw materials one deals with the screen classification of finely grained materials (Banaszewski, 1990; Wodziński, 1981, 1997; Meinel and Schubert, 1971; Book and Kramer, 1984). It is evident from the preliminary results of the investigations, that the modern construction of a double-frequency screen is an ideal solution to the realisation of the process of fine grain screening (Wodziński, 2008).

A vital field of the industry in which one may utilize the double-frequency screen is processing of minerals. The authors of the present study intend to propose the

* Faculty of Process and Environmental Engineering, Technical University of Lodz, Wolczanska 213, 90-094 Lodz, e-mail: wodzinsk@wipos.p.lodz.pl

double-frequency screen for the application to the Polish copper industry. The classification of copper ores is a difficult process due to various physicochemical properties of those media and, additionally, due to high process efficiencies with which one deals.

A DOUBLE-FREQUENCY SCREEN

The experimental screen which is the focal point of the study was constructed in the Department of Process Equipment, Technical University of Lodz. The dimensions of the screen are demonstrated in Figure 1. As the most characteristic feature of this construction one may recognise the drive which is composed of two inert vibrators operating at various rotational speeds thereby causing the complex movement of the screen.

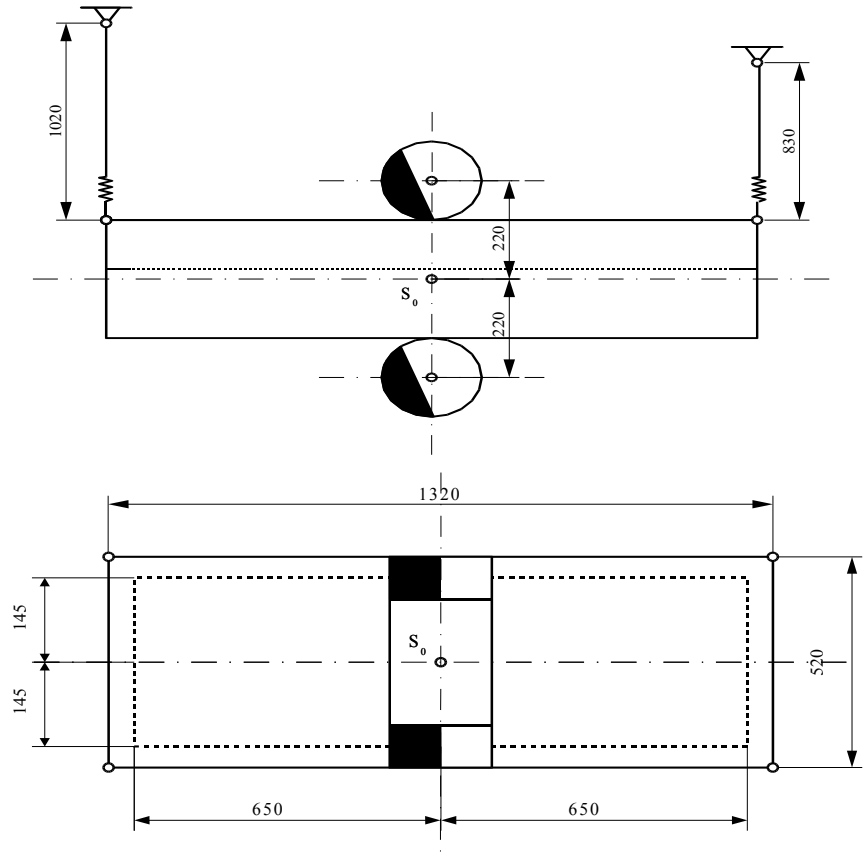

Fig. 1. The basic dimensions of the experimental screen

The construction of the screen allows the regulation (for research needs) of all basic machine operation parameters, in particular such as:

- the inclination of the sieve against the level – α ;
- the arrangement of the engine against the middle part of the sieve – β ;
- the exciting forces generated by the engines – F ;
- the rotational speeds of the engines.

A highly important parameter characterizing the operation of the double-frequency screen is the speed coefficient defined as follows (Turkiewicz i Banaszewski, 1982):

$$\xi = \frac{\omega_1}{\omega_2} = \frac{n_1}{n_2} . \tag{1}$$

This quantity defines how much the angular velocities (or rotational speeds) of two rotational vibrators are different from one another.

The regulation of the rotational speed of the engines was performed using inverters. The investigations were carried out for combinations of rotational frequencies of both vibrators as it is summarized in Table 1. For both vibrators: an upper and bottom one, the rotation in the right direction, i.e. in accordance with the clockwise direction, was assumed as a positive direction of rotations.

Table 1. Rotational frequencies of vibrators

Vibrator	Vibrator	Vibrator	Vibrator	Vibrator	Vibrator	Vibrator	Vibrator
Upper (ω_1)	Bottom (ω_2)	Upper (ω_1)	Bottom (ω_2)	Upper (ω_1)	Bottom (ω_2)	Upper (ω_1)	Bottom (ω_2)
Right (+)	Right (+)	Right (+)	Left (-)	Left (-)	Right (+)	Left (-)	Left (-)
rot/min		rot/min		rot/min		rot/min	
1500	1500	1500	1500	1500	1500	1500	1500
750	1500	750	1500	750	1500	750	1500
1500	750	1500	750	1500	750	1500	750
1500	1000	1500	1000	1500	1000	1500	1000
1000	1500	1000	1500	1000	1500	1000	1500
1500	500	1500	500	1500	500	1500	500
500	1500	500	1500	500	1500	500	1500

PROCESS INVESTIGATIONS OF A DOUBLE-FREQUENCY SCREEN

Agalite (as a model material of spherical grains), sand (irregular grains) and marble aggregate (sharp-edge grains) were utilized as loose material in the investigations. The shape of grains is presented in Figure 2.

The material had been appropriately prepared beforehand, i.e. screened in laboratory shakers in such a way that half of material mass constituted an upper fraction. In other words grains greater than 0.63 mm and another half constituted the

bottom fraction. Further process examinations were carried out on a metal woven sieve of a square opening and sieve mesh side $l = 0.63$ mm (Figure 3).

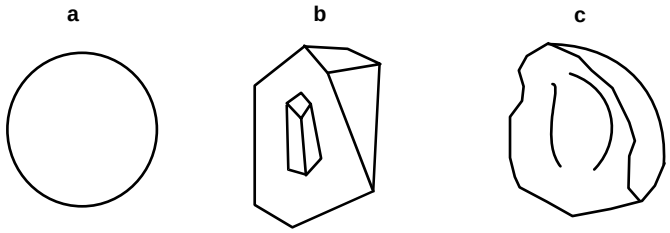

Fig. 2. Shapes of grains of model materials: a) agalite; b) aggregate; c) sand

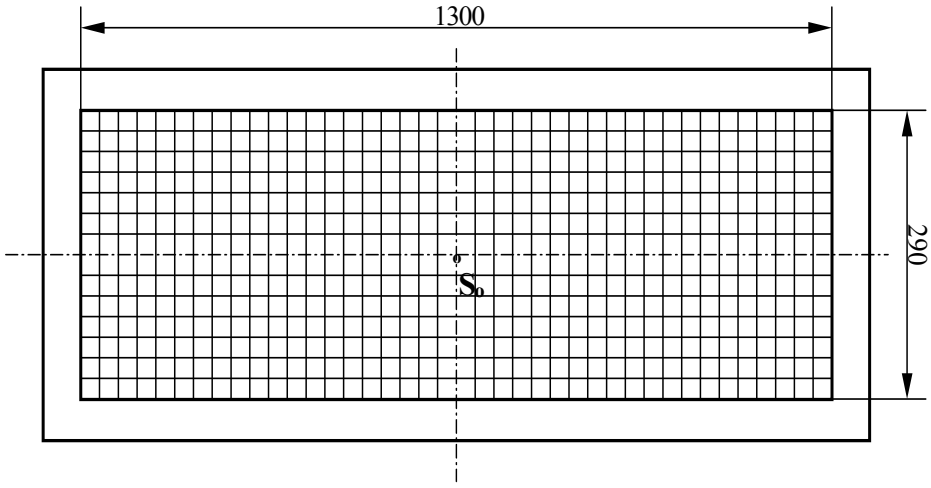

Fig. 3. The dimensions of sieve of the experimental screen

The granulometric composition of the material is summarised in Table 2 provided underneath. For all materials used the granulmetric composition coincided. In Figure 4 the composition of the material is given in the form of the curve of outflow and the curve of the material gathered on the sieve.

Table 2. Granulometric composition of used material

Grain class d [mm]	Percentage of share U [%]		Mass of sand class [kg]	sum [kg]
0.2	11.25	50%	3.38	
0.4	16.25		4.88	
0.63	22.5		6.75	30
0.85	22.5	50%	6.75	
1	16.25		4.88	
2	11.25		3.38	

In the course of the investigations a few tens of series tests were performed. Each cycle of tests consisted of the experimental screening of the material prepared beforehand and its separation into two products, i.e. upper and bottom ones. On completion of screening the following products were weighted, i.e. the products which were above the sieve (m_g) and under the sieve *(*m_g). The results were summarized in Table 2. Next, both fractions were thoroughly mixed and they were used in a subsequent test cycle. The parameters of work of the screen drive were set for each cycle. Additionally, the mass flow rate of material outflow was regulated through the increase and decrease of the outflow gap in a feeder.

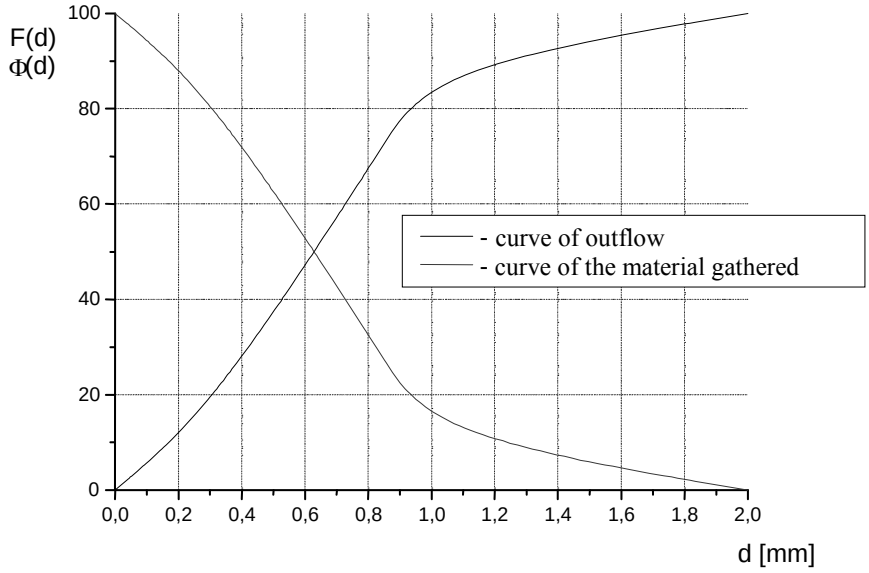

Fig. 4. The characteristics of the materials examined

The results of the research were presented in the graphical form. Each of the graphs was constructed on the basis of three test cycles, corresponding to three different rates of material feeding. The screen capacity was marked on two x-axes. The bottom axis was scaled in [$^{kg}/_{s}$] (mass flow rate of material inflow) whereas the axis of ordinates presents the efficiency of the screen.

To calculate the efficiency of the screening process the following dependence was used:

$$\eta = \frac{m_d}{m_n \cdot K_d} \tag{2}$$

where: m_d – the mass of the product under the sieve, kg, determined experimentally
m_n – the mass of the material, kg

K_d – the participation of the bottom class in the material – 50%.

Figures 5 – 7 show the course of chosen curves concerning the efficiency and capacity for various settings of the screen drive.

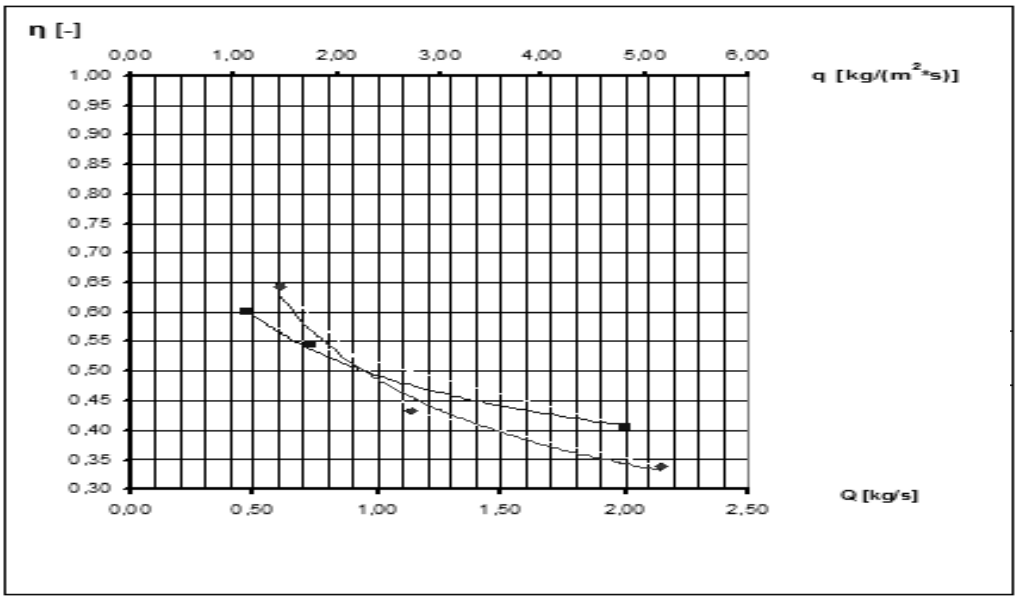

Fig. 5. The results for the following settings: α=15º, β=0º, F=2kN, $\omega_1 / \frac{1}{2}\omega_2$

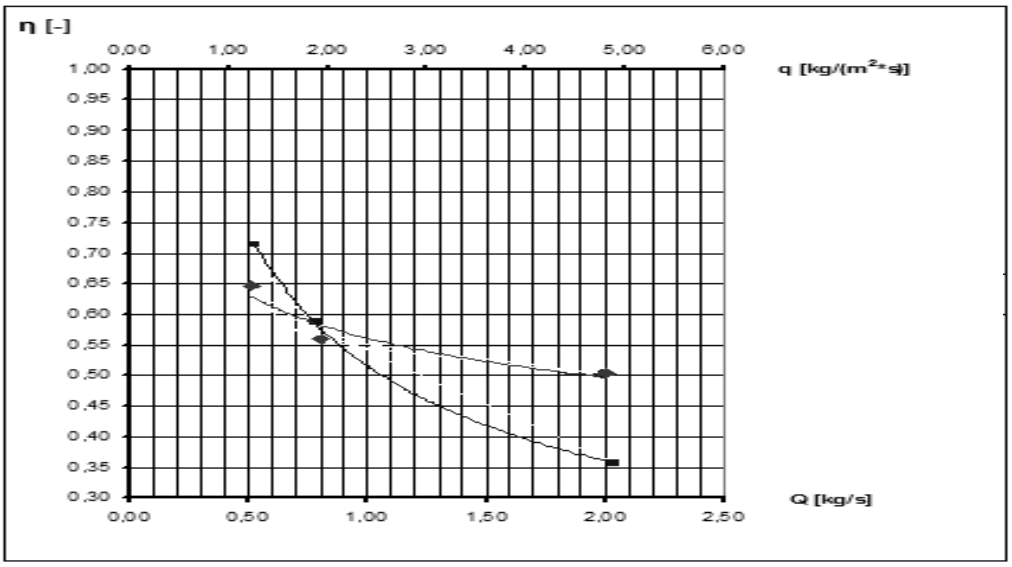

Fig. 6. The results for the following settings: α=15º, β=0º, F=2kN, $\omega_1 / \frac{1}{3}\omega_2$

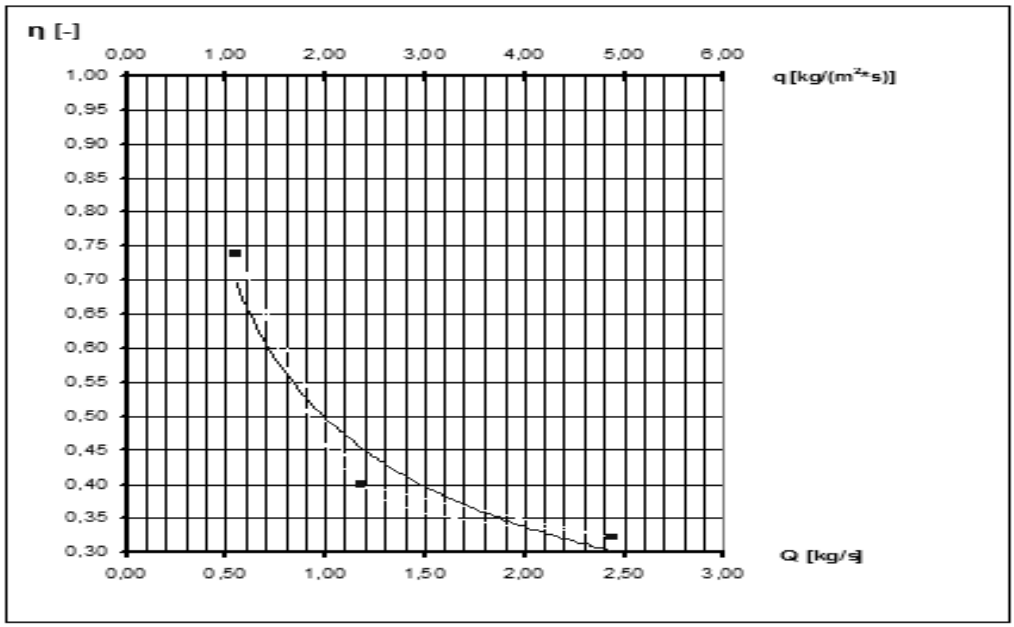

Fig. 7. The results for the following settings: α=15º, β=42,2º, F=2kN, ω_1 / ω_2

It must be underscored that in certain cases the material motion on the sieve was not ensured which took place at the concurrent synchronization, maximal exciting force and the frequency ratio ω_1 / $^{1}/_{2}\omega_2$. Such configuration of the sieve contributed to the generation of torsional vibrations, i.e. the beginning and end of the sieve moved at maximal amplitudes whereas the middle part was almost still. The effect of torsional vibrations was the accumulation of the granular material in the central part of the sieve which, in turn, led to the blocking of the whole process of material flow. In this way, the circulation occurred in the material layer generated, in the course of which the material was flowing on the sides of the sieve down the screen to circa ¼ of its length and, subsequently, was reversed in the direction of the central part of the sieve. The process of screening occurred, however not sufficiently effective.

THE POSSIBILITIES OF APPLICATIONS OF DOUBLE-FREQUENCY SCREENS

To the advantages of double-frequency screens one may account:

- the simplicity of construction with a number of configurations of the driving system which are not encountered in the other machines of this type,
- the possibility of using of the components typical of other screens such as, for instance, sieves, spring suspensions, main frames, mounting mechanisms of

sieves, sieves alone, rotational vibrations and other elements tested in the industrial practice,

- quite high efficiency: for the tested range of material inflow rate (0,5 – 2,5 kg/m^{2}s), the efficiency of the process exceeded 50% in the vast majority of cases, even for such a difficult material for screening as marble aggregate.

In the Ore Enrichment Plants of the KGHM "Polish CopperCo., the granulometric classification of crude ore on the sieves, prior to the process of grinding of this ore, is carried out. The screening of crude ore is performed with an insufficient efficiency due to the fact that the existing screens are supplied with the flux of ore of too high mass flow rate. On screen beds one may observe a too thick granular layer which does not allow the efficacious separation of the bottom class from the upper one. The modernization of the copper ore screen classification may be obtained thanks to the double-frequency screen application and the increase of screen beds in this machine which will allow the quicker separation of the thicker classes from the material.

It is widely accepted that big machines, i.e. screens operating in the extractive and processing industry should be driven using non-balanced shafts, located directly on the sides of screens. Such a constructional solution is realistic also in the case of a double-frequency screen.

As it may be seen, a double-frequency screen is a universal screen encompassing the experience which has been gained so far regarding the structure and exploitation of screening machines. Furthermore, this screen is characterized by a uniform distribution of the oscillating masses which does not take place in the case of the constructions which have been known up to the present moment.

CONCLUSIONS

The main feature of the double-frequency screen is the possibility of free configuration of the inertia drive and, thus the possibility of its compliance with the requirements set by the process of screening of the concrete granular material. The optimization of operation of the drive is carried out through the regulation of the vibrators rotational frequency, their exciting force and mutual location and the direction of rotations.

As a criterion of the device operation quality evaluation the screen efficiency and mass capacity were assumed. These parameters have a significant meaning from the point of view of the process economy. The process investigations constitute the only way to achieve the aim which is the optimization of the drive system due to the fact that even the appropriate operation of the mechanical systems does not mean the ensuring of the sufficiently good screening conditions.

Based on the preliminary examination it may be stated that:

- the countercurrent synchronization of vibrators is better from the process point of view;
- smaller inclination of the sieve ensures better screening conditions;
- the application of vibrators of considerable power is not economically justified;
- the location of vibrators with regard to the mass centre does not affect the process.

The analysis of the results of the investigations makes one draw a number of more general conclusions which are as follows:

- screen drive system allows one to obtain the complex sieve motion which, in turn, enables to attain high screening efficiency;
- double-frequency screen should be assigned to the screening of finely grained materials and those which are screened with difficulty due to the fact that the machine brings about the intensive loosening of material on the sieve;
- condition of the proper operation of the screen is to ensure the rigidity of the sieve on the plane of vibration trajectories;
- phenomenon of driving vibrators self-synchronization enables to simplify the construction of the screen because it is not necessary to apply any devices which would trigger the synchronization. As it is reported, self-synchronization is a durable phenomenon; in the course of the measurements the motion once started occurred in trajectories which depended exclusively upon the configuration of the driving system;
- construction of the line-elliptic screen allows the application of all known construction elements of the screening machines which makes it easier to apply this screen practically to industry.

REFERENCES

BANASZEWSKI T., 1990 *Przesiewacze*; Wydawnictwo „Śląsk”

WODZIŃSKI P., 1997 *Przesiewanie i przesiewacze*; Wydawnictwo Politechniki Łódzkiej.

WODZIŃSKI P., 1981 *Odsiewanie materiałów ziarnistych* Zeszyty Naukowe PŁ, Rozprwy naukowe z. 40.

MEINEL A., SCHUBERT H., 1971 *Zu den Grundlagen der Feinsiebung. Aufbereitungs – Technik*, BOCK B., KRAEMER T., 1984 *Siebung mit Gummisiebböden unterschiedlicher Lochformen. Aufbereitungs – Technik*.

TURKIEWICZ W., BANASZEWSKI T., 1982 *Wzrost amplitudy drgań podczas zatrzymywania przesiewaczy z napędami bezwładnościowymi*. Archiwum Górnictwa.

WODZIŃSKI P., 2000 *Przesiewacze wieloczęstościowe*, Praca wykonana w ramach projektu badawczo – rozwojowego MNiSzW nr R 1401403.

Modrzewski R., Wodziński P., Wyniki *badań procesowych przesiewacza dwuczęstościowego*, Physicochemical Problems of Mineral Processing, 44 (2010), 169-178 (w jęz. ang), http://www.minproc.pwr.wroc.pl/journal

W niniejszej pracy zaprezentowano wstępne wyniki badań procesowych, będących częścią programu badawczego, jaki jest prowadzony w Katedrze Aparatury Procesowej Politechniki Łódzkiej. Prace te mają na celu przebadanie procesowe nowego przesiewacza doświadczalnego – dwuczęstościowego, pod kątem jego przydatności do przesiewania drobno uziarnionych materiałów sypkich. Głównym celem niniejszego opracowania jest przedstawienie wyników badań procesowych tego przesiewacza dla różnych konfiguracji napędu, w postaci graficznych zależności sprawnościowo-wydajnościowych.

słowa kluczowe: klasyfikacja, sita wibracyjne, częstotliwość rotacji, wibrator

Physicochem. Probl. Miner. Process. 44(2010) 179-186

journal homepage
www.minproc.pwr.wroc.pl/journal/

Physicochemical Problems of Mineral Processing

Index No. 32213X ISSN 1643-1049

A. Nowik-Zając*, C. Kozłowski*, W. Walkowiak**

TRANSPORT OF PERRHENATE ANIONS ACROSS PLASTICIZER MEMBRANES WITH BASIC ION CARRIERS

Received January 9, 2009; reviewed; accepted April 13, 2009

Transport experiments across polymer inclusion membranes (PIMs) are presented. The physical immobilization of trioctylamine (TOA) or methyltrioctylammonium chloride (TOMACl) as the ion carriers and *o*-nitrophenyl octyl ether as the plasticizer in cellulose triacetate as the support were used to prepare polymer inclusion membranes. The competitive transport of ReO_4^- ions from nitrate aqueous solutions through a PIM with TOA or TOMACl was investigated. The effect of the pH of the source aqueous phase on ReO_4^- transport from nitrate solution was studied. The higher efficiency of ReO_4^- removal was observed with use of the basic carrier. TOMACl. The selectivity of competitive oxoanions transport from the source phase decreases as follows: $ReO_4^- > NO_3^- > SO_4^{2-}$. This order of permeability correlates well with the energy of transported anions hydration.

key words: polymer inclusion membranes, oxoanions, separation, perrhenate

INTRODUCTION

The selectivity and removal of toxic metal cations from water has frequently been addressed in membrane separation systems. Toxic metal anions have not received significant attention. There are specific reasons why anion receptors are more challenging to design than cation receptors (Gale, 2003).

* Institute of Chemistry and Environment Protection, Jan Dlugosz University of Czestochowa, 42-201 Czestochowa, Armii Krajowej 13, Poland, Corresponding author address: c.kozlowski@ajd.czest.pl
** Chemical Metallurgy Division, Faculty of Chemistry, Wroclaw University of Technology, 50-370 Wroclaw, Wybrzeze Wyspianskiego 27, Poland

Anion separations are important for a number of reasons. Some anions, when introduced into the environment in sufficient quantities, pose health risks to humans and animals (Vandergrift et al., 1992). Fertilizers, feedlots, livestock waste and human waste from highly populated areas produce large amounts of nitrates, phosphates and sulfates.

Another important target of metal anion separation is technetium. Nuclear wastes contain radioactive ^{99}Tc, which is often present in solution as pertechnetate (Manahan, 1994). It would be desirable to remove the radioactive pertechnetate from nuclear wastes at the reprocessing plant. Also, radioactive ^{99}Tc and ^{188}Re are generated in isotonic solutions as pertechnetate or perrhenate for use in medical diagnostic and therapeutics (Brix et al., 2001a). Furthermore, non-radioactive perrhenate is often used as a model anion to simulate binding of radioactive pertechnetate, since the perrhenate anion has the same charge and a similar radius as pertechnetate (Brix et al., 2001b). Permeability was higher for the oxoanions than for halide anions although hydration energies for the monovalent oxoanions are comparable to those of the halides, while hydration energies of the other oxoanions are higher.

Transport of anions was attenuated significantly in a number of cases, and very high selectivity for perrhenates was observed. Perrhenates transport was selective over the divalent anions. The selectivity for perrhenate over the divalent metal cations was also observed (Gardner et. al., 2006).

Recently, ion exchange methods such as solvent extraction (Kasikov et al., 2007; Zhou et al., 1999), liquid membrane transport (Gardner et al., 2006) and polymer inclusion membrane (Marcus, 1991) in separation of perrhenate anions were presented. Marcus (1991) observed anion transport selectivity in PIM transport for ReO_4^- over NO_3^-. This trend in anion transport selectivity follows the trend of calculated hydration energy values. NO_3^- has a higher hydration energy and is transported slower than ReO_4^-, which has a lower hydration energy. Lamb et al., (2008) showed that ReO_4^- is selectively transported over NO_3^-. In the presence of K^+ and Na^+, ReO_4^- transport is promising, while Pb^{2+} promotes NO_3^- removal. Kudo et al. (2007) determined equilibrium constants for the formation of Na^+-ReO_4^--crown ether complex. Kopunec et al., (Kopunec et al., 1998) showed that the extraction constant for Ph_4P^+-ReO_4^- ion pair is several times higher than that for Ph_4As^+-ReO_4^-

This paper describes the competitive transport of perrhenate, sulfate and nitrate anions from aqueous solutions through PIMs with the basic carries tri-n-octylamine (TOA) and methyltrioctylammonium chloride (TOMACl). The influence of ion carriers and pH of source phase on the transport efficiency is reported. The separation of ReO_4^-, NO_3^-, SO_4^{2-} from acidic aqueous solutions across PIM with TOMACl was also studied.

MATERIALS AND METHODS

REAGENTS

Inorganic chemicals such as sodium perrhenate, sodium hydroxide, sulfuric and hydrochloric acids were of analytical grade and were purchased from POCh (Gliwice, Poland). Organic reagents, such as cellulose triacetate (CTA), *o*-nitrophenyl octyl ether (ONPOE), tri-n-octylamine (TOA), methyltrioctylammonium chloride (TOMACl) and dichloromethane were also of analytical grade and were purchased from Fluka and used without further purification. Aqueous solutions were prepared with double distilled water with a conductivity of 0.1 μS cm^{-1}.

PREPARATION OF POLYMER INCLUSION MEMBRANES

A solution containing cellulose triacetate as the support, o-nitrophenyl octyl ether as the plasticizer, and tri-n-octylamine or methyltrioctylammonium chloride as the ionic carrier in dichloromethane as the organic solvent was prepared. A specified portion of this organic solution was poured into a glass Petri dish consisting of a 9.0 cm glass ring attached to a glass plate with cellulose triacetate-dichloromethane glue. The dichloromethane was evaporated overnight, and the resulting membrane was separated from the glass plate by immersion in cold water. Two samples of membrane were cut out from the same membrane for duplicate transport experiments.

TRANSPORT STUDIES

Transport experiments were carried out in a permeation cell in which the membrane film (4.9 cm^2 effective surface) was tightly clamped between two compartments. The aqueous receiving phase was a 0.10 mol dm^{-3} aqueous solution of sodium hydroxide (50 cm^3). Transport was conducted at a room temperature (23 to 25 ^{0}C) and both the source and receiving aqueous phases were stirred at 600 rpm with synchronous motors. Samples (0.010 cm^3) of the aqueous receiving phase were removed periodically via a sampling port with a syringe and analyzed to determine the concentrations of ReO_4^-, NO_3^- and SO_4^{2-}. The source phase acidity was monitored using a pH meter (multifunctional pH meter, CX-731 Elmetron, with combine pH electrode, ERH-136, Hydromet, Poland). The kinetics of the transport process through the polymer inclusion membrane is described by a first-order reaction in respect to metal ion concentration (Danesi, 1984):

$$\ln(c / c_i) = -kt \tag{1}$$

where c is the metal ion concentration (mol dm^{-3}) in the source phase at a given time; c_i is the initial ReO_4^- concentration in the source phase; k is the rate constant (s^{-1}); and t is the transport time (s).

To calculate the k value, a plot of $\ln(c/c_i)$ versus time was made. The rate constant value for the duplicate transport experiment was the averaged, and the standard deviation was calculated. The permeability coefficient (P) was calculated as follows:

$$P = -(\mathrm{V}/\mathrm{A})k \tag{2}$$

where V is the volume of aqueous source phase, and A is the area of membrane.

The initial flux (J_i) was calculated as follows:

$$J_i = Pc_i \tag{3}$$

To describe the efficiency of metal ion removal from the source phase, the recovery factor (RF) was calculated as follows:

$$RF = \frac{c_i - c}{c_i} \cdot 100\,\% \tag{4}$$

A capillary electrophoresis system with an ultraviolet (UV) detector (Capel-105, Russia) was used to determine the concentrations of perrhenate, sulfate, nitrate, and chloride anions. The electrophoretic buffer consisted of $5.0 \cdot 10^{-3}$ M chromium(VI) oxide, $2 \cdot 10^{-2}$ M diethanolamine, and $1.65 \cdot 10^{-3}$ M metyltrioctylammonium chloride (from Fluka), at a voltage of 17 kV. The detection limits in this method for the ReO_4^-, NO_3^-, and SO_4^{2-} anions were 0.10 ± 0.02, 0.15 ± 0.05 and 0.20 ± 0.03 mg/dm^3, respectively.

RESULTS AND DISCUSSION

At first, the influence of ion carriers TOA or TOMACl immobilized in cellulose triacetate membrane on perrhenate anions transport was studied. Blank experiments in the absence of the carrier yielded no significant flux across PIM with support and plasticizer only. In previous studies on chromium(VI) transport across PIM, we observed that tertiary amines, such as TOA, also have plasticizing properties (Kozlowski and Walkowiak, 2002, 2005). The polymeric inclusion membranes investigated contained 77 wt. % CTA and 23 wt. % ion carrier. As source and receiving phases, 0.10 M HNO_3 and 0.10 M NaOH aqueous solutions were used, respectively. The results shown in Fig. 1 demonstrate transport of perrhenate anions from 0.10 M nitric acid across the PIM containing TOA or TOMACl. The transport conditions were set up for a high excess of NO_3^- over ReO_4^-.

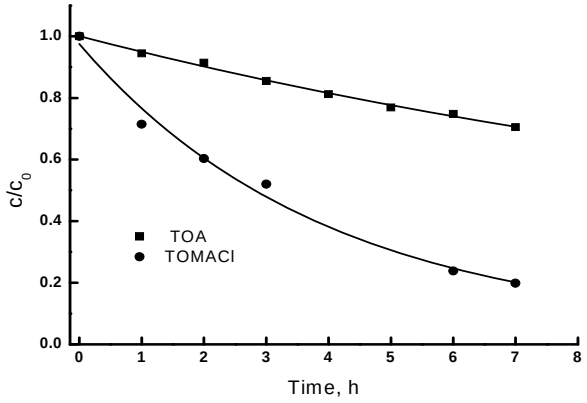

Fig. 1. Kinetics curves of perrhenate anions transport across PIM with TOA and TOMACl
PIMs: 77 wt. % CTA, and 23 wt. % ion carrier; source phase: 0.0050 M ReO_4^- in 0.10 M HNO_3; receiving phase: 0.10 M NaOH

The recovery factors (RF) of nitrate anions for transport with TOA and TOMACl after seven hours were equal to 5.0 % and 3.0 %, respectively. Fig. 1 shows an exponential decrease of ReO_4^-concentration in the source phase versus time. The kinetics of the ReO_4^- transport across the membrane is described by the first order. For transport across PIM with TOMACl and TOA, the fluxes were equal to 3.5 and 0.7 μmol/m^2s, respectively.

Perrhenate removal was observed only in membranes with support (CTA) and ion carriers (TOA or TOMACl). We also applied polymer inclusion membranes containing the typical plasticizer, *o*-nitrophenyl octyl ether. The influence of source phase acidity on ReO_4^- transport through PIM was studied. PIM composition was 40 wt. % of cellulose triacetate as the support, 25 wt. % of tri-n-octylamine or methyltrioctylamonium chloride as the ion carrier, and 35 wt. % of *o*-nitrophenyl octyl ether as the plasticizer. These membranes containing ONPOE as the plasticizer showed much faster transport of ReO_4^- anions. The effect of perrhenate initial fluxes values on pH of source phase is shown in Fig. 2. Comparison of the perrhenate transport across PIM with TOA and TOMACl indicates that the transport rate is twice as high for quaternary ammonium salt (TOMACl), which is a more basic carrier. The results in Fig. 2 show the linear decrease of perrhenate transport flux (in log-log scale) with the pH increase values from 1 to 5. The initial transport flux value achieved for TOMACl at pH 1.0 was equal to 11.68 μmol/m^2s.

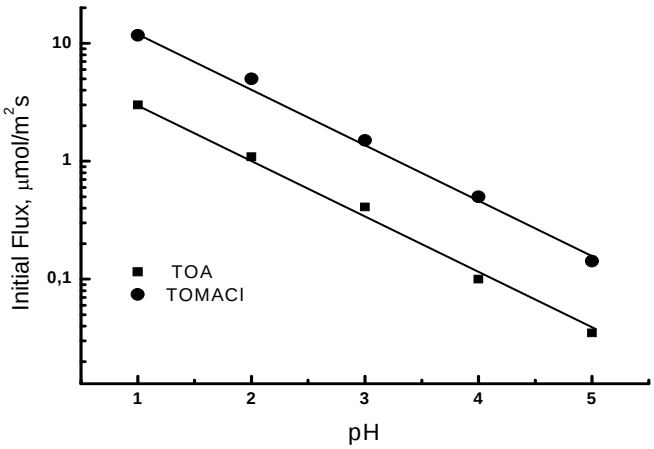

Fig. 2. Iinitial flux values vs. pH of the source phase. Membrane: 0.8 cm^3 ONPOE / 1.0 g CTA, 1.0 M carriers (TOA, TOMACl); source phase: $5 \cdot 10^{-3}$ M ReO_4^-, H(Na)NO_3 I=0.1 M

Finally, competitive transport of perrhenate, nitric and sulfuric anions from acidic solutions was performed. As the aqueous source phase the solution containing $5 \cdot 10^{-4}$ M ReO_4^- in 0.05 M HNO_3 and 0.05 M H_2SO_4 was used. The used membrane contained: 1.0 M carrier (TOMACl) and 0.8 cm^3 ONPOE/1.0 g CTA. As the receiving phase, 0.1 M NaOH was applied. The dependence of recovery factors (RF) for perrhenate, nitrate and sulfate anions *vs.* time in transport across PIM with TOMACl as ionic carrier is shown in Fig. 3.

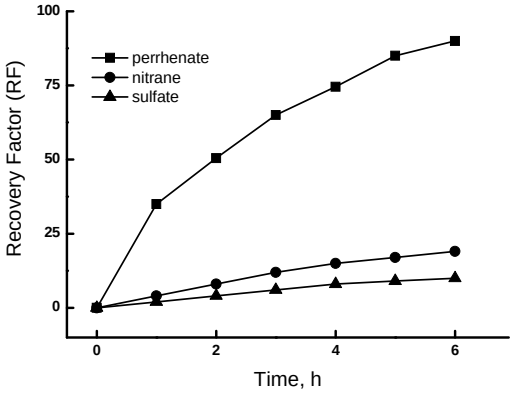

Fig. 3. Recovery factor (RF) vs. competitive transport of perrhenate, nitrate and sulfate on PIM with TOMACl. PIM: 1.0 M TOMACl, 0.8 cm^3 ONPOE / 1.0 g CTA; source phase: $5 \cdot 10^{-4}$ M ReO_4^- in 0.05 M HNO_3 and 0.05 M H_2SO_4; receiving phase: 0.10 M NaOH

As can be seen from Fig. 3, the selectivity order of transport through PIM with TOMACl was as follows: $ReO_4^- > NO_3^- > SO_4^{2-}$. The removal of perrhenate was

higher than that of sulfate and nitrate anions in spite of the high excess of NO_3^- and SO_4^{2-} anions. For these transport conditions the selectivity coefficients for perrhenate/nitrate and perrhenate/sulfate were: 11.1 and 8.2, respectively. The hydration energy of SO_4^{2-}, NO_3^- and ReO_4^- anions were -1103 kJ mol^{-1}, -314 kJ mol^{-1} and -240 kJ mol^{-1}, respectively (Gardner et al., 2006). Hydration energy was highest for SO_4^{2-}, and lowest for ReO_4^- anions. There is the correlation between selectively sequence of anions transported,. $ReO_4^- > NO_3^- > SO_4^{2-}$, and hydrophobicity. The highest transported anions are perrhenates, which are the least hydrated.

CONCLUSIONS

Perrhenate anions can be effectively separated from aqueous solutions containing high excess of sulfate and nitrate anions by polymer inclusion membrane transport with basic ion carrier, such as TOMACl. For both TOA and TOMACl, the initial fluxes decreased as the pH of the source phase increased. For competitive transport, the removal of sulfates and nitrates is lower that of perrhenates, in spite of the high excess of NO_3^- and SO_4^{2-} anions. The selectivity order sequence for anions fluxes transported across the polymer inclusion membrane with TOMACl was $ReO_4^- > NO_3^- > SO_4^{2-}$. This correlates well with the hydrophobicity of these anions.

REFERENCES

BRIX K.V., HENDERSON D.G., ADAMS W.J., REASH R.J., CARLTON R. G., McINTYRE D.O., (2001a), *Acute toxicity of sodium selenate to two daphnids and three amphipods*, Environ. Toxicol. Chem. 16, 142-150.

BRIX K. V., VOLOSIN J. S., ADAMS W. J., REASH R. J., CARLTON R. G., McINTYRE D.O., (2001b), *Effects of sulfate on the acute toxicity of selenate to freshwater organisms*, Environ. Toxicol. Chem. 20, 1037-1045.

CIMPEANU C., SAHAGIA M., (2002), *High specific activity ^{186}Re perrhenates to be used for biomolecule labeling*, J. Radiol. Nucl. Chem.. Vol.252, 601-604.

FERGUSON J. E., (1982), *Inorganic Chemistry and the Earth*, Pergamon, Oxford.

GALE P.A., (2003), For reviews on anion receptors: *35 years of synthetic anion receptor chemistry 1968-2003,* Coord. Chem. Rev. 240, 1-221.

GARDNER J. S., PETERSON Q. P., WALKER J. O., JENSEN B. D., ADHIKARY B., HARRISON R. G., LAMB J. D., (2006), *Anion transport through polymer inclusion membranes facilitated by transition metal containing carriers*, J. Membr. Sci. 277, 165-176.

KASIKOV A. G., PETROVA A. M., (2007), *Effect of the structure of Octanols on Their Extraction Capacity for Rhenium(VII) in Sulfuric Acid Solutions*, Russian J. Appl. Chem., Vol. 80, 672-674.

KOPUNEC R., ABUDEAB F. N., SKRAŠKOVA S., (1998), *Extraction of pertechnetate with tetraphenylphosphonium in the presence of various acids, salts and hydroxides*, J. Rad. and Nucl. Chem.. Vol. 230, 51-60.

KOZLOWSKI C.A., WALKOWIAK W., (2002), *Removal of chromium(VI) from aqueous solutions by polymer inclusion membranes*, Water Research 36, 4870-4876.

KOZLOWSKI C.A., WALKOWIAK W., (2005), *Applicability of liquid membranes in chromium(VI) transport with amines as ion carriers,* J. Membr. Sci. 266, 143-150.

KUDO Y., FIJIHARA R., KATSUTA S., TAKEDA Y., (2007), *Solvent extraction of sodium perrhenate by 3m-crown-m ethers (m=5,6) and their mono-benzo-derivatives into 1,2-dichloroethane: Elucidation of fan overall extraction equilibrium based on component equilibria containing an ion-pair formation in water*, Talanta 71, 656-661.

LAMB J. D., MORRIS C. A., WEST J. N., MORRIS K. T., HARRISON R. G., (2008), *Cation effect on anion separation by aza-crown ligands in liquid membranes,* J. Membr. Sci. 321, 15-21.

MANAHAN S. E, (1994), *Environmental Chemistry*, Sixth ed., CRC Press, Inc., Boca Raton, USA.

MARCUS Y., (1991), *Thermodynamics of salvation of ions*. Part 5. Gibbs free energy of hydration at 298,15 K, J. Chem. Soc. Faraday Trans. 87, 2995-2999.

ROUNDHILL D. M., KOCH H. F., (2002), *Methods and techniques for the selective extraction and recovery of oxoanions*, Chem**.** Soc. Rev. 31, 60.

VANDERGRIFT G. F., REED D. T., TASKER I. R., (1992), *Environmental Remediation*, ACS, Washington DC.

ZHOU Z., XING Y., WU Y., (1999), *Solvent extraction of perrhenate with 25,26,27,28-tetrakis[(ethoxycarbonyl)methoxy]-p-tert-butylcalix[4]arene and crystal structure of the extracted complex*, J. Incl. Phenom. Macro. Chem.. 34, 219-231.

Nowik-Zając A., Kozłowski C., Walkowiak W., *Transport anionów nadrenianowych przez polimerowe membrany zawierające zasadowe przenośniki jonowe,* Physicochemical Problems of Mineral Processing, 44 (2010), 179-186 (w jęz. ang), http://www.minproc.pwr.wroc.pl/journal

W pracy opisano badania laboratoryjne dotyczące selektywnego wydzielania anionów nadrenianowych z roztworów azotanowych przez polimerowe membrany inkluzyjne zawierające w roli przenośników jonów trioktyloaminę lub chlorek metylotrioktyloamoniowy oraz trioctan celulozy jako matrycę. Określono również wpływ pH fazy zasilającej na efektywność transportu RO_4^- przy użyciu polimerowej membrany inkluzyjnej zawierającej w/w przenośniki jonów, plastyfikator, tj. eter *o*-nitrofenylooktylowy, immobilizowane do matrycy z trioctanu celulozy. Wykazano, że chlorek metylotrioktyloamoniowy z roztworów silnie kwaśnych efektywnie transportował aniony nadrenianowe niż trioktyloamina. Zbadano również konkurencyjny transport oxoanionów przez plastyfikowaną membranę zawierającą chlorek metylotrioktyloamoniowy i eter *o*-nitrofenylooktylowy. Z porównania szybkości transportu wynika, że malała ona w szeregu $ReO_4^- > NO_3^- > SO_4^{2-}$. Selektywność badanego układu membranowego powiązano z procesem dehydratacji anionów selektywnie transportowanych przez membranę zawierającą czwartorzędową sól amoniową

słowa kluczowe: nadreniany, separacja, polimerowe membrany inkluzyjne

Physicochem. Probl. Miner. Process. 44(2010) 187-194

journal homepage
www.minproc.pwr.wroc.pl/journal/

Physicochemical Problems of Mineral Processing

Index No. 32213X ISSN 1643-1049

T. P. Olejnik*

KINETICS OF GRINDING CERAMIC BULK CONSIDERING GRINDING MEDIA CONTACT POINTS

Received January 5, 2009; reviewed; accepted March 28, 2009

Results of experiments carried out in a pilot-plant ball mill are discussed in the paper. The objective of the experiments was to determine the effect of the number of contact points between grinding media on the rate of grinding. The experimental material was ceramic body used in the production of floor and wall tiles. Main component of the feed was a mixture of feldspar and clay with antiemulsifiers. The feed was subjected to wet grinding. During grinding the rate of comminution of particular size fractions was determined. Changes in particle size distribution of ground material in time were analysed and the effect of ball size, mill filling with the feed and the number of grinding media on the process rate was described.

Main objective of the study was to define the effect of changes in the number of grinding media contact points on the grinding rate. Additionally, the effect of mill filling with the feed on changing specific rate of grinding of particle fractions was determined. The change in time of the particle size composition enabled to calculate the grinding rate of particular fractions. In the calculations Gardner and Austin differential equation was used for discrete values of fractions.

key words: ball mill, specific grinding rate

INTRODUCTION

The process of grinding in ball mills is determined by a complex character of grinding media impact on the raw material being ground. Basic geometric dimensions of the drum and the size and type of grinding media motion have an influence on the process rate and final composition of the ground product.

* Faculty of Process and Environmental Engineering, Technical University of Lodz, Wolczanska 213, 90-094 Lodz, e-mail: tolejnik@p.lodz.pl

The comminution process proceeds mainly due to complex action of grinding media on the material being ground and additionally the interactions between grinding elements and the inner drum surface. Material which is between the surfaces of moving balls is subjected to attrition and shearing with possible crushing (Drzymała et al., 1990; and Mattan, 1971; Lynch, 1974; Shipway, 1994). These mechanisms of comminution occur mainly in the avalanche motion of grinding media. The cascade motion of balls involves additionally an impact mechanism resulting from collisions of balls falling down to the bed of balls and feed which is at the bottom of the drum (Heim et al., 2004) and (Heim et al., 2004). The type of motion at which impact mechanisms prevail, occurs at rotations frequency close to the critical frequency. This phenomenon is very desirable because of grinding intensity, but the size of industrial ball mills and resulting inertia forces reduce the character of mill operation at velocities close to the critical frequency. For this reason, if we choose lower rotations speeds of the mill, the contribution of particular comminution mechanisms can be changed by changing the size and number of grinding media. It is obvious that at the same volume of the bed of grinding media and ball filling of the mill, the bigger are the balls, the smaller is their number. An increase of the ball size determines an increase of a single ball mass and extension of mutual interactions between the grinding media. An enlarged size of the grinding media, at unchanged ball filling of the mill, causes a decrease of the number of contact points. This induces a decrease of mini-regions in which breaking stresses may occur leading to destruction of ground material particles. Ball diameters are selected according to the ground material strength and particle diameter of the mill feed. For bigger particles that require a higher breaking strength, the balls should be bigger, while for smaller particles and materials with lower strength better results are obtained when the number of ball contacts, and consequently the number of balls, increases at the cost of their diameters.

Simplicity of the mill construction does not keep up with grinding process efficiency. Low process efficiency makes technologists look for such a composition of balls and ball filling of the mill at which the mean particle diameter decreases at the fastest rate. This will enable a more economic use of the mill operating time.

Having this in mind, results of comminution in a mill with different number and size of balls as well as different load filling of the mill were analysed. Ceramic body was subjected to wet grinding.

GRINDING PROCESS AND EQUIPMENT PARAMETERS

Changes of particle size distribution in time were studied in a pilot-plant mill. Basic technical data of the mill are given in Table 1.

Table 1. Main parameters of a pilot-plant mill

Inner diameter [m]	0.5
Total volume [m^3]	0.112
Rotations speed n[min^{-1}]	31
n/n_{kr}	0.54

The comminution process was carried out in wet regime (water solution with antiemulsifiers). The feed was a mixture of rock material, mainly feldspar and clay. Grinding was performed for different feed compositions. The difference in feed composition was determined by the assignment of the ground product and was related directly to the assortment of final products obtained from the ceramic body. A differentiated feed composition depended on specific utility requirements. The technology of ceramic body production for floor tiles requires an increased percentage of harder components (feldspars). In wall tiles the feldspar percentage is reduced to a minimum. Table 2 gives compositions of feed comminuted in the tested mill for two groups of products, wall and floor tiles.

Ball charge of the mill was assumed to be 45% of the mill volume for the full feed load. The ceramic body was ground at changing ball composition. Mass of size fractions and ball dimensions for each experimental series are given in Table 3. To differentiate grinding series according to ball composition, each of them was given a symbol A, B and C.

Table 2. Components of raw material used in the production of wall and floor tiles

	Wall tiles	Floor tiles
Solid components [kg]	66	66
- feldspar [kg]	18	36
- clay [kg]	29	25
- quartz [kg]	11	5
- carbonates [kg]	8	-
Liquid components [kg]	19.7	19.7
- water [kg]	19.5	19.5
- sodium tripolyphosphate [kg]	-	0.2
- liquid glass [kg]	0.2	-

RESULTS AND DISCUSSION

Grinding was a batch process. Samples of ground material were taken at every 1000 revolutions of the mill. Particle size analysis of the samples was made using an ANALYSETTE 22 laser particle size analyser (FRITSCH).

Table 3. Composition and dimensions of balls

Series	A	B	C
Ball diameter, [mm]	Ball mass, [kg]		
10	12.4	2	-
20	24.6	25	22.6
30	24.6	25	29.4
40	20.4	30	30
Total, [kg]	82	82	82

On the basis of the particle size analysis comminution rates were calculated for particular size fractions. In the calculations, Gardner and Austin equation (1) was used in the differential form for discrete values of the fractions, assuming an ideal mixing of the ground material.

$$\frac{\mathrm{d}w_i(t)}{\mathrm{d}t} = -S_i w_i(t) + \sum_{j=1,i>1}^{i-1} S_j b_{i,j} \cdot w_j(t) \tag{1}$$

The form of equation describing a change of coefficient $b_{i,j}$ was also assumed:

$$b_{i,j} = \phi\left(\frac{d_i}{d_j}\right)^{\gamma} + (1-\phi)\left(\frac{d_i}{d_j}\right)^{\beta} \tag{2}$$

Rate coefficients S_i in equation (1) for grinding of material used for wall tiles production for series A, B and C are given in Table 4. Similar calculations of rate coefficient S_i in equation (1) were made for grinding of material used in the production of floor tiles.

Knowing the particle size distribution also the mean particle size was calculated from the formula

$$d_s = \sum_{i=1}^{n} d_{si} \cdot x_i \tag{3}$$

Using Statistica®, the correlation equations of changes in the comminution rate as a function of particle size fraction d_i were generated. This allowed us to present process kinetics in the form of a relationship between the rates S_i for particular size fractions and the filling of mill with the feed and grinding media.

As an equation describing the rate of grinding particular size fractions, the following function was used:

$$S(i) = K_S \cdot d_S(i)^{n_s} \cdot e^{-b_s \cdot d_{si}} \tag{4}$$

Coefficients K_S, n_s and b_s for each measuring series are given in Table 5.

Table 4. Rate coefficients S_i for grinding of wall tile material in series A, B and C

Ball composition	Series A	Series B	Series C
d_{sr}	S_{iA} x 10000	S_{iB} • 10000	S_{iC} • 10000
704.28	5.25	6.01	18.8
545.115	7.2	1.18	48.7
418.03	10.9	28.4	8.03
320.34	19.9	51.2	6.53
245.565	19	29.1	36.9
188.25	7.05	0.67	22.3
`144.31	3.16	1.67	12
110.625	2.65	1.96	6.47
84.805	2.22	1.79	4.3
65.01	1.27	1.08	4.5
49.835	0.198	0.15	3.13
38.205	0.368	5.74	1.19
29.29	0.532	7.31	1.29
22.45	0.65	7.98	1.65
15.695	0.713	0.83	3.07
10.115	0.714	0.81	5.66
7.755	-0.66	0.69	7.42
5.945	-0.606	-0.53	7.28
4.555	-0.594	-0.4	5.99
3.49	-0.605	-0.32	4.3
2.675	-0.577	-0.27	2.7
2.05	-0.496	-0.26	1.56
1.575	-0.399	-0.25	0.88
1.21	-0.316	-0.24	0.47
0.925	-0.255	-0.23	0.22
0.71	-0.215	-0.23	0.04
0.545	-0.19	-0.24	-0.11
0.415	-0.195	-0.28	-0.19
0.32	-0.212	-0.35	-0.26
0.245	-1	-1.22	-0.34

Table 5. Coefficients γ, β and ϕ in equation (2) and K_s, b_s and n_s in equation (4)

Parameter / Series		γ	β	φ	$K_S * 10^6$	b_s	n_s	R^2
Wall tiles	A	3.227	3.114	0.618	0.128	0.0146	3.9	0.83
	B	1.066	1.083	0.756	0.0061	0.0139	3.4	0.72
	C	0.15	3.4	0.88	35.5	0.0073	2.5	0.98
Floor tiles	A	4.8	4.15	0.78	58.9	0.0135	2.4	0.80
	B	3.654	1.538	0.7973	5.18	0.0199	3.6	0.82
	C	0.1496	2.465	0.6269	393	0.0141	2.2	0.74

To present a clearer picture of the change in comminution rate of particular size fractions of the feed, the range of changes in the mean particle diameter d_s was reduced to 200 μm (Fig. 1). As follows from calculated coefficients of equations 2 to 4 and from the diagram shown in Fig. 1, the best results were obtained for series B and a mixture of raw materials used in the production of floor tiles – line gB. Series B was characterised by the most differentiated composition of balls with the largest differences between the smallest and the biggest ball diameter. Slightly worse, although still relatively high grinding rates were obtained for series mC (material for wall tile production). Series C was characterised by the greatest number of balls with the biggest diameters. They determine the biggest breaking forces required to comminute the material. Within the size fraction above 250 μm, the grinding rate is the highest for series C (Fig. 2.). The lowest grinding rate in the whole range of particle size changes was obtained in series A with grinding of the raw material used in the production of floor tiles – curve fA. For other measuring series, the grinding rates were similar in the whole size range of particles.

Interesting are the profiles of curves wC and fB. A bigger number of balls with increased diameters (series C) determines the stronger impact forces which has a favourable effect on grinding of big size fractions. For small particle sizes, smaller than ca. 220 μm, the rate of grinding depended not on the ball sizes but on an increased number of contact points of feed with grinding media.

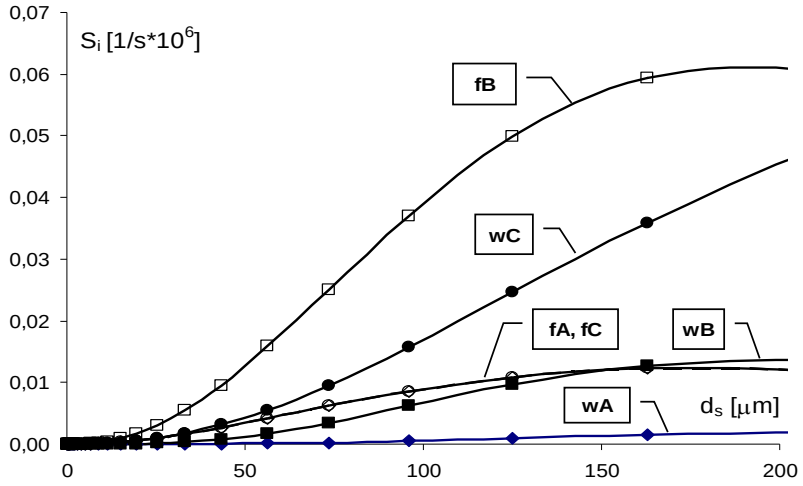

Fig. 1. Change of comminution rate S_i of wall tile material (*w*) and floor tile material (*f*) for series A, B and C. Correlation function (4), range of particle size changes 0÷200 μm

This tendency was more pronounced with the increase of the number of particles with high mechanical strength in the mill feed. In the mixture used in floor tile production, the content of hard feldspar fractions was twice as high as in the mixture used in the production of wall tiles. The calculation shows that negative values of comminution rate (Table 4) occurred for particle size fraction below 5 μm. This can be explained by

agglomeration of the smallest particles of the feed which was caused by interparticle interactions. This is an unfavourable phenomenon that has an influence on grinding of coarser fractions. The smallest fractions can stick to the grinding media decreasing in this way the impact of grinding media on the comminuted material.

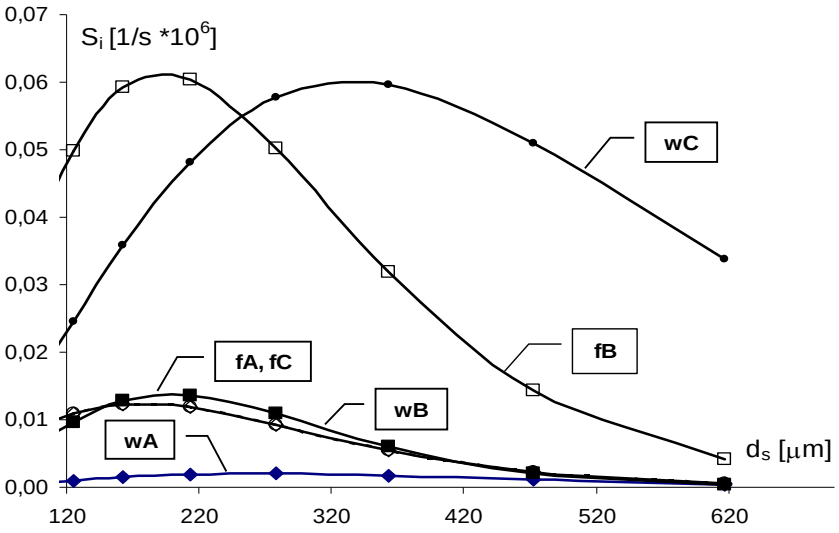

Fig. 2. Change in comminution rate S_i of wall (*w*) and floor (*f*) tile material in series A, B and C. Correlation function (4), range of particle size change 120 – 620 μm.

CONCLUSIONS

The following conclusions can be drawn on the basis of the results presented in this study.

The process of grinding in ball mills during the initial period when feed particles are relatively coarse, is affected by the size of balls and mill filling which determines the forces with which the balls act on each other.

After that, when particle size of ground material is much finer, we can observe the effect of the number of balls, or more precisely the number of contact points of grinding media between which material particles are comminuted.

The highest comminution rates for big fractions of the feed were obtained for the balls with the biggest diameters. Decreasing the number of balls with big diameters and replacing them with grinding media of smaller diameter cause a significant reduction of the comminution rate and lower variability of this parameter in the whole size range of the ground product.

NOMENCLATURE

$b_{i,j}$ – particle size distribution function
b_s, K_s, n_s – parameters in correlation equation (4)
d_i, d_j – particle diameters in size fractions *i* and *j,* respectively
d_s, d_{si} – mean particle size and mean (arithmetic) size of particles in size fraction *i*, respectively
S_i, S_j – specific rate (separation parameter) of grinding particles from fraction *i* or *j,* $w_i(t)$, $w_j(t)$ – weight fraction of particles *i* or *j* after grinding time *t*
x_i – mass fraction of particles from size fraction *i* respectively
β, φ, γ, – parameters in equation (*2).*

ACKNOWLEDGEMENTS

This study was carried out within research project no. W-10/1/2009 Dz.St 1

REFERENCES

DRZYMALA Z. (1992), *Badania i podstawy konstrukcji młynów specjalnych*. PWN. Warszawa.
MATTAN J. (1971), *How to step up ball mill efficiency*. Rock Products, Nr 5.
LYNCH A.J. (1974), *Mineral crushing and grinding circuits*. Amsterdam, Oxford, New York.
SHIPWAY P. H., HUTCHINGS I. M. (1993), *Attrition of brittle spheres by fracture under compression and impact loading*. Powder Tech. 76, 23-30.
HEIM A., OLEJNIKl T.P., PAWLAK A. (2004), *Analiza porównawcza pracy wybranych przemysłowych młynów kulowych (Comparision analysis of some industrial ball mills)*, KOMEKO.
HEIM A., OLEJNIK T.P., PAWLAK A. (2004), *Effect of the number od grinding media contact points on ceramide body grinding rate,* Proceedings of 16 th International Congress of Chemical and Process Engineering (Praha 22-26.08), P5.270, pp.1-13.

Olejnik T.P., *Kinetyka rozdrabniania masy ceramicznej z uwzględnieniem liczby punktów kontaktów mielników***,** Physicochemical Problems of Mineral Processing, 44 (2010), 187-194 (w jęz. ang), http://www.minproc.pwr.wroc.pl/journal

W artykule omówiono wyniki badań przeprowadzonych w pół-przemysłowym młynie kulowym. Celem badań było określenie wpływu liczby punktów kontaktu, pomiędzy mielnikami a nadawą, na szybkość przemiału. Do eksperymentu użyto kul materiałów skalnych wykorzystywanych w produkcji ceramiki budowlanej. Rozdrabniany materiał składał się z mieszaniny skaleni oraz glinki z dodatkiem antyemulgatorów. Przemiał wykonano na mokro. W trakcie przemiału określano skład granulometryczny mielonego surowca. Zmiany wymiarów ziarna średniego w czasie, poddano analizie ze względu na wpływ wielkości mielników, wypełnienia młyna oraz liczby mielników, określając szybkość procesu rozdrabniania. Główny cel badań dotyczył określenia wpływu zmiany liczby punktów kontaktu mielników na szybkość właściwą rozdrabniania nadawy. Zmiana w czasie rozmiaru ziarn pozwoliła na określenie szybkości procesu dla poszczególnych klas rozmiarowych. Do obliczeń wykorzystano równanie Gardnera i Austina w formie dyskretnej.

słowa kluczowe: młyn kulowy, szybkość przemiału

Physicochem. Probl. Miner. Process. 44(2010) 195-204

journal homepage
www.minproc.pwr.wroc.pl/journal/

Physicochemical Problems of Mineral Processing

Index No. 32213X ISSN 1643-1049

B. Pospiech[*], W. Walkowiak[**]

STUDIES ON IRON(III) REMOVAL FROM CHLORIDE AQUEOUS SOLUTIONS BY SOLVENT EXTRACTION AND TRANSPORT THROUGH POLYMER INCLUSION MEMBRANES WITH D2EHPA

Received March 20, 2009; reviewed; accepted July 7, 2009

The removal of iron(III) from chloride acidic aqueous solutions in solvent extraction and transport through polymer inclusion membranes (PIMs) has been studied. D2EHPA was used as the extractant/ion carrier in these processes. The extraction of Fe(III), Mn(II), Ni(II), Cu(II) and Co(II) with 0.5 M D2EHPA was: 73.4 %, 11.2 %, 15.3 %, 7.8 % and 23.9 %, respectively. Separation factors *(S)* for metal ions were calculated and reported. The transport across PIM containing cellulose triacatate (CTA) as the support and *o*-nitrophenyl octylether (ONPOE) as the plasticizer was found to be the effective and selective method of Fe(III) ions removal from aqueous chloride solutions containing Mn(II), Ni(II), Cu(II) and Co(II) ions. The stability of PIMs was also studied. Present studies indicate that the transport across PIM has the long term integrity.

key words: iron(III), D2EHPA, solvent extraction, polymer inclusion membranes

INTRODUCTION

Iron(III) is present in the solutions after hydrometallurgical processes of recovering a number of nonferrous metal ions such as nickel(II), cobalt(II) and copper(II). The removal of iron(III) from aqueous solutions is a very difficult. Studies on application of tributyl phosphate (TBP) in selective removal of iron(III) from

[*] Department of Chemistry, Czestochowa University of Technology, 42-200 Czestochowa, Poland

[**] Division of Chemical Metallurgy, Wroclaw University of Technology, 50-370 Wroclaw, Poland, e-mail: wladyslaw.walkowiak@pwr.wroc.pl

solution containing manganese(II), copper(II), nickel(II) and cobalt(II) by solvent extraction and transport through polymer inclusion membranes processes were studied (Pospiech and Walkowiak 2005). The commercial cationic and neutral extractans have been proposed for the extraction in order to separate iron(III) from other metal ions. Several publications have dealt with the application of organophosphorus acids and the derivatives of organophosphorus compounds in separation of iron(III) from aqueous chloride and sulphate solutions, i.e. di(2-ethylhexyl)phosphoric acid (D2EHPA) and di(2-ethylhexyl)phosphonic acid (PC - 88A) (Lupi and Pilone 2000; Biswas and Begum 1998, 1999, 2001; Jayachandran and Dhake 1997), tributyl phosphate (TBP) and methyl *iso*-butyl ketone (MIBK) (Saji and Reddy 2001), trioctylphosphine oxide (TOPO) and Cyanex 923 (Saji et al. 1998; Gupta et al. 2003). Separation of iron(III) and nickel(II) from a spent $FeCl_3$ by solvent extraction using Alamine 336, MIBK and PC 88A as extractants were also investigated (Lee et al. 2005). Comparative study of iron(III) separation from zinc sulphate-sulphuric acid solutions by D2EHPA was performed (Principe and Demopoulos 2004). Separation of iron(III), copper(II) and zinc(II) from a mixed sulphate/chloride solution was carried out using the extractants TBP, LIX 84I and Cyanex 921 in kerosene (Sarangi et al. 2007).

The supported liquid membranes (SLM) and polymer inclusion membranes (PIMs) are used to separate different metal ions such as copper(II), nickel(II), cobalt(II), iron(III) and zinc(II) (Gill et al. 2000, Pospiech and Walkowiak 2007; Parhi and Sarangi 2008; Walkowiak and Kozlowski 2009). Transport of iron(III) through SLM with the phosphine oxide (Cyanex 921) as ion carrier is a very effective method of removal of iron(III) from aqueous solutions (Alguacil and Alonso 2000). For concentration of Cyanex 921 higher than 0.26 M, permeability coefficient was found to be 23 μm/s and the transport process was controlled by the diffusion in the aqueous stagnant film. Iron(III) can be selectively transported from 2.0 M HCl aqueous solutions containing chromium(VI) by using SLM containing the phosphine oxide (Cyanex 923) as a carrier (Alguacil and Martinez 2000).

The long-term stability of the SLM is a major problem for its wide scale industrial applications. In general, the PIMs are analogous to SLMs in terms of mechanism of ion transport but show better stability as compared to SLM (Scindia et al. 2005). One of the important aspects of PIMs is the distribution of organic carrier in the polymer matrix, which determines their transport efficiency (Tripathi et al. 2003). PIMs have been reported to have better mechanical properties than traditional SLMs and good chemical resistance. The addition of plasticizers is reported to improve the compatibility of the carrier with the polymer, and additionally improve the brittleness and elasticity by creating a polymeric solution. Although PIMs have a higher internal viscosity than SLMs, it has been reported that, for a number of systems the fluxes across both types of membranes are comparable. In other cases higher fluxes of transport across PIMs have been investigated (Salazar-Alvarez et al. 2005, Gardner et

al. 2004). A number of new types of PIMs using various cellulose derivatives were described These membranes have been characterized with respect to their durability against hydrolysis under alkaline and acidic conditions.

Recently the transport of metal ions by polymer inclusion membranes has been reviewed (Nghiem et al. 2007). The competitive transport of metal ions such as Cr(VI), Cd(II), Zn(II), Sr(II), Cs(I) and Co(II) across PIMs was investigated (Kozlowski et al. 2002, 2007, 2008).

The present work examines the possibility of iron(III) separation from solution containing manganese(II), copper(II), nickel(II) and cobalt(II) by solvent extraction and transport through polymeric inclusion membranes processes with D2EHPA as the extractant/ion carrier. The effect of extractant concentration, the kinetics and efficiency parameters of transport through polymer inclusion membranes have been investigated. The stability of polymer inclusion membranes has also been studied.

EXPERIMENTAL

REAGENTS

Inorganic chemicals, i.e. iron(III), manganese(II), nickel(II), cobalt(II) and copper(II) chlorides, sodium chloride and hydrochloric acid were of analytical grade and were purchased from POCh (Gliwice, Poland). Organic reagents, i.e. cellulose triacetate (CTA), *o*-nitrophenyl octyl ether (ONPOE), di(2-ethylheksyl)phosphoric acid (D2EHPA) and dichloromethane were of analytical reagent grade (Fluka) and used without further purification. Distilled kerosene was used as the diluent in solvent extraction. The density of plasticizer, i.e. ONPOE, was 1.04 g cm^{-3}. Aqueous solutions were prepared with twice distilled water, with a conductivity of 0.1 μSm^{-1}.

PROCEDURE

SOLVENT EXTRACTION

Solvent extraction was carried out using equal volumes of both phases (10 cm^3 each) which were mechanically shaken (200 min^{-1}) for 20 minutes at the constant temperature (25 ± 2 °C). The metal ions content in the aqueous phase has been determinated by means of AAS Solaar 939 (Unicam) spectrophotometer, while the pH value has been measured with a CX-731 (Elmetron) pH-meter. The concentration of metals in the organic phase was calculated from the mass balance.

POLYMER INCLUSION MEMBRANE

Organic solutions of cellulose triacetate (CTA), ion carriers (D2EHPA), and plasticizer (ONPOE) in dichloromethane were prepared. A portion of solution was poured into a membrane mold comprised of a 6.0 cm glass ring attached to a glass plate with CTA-dichloromethane glue. The organic solvent was allowed to evaporate overnight and the resultant membrane was separeted from the glass plate by immersion in cold water. The membrane was soaked in 0.10 M HCl aqueous solution for 12 hours and stored in distilled water.

MEMBRANE TRANSPORT EXPERIMENTS

The transport across PIMs was carried out in a permeation cell in which the membrane film was tightly clamped between two cell compartments. The effective membrane area, which was exposed to both phases, was 3.14 cm^2. Both, the source and receiving aqueous phases (50 cm^3 each) were stirred at 600 rpm with synchronous motors. The PIM transport experiments were conducted at room temperature (22-25 °C). The permeation of iron(III) was monitored by periodical sampling (0.1 cm^3 each) of the source phase. After appropriate dilution, samples were analyzed by an atomic absorption spectrophotometer. The source phase acidity was controlled by pH-meter (Cx-731 Elmetron, with a combined pH electrode, EFH-136, Hydromet, Poland), pH was kept constant by adding to the source phase periodically aqueous solution of 2.0 M HCl.

RESULTS AND DISCUSSION

The solvent extraction of Fe(III) from aqueous chloride solutions containing Mn(II), Ni(II), Co(II), and Cu(II)

The extraction behavior of 0.10 M Fe(III), 0.30 M Mn(II), 0.020 M Ni(II), 0.010 M Cu(II), 0.0020 M Co(II) from 1.0 M hydrochloric acid and 2.0 M sodium chloride with D2EHPA in kerosene as the solvent has been studied. The composition of this aqueous solution is very similar to aqueous solutions after leaching of polymetallic nodules (Jana 1993). Percent extraction of Fe(III) increased with increasing extractant concentration in organic phase (Fig. 1).

As it can be seen from this figure extraction of Fe(III) was the highest for 0.5 M D2EHPA and equal to 73.4 %. Extraction of others metal ions was much lower. Extraction of Mn(II), Ni(II), Cu(II) and Co(II) with 0.5 M D2EHPA was low and amounted to: 11.2 %, 15.3 %, 7.8 % and 23.9 %, respectively. The values of selectivity coefficients are presented in Table 1.

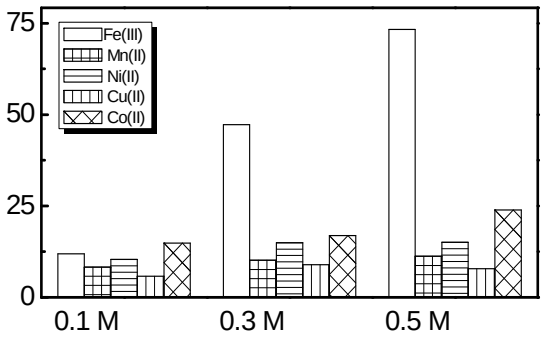

Fig. 1. The dependence of Fe(III), Mn(II), Ni(II), Cu(II) and Co(II) extraction percent (% E) from chloride solution on D2EHPA concentration. Organic phase: 0.1 - 0.5 M D2EHPA in kerosene. Aqueous phase: of 0.10 M Fe(III), 0.30 M Mn(II), 0.020 M Ni(II), 0.010 M Cu(II), 0.0020 M Co(II), 1.0 M HCl and 2.0 M NaCl.

Table 1. Selectivity coefficients of Fe(III) over Mn(II), Ni(II), Co(II) and Cu(II) for different D2EHPA concentrations in solvent extraction process.. Conditions of experiments as in Fig. 1

Selectivity coefficient, S	D2EHPA, M		
	0.1	0.3	0.5
$S_{Fe(III)/Mn(II)}$	1.50	7.40	21.23
$S_{Fe(III)/Ni(II)}$	1.13	4.94	15.27
$S_{Fe(III)/Cu(II)}$	2.21	9.08	32.35
$S_{Fe(III)/Co(II)}$	0.79	4.45	8.87

The selectivity of Fe(III) over the other metals ions is a very important process parameter. The investigation found that the selectivity coefficient depends on the extractant concentration in organic phase. The results indicate that the selectivity coefficient increases with increasing D2EHPA concentration.

In this project a preliminary attempt was to find out which iron(III) species are preferably extracted. Literature reports that iron(III) forms various chloride complexes with increase of chloride concentration in aqueous phase. Dependence of the fractions of Fe^{3+}-Cl^- ($\alpha_n \cdot 100\%$) on chloride ions concentration in aqueous solution (on the ground of the values of stability constants of metal-ion complexes at constant ionic strength I = 4.0 for Fe(III), *(Stability Constans of Metal-Ion Complexes, Part A: Inorganic Ligands, Pergamon Press)* was presented in Fig. 2.

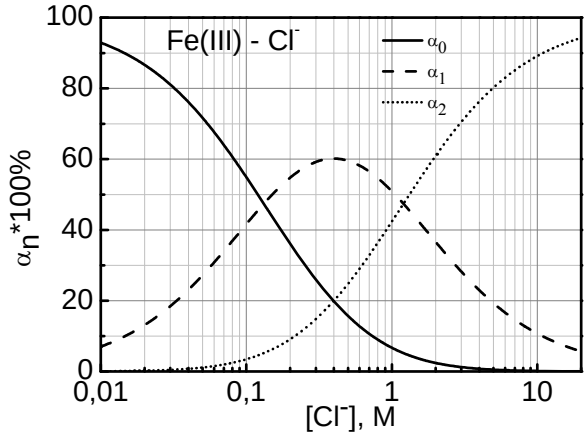

Fig. 2. Dependence of the fractions of Fe^{3+}-Cl^- ($\alpha_n \cdot 100\%$) on chloride ions concentration in aqueous solution *(Stability Constans of Metal-Ion Complexes, Pergamon Press, 1998)*.

The results presented in Fig. 2 indicate that at 4.0 M Cl^- concentrations in the aqueous solution, iron(III) exists as 0.70 % Fe^{3+}, 22.47 % $FeCl^{2+}$ and 76.83% $FeCl_2^+$. The difference in extraction behaviour of these metals was attributed to the fact that the extraction of Fe(III) is favored from chloride media under these conditions in comparison with other metal ions. It would be possible to separate iron(III) and manganese(II), nickel(II), cobalt(II) and copper(II).

TRANSPORT OF IRON(III) ACROSS POLYMER INCLUSION MEMBRANES FROM AQUEOUS CHLORIDE SOLUTIONS

THE KINETICS OF PIM TRANSPORT

The polymer inclusion membranes transport of iron(III) from aqueous solution containing 0.10 M Fe(III), 0.30 M Mn(II), 0.020 M Ni(II), 0.010 M Cu(II) and 0.0020 M Co(II), in 1.0 M HCl and 2.0 M NaCl was also studied. D2EHPA as the ion carrier was used. The polymer inclusion membrane contained: 0.0375 g CTA, 2.0 M ion carrier (based on plasticizer and carrier) and 2.66 cm^3 ONPOE/1 g CTA. The incluision membrane composed of: CTA – 19.28 %, ONPOE – 53.47 % and D2EHPA – 27.25 %. The kinetics of PIM transport was calculated by a first order reaction rate:

$$\ln\left(\frac{c}{c_i}\right) = -kt \tag{1}$$

where: c is the metal ion concentration (M) in the source phase at some given time, c_i is the initial metal ion concentration (M) in the source phase, k is the rate constant (s^1), and t is the time of transport (s).

To calculate the k value, a plot of $\ln(c/c_i)$ versus time was prepared. The rate constant value for the duplicate transport experiment was averaged and standard deviation was calculated. The initial input flux (J_i) was determined as equal to:

$$J_i = \frac{V}{A} \cdot k \cdot c_i \tag{2}$$

where V is volume of the aqueous source phase (m^3), and A is an area of effective membrane (m^2).

The results obtained for the iron(III) transport into distilled water as the receiving phase are presented in Fig. 3.

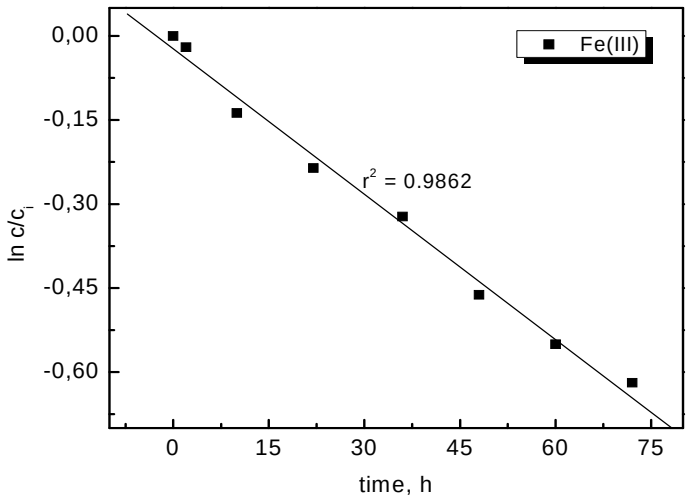

Fig. 3. Kinetics of 0.10 M Fe(III) transport through PIM with 2.0 M D2EHPA. Receiving phase: distilled water; PIM: 0.0375 g CTA, 2.66 cm^3 ONPOE/1 g CTA.

As it can be seen from this figure the initial flux was equal to 15.87 $\mu molm^{-2}s^{-1}$. To calculate the k value, the plot of $\ln(c/c_i)$ versus time was made. The relation of $\ln(c/c_i)$ versus time is linear, which was confirmed by high values of determination coefficients (r^2). The value of this coefficients was equal to 0.98. In this experiment of polymer inclusion membrane transport no manganese(II), nickel(II), copper(II) and cobalt(II) ions were detected in the receiving phase. That shows that under the conditions of the experiment iron(III) can be effectively separated from other metal ions present in this source aquous phase with investigatigated ion carrier.

LONG TERM STABILITY OF THE POLYMER INCLUSION MEMBRANES

Membrane stability was also investigated by performing three transport cycles in 72 h. After each cycle, the solutions were removed from the permration cell and the membrane was washed: feed and strip compartments were filled with fresh distilled water (30 min.). The stability of PIMs in the transport of iron(III) was studied using D2EHPA as the carrier. We used the same membrane with 2.0 M D2EHPA. The flux of Fe(III) varied slightly at the beginning, but after tree cycle the flux decreased considerably. Results are summarized in Table 2.

Table 2. Values of the permeability coefficient (P) after each cycle in Fig. 4

Cycle number	Permeability coefficient, $P\ (\mu ms^{-1})$
1	0.158
2	0.142
3	0.111

The fact that stability of liquid membrane depended on different parameters (Szpakowska and Nagy 1997) suggested that solute-solvent (and polymer solvent) interactions play a dominant role in membrane stability. The influence of different experimental conditions on the transport rate allowed to establish various factors determining membrane stability. One of the major factors is that the membrane solvent and the organic carrier are lost to the aqueous phase, limiting the durability of the membrane. Several authors have reported that polymer inclusion membranes show good long – term stabilities, although in general lower fluxes can be obtained with this kind of membranes due to their high viscosity (Aguilar et al. 2001).

CONCLUSION

Di(2-ethylhexyl)phosphoric acid (D2EHPA) used as extractants in solvent extraction process allow for selective removal of iron(III) from acidic aqueous solutions containing Mn(II), Ni(II), Co(II), and Cu(II). The investigation indicated that the selectivity coefficient depended on the extractant concentration in organic phase. Also, transport across polymer inclusion membranes with D2EHPA as the ionic carrier, *orto*-nitrophenyl octylether (ONPOE) as the plasticizer, and cellulose triacetate as the support into hydrochloric acid aqueous solution as the receiving phase was found to be very selective for iron(III) removal from acidic aqueous chloride solutions containing Mn(II), Ni(II), Co(II), and Cu(II). No other metals excluding Fe(III) were detected in the receiving aqueous phase.

The results of this study show that in order to achieve long-term stability of the PIM the organophosphorous acid (D2EHPA) as the ion carrier can be used.

REFERENCES

AGUILAR J.C., SANCHEZ-CASTELLANOS M., RODRIGEZ DE SAN MIGUEL E., GYVES J. (2001), *Cd(II) and Pb(II) extraction and transport modeling in SLM and PIM systems using Kelex 100 as carrier*, Journal of Membrane Science 190, 107-118.

ALGUACIL F.J., ALONSO M. (2000), *Iron(III) transport using a supported liquid membrane containing Cyanex 921,* Hydrometallurgy 58, 81-88.

ALGUACIL F.J., MARTINEZ S. (2000), *Permeation of iron(III) by an immobilised liquid membrane using Cyanex 923 as mobile carrier,* Journal of Membrane Science 176, 249-255.

BISWAS R.K., BEGUM D.A. (1998), *Solvent extraction of Fe^{3+} from chloride solution by D2EHPA in kerosene,* Hydrometallurgy 50, 153-168.

BISWAS R.K., BEGUM D.A. (1999), *Study of kinetics of forward extraction of Fe(III) from chloride medium by di-2-ethylhexylphophoric acid in kerosene using the single drop technique,* Hydrometallurgy 54, 1-23.

BISWAS R.K., BEGUM D.A. (2001), *Kinetics of stripping of Fe^{3+} - D2EHPA complexes from D2EHPA-kerosene phase by aqueous HCl-Cl^- phase using the single drop technique,* Hydrometallurgy 60, 81-97.

GARDNER J.S., WALKER J.O., LAMB J.D. (2004), Permeability and durability effects of cellulose polymer variation in polymer inclusion membranes, *Journal of Membrane Science* 229, 87-93.

GILL J.S., SINGH H., GUPTA C.K. (2000), *Studies on supported liquid membrane for simultaneous separation of Fe(III), Cu(II) and Ni(II) from dilute feed,* Hydrometallurgy 55, 113-116.

GUPTA B., DEEP A., SINGH V., TANDON S.N. (2003), *Recovery of cobalt, nickel, and copper from sea nodules by their extraction with alkylphosphines,* Hydrometallurgy 70, 121-129.

JANA R.K. (1993), Leaching of sea nodules in acidic chloride-sulphide media, *Trans. Inst. Min. Metall* 102, C191-C194.

JAYACHANDRAN J., DHAKE P.M. (1997), *Liquid-liquid extraction separation of iron(III) with 2-ethyl hexyl phosphonic acid mono 2 - ethyl hexyl ester,* Talanta 44, 1285-1290.

KOZLOWSKI C.A., WALKOWIAK W. (2002), *Removal of chromium(VI) from aqueous solutions by polymer inclusion membranes,* Water Research 36, 4870-4876.

KOZLOWSKI C.A., (2007), *Kinetics of chromium(VI) transport from mineral acids across cellulose triacetate (CTA) plasticized membranes immobilized by tri-n-octylamine*, Industrial & Engineering Chemistry Research 46 (2007) 5420-5428.

KOZLOWKI C.A., WALKOWIAK W., GIREK T. (2008), *Kinetics of chromium (VI) transport from mineral acids across cellulose triacetate (CTA) plasticized membranes immobilized by tri-n-octylamine*, Journal of Membrane Science, 310, 312-320.

LEE M.S., LEE K.J. (2005), *Separation of iron and nickel from a spent $FeCl_3$ etching solution by solvent extraction,* Hydrometallurgy 80, 163-169.

LUPI C., PILONE D. (2000), *Reductive strpping in vacuum of Fe(III) from D2EHPA.* Hydrometallurgy 57, 201-207.

NGHIEM L.D., MORNANE P., POTTER I.D., PERERA J.M., CATTRALL R.W., KOLEV S.D. (2006), *Extraction and transport of metal ions and small organic compounds using polymer inclusion membranes (PIMs),* Journal of Membrane Science 281, 7-41.

PARHI P.K., SARANGI K. (2008), *Separation of copper, zinc, cobalt and nickel ions by supported liquid membrane technique using LIX 84I, TOPS-99 and Cyanex 272*, Separation and Purification Technology 59, 169-174.

POSPIECH, B., WALKOWIAK W. (2005), *Application of TBP in selective removal of iron(III) in solvent extraction and transport through polymer inclusion membranes processes,* Physicochemical Problems of Mineral Processing 39, 89-98.

POSPIECH B., WALKOWIAK W. (2007), *Separation of copper(II), cobalt(II) and nickel(II) from chloride solutions by polymer inclusion membranes,* Sep. and Purification Technology 57, 461-465.

PRINCIPE, F., DEMOPOULOS, G.P. (2004), Comparative study of iron(III) separation from zinc sulphate–sulphuric acid solutions using the organophosphorus extractants, OPAP and D2EHPA, Hydrometallurgy 74, 93–102.

SAJI J., REDDY M.L.P. (2001), *Liquid - liquid extraction separation of iron(III) from titania wastes using TBP-MIBK mixed solvent system*, Hydrometallurgy 61, 81-87.

SAJI J., PRASADA RT., IYER C.S.P., REDDY M.L.P. (1998), *Extraction of iron(III) from acidic chloride solutions by Cyanex 923,* Hydrometallurgy 49, 289-296.

SALAZAR-ALVAREZ G., BAUTISTA-FLORES A.N., RODRIGUEZ DE SAN MIGUEL, MUHAMMED M., GYVES J. (2005), *Transport characterization of a PIM system used for the extraction of Pb(II) using D2EHPA as carrier,* Journal of Membrane Science 250, 247-257.

SARANGI K., PARHI. P.K., PADHAN E., PALAI A.K., NATHSARMA K.C., PARK K.H. (2007), *Separation of iron(III), copper(II0, and zinc(II) from mixed sulphate/chloride solution using TBP, LIX 84I and Cyanex 923,* Separation and Purification Technology 55, 44-49

SCINDIA Y.M., PANDEY A.K., REDDY A.V.R. (2005), *Coupled-diffusion transport of Cr(VI) across anion-exchange membranes prepared by physical and chemical immobilization methods,* Journal of Membrane Science 249, 143-152.

STABILITY CONSTANS OF METAL-ION COMPLEXES, Part A: Inorganic Ligands, Pergamon Press (1998), New York

SZPAKOWSKA M., NAGY O.B. (1997), *Stability of supported liquid membranes containing Acorga P-50 as carrier*, Journal of Membrane Science 129, 251-261.

TRIPATHI R., PANDEY A.K., SODAYE S., TOMAR B.S., MANOHAR S.B., SANTRA S., MAHATA K., SINGH P., KAILAS S. (2003), *Backscattering spectrometry studies on metal ion distribution in polymer inclusion membranes,* Nuclear Instruments and Methods in Physics Research B, Nuclear Instruments and Methods in Physics Research 211, 138-144.

WALKOWIAK W., KOZLOWSKI C.A. (2009), Macrocycle carriers for separation of metal ions in liquid membrane processes – a review, Desalination 240, 186-196

Pospiech P., Walkowiak W., *Badania nad usuwaniem żelaza(Iii) z wodnych roztworów chlorkowych w procesie ekstrakcji cieczowej i transportu przez polimerowe membrany inkluzyjne za pomocą D2EHPA*, Physicochemical Problems of Mineral Processing, 44 (2010), 195-204, (w jęz. ang) http://www.minproc.pwr.wroc.pl/journal

Zbadano proces usuwania żelaza(III) z wodnych roztworów chlorkowych zawierających w procesie ekstrakcji cieczowej i transportu przez polimerowe membrany inkluzyjne (PIMs). W roli ekstrahenta/przenośnika jonów użyto kwasu di(2-etyloheksylo)fosforowego (D2EHPA). Procent ekstrakcji jonów Fe(III), Mn(II), Ni(II), Cu(II) i Co(II) za pomocą 0,5 m D2EHPA wynosił odpowiednio: 73.4 %, 11.2 %, 15.3 %, 7.8 % i 23.9 %. Obliczono i przedstawiono także współczynnik separacji (S) poszczególnych metali. Stwierdzono, że transport przez polimerową membranę zawierającą trioktan celulozy (CTA) w roli polimerowej matrycy, eter o-nitrofenylooktylowy (ONPOE) jako plastyfikator i D2EHPA jest efektywną i selektywna metodą usuwania jonów Fe(III) z wodnych roztworów chlorkowych zawierających jony Mn(II), Ni(II), Cu(II) i Co(II). Wyniki badań wskazują na stosunkowo długi okres trwałości tych membran w tych warunkach.

słowa kluczowe: żelazo(III), DZEHPA, ekstrakcja, membrany

Physicochem. Probl. Miner. Process. 44(2010) 205-214

journal homepage
www.minproc.pwr.wroc.pl/journal/

Physicochemical Problems of Mineral Processing

Index No. 32213X ISSN 1643-1049

Z. Sadowski*, I. Polowczyk*, A. Frąckowiak*, T. Koźlecki*, S. Chibowski**

BIOINSPIRED SYNTHESIS OF CALCIUM CARBONATE COLLOID PARTICLES

Received April 16, 2009; reviewed; accepted July 30, 2009

Biomimetic procedure for nucleation and growth of $CaCO_3$ has been presented. The wet chemical syntheses of $CaCO_3$ colloidal particles have been carried out. The characterization of precipitated particles of $CaCO_3$ has been done using the particle size distribution analysis. The effect of physical and chemical parameters on the size of precipitated particles of $CaCO_3$ has been investigated. This research may provide new insight into the precipitation of calcium carbonate.

key words: calcium carbonate, nanoparticles, synthesis, size distribution

INTRODUCTION

The concept of calcium carbonate synthesis inspired by natural processes has expanded greatly during three past decades (Mann, 2001). It is well known that biomineralization is achieved through the calcification process in a single cell organism. Biominerals of over 40 different types occur in organisms, ranging from bacteria to mammals. Biominerals are biocomposites of inorganic-organic hybrid materials, consisting of broad group of biological minerals (Dujardin et al., 2003).

Among biological minerals, calcium carbonate has a special place since it is the main constituent of bones and shells. In both materials, the inorganic mineral is associated with biopolymers (Hunter 1996).

* Wroclaw University of Technology, Faculty of Chemistry, e-mail: Zygmunt.Sadowski@pwr.wroc.pl

** Maria Curie-Sklodowska University, Lublin, Faculty of Chemistry, e-mail: rad1@hermes.ums.lubli.pl

Eggshell is natural composite bioceramics containing 5% of organic and 95% of calcite components (Arias and Fernandez 2003). The eggshell biomineralization is affected by macromolecules which are produced by specialized cells. These biomineral crystals appear to be nucleated on the mammillary knobs which is proteoglycan containing oversulfated keratin sulfate. The calcite crystals growth on the knobs is affected by oveglycan. These organic components are polyanionics and polyacids, which have a high calcium affinity (Arias and Fernandez 2003).

Shells are composed of pure calcium carbonate, usually both in the form of calcite and aragonite. The precipitation of calcium carbonate can be realized inside the organism cell (the inner shell) or outside the cell.

The morphology and structural properties of calcium carbonate can be controlled by the use of specific organic additives. For instance, proteins isolated from mollusk shells shown control on the structure of calcium carbonate crystals (Feng et al., 2000). The function of proteins during biomineralization was studied by application of proteins extracted from mollusk shells (*Mylilus edulis)*. The proteins from different layers of shell were used. It was shown, that proteins extracted from nacreous layer induced aragonite formation, while those extracted from prismatic layer induced calcite formation. Additionally, it was shown that the morphology of precipitated calcium carbonate crystals was controlled mainly by soluble proteins.

The effect of lysozyme on the precipitation kinetics and morphology of calcite crystals was examined (Jimenes-Lopez et al., 2003). It was found that lysozyme favored the nucleation of calcium carbonate and modified the morphology of crystals. The degree of modification was changed with the lysozyme concentration. The presence of lysozyme during the calcite precipitation process led to the formation of spherical particles. The particle size distribution depended on the lysozyme concentration (Voinescu et al., 2007).

Similar findings were reported for alcohols like ethanol, isopropanol or diethylene glycol which also were used to influence the $CaCO_3$ morphology (Cölfen, 2003).

The main role of biomacromolecules is an induction of calcium carbonate nucleation process. However, the experimental results showed (Sen et al., 2002) that the growth of calcium carbonate was more and more inhibited by an increasing concentration of collagen. The inhibition of calcite growth by collagen is caused because collagen is non-uniformly incorporated into the calcite crystal planes.

The cooperative influence of collagen and magnesium ions on calcium carbonate precipitation has been investigated (Jiao et al., 2006). The experimental data suggested that collagen acts in combination with magnesium ions to inhibit $CaCO_3$ crystal growth. Also, the influence of Mg/Ca ratio on polymorph of $CaCO_3$ was tested. When the ratio of Mg/Ca was in the range of 0-1, only calcite crystals were formed. When the Mg/Ca ratio was in the range 2-4 some vaterite and aragonite crystals were precipitated. However, when the ratio of Mg/Ca attains 4, most crystals were aragonite (Jiao et al., 2006).

The density and structural geometry of calcium carbonate can be easily regulated by changing the kind and the amount of the water soluble polyelectrolytes. The polyelectrolyte assembly creates a microenvironment for both the nucleation and crystal growth. It was shown (Falini, 2000), that the collagenous matrix with entrapped poly-Asp is able to control calcite and aragonite precipitation.

The results of calcium carbonate crystallization into the β-chitin scaffold has been presented (Falini et al., 2002). The three main polymorph of calcium carbonate were observed. Calcite and vaterite were precipitated in an absence of magnesium ions in solution. In the presence of Mg^{2+} ions, aragonite deposition slightly increases with crystallization time. The optimal aragonite crystallization time was 24 h.

Hydrogels of polyacrylamide modified by copolymerization with acrylic acid were used as growth medium for $CaCO_3$ precipitation. This procedure gives an organic microstructure similar to natural biomineralization process (Grassman and Löbman, 2004). The introduction of –COOH group by poly-organic acid into hydrogel altered both the morphology and stability of calcium carbonate.

Polyacrylamide was also used as an organic substrate to induce the nucleation and growth of calcium carbonate. The calcium carbonate precipitation was realized by bubbling of CO_2/N_2 gas mixture through the water solution of calcium hydroxide with polyacrylamide. It was shown (Wang et al., 2006), that the concentration of organic substrate and temperature influence the nucleation, growth and morphology of calcium carbonate particles.

Recently, dendrimers were discovered as active additive for the controlled $CaCO_3$ precipitation (Cölfen, 2003).

SYNTHESIS OF NANO-SIZED PARTICLES OF METAL CARBONATES

Recently calcium inorganic particles in micro- and nano-size are prepared by various methods for the various applications. Several synthetic procedures have been designed for control of the formation of naoparticles of metal carbonates. Two routes seem important: precipitation from homogeneous solution and synthesis in microemulsion (reversed micelles).

The nanosize calcium carbonate was synthesized by an *in situ* deposition technique (Mishra et al., 2005). Using this procedure, calcium chloride solution was mixed with PEG solution. This mixture was blended with K_2CO_3 water solution. Four different molar ratios (1:4; 1:8; 1:12 and 1:16) were used. Calcium carbonate precipitate was filtered off, washed with water, and dried in vacuum.

Microemulsions are used as special microreactors to limit the size of nano-particles (Karagiozov and Momchilova, 2005). Nano-size particles of $CaCO_3$ and $BaCO_3$ were obtained using chemical reaction in water-in-oil microemulsion. Nano-particles synthesized in this way have a spherical shape and almost equal size varying from 20

to 30 nm. Chemical interaction between CO_2 and the corresponding drops of microemulsions takes place in the reactor equipped with cooling jacket. The process of metal carbonate precipitation is endothermic. The microemulsion used in these experiments was aqueous alkali solution in oil (w/o) where the water drops contained dissolved calcium or barium hydroxide, and organic phase was n-hexane. The synthesis was carried out at temperature 20-23^oC at constant flow rate for 60 min.

The growth of calcium carbonate in a reverse macroemulsion system based on n-stearoyl acid surfactant has been described (Menahem and Mastai, 2008). X-ray diffraction data showed that crystallization of $CaCO_3$ in macroemulsion led to the formation of vaterite and calcite nanocrystals.

The formation of nanoparticles using the microemulsion method is completely governed by the droplet exchange, which provides new reactants in small amounts of few molecules from other droplets.

A new method for preparation of nanoparticles was based on using two types of foams. Foam one was formed by the aqueous solution of $CaCl_2$ with anionic surfactant. The second foam was created by aqueous solution of Na_2CO_3 and cationic surfactant. Two types of foam were contacted each other in a specially designed apparatus (Guo et al., 2007). The size of nanoparticles can be controlled by changing the solution concentration,

Many nanoparticles have been studied for the use in drug delivery systems (DDS). The study of incorporation of bioactive proteins into nano-$CaCO_3$ has been carried out (Uano et al., 2005).

Among the various method employed to the drag delivery, $CaCO_3$ microcapsules seem be useful in numerous clinical applications (Fischer et al., 2000).

The preparation of $CaCO_3$ microcapsules encapsulating some biomacromolecules has been reported (Fujiwara et al., 2008). Proteins, such as bovine serum albumin was added to the $(NH_4)_2CO_3$ water solution. No change of the solution occurred after the protein addition into the $(NH_4)_2CO_3$ solution. It was shown that the contents of protein in $CaCO_3$ microcapsules strongly depended on their molecular weight.

The purpose of this study was to synthesize precipitated calcium carbonate of various sizes using different methods. The data are presented as particle size distribution curves.

MATERIALS AND METHODS

All chemicals used in these syntheses were commercial available (POCh, Poland) and were used without further purification. The poly(ethylene glycol) PEG of molecular weight 1000, 6000, 20000, 300000, and 5000000 was used.

Some bacteria cultures were isolated from soil samples. From isolated bacteria cultures two bacterial strains: *Bacillus circulans* and *Streptomyces* sp. were separated

for further investigations. The biosurfactant production was determined by the measurements of the surface tension. Biosurfactants produced by *Bacillus circulans* reduced the surface tension from 74 to 28.66 mN/m after 20h period of bacteria growth. Biosurfactants produced by *Streptomyces* sp. reduced the surface tension to 29.30 mN/m. The filtrates of microorganisms culture were marked B4 and B6, respectively.

The preparation of $CaCO_3$ colloid particles was carried out in the Erlenmeyer flasks at the speed of the magnetic stirrer 300 rpm, using three reaction systems:

i. Na_2CO_3 0.01M in H_2O (100 ml) + $CaCl_2$ 0.01M in H_2O (100 ml);
ii. Na_2CO_3 0.01M in PEG 0.1 or 0.7% aqueous solution (100 ml) + $CaCl_2$ 0.01M in PEG 0.1 or 0.7% aqueous solution (100 ml);
iii. Na_2CO_3 0.01M in filtrate 10% aqueous solution (100 ml) + $CaCl_2$ 0.01M in filtrate 10% aqueous solution (100 ml).

The solutions of sodium carbonate and calcium chloride with PEG and filtrate were prepared one day before the calcium carbonate synthesis and have been stirred overnight. The precipitation experiments were carried out at 25^{o}C. The pH of solutions in which precipitation has occured was 11.2 (without any additives), and 12.6-13 with PEG or broth. The particle size distribution of the colloidal $CaCO_3$ particles was measured using a laser diffraction technique (Mastersizer 2000, Malvern).

RESULTS AND DISCUSSION

The objective of this work was to synthesize calcium carbonate of various sizes using the precipitation technique. The synthesis of $CaCO_3$ was followed by basic synthetic route. The aqueous solutions of Na_2CO_3 and $CaCl_2$ were combined. Additionally, the precipitated calcium carbonate suspensions were homogenized for the time period of 5 and 10 min. The effect of time and homogenization on the size of precipitated calcium carbonate was compared. Figure 1. presents the changes of distribution curves of precipitated $CaCO_3$ in time and after the homogenization of the precipitate. After one day the particles become larger due to recrystallization process (Rodriguez-Navarro et al., 2007). On the other hand, the mechanical homogenization of formed particles decreased the size of precipitated calcium carbonate, but not considerably.

The second experimental part has been realized using the way described by Mishra et al. (2005). Calcite precipitation experiments were conducted in the presence of poly(ethylene glycol) PEG. The experimental procedure was as follows: 100 ml of 0,01M $CaCl_2$ (and Na_2CO_3, simultaneously) solution was mixed with appropriate amount of PEG. After one day two mixtures were combined while mixing on the magnetic stirrer.

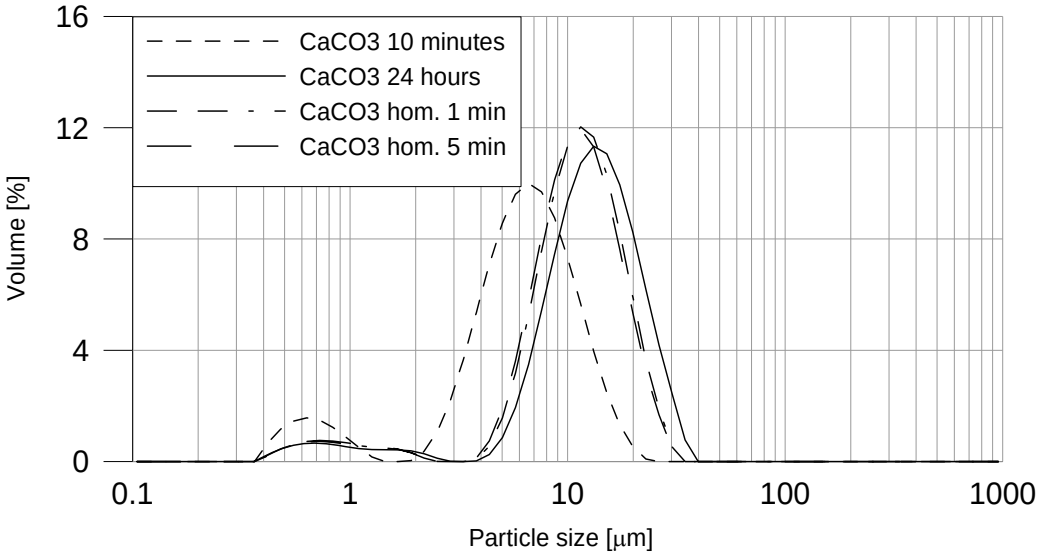

Fig. 1. Changes of size distribution curves for precipitated $CaCO_3$ in time and after homogenization at 24 000 rpm

Two concentrations (0.1 and 0.7%) of PEG 1000 were applied. The results obtained after 24 hours of synthesis (Fig. 2) were compared with the size distribution of precipitated $CaCO_3$ without polymer.

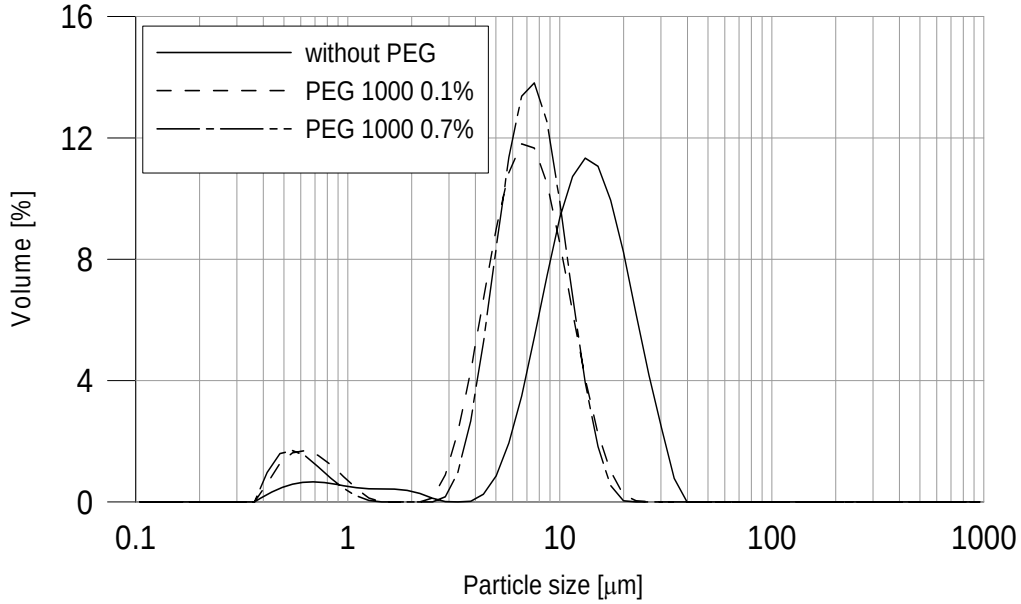

Fig. 2. The effect of PEG concentration on the size distribution curves of $CaCO_3$

The effect of molecular weight of polymer (PEG) at the same concentration (0.1%) was tested at the next series of experiments. As can be seen in Fig. 3 a and b, small changes of size distribution can be observed when the molecular weight of polymer has been changed from 1000 to 5000000.

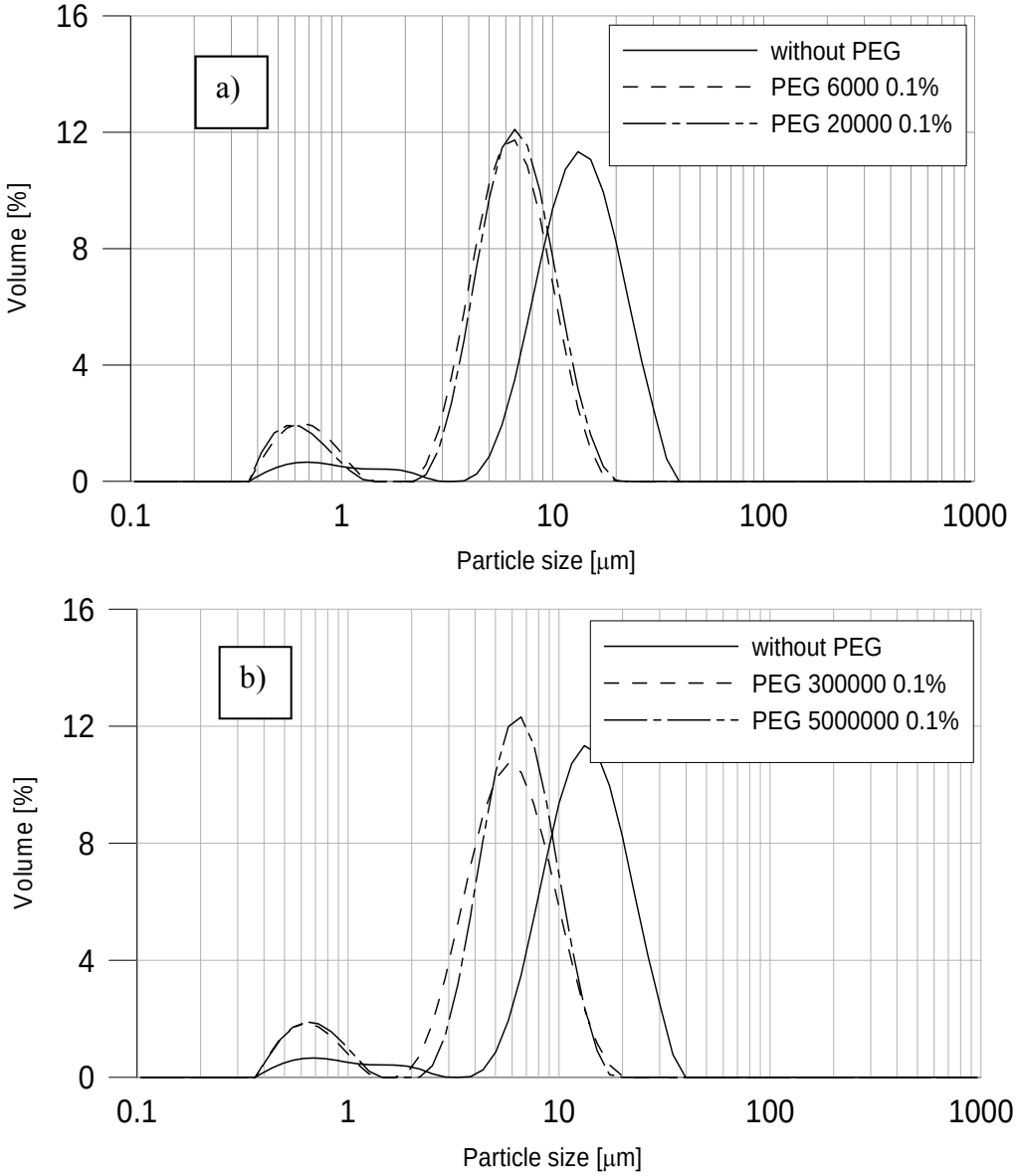

Fig. 3 a and b. The effect of the molecular weight of PEG on the size distribution of $CaCO_3$

The same procedure of salt solutions preparation was used for calcium ions precipitation in the presence of microbial filtrates (B4 and B6). Figure 4 (a,b) shows

the influence of both biosurfactant solutions (B4 and B6) on the size distribution of precipitated calcite particles. It is clear that the size distribution curve of calcium carbonate in the presence of B4 broth has changed as a function of time. This phenomenon can be explained by a specific interaction between biosurfactant and inorganic materials. It is known that biosurfactants play a role of the template to synthesize lithium iron phosphate (Li et al., 2009) or mesoporous hydroxyapatite (Zhao et al., 2008).

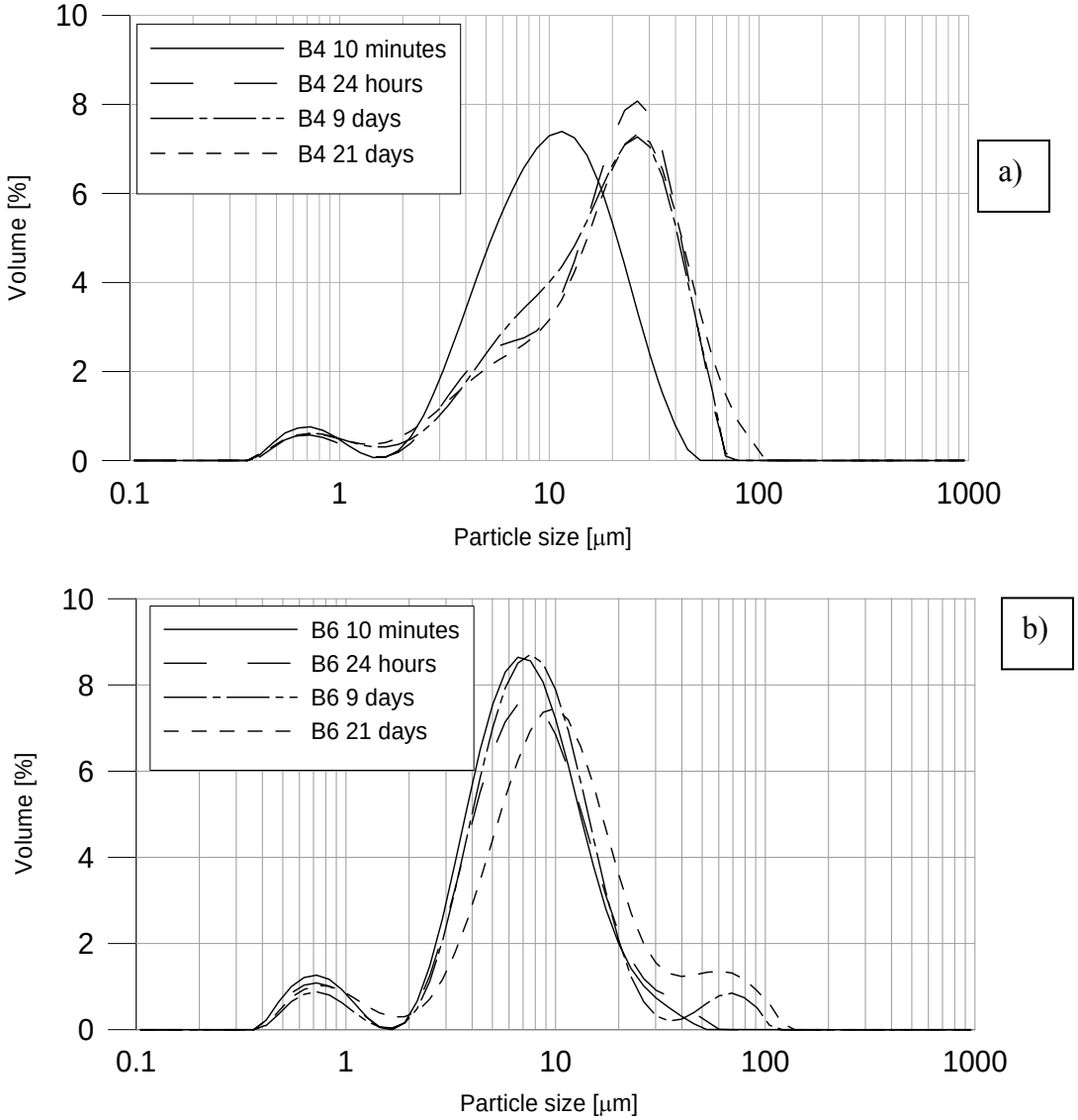

Fig. 4 a and b. The size distribution curves of $CaCO_3$ precipitated in the presence of the microbial filtrate

CONCLUSIONS

The calcium carbonate precipitation experiments were conducted to examine the effect of physical and chemical conditions of calcite synthesis on the size distribution of precipitated particles. From these experiments the following conclusions can be drawn:

1. The length of mixing period and the stirring speed have an essential influence on the size distribution of precipitated calcium carbonate.
2. The homogenization caused the aggregates' destruction.
3. The polymer (PEG) addition brings about smaller particles of $CaCO_3$. The size of particles depends on the polymer concentration. The molecular weight of polymer does not affect the particles size significantly.
4. The particles of $CaCO_3$ synthesized in the presence of microbial filtrate (B4) showed an increase of size in time. It can suggest a specific interaction between biosurfactant and precipitated particles.

ACKNOWLEDGMENT

This work was partially support by MNiSzW grant N N204 290134 and SURUZ scientific network.

REFERENCES

ARAS J.L., FERNANDEZ S.M., 2003, Biomimetic process through the study of mineralized shells, *Materials Characterization,* 50, 189-195.

CÖLFEN H., 2003, Precipitation of carbonates: recent progress in controlled production of complex shapes, *Current Opinion Colloid Inter. Sci.,* 8, 23-31.

DUJARDIN E., MANN S., 2002, Bio-inspired materials chemistry, *Advanced Materials*, 14 (11), 1-14.

FALINI G., 2000, Crystallization of calcium carbonates in biologically inspired collagenous matrices, *Inter. J. Inorganic materials*, 2, 455-461.

FALINI G., FERMANI S., RIPAMONTI A., 2002, Crystallization of calcium carbonate salts into beta-chitin scaffold, *J. Inorganic Biochemistry,* 91, 475-480.

FENG L.Q., PU G., PEI Y., CUI Z.F., LI D.H., KIM N.T. 2000, Polymorph and morphology of calcium carbonate crystals induced by proteins extracted from mollusk shell, *J.Crystal Growth*, 216, 459-465.

FISCHER K.E., ALEMAN J.B., TAO L.S, DANIELS H.R., LI M.E., BUNGER D.M., NAGARAJ G., SIGH P., ZETTL A., DESAI A.T., 2009, Biomimetic nanowire coatings for next generation adhesive drug delivery systems, *Nano Letter*, 9, (2), 716-720.

FUJIWARA M., SHIOKAWA K., MORIGAKI K., ZHU Y., NAKAHARA Y., 2008, Calcium carbonate microcapsules encapsulating biomacromolecules, *Chemical Engin. J.*, 137. 14-22.

GROSSMANN O., LÖBMAN P., 2004, Biomimetic nucleation and growth of $CaCO_3$ in hydrogels incorporating carboxylate groups, *Biomaterials*, 25,277-282.

GUO F., LI Y., HU H-X., ZHAO Q-G., HE X-J., 2007, Size-controllable synthesis of calcium carbonate nanoparticles using aqueous foam films as templates, *Material Letters*, 61, 4937-4939.
GUPTA R., 2004, Synthesis of precipitated calcium carbonate nanoparticles using modified emulsion membranes, Master thesis, Georgia Institute of Technology, USA.
HUNTER K.G., 1996, Interface aspects of biomineralization, *Current Opinion Solid State & Materials Sci.,* 1, 430-435.
JIAO Y., FENG Q., LI X., 2006, The co-effect of collagen and magnesium ions on calcium carbonate biomineralization, *Materials Sci., Engin., C.,* 26, 648-652.
KARAGIOZOV C., MOMCHILOVA D., 2005, Synthesis of nano-sized particles from metal carbonates by the method of reversed micells, *Chemical Eng. Process.,* 44, 115-119.
LI P., HE W., ZHOA H., WANG S., 2009, Biomimetic synthesis and characterization of the positive electrode material $LiFePO_4$, *J. Alloys Compounds*, 471, 536-538.
MANN S., 2001, Biomineralization principles and concepts in bioinorganic materials chemistry, Oxford University Press,
MENAHEM T., MASTAI Y., 2008, Controlled crystallization of calcium carbonate susperstructures in macroemulsions, *J. Crystal Growth*, 310, 3552-2556.
MISHRA S., SONAWANE H.S., SINGH P.R., 2005, Studies on characterization of nano $CaCO_3$, prepared by the in situ deposition technique and it application in PP-nano $CaCO_3$ composites, *J. Polym. Sci., B.,* 43, 107-113.
RODRIGUEZ-NAVARRO C., JIMENEZ-LOPEZ C., RODRIGEUEZ-NAVARRO a., GONZALEZ-MUNOZ T.M., RODRIGUEZ-GALLEGO M., 2007, Bacteria mediated mineralization of veterite, *Geochem. Cosmochim. Acta,* 71, 1197-1213.
SHEN H.F., FENG L.Q., WANG M.C., 2002, The modulation of callogen on crystal morphology of calcium carbonate, *J.Crystal Growth*, 242, 239-244.
UENO Y., FUTAGAWA h., TAKAGI Y., UENO A., MIZUSHIMA Y., 2005, Drug-incorporating calcium carbonate nanoparticles for a new delivery system, *J.Controlled Release*, 103, 93-98.
VOINESCU E.A., TOURAUD D., LECKER A. PFITZNER A., KUNZ W., NINHAM W B., 2007, Mineralization of $CaCO_3$ in the presence of egg white lysozyme, *Langmuir*, 23, 12269-12274.
WANG C., ZHAO J., ZHAO X., BALA H., WANG Z., 2006, Synthesis of nanosized calcium carbonate (aragonite) via a polyacrylamid inducing process, *Powder Technology*, 163, 134-138.
ZHAO h., HE W., WANG Y., YUE Y., GAO X., LI Z., YAN S., ZHOU W., ZHANG X., 2008, Biomineralizing synthesis of mesoporous hydroxyapatite-calcium pyrophosphate polycristal using ovalbumin as biosurfactant, *Materials Chemistry Physics*, 111, 265-270.

Sadowski Z., Polowczyk I., Frąckowiak A., Koźlecki T., Chibowski S., *Bioinspirowana synteza koloidalnych ziarn węglanu wapnia,* Physicochemical Problems of Mineral Processing, 44 (2010), 205-214, (w jęz. ang), http://www.minproc.pwr.wroc.pl/journal

Zaprezentowano biomimetyczną procedurę zarodkowania wzrostu $CaCO_3$ przeprowadzając chemiczna syntezę „na mokro" koloidalnych cząstek $CaCO_3$. Dokonano charakterystyki wytrąconych cząstek przez wyznaczenie ich składu ziarnowy. Badano też fizyczne i chemiczne parametry wytrąconych ziarn $CaCO_3$. Badania te mogą dostarczyć nowego spojrzenia na precypitację węglanu wapnia.

słowa kluczowe: węglan wapnia, nanoziarna, synteza, skład ziarnowy

Physicochem. Probl. Miner. Process. 44(2010) 215-230

journal homepage
www.minproc.pwr.wroc.pl/journal/

Physicochemical Problems of Mineral Processing

Index No. 32213X ISSN 1643-1049

A. M. Saleh*

A STUDY ON THE PERFORMANCE OF SECOND ORDER MODELS AND TWO PHASE MODELS IN IRON ORE FLOTATION

Received May 4, 2009; reviewed; accepted July 8, 2009

In this study, the fit to the experimental data of two second order models and two phase model were compared with first order models. The best fit was observed with the two parameter model with rectangular distribution of floatabilities (model II) and the three parameter fast/slow floating particles model (model I). Also, the three parameter gamma distribution model (model VI) showed good fit to the experimental data. The worst fit was observed with first order two stage kinetic model (model V) which indicates that there is no need to divide the flotation rate into two flotation rates. Model VII which includes six parameters gave acceptable fit to experimental data. This result is in contrast with the results obtained by other investigators which states that increase of parameters in model leads to parameter dilution and increase on model error. Hence, it may be concluded that the number of parameters to obtain an adequate model needs more investigation. The confidence intervals for the three best models (model I, model II and model VI) were estimated at 95% confidence level. Also, model II shows more discrete regions with regard to flotation rate and recovery than model VI. This result indicates the ability of such model to express the changes in flotation reagents and/or flotation conditions over other tested models.

key words: flotation, modeling, second order models, two phase models

INTRODUCTION

The importance of describing the flotation process by a mathematical model has been realized by numerous researchers (Arbiter and Harris 1962, Jowett and Ghosh 1965). Models provide the worker with a means to assess and predict flotation cell performance and hence the opportunity to improve operation of the cell.

* Mining & Pet. Dept., Faculty of Engineering, Al-Azhar University, Nasr City, Cairo, Egypt, e-mail: amsaleh2006@yahoo.com

Distinguishing between the performance of different flotation cells and evaluating the effects of operating parameters (Such as aeration rate and agitation intensity) can also be accomplished by use of a flotation model (Mehrotra and Kapur 1974, Mika and Fuerstenau 1969). Examination of the literature dealing with the modeling of flotation process reveals that a number of varying models have been presented (Woodburn et al. 1976, Woodburn 1970). No particular model has gained predominant acceptance amongst flotation researchers.

The mathematical modeling of flotation was applied in many areas in the flotation literature. Gulsoy (2005) analyzed the entrainment behaviour of both hydrophilic and hydrophobic particles in flotation. Empirical model equation was proposed and checked with experimental observations. The results provided accurate interpretation of hydrophilic and hydrophobic particles entrainment. Mathe et al. (2000) studied also the effect of entrainment of hydrophilic particles on modeling of recovery of mineral grains in concentrate. Heindel (1997) analyzed the microprocesses associated with the deinking flotation. He made a comparison between deinking and mineral flotation and concluded that modeling deinking flotation is possible. Heindel and Bloom (2006) mentioned that although there are many differences between conventional mineral flotation and dispersed air flotation, the latter can be modeled and they gave some guidelines for modeling such complex process.

Yianatos (2007) reviewed the flotation models that depend on fluid flow and models that depend on kinetics of related processes in conventional and column flotation. He mentioned that due to deviation of mechanical cells from perfect mixing conditions, the fluid flow regime, mass transport between pulp/froth interface and froth transport mechanism are better understood. The simulation of flotation process/circuits was also attempted. The results of such simulations are found for example in (Harris 1997, Alexander et al. 2000).

In a previous study (Saleh 2009) statistical model analysis was carried out on single phase first order models. The results showed that the three parameter fast/slow floating particles model and the two parameter model with rectangular distribution of floatabilities were the best models. In the present investigation, models of second order and two phase type are tested, evaluated and compared with first order models in iron ore flotation.

CONSIDERED FLOTATION MODELS

The following models are tested and analyzed in this work.

1 – Three parameters fast/slow floating particles model (named model I). This model mathematically expressed as:

$$r = (1-\Phi)[1-\exp(-K_f t)] + \Phi[1-\exp(-K_s t)] \quad (1)$$

where r is recovery at time (t), Φ is the fraction of flotation components with slow rate constant, K_f, K_s are the rate constants for fast and slow components (min^{-1}). This

model incorporates two rate terms instead of one rate constant (Kelsall 1961). The model does not include an ultimate recovery parameter but rather the ultimate fractional recovery is assumed to be 1.0. When K_s parameter approaches 0, the parameter *(Φ)* will then represent the fraction not recovered and the term *(1 - Φ)* becomes analogous to ultimate recovery and the model reduces to two parameter model.

2 – Two parameter model with rectangular distribution of floatabilities (named model II). Mathematically, this model is described as:

$$r = R[1 - \frac{1}{Kt}(1 - \exp(-Kt))] \tag{2}$$

where R is the ultimate recovery at long flotation times, K is the rectangular rate constant representing the largest allowed value of rectangular distribution (min^{-1}) and r as in model I. This model assumes a rectangular distribution of rate constants (Meyer and Klimpel 1984). The model describes a first order reaction. The predicted recovery is based on both ultimate recovery and a rectangularly distributed rate constant.

3 – Second order kinetic model (named model III). Because a first order equation appears to apply to a limited number of time – recovery profiles, it is not a sufficient criterion alone to establish the order of a flotation rate equation. This model is developed by assuming n=2 in the rate equation $(dc/dt = -Kc^n)$ where c is the concentration of a particular floatable component, K is the rate constant and n is the order of rate constant. Mathematically it is expressed as:

$$r = \frac{R^2 Kt}{1 + RKt} \tag{3}$$

R is the ultimate recovery and K is the flotation rate constant. This model is a two parameter expression describing the flotation of a monodisperse feed with particles having a constant floatability (Arbiter, 1951). The terms *r, R* and *K* are the same as mentioned in model II.

4 – Second order kinetic model with rectangular distribution of floatabilities (named model IV). This model was proposed by Klimpel (1980). The mathematical form of this two parameter model is given as:

$$r = R\{1 - \frac{1}{Kt}[\ln(1 + Kt)]\} \tag{4}$$

The terms *r, R* and *K* are the same as in model II. This model assumes a rectangular distribution of floatabilities.

5 – First order two stage kinetic model (named model V). This model was developed by considering the flotation system as being composed of discrete pulp and froth volumes. The model as proposed by Klimpel (Klimpel, 1984) incorporates two rate terms describing the mass transfer of a component from the pulp to the froth and finally to the concentrate. By assuming that the rate of drainage from the froth is minimal, the mathematical form of this model is derived as:

$$r = R\{(\frac{K}{K-K'})(1-\exp(-K't)) - (\frac{K'}{K-K'})(1-\exp(-Kt))\} \quad (5)$$

K is the rate of transfer from pulp to froth and K' is rate of transfer from froth to concentrate. Equation (5) is a three parameter model, describing a first order, two stage reaction. The particles are assumed to be present in a monodisperse feed with constant floatabilities. As K (rate of transfer from pulp to froth) is always much greater than K' (rate of transfer from froth to concentrate), transfer from froth to concentrate is the rate limiting step.

6. Three parameter gamma distribution model (named model VI). This model assumes a gamma distribution of floatabilities instead of rectangular distribution and was developed by (Huber–Panu et al., 1976). It is mathematically expressed in the following form:

$$r = R\{1-[\frac{\lambda}{\lambda+t}]^P\}. \quad (6)$$

The gamma distribution can be described as being composed of the summation of P exponential distributions. When P = 1.0, this model will be reduced to a two parameter form.

7. Six parameter model (named model VII). This model discretises the floating material into fast, medium and slow floating components (Apling and Ersayin ,1986). It may be represented by the equation:

$$\mathrm{r} = \sum_{i=1}^{n} \mathrm{a_i}(1-\exp(-K_i t) \quad (7)$$

where r is the recovery of the grains at time (t) and a_i is the fraction of the grains that is characterized by rate constant K_i such that:

$$\sum_{i=1}^{n} \mathrm{a_i} = 1.0. \quad (8)$$

Models I and II were tested for coal flotation in a previous study (Saleh 2009) and obtained the best fit among other models tested, with model I better than model II. It was aim of this investigation to test these models and compare them to the performance of second order and two phase models for iron flotation.

EXPERIMENT

MATERIAL

Iron ore sample used in this study was obtained from Um-Hebal region, South-East of Aswan, Egypt. The sample was first crushed in a hammer mill and then ground in a disc crusher. The ground product was screened on a 0.5 mm wedge wire screen using Rotap Shaker. The undersize material was collected and the oversize product

was returned to disc mill and screened again until all material passed 0.5 mm sieve. The collected material [-0.5 mm] represents the flotation feed (-500 μm). A representative sample from the flotation feed was taken and analyzed. The chemical analysis of this sample are: K_2O=0.1%, Na_2O<0.1%, TiO_2 = 0.55, MnO = 1.57, Fe_2O_3 = 57.5%, SiO_2 = 17%, Al_2O_3 = 3.57, CaO = 5.38%, P_2O_5 = 3.02% and L.O.I. = 9.35%. The flotation feed was screened and analyzed for Fe content. The size distribution and iron content of different size fractions are shown in Table 1. Oleic acid was applied as a collector and pine oil was used a frother.

Table 1. Size distribution and iron content of flotation feed

Size, micron	Yield *(γi)* wt%	Cumulative yield *(Σγi)*	Fe content %
-500+355	9.38	100	35.90
-355+250	15.48	90.62	38.10
-250+125	35.54	75.14	38.05
-125+62	32.82	39.60	40.00
-62+32	11.88	15.78	44.70
-32	3.90	3.90	48.00
Feed Sample	100		38

METHODS

Flotation experiments were carried out in Denver laboratory sub aeration machine of one dm^3 capacity using tap water. The operating conditions are shown in Table 2.

The ore was well mixed and sampled using standard riffling procedure. The 100 g samples were taken, placed in bags and stored in a dry environment until testing. The froth was removed manually. After the ground material was transferred to the cell, the pulp level was adjusted to the appropriate height. It was found that the applied frother concentration was sufficient to produce a stable froth persistent for entire flotation time (8 min).

Table 2. Operating conditions

Operating Variable	Value
Oleic acid collector	2 kg/Mg and 3 kg/Mg
Pine oil frother	60 mg/l
Solid/liquid ratio	10%
Aeration rate	6 l/min
Flotation time	0.5, 1.0, 2.0, 4.0, 6.0, 8.0 min
r. p. m.	1000
pH	8

The collector reagent is used industrially for this type of ore. The collector was provided by the supplier in a purified state, used as it received and added to the flotation cell using clean, calibrated pipette.

In carrying out a flotation test, the pulp was first agitated for 5 min and then conditioned with oleic acid collector for another 5 min. The pine oil frother was added 1 min before aeration.

To study the flotation kinetics, the collection of concentrate was taken at time intervals 0.5, 1.0, 2.0, 4.0, 6.0 and 8.0 min. The concentrate and tailing from each test were filtered, dried, weighed, sampled and assayed for Fe content and the fractional recovery.

RESULTS AND DISCUSSION

The optimal flotation model parameters were determined by a generalized parameter estimation computer program (Ureka-the solver). The criteria used for estimation of parameter values is the minimization of the absolute sum of the squares of the deviations at a given time between observed (experimental) and calculated recovery. Having the optimal parameters for a given model, a procedure for selecting the best flotation model remains to be found.

EVALUATION OF FLOTATION MODELS

A method of model discrimination used is based on a statistical analysis of the model error resulting from curve fitting as compared to the true experimental error. The requirements of a floatation model are first: a model must fit the observed data and, second: each model parameter must have a range of statistical significance narrow enough such that changes in flotation system can be confidently assessed. By using standard deviation of estimate, S_r, the fit of the observed to the calculated data can be measured (Eq. 9).

$$S_r = \sqrt{\frac{\sum_{i}^{n} (r_{i,cal} - r_{i,\,obs})^2}{n-m}} \tag{9}$$

In this equation, n equal to number of data points, m is the number of model parameters; $r_{i,cal}$ is the calculated recovery at time i and $r_{i,obs}$ is the observed or experimental recovery rate at time i.

Hence, flotation models have been evaluated on the basis of the quality of fit of the experimental data. Model that gives parameters when evaluated at various flotation times will give a predicted flotation time-recovery profile that is nearly identical to the observed flotation time-recovery profile is assumed to be the best model. Because the experimental error is constant in all tests, the difference between experimental profile and predicted profile of two models will be a direct measure of the difference in the model errors.

Figure 1 shows the flotation response of the iron ore sample tested. It represents the flotation recovery % versus flotation time (min) at collector dosage of 2 kg/Mg and 3 kg/Mg. It is clear that the recovery increases with increasing flotation time. The increase in flotation recovery is small at high flotation times and the recovery tends to be, more or less, constant after 6 minutes. The flotation response of feed sample is poor where the maximum obtained flotation recovery (at 2 kg/Mg collector) is about 50% after long flotation time (about 8 min). The poor flotation response may be related to the geological nature of the flotation feed, i.e. the valuable mineral (hematite) may be finely disseminated in the ore matrix which needs extensive grinding to achieve acceptable mineral liberation. This is clear from Fig. 1 where increase collector dosage from 2 kg/Mg to 3 kg/Mg does not lead to a significant increase of recovery (55% vs. 50%) with the same concentrate grade 48% Fe compared with the feed grade 38% Fe.

The optimal model parameters for models (I-VII) as well as the maximum error in predicted flotation recovery and the standard error of *estimate* (S_r) are shown in Table 3. The results of simulation of the investigated models are shown in Figures 2 through 5. All tested flotation models expressed the recovery-time profile successfully as the standard error of estimate may be more or less acceptable where it is ranging from 0.010 to 0.034, i.e., from 1%-3%. The lowest performance is observed with the first order two stage kinetic model (model V) which include two stage rate constants. The first expresses the transfer of particles from pulp to froth and the second expresses the rate of transfer of particles from froth to concentrate.

Table 3. Model parameters, maximum error and standard error of estimate (S_r) at flotation dose 2 kg/Mg collector

Model	Parameters			Max. error	S_r
I	K_f=1.3374	K_s=0.0349	Φ =0.6222	0.0254	0.0130
II	K =2.0522	R =0.5221		0.0129	0.0100
III	K=2.1663	R=0.5494		0.0231	0.0148
IV	K=2.5609	R=0.5901		0.0286	0.0184
V	K=2.3432	K'=2.4014	R=0.4637	0.0342	0.0341
VI	λ=2.6595	P=2.9025	R=0.4959	0.0128	0.0130
VII	a_1=0.4095 K_1=1.2020	a_2=0.0106 K_2=0.7050	a_3=0.5800 K_3=0.0171	0.0098	0.0138

This indicates that dividing flotation rate constant into two rate constants, i.e. considering that flotation process consists of two stages instead of single stage is useless or have no additional benefit. The best fit to the experimental data is obtained with the first order two parameters model with rectangular distribution of

floatabilities (model II) and the three parameter fast/slow floating particles model (model I). This result is in agreement with the obtained results in a previous work carried out on coal flotation (Saleh 2009). In that investigation, these models recorded the best performance among other tested first order models. This work indicates that the performance of first order models is better than second order models as better fit to experimental data is observed.

Three parameter gamma distribution model gave better fit than second order models. This result shows that the flotation process can be better described as first order process than other high order processes. The six parameter model (model VII) which includes classification of floating particles into three fractions (a_1, a_2, a_3) with fast, medium and slow flotation rates (K_1, K_2, K_3) has good fit to the experimental results better than second order models. This result is in contrast with other results obtained by other investigators (Apling and Ersayin 1986) which stated that no benefit is gained from increasing number of parameters in the flotation model. Hence, it seems that this conclusion needs more investigation in the future studies. The performance of tested models with regard to fit is in following order: model II > model I = model VI > model VII > model III > model IV > model V.

The best two models (model I and model II) were tested also with dosage 3 kg/Mg oleic acid collector. The standard error of estimate *(Sr)* were 0.024 and 0.023 respectively compared with 0.013 and 0.010 at 2 kg/Mg collector. It is clear that the standard error of estimate depends on the flotation conditions and increases with collector dosage increase. It's worth to mention that among the tested models, two parameters model with rectangular distribution of floatabilities (model II) and second order kinetic model with rectangular distribution of floatabilities (model IV) don't respond at the point of zero time. Among tested second order models (models III, IV), second order kinetic model (model III) obtained better results.

Better performance of model II over model I may be related to the assumption that the ultimate recovery is 1.0. It is believed that the rectangular distribution of floatabilities gives this model flexibility and therefore, should be a better form of the first order process. Quality of fit for model II is the best of all models. Because the mathematical form of model III includes the square of the ultimate recovery parameter and due to assumption of the second order, additional model error over and above that inherent in first order models may be introduced. However, as in model III, the second order form in model IV introduced additional parameter dilution. In model VI the fit to the observed data is excellent and better than of some two parameter forms. Although it was concluded that little or no benefit is derived from increasing number of parameters in the model, i.e., the smaller the number of parameters that are required by a model to achieve an adequate fit to experimental data, the easier the model relates changes in their magnitude to changes in operational variables (Apling and Ersayin 1986), six parameter model (model VII) shows good fit to the observed data.

PARAMETER CONFIDENCE REGIONS

The parameter confidence regions were estimated for the three best models, namely, model I, model II and model VI.

Due to the non-linear nature of the flotation models, confidence limit estimates of parameters based on linear model methodology can not be applied. Instead, logical sensitivity test procedure was applied (Klimpel and Austin 1984).This procedure involved a stepwise change (±10%,±25%,±50%) in one of the optimal model parameters values. By holding the changed parameter constant and allowing the computer program to reoptimize, a new estimate of model parameters and the sum of squares between observed recovery and calculated recovery was determined. The sum of squares is then used to calculate the model variance (S^2_r) which used in statistical *F-Test*. By comparing the optimal model variance to the model variance from a given change in the parameter being assessed, a calculated *F*-value can be determined. By repeating this process, a plot of calculated *F* versus the parameter value can be made. If calculated *F*-value is less than the *F*-distribution (*F*-value from the tables, i.e., F_{crit}) then there is no significant difference between

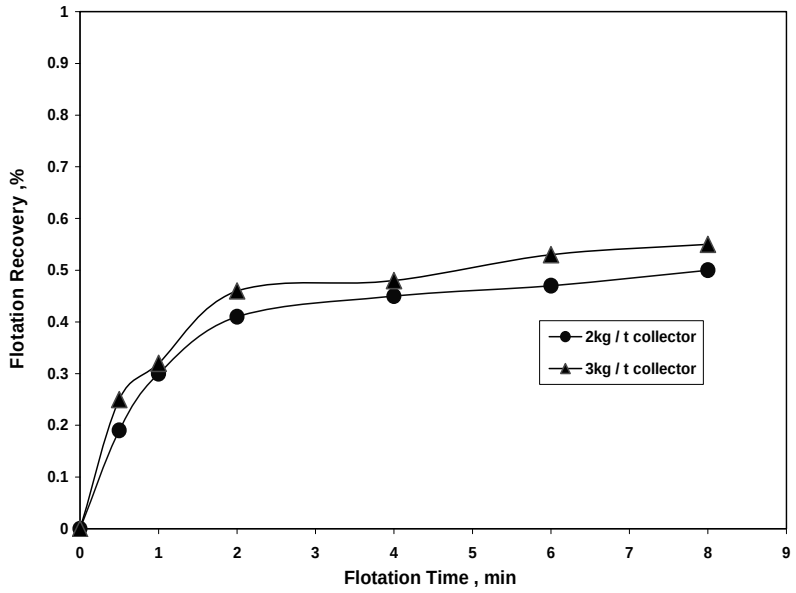

Fig. 1. Flotation response of considered feed sample at 2 kg / Mg and 3 kg / Mg collector

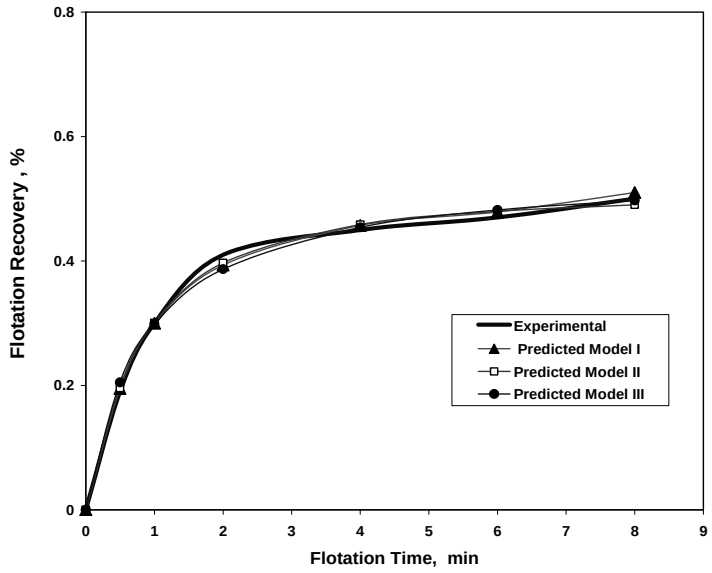

Fig. 2. Experimental and predicted flotation recovery for models I , II and III

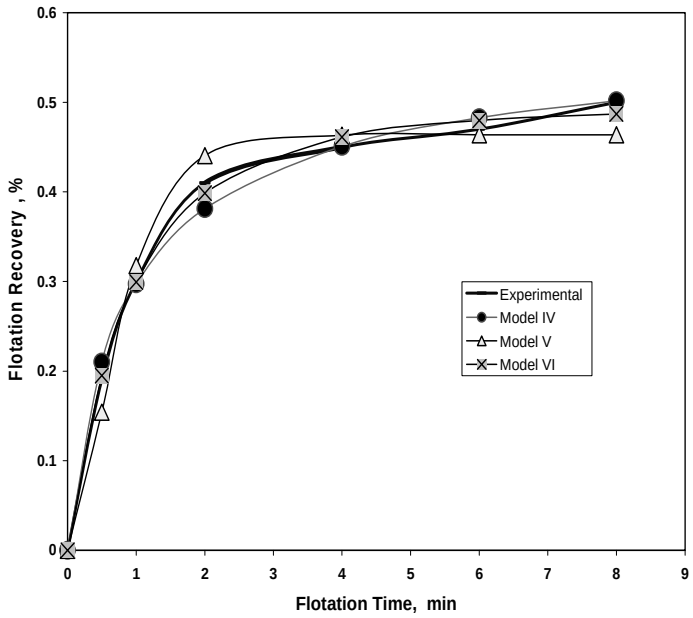

Fig. 3. Experimental and predicted flotation recovery for models IV, V, and VI at 2kg / Mg collector

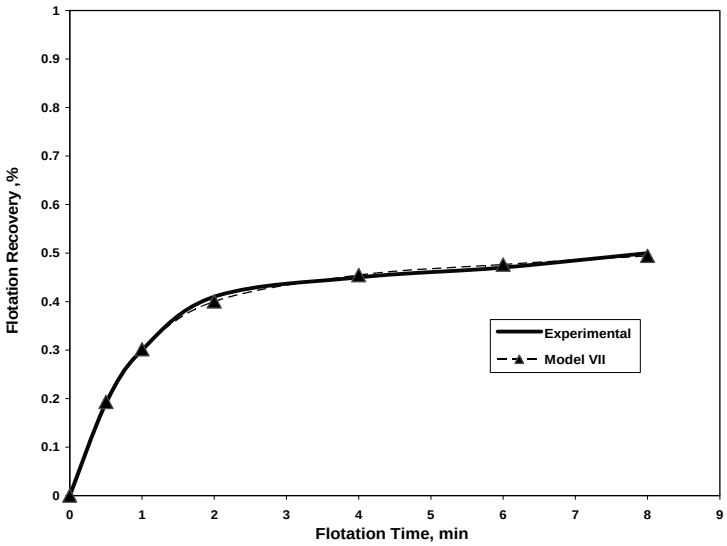

Fig. 4. Experimental and predicted flotation recovery for model VII at 2 kg / Mg collector

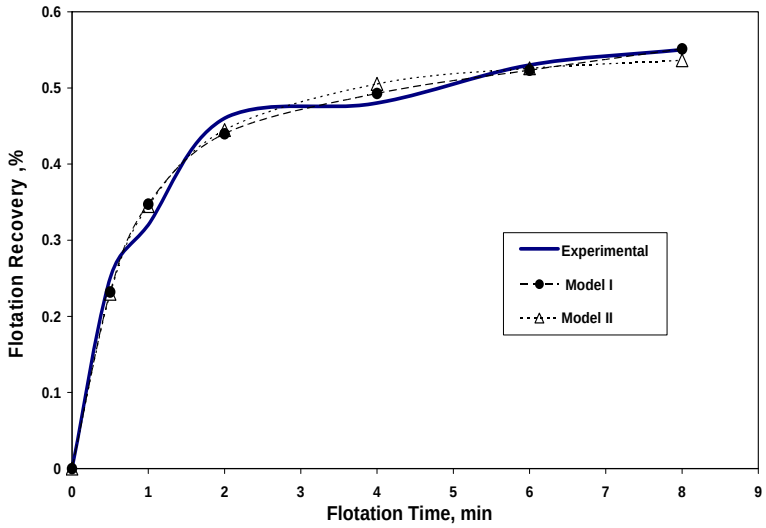

Fig. 5. Experimental and predicted flotation recovery for models I and II at 3 kg / Mg collector

the optimum parameter value and the changed parameter value and null hypothesis (H_o) is applied. On the other hand, if calculated F-value is greater than the $F_{crit,}$ the

alternative hypothesis (H_1) is applied which states that there is a significant difference between the optimum parameter value and the charged parameter value.

If a model gives parameters with a wide range of statistical significance, the differences that can be observed between different tests become diluted or completely masked and it's impossible to make firm quantitative comparison of various test conditions. On the other hand, if the model gives parameters with a narrow range of statistical significance, differences between tests become apparent.

This method of calculation is illustrated in a working example for model II in tables (4, 5). The confidence limits for K and R parameters were determined by the graphical technique at 95% confidence level and shown in Figures (6, 7).

Figure (8) shows comparison of confidence intervals for ultimate recoveries of models II and VI. The approach was continued for each parameter in each of considered models (I, II, VI). Table (6) shows the confidence limits of the three best models, i. e, model I, model II and model VI.

It's clear that for model II while the confidence regions of K is symmetrical, the confidence region of R is not. The confidence region of R of model VI is also, more or less, symmetrical as shown on Fig. 8.

Investigating the above results indicates that with regard to (R), the range of statistical significance in model VI is less than model II. The confidence limits for R and K are very narrow for model II. The confidence limits for Φ and R in models I and VI are, more or less, the same. It is expected that additional parameters in model VI may introduce model error and parameter dilution comparing with simpler form of model II. Determination of confidence intervals for second order models are recommended in future work to be compared with that of first order models. Among the tested models and with regard to quality of fit and confidence intervals, the two parameter model with rectangular distribution of floatabilities (model II) is the best model. The increase in model parameters still needs more investigation in the future studies. The first order models recorded better performance than second order models. Three parameter gamma distribution (model VI) shows a fit to the experimental data more or less similar to that observed with three parameter fast/slow floating particles model (model I). Models I, II obtained the best fit to the experimental data as previously observed in coal flotation (Saleh 2009). The worst fit was observed with the first order two stage kinetic model (model V).

Table 4. Determination of parameter confidence range of K by F-Test at 95% confidence level for model II

	K	R	SSQ	S_r^2	F
Opt.	2.0522	0.5221	0.00045	0.00010	1.0
+10%	2.2574	0.5129	0.00070	0.00018	18
-10%	1.8470	0.5329	0.00077	0.00019	19
+25%	2.5653	0.5013	0.00182	0.00045	45
-25%	1.5391	0.5531	0.00286	0.00072	72

Table 5. Determination of parameter confidence range of *R* by *F*-Test at 95% confidence level for model II

	K	*R*	*SSQ*	S_r^2	*F*
Opt.	2.0522	0.5221	0.00045	0.00010	1.0
+10%	1.8316	0.5743	0.00109	0.00027	2.7
-10%	2.2855	0.4699	0.00048	0.00012	1.2
+25%	1.5163	0.6526	0.00484	0.00121	12.1
-25%	2.6676	0.3916	0.00409	0.00102	10.2

SSQ=sum of squares of differences

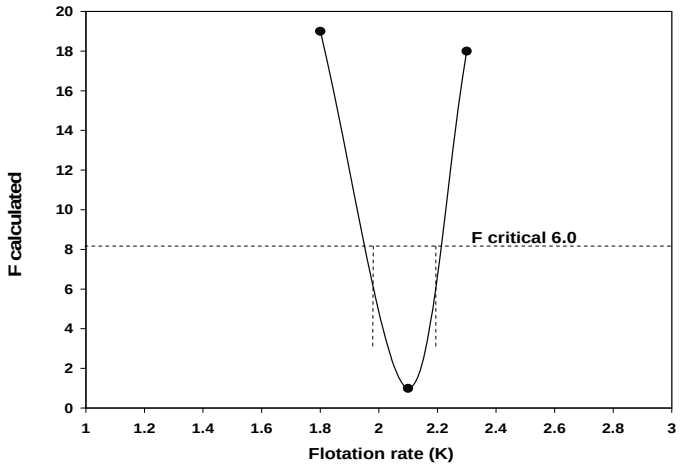

Fig. 6. Graphical determination of parameter confidence ranges for flotation rate (*K*) for model II

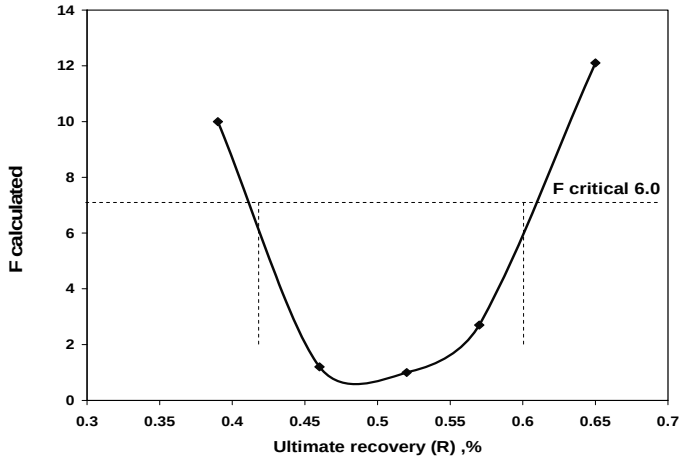

Fig. 7. Graphical determination of parameter confidence ranges for ultimate recovery (*R)* for model II

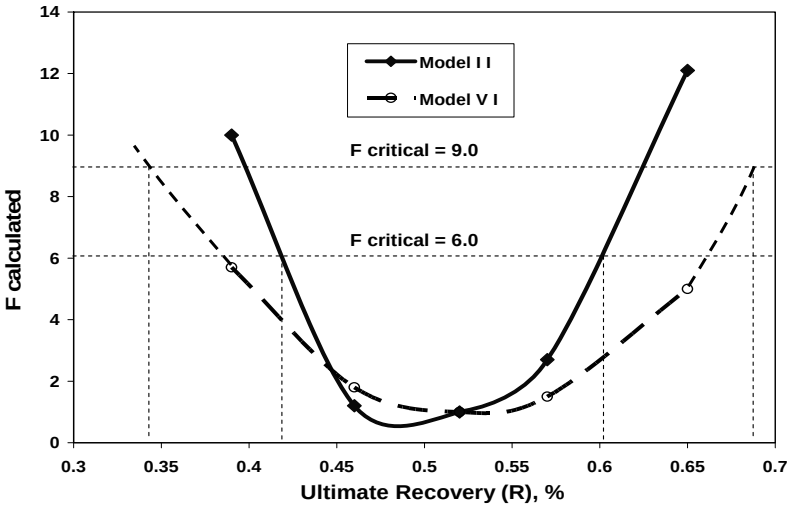

Fig. 8. Comparison of confidence ranges for ultimate recovery (R) for models II and VI

Table 6. Confidence intervals for model I, model II and model VI

Model	Parameter	Optimum	Range
I	K_f	1.3374	0.75 - 2.25
	K_s	0.0349	*
	Φ	0.6222	0.40 - 0.75
II	K	2.0522	1.97 - 2.20
	R	0.5221	0.42 - 0.60
VI	λ	`2.6595	*
	P	2.9025	*
	R	0.4959	0.34 - 0.68

* Parameter insensitive to 50% change

CONCLUSIONS

In this investigation, seven flotation models were tested in iron ore flotation. These models include, three parameter fast/slow floating particles model (model I), two parameter model with rectangular distribution of floatabilities (model II), second order kinetic model (model III), second order kinetic model with rectangular distribution of floatabilities (model IV), first order two stage kinetic model (V), three parameter gamma distribution model (model VI) and six parameter model (model VII). The best fit was observed for models I and II with model II better than model I.

The fit to the experimental data is found in following order: model II > model I = model VI > model VII > model III > model IV > model V. The first order models obtained better performance than second order models. The tested six parameter model (VII) showed also good fit to the experimental data. This result shows need for more investigation to illustrate the effect of increase parameters in model and to determine their upper limit to provide an adequate model. The worst fit was observed with the first order two stage kinetic model (model V) which indicates that dividing flotation rate into two rates, the first for transfer particles from pulp to froth and the second for transfer particles from froth to concentrate is incorrect.

The confidence intervals for the three best models (model I, II, VI) were estimated by the graphical technique at 95% confidence level. It was found that model II shows discrete confidence regions which illustrates the ability of this model to express changes in flotation conditions. In comparison with model II, and with regard to flotation recovery, model VI showed less discrete (wide) confidence regions.

REFERENCES

ARBITER, N AND HARRIS, C.C., 1962 "Flotation Kinetics" – in Froth flotation: 50th Anniversary volume, New York, American Institute of Mining, Metallurgical and petroleum Engineers, PP. 215-246.

ARBITER, N., 1951, "Flotation rates and flotation efficiency" Trans. AIME, Vol. 190, , PP. 791-796.

ALEXANDER, D.J., RUNGE, K.C., FRANZIDIS, J.P. AND MANLAPIG, E.V., 2000, "The application of multi-component floatability to full scale flotation circuists" Proceedings of the Aus IMM, 7th Mill operators conference, Kalgoorlie, PP. 167-178.

APLING, A.C. AND ERSAYIN, S., 1986, "Reproducibility of semi-batch flotation testwork with the leeds open-Top cell and of derived kinetic parameters "Trans Instn. Min., Metall. (sec. C: Mineral Processing Extr. Metall.), 95, June , pp. C83-C88.

GULSOY, O.Y., 2005, "A simple model for the calculation of entrainment flotation" Korean Journal of chemical Engineering, Vol. 22, number 4, July , PP. 628-634.

HEINDEL, T.J. , 1997, "The fundamentals of flotation deinking "TAPPI pulping conference, San Francisco, California, Oct. , PP. 19-23.

HEINDEL, T.J., BLOOM, F., 2006, "Dispersed air flotation theory" Encyclopedia of surface and colloid science, subject-Material science, Somasundaran, P. and Hubbard, A (eds). published in Aug 15, 2006.

HARRIS, M.C., 1997, "A practical framework for flotation circuit modeling and simulation" presented at the SAIchE,, the 8th national meeting of the South African Institute of chemical Engineers, Cape Town, April 16-18.

HUBER-PANU, I., ENE- DANALACHE E., COJOCARIU, D.,G, 1976, "Mathematical models of batch and continuous flotation" flotation- A.M. Gaudin Memorial Volume, M.C. Fuerstenau, (ed) AIME, New York, NY, Vol. 2 chapter 5, PP. 675-724.

JOWETT, A., GHOSH, S.K., 1965, "Flotation Kinetics: Investigations leading to process optimization" 7th int. mineral processing congr., New York., PP. 175-184.

KELSALL, D.F. , 1961, "Application of probability in assessment of flotation systems" Trans. IMM, Vol. 70, PP. 191-204.

KLIMPEL, R.R., 1980, " Selection of chemical reagents for flotation " Mineral processing plant design, 2nd edition, Mular, A.L. and Bhappu, R.B.(eds), chapter 45, AIME, New York, NY, PP. 907-934.

KLIMPEL, R.R., 1984, "The effect of chemical reagents on the flotation recovery of minerals" chemical Engineering, Vol. 91. No. 18, sept. 1984.
KLIMPEL, R.R., AUSTIN, L.G., 1984, “The back calculation of specific rates of breakage from continuous mill data” Powder Technology, Vol. 38, pp. 77-91.
MEHROTRA, S.P. AND KAPUR, P.C., 1974, "The effects of aeration rate, particle size and density on the flotation rate distributions "Powder Tech., Vol. 9, PP. 213-219.
MIKA, T.S., FUERSTENAU, D.W., 1969, "A microscopic model of the flotation process "8th int. mineral processing congr. Leningrad, 1968, Paper S4.
MATHE, Z.T., HARRIS, M.C., O'CONNER, C.T., 2000, "A review of methods to model the froth phase in non-steady state flotation systems" Minerals Engineering, Vol. 13, No. 2, PP. 127-140.
MEYER, W.E. AND KLIMPEL, R.R., 1984, "Rate limitations in froth flotation" Trans AIME, Vol. 274, PP. 1852-1858
SALEH, A.M.,2009, “Assessment of first order batch flotation models in coal flotation” Journal of Al-Azhar University Engineering sector (JAUES) Vol. 4, No. 12, July 2009, PP. 467-476.
WOODBURN, E.T., KROPHOLLER, H.W., GREENE, J.C.A., 1976, "The utilization and limitations of mathematical modeling in the prediction of flotation networks "in Flotation: A.M. Gaudin Memorial volume, 2, AIME, Fuerstenau M.C. (ed), PP.638-674.
WOODBURN, E.T., 1970, "Mathematical modeling of flotation processes" Minerals Sci. Engng. 2(1), PP. 3-17.
YIANATOS, J.B., 2007, "Fluid flow and kinetic modeling of flotation related processes in columns and mechanically agitated cells- Review" Chemical Engineering Research and design, Vol. 85, Issue Al2, Dec. 2007, PP. 1591-1603.

Saleh A.M., *Badania modeli drugiego rzędu oraz dwufazowych we flotacji rud żelaza*, Physicochemical Problems of Mineral Processing, 44 (2010), 215-230, (w jęz. ang), http://www.minproc.pwr.wroc.pl/journal

Porównano wierność opisu danych pomiarowych za pomocą kinetycznych modeli drugiego rzędu i modeli dwufazowych. Najlepszy opis odnotowano za pomocą modelu dwuparametrowego z potęgową dystrybucją flotowalności (model II) oraz trójparametrowego modelu dla szybko/wolno flotujących ziarn (model I). Także trójparametrowy model oparty o γ-dystrybucję (model VI) dobrze opisywał dane pomiarowe. Najgorsze dopasowanie obserwowano dla modelu pierwszego rzędu dwustopniowego modelu kinetycznego (model V), co wskazuje, że nie ma potrzeby dzielenia szybkości flotacji na dwie części. Model VII, który zawiera sześć parametrów, także daje poprawny opis danych. Wynik ten kontrastuje z wynikami otrzymanymi przez innych badaczy twierdzących, że wzrost liczby parametrów modelu prowadzi do rozmycia oraz wzrostu błędu modelu. Przy 95% poziomie ufności wyznaczono przedziały ufności dla najlepszych modeli I, II oraz VI. Ponadto model II wykazał więcej dyskretnych obszarów w odniesieniu do prędkości flotacji i uzysku, niż model VI. Wskazuje to na lepszą zdolność tych modeli do opisu zmian w procesie flotacji.

słowa kluczowe: flotacja. modelowanie, modele drugiego rzędu, model dwufazowe

Physicochem. Probl. Miner. Process. 44(2010) 231-244

journal homepage
www.minproc.pwr.wroc.pl/journal/

Physicochemical Problems of Mineral Processing

Index No. 32213X ISSN 1643-1049

K. Siwińska-Stefańska[*], A. Krysztafkiewicz[*], F. Ciesielczyk[*], D. Paukszta[*], J. Sójka-Ledakowicz[**], T. Jesionowski[*]

PHYSICOCHEMICAL AND STRUCTURAL PROPERTIES OF TiO_2 PRECIPITATED IN AN EMULSION SYSTEM

Received January 15, 2009; reviewed; accepted May 15, 20009

Precipitation of titania using titanium(IV) sulphate(VI) as the precursor in the emulsion system has been studied. Tytanpol® R-210 of the rutile type structure was used as a standard. The basic physicochemical parameters of the titanium dioxide such as bulk density, the absorption capacity of water, paraffin oil and dibutyl phthalate have been determined along with the moisture content and oil number. Morphology and dispersive characteristics of the titanium dioxide precipitated have been evaluated by the SEM and NIBS techniques. The TiO_2 powders have been also studied by XRD and colorimetric method. In the emulsion system proposed titania of rutile structure has been successfully precipitated. It has been established that the properties of the titanium dioxide obtained depend not only on the composition of the emulsion but also on the amount of the emulsifier applied.

key words: TiO_2, precipitation, emulsion system, rutile and anatase structure, agglomeration

INTRODUCTION

Titania is the most important and most commonly applied inorganic pigment. Chemically it is titanium dioxide (TiO_2) occurring in three polymorphous varieties: tetragonal rutile, anatase and rhombic brukite. Its widespread use is a consequence of

[*] Poznan University of Technology, Institute of Chemical Technology and Engineering
M. Sklodowskiej-Curie 2 Sq., 60-965 Poznan, Poland
e-mail: Teofil.Jesionowski@put.poznan.pl, phone:+48(61)6653720, fax:+48(61)6653649

[**] Textile Research Institute (IW), Brzezinska 5/15 St., 92-103 Lodz, Poland

its unique optical and physicochemical properties such as excellent whitening ability, covering power, brightening and lustre ability and resistance to colour change. Excellent pigmentation value is supplemented with the ability to absorb ultraviolet radiation, chemical inertness, high thermal stability and non-toxicity (Wypych 1999, Braun 1992, 1997, Morgans 1990, Buxbaum 1993, The Merck Index 1996, Rentschler 1999, Jesionowski 2002, Doerr 1989, Luo 2007, Chen 2003, Hu 1999).

Titanium dioxide is obtained from natural raw materials such as rock ilmenites, leucoxen, ilmenite sands, or from enriched ores such as enriched ilmenites, synthetic rutiles or titanium slags. Titania pigments are produced by two distinct technologies: the sulphate technology and the chloride technology (Wypych 1999, The Merck Index 1996).

The properties of TiO_2 nanoparticles depend on their morphology, size of crystallites and crystallographic structure. A few methods have been proposed for obtaining nanocrystalline particles of titanium dioxide, including hydrolysis (chemical precipitation), microemulsion method (inversed micelles), sol-gel method and hydrothermal crystallisation (Dąbrowski 2001).

TiO_2 nanoparticles have been obtained by the sol-gel method during hydrolysis of titanium precursors (Kim 2002, Liu 2002, Reddy 2001, Manorama 2001, Sugimoto 1987, 1997, 2002a, 2002b, 2003a, 2003b). Usually this process involves hydrolysis of titanium(IV) alkoxides in the presence of an acid catalyst and followed by condensation. The process of obtaining TiO_2 nanoparticles of different shapes and size by the sol-gel method has been studied by Sugimoto et al. (Sugimoto 1987, 1997, 2002a, 2002b, 2003a, 2003b). Eiden-Assmann and co-authors have described a method of obtaining TiO_2 particles of specific target size (Eiden-Assmann 2004). They proposed the use of titanium alkoxide as the initial substance in the alcoholic solution to produce TiO_2. Unfortunately, this method was proven ineffective as it resulted in often aggregations with a small number of colloidal spherical molecules.

Another method is the non-hydrolytic sol-gel process based on the reaction of titanium tetrachloride with different oxygen-donating compounds such as metal alkoxides or ethers (Niederberger 2002, Parala 2002, Arnal 1996, Burnside 1998). The hydrothermal method has been widely applied to produce particles, mostly of titanium oxides of small diameters for ceramic industry. The nanoparticles of TiO_2 are obtained during hydrothermal treatment by peptisation of titanium precursors with water. The hydrothermal method has many advantages as it needs a lower temperature of crystallisation than in a typical thermal process. The agglomeration of particles can be eliminated or reduced by conducting crystallisation under high pressure. Moreover, high quality products can be obtained without calcination and milling. This method enables control of the shape and size of particles but the process is slow and cannot be implemented on industrial scale (Wu 2002).

The principal users of titania is the paint, varnish, plastic and paper industries. It is also used in production of textiles, pharmaceutical products, cosmetics, cement and

rubber. Recently increasing attention is paid to ultrafine pigments, known as nanopigments, characterised by excellent absorption of ultraviolet radiation and photocatalytic properties. This wide scope of application of this pigment has brought a wide range of commercially available types of titanium dioxide pigments differing in the technology of production, crystalline form, type of surface processing and properties. Increasing demand for titania prompts efforts to improve its quality and to modify certain properties and extension of the gamut of this pigment quality (Braun 1992, Rentschler 1999, Andrzejewska 2004, Jesionowski 2001, 2002a, 2002b, Doerr 1989, Luo 2007, Chen 2003, Hu 1999, Tadros 1996, Tang 2002).

The aim of the study was to obtain titania by precipitation in the emulsion system using titanium(IV) sulphate(VI) as the precursor. The method proposed will permit obtaining pigments based on titanium of anatase-rutile crystallographic structure and hydrophilic/hydrophobic properties.

EXPERIMENTAL

MATERIALS

The Tytanpol® R-210 is the rutile variety of the pigment whose surface is processed by aluminium and silicon compounds in the amount of 3% Al_2O_3 and 1% SiO_2 and modified by organic compounds of hydrophilic/hydrophobic nature. The basic parameters describing the properties of this pigment, produced by applying the sulphate method by Chemical Works Police S.A., are given in Table 1.

Table 1. Principal properties of the titanium dioxide R-210

Physicochemical variable	Titanium dioxide R-210
Content of titanium dioxide (wt. %)	94
Content of volatile substances at 105°C (wt. %)	0.5
Content of water soluble materials (wt. %)	0.5
Residue on a sieve of 45 μm (wt. %)	0.02
Lightness	95
Shade in a white paste	-7.0
Relative scattering ability	100
Ability to tone down the shade	1850
Shade in a gray paste	2.5
pH in water suspension	7.7

The substrates used to obtain titania in the emulsion system included: (i) the hydrophobising agent Rokanol K7, oxyethylenated unsaturated fatty alcohol made by

PCC ROKITA S.A.; (ii) cyclohexane (made by POCh S.A.) as the organic phase in the emulsion; (iii) 25% solution of sodium hydroxide (POCh S.A.); (iiii) titanium(IV) sulphate(VI) as the precipitating agent (Chemical Works Police S.A.).

PROCEDURES

Precipitation of titania was carried out in a reactor of 500 cm^3 in capacity, in which was placed earlier prepared emulsion of 66 cm^3 of cyclohexane, 70 cm^3 of a 25% solution of NaOH, Rokanol K7: 3.2–4.4 g. The reagents were vigorously stirred by a homogeniser IKA Werke T25 basic, working at the rate of 13500 rpm. Upon homogenisation the precipitating agent – titanium(IV) sulphate(VI) – was introduced into the reactor at a constant rate of 2.6 cm^3/min. by a peristaltic pump ISM833A (Ismatec). Prior to introduction the titanium(IV) sulphate(VI) solution was centrifuged by a high-speed Eppendorf Centrifuge 5804.

The hydrated titanium dioxide was separated from the post-reaction mixture and the salts by filtration under reduced pressure and washed with distilled water on the filter. The product was dried in a stationary dryer at 105ºC for about 8h. The dried pigment was calcined in an oven at 920ºC for 90 min. In total 7 samples were obtained differing in the amount of the emulsifier used in preparation of the emulsion: sample P1 precipitated from the emulsion containing 3.2 g, P2 – 3.4 g, P3 – 3.6 g, P4 – 3.8 g, P5 – 4.0 g, P6 – 4.2 g and P7 – 4.4 g of Rokanol K7.

PHYSICOCHEMICAL PROPERTIES EVALUATION

Bulk density, absorbing capacity of water, dibutyl phthalate, paraffin oil, oil number and moisture content of the product obtained were measured. The morphology and surface structure of the titanium oxides were analysed by a scanning electron microscope (Zeiss VO40). The particle size and its distribution were measured using the non-invasive backscattering technique (NIBS) on Zetasizer Nano ZS instrument (Malvern Instruments Ltd.). On the basis of the particle size distribution curves the polydispersity was found. The polymorphous variety of the samples was verified by X-ray diffraction on a diffractometer TUR-M62. The colorimetric data of the obtained titanium pigments were documented using an instrumented colorimeter (SPECBOS 4000, JETI Technische Instrumente GmbH), which was calibrated using a white colour standard tile with tristimulus values: X=80.57, Y=84.79, and Z=88.33 (Tytanpol® R-210). Daylight (D65) was used as a standardised light source. A fixed amount of pigment sample was poured into the measurement cup. The instrument provided the colour in terms of the CIE $L^*a^*b^*$ colour space system. In this colour space, L^* represented the lightness (or brightness), a^* and b^* were colour coordinates, where $+a^*$ was the red direction, $-a^*$ was the green direction, $+b^*$ was the yellow

direction, and $-b^*$ was the blue direction. Moreover, changes in individual components allowed to estimate the total change of colour ΔE^*. On the other hand, C^* denoted chrome, and h^* determined hue.

RESULTS AND DISCUSSION

The parameters describing the basic physicochemical properties of the TiO_2 powders obtained in the emulsion system are given in Table 2.

Table 2. Principal physicochemical parameters of titania

Sample name	Emulsifier content (g)	Bulk density (g/dm^3)	Absorbing capacity of ($cm^3/100g$)			Oil number ($cm^3/100g$)	Lightness L*
			water	dibutyl phthalate	paraffin oil		
R-210	-	600	100	95	250	27	93.8
P1	3.2	660	60	50	160	29	89.8
P2	3.4	430	95	65	120	28	93.3
P3	3.6	580	90	60	190	28	89.2
P4	3.8	540	90	60	185	30	88.4
P5	4.0	410	90	65	230	30	93.4
P6	4.2	390	100	70	255	35	93.2
P7	4.4	430	100	85	260	27	88.2

Analysis of the results has shown that the bulk density of the titania precipitated decreases with increasing content of the emulsifier in the emulsion, even to a value below 400 g/dm^3 (the standard sample R-210 density is 600 g/dm^3). The absorbing capacities of water, dibutyl phthalate and paraffin oil of the titania precipitated from the emulsion containing 4.4 g of Rokanol K7 (sample P7) are close to the corresponding values of the standard sample of Tytanpol® R-210. For both samples, i.e. sample P7 and the standard, the absorbing capacities of water was 100 $cm^3/100g$, of dibutyl phthalate it was 95 $cm^3/100g$ for R-210 and 85 $cm^3/100g$ for P7 and of paraffin oil it was 250 $cm^3/100g$ for R-210 and 260 $cm^3/100g$ for P7. The oil number of the sample labelled as P7 is 27 $cm^3/100g$, which is the same as that of the standard R-210. For the other samples obtained the oil numbers are slightly higher. The increasing amount of the surfactant used for the emulsion preparation was found to have insignificant effect on the oil number.

Figure 1 presents graphic illustration of the changes in the colorimetric parameters. The lightness (L*) of the standard sample R-210 is 93.8. The highest value of L* was measured for the samples precipitated from the emulsion containing Rokanol K7 in the amounts of 3.4, 4.0 and 4.2 g, labelled as P2 ($L^* = 93.3$), P5 ($L^* = 93.4$) and P6 ($L^* = 93.2$), respectively. For the other samples L* values were lower and the lowest value

of 88.2 was measured for sample P7. This sample was also found to show the highest hue parameter h^* of 95.5 and the lowest colour saturation parameter (C^*) of 3.5. The lowest h^* of 87.0 was determined for sample P1 precipitated from the emulsion containing 3.2 g of Rokanol K7, while the highest difference in the colour relative to that of the standard

ΔE^* of 9.8 was found for sample P3 precipitated from the emulsion containing 3.6 g of Rokanol K7.

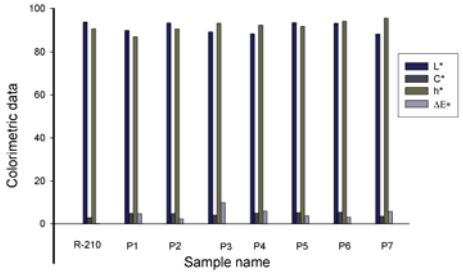

Fig.1. Colorimetric parameters of titania samples precipitated in the emulsion system

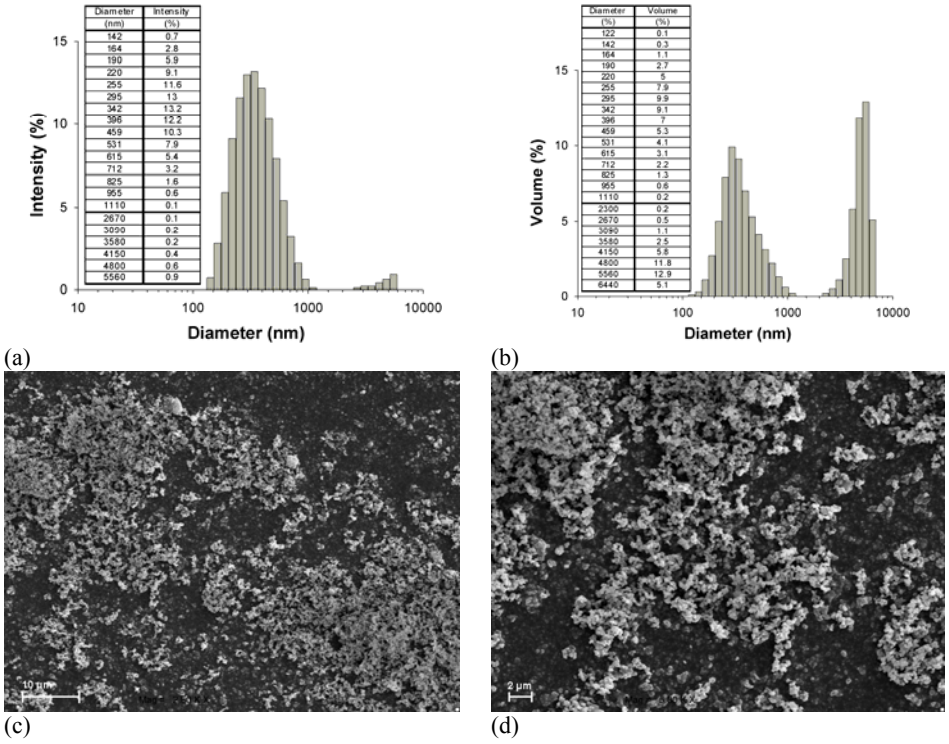

Fig. 2. Particle size distributions: (a) by intensity, (b) by volume and SEM images (c, d) of titanium dioxide R-210 (at different magnifications)

Figure 2 presents the particle size distributions in the form of the percent intensity and volume contribution of particles of a given diameter and the SEM images of the standard sample R-210.

The particle size distribution expressed by the percent intensity contribution of particles of a given diameter (Fig. 2a) shows two bands. The more intense band in the range 142–1110 nm, with the maximum of 13.2% corresponding to the particles of 342 nm in diameter, is assigned to the particles of primary agglomerates. The other band covers the range 2670–5560 nm and is assigned to secondary agglomerates, its maximum intensity of 0.9% corresponds to the particles of 5560 nm in diameter. The polydispersity of R-210 sample related to the particle size distribution is 0.189. The particle size distribution expressed by the percent volume contribution of particles of a given diameter (Fig. 2b) also reveals two bands of similar intensity. The first band in the range 122–1110 nm, with the maximum of 9.9% corresponding to the particles of 295 nm in diameter, is assigned to primary agglomerates. The other band at 2300–6440 nm with the maximum of 12.9% corresponding to the particles of 5560 nm, demonstrates the presence of agglomerates of greater diameters than those of the primary agglomerates. It is concluded from the SEM images, Fig. 2c and d, that the powders are spherical in shape, of small diameters and associate in aggregations and agglomerations.

Figure 3 presents the particle size distributions in the form of the percent intensity and volume contribution of particles of a given diameter and SEM images of sample P1. The particle size distribution expressed as the percent intensity contribution of particles of a given diameter (Fig. 3a) shows two bands. The first more intense band in the range 190–1280 nm, with a maximum of 21.1% for the particles of 396 nm in diameter, is assigned to the primary agglomerates. The other band covering the range 3580–5560 nm, with a maximum of 0.7% corresponding to the particles of 5560 nm in diameter, is assigned to secondary agglomerates. The polydispersity of sample P1 is 0.234, which is higher than that of the standard. The particle size distribution expressed as the percent volume contribution of particles of a given diameter (Fig. 3b) shows two bands. The first at 122–2300 nm, with a maximum of 11.9% for the particles of 396 nm in diameter, is assigned to primary agglomerates. The other band at 4150–6440 nm, with a maximum of 2.6% corresponding to the particles of 4800 nm in diameter, testifies to the presence of secondary agglomerates. The SEM images, shown in Fig. 3c and d, prove the presence of low-diameter particles that are forming aggregations and agglomerations.

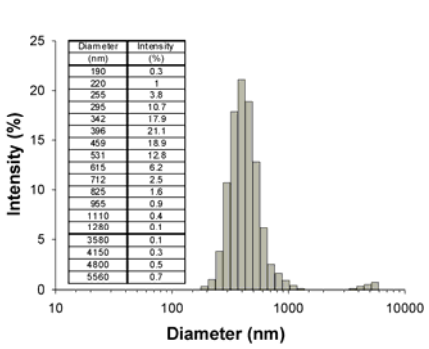

(a)

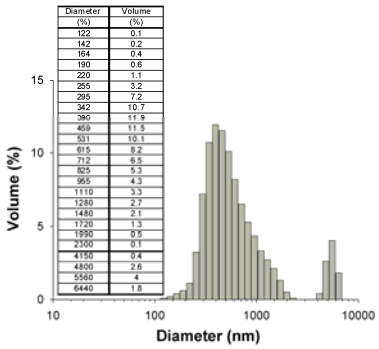

(b)

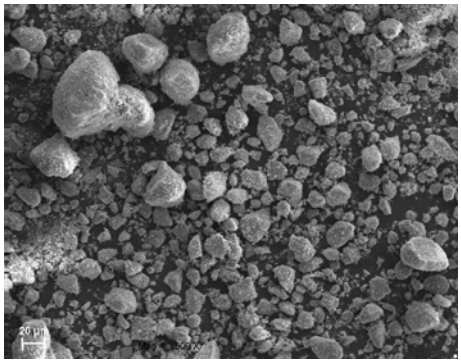

(c)

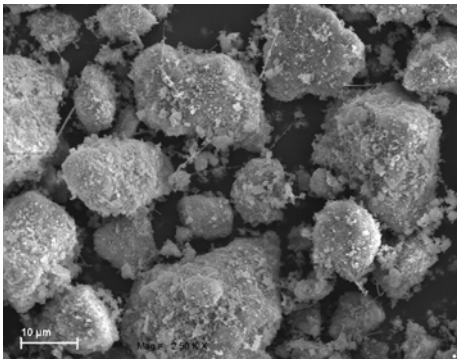

(d)

Fig. 3**.** Particle size distributions: (a) by intensity, (b) by volume and SEM images (c, d) of titanium dioxide precipitated from the emulsion containing 3.2 g of Rokanol K7 (sample P1)

Figure 4 presents the particle size distributions and SEM photographs for sample P3 precipitated from the emulsion containing 3.6 g of Rokanol K7. The particle size distribution expressed by the percent intensity contribution of particles of a given diameter (Fig. 4a) reveals one band only. This band at 220–4150 nm with a maximum of 18.8% corresponding to the particles of 615 nm in diameter, is related to the presence of primary and secondary aggregates. The polydispersity of sample P3 is 0.202. The particle size distribution expressed as the percent volume contribution of particles of a given diameter (Fig. 4b) also shows only one band. This one band covering the range 220–5560 nm, with a maximum of 13.3% for the particles of 615 nm in diameter, is assigned to secondary agglomerates. The SEM images of sample P3, Fig. 4c and d, demonstrate the presence of particles of secondary aggregates associating into agglomerates.

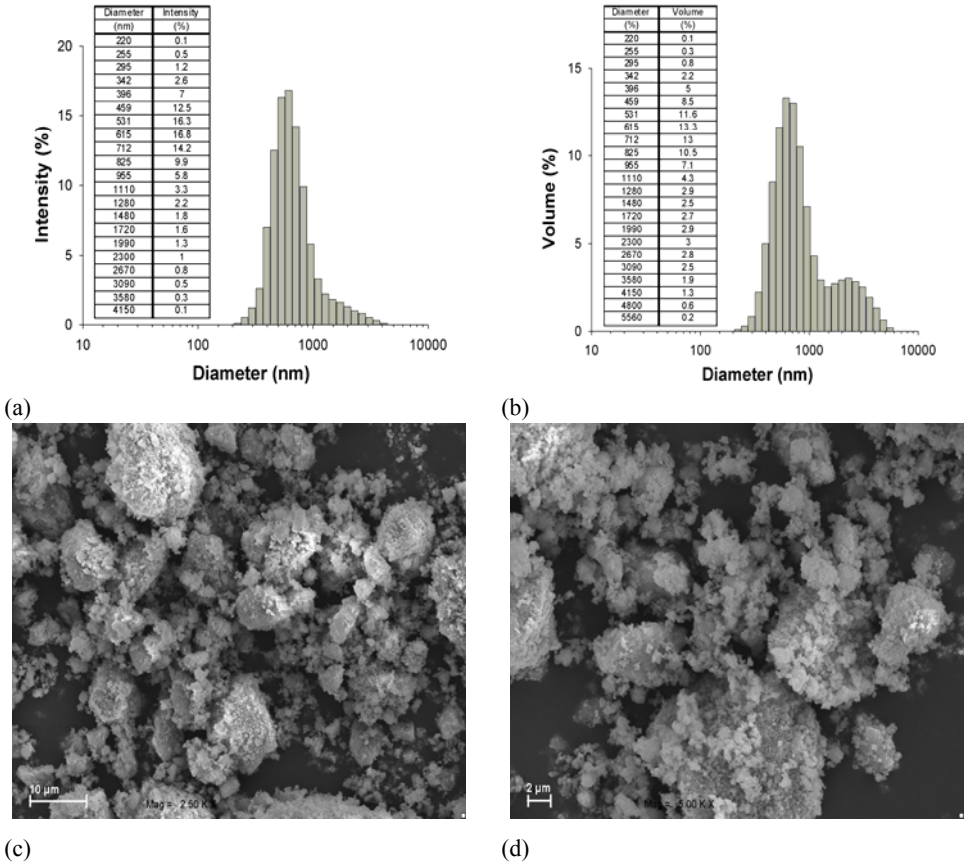

Fig. 4. Particle size distributions: (a) by intensity, (b) by volume and SEM images (c, d) of titanium dioxide precipitated from the emulsion containing 3.6 g of Rokanol K7 (sample P3)

The analogous data and SEM images for sample P5 obtained from the emulsion containing 4.0 g of Rokanol K7 are displayed in Fig. 5.

The particle size distribution expressed by the percent intensity contribution of particles of a given diameter, Fig. 5a, shows one band covering the range 122–5560 nm, with a maximum of 8.3% for the particles of 295 nm in diameter, is assigned to the primary and secondary agglomerates. The particle size distribution expressed by the percent volume contribution of particles of a given diameter, Fig. 5b, also reveals one band in the range 122–6440 nm with a maximum of 6.4% for the agglomerates of 1990 nm indiameter, and is assigned to the primary and secondary agglomerates. The polydispersity of this sample is 0.318, which is greater than that of the above discussed samples (R-210, P1 and P3). The SEM images (Fig. 5c and d) confirm the presence of particles of diameters varying in a wide range.

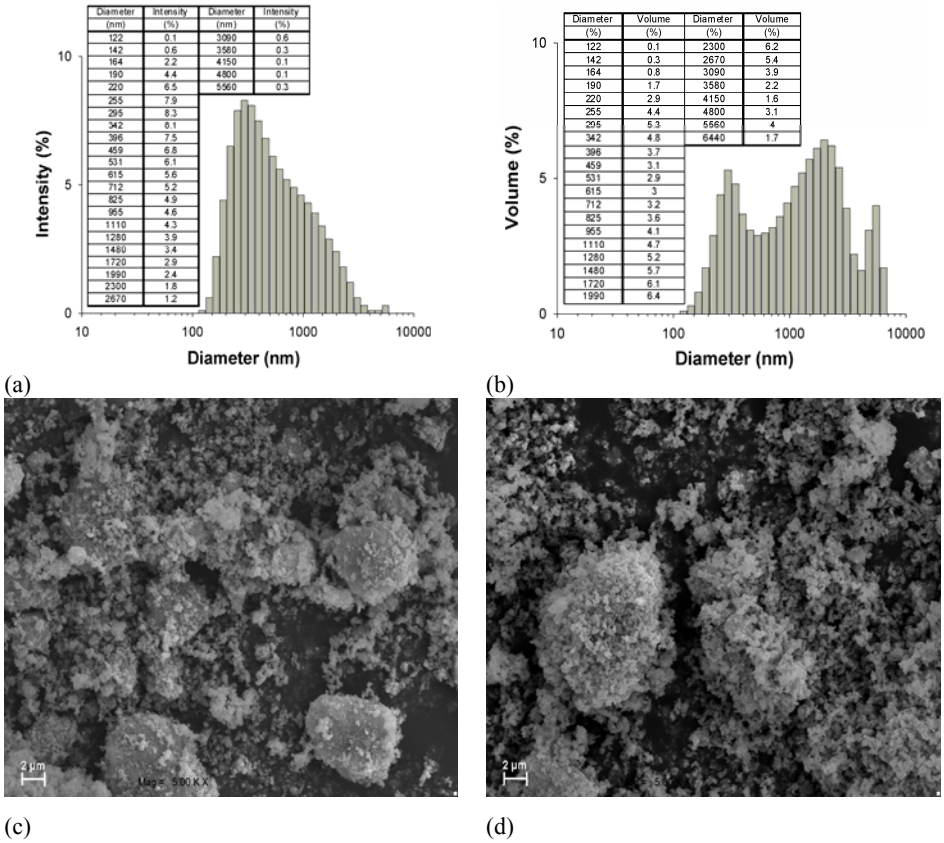

Fig. 5. Particle size distributions: (a) by intensity, (b) by volume and SEM images (c, d) of titania precipitated from the emulsion with 4.0 g of Rokanol K7 (sample P5)

The particle size distributions and SEM images for sample P7 precipitated from the emulsion with 4.4 g of Rokanol K7 are shown in Fig. 6. The particle size distribution expressed by the percent intensity contribution of particles of a given diameter (Fig. 6a) reveals two bands. The first more intense band at 122–1990 nm with a maximum of 14.5% for the particles of 342 in diameter is related to the presence of primary agglomerates. The other band of much lower intensity is assigned to the agglomerates of the diameters from the range 4800–5560 nm. The particle size distribution expressed by the percent volume contribution of particles of a given diameter (Fig. 6b) also shows two bands. The first band, covering the range 122–2300 nm with a maximum of 12.6% for the particles of 342 in diameter, corresponds to the primary agglomerates, while the other, in the range 3580–6440 nm with a maximum of 6.3% for the particles of 5560 nm in diameter, corresponds to secondary agglomerates. The polydispersity of sample P7 is 0.262.

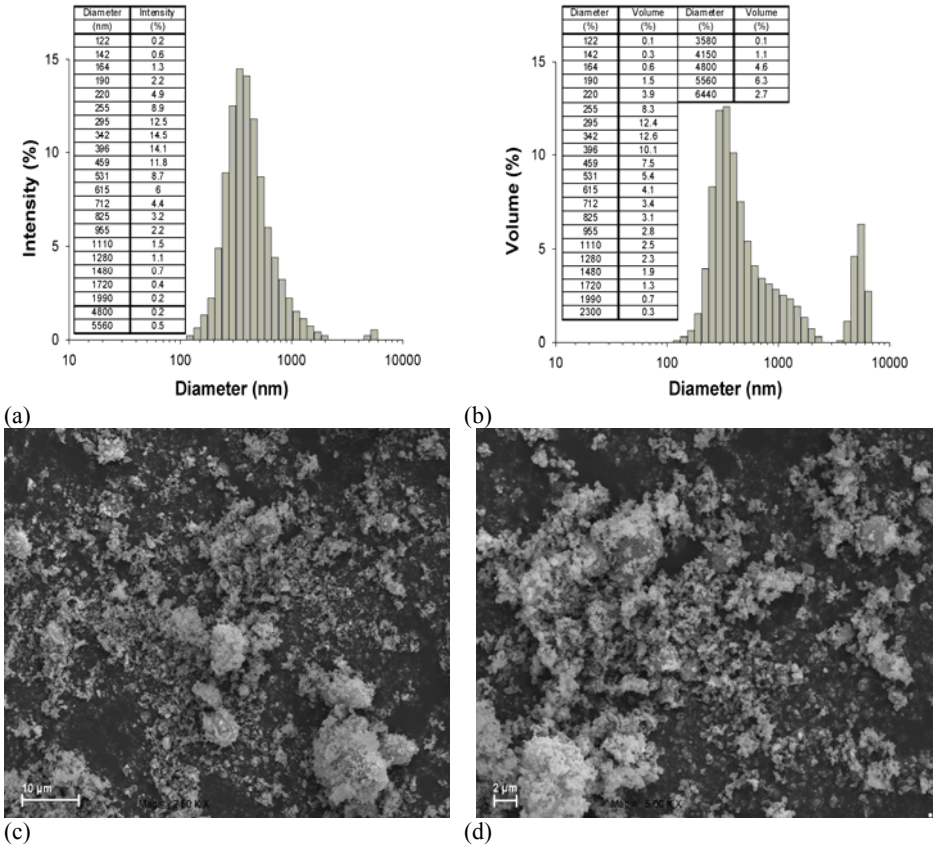

Fig. 6. Particle size distributions: (a) by intensity, (b) by volume and SEM images (c, d) of titania precipitated from the emulsion containing 4.4 g of Rokanol K7 (sample P7)

The crystalline structure of the titania samples obtained by precipitation was determined by X-ray diffraction. Selected diffractograms are shown in Fig. 7. Figure 7a presents the XRD pattern of the standard R-210 sample of rutile type structure, characterised by the maxima for the following values of the angle 2θ: 28, 36, 39, 41, 44, 54, 57. The occurrence of maxima at these values of the angle theta permits identification of the rutile type structure. The X-ray diffraction patterns recorded and shown in Fig. 7b–d confirm the rutile type of the titanium dioxide samples obtained by precipitation, but reveal also samples of anatase type structure, identified on the basis of the maxima for the angle 2θ: 25, 32, 33, 33.5, 48, 54, 55. The X-ray diffractograph of sample P4 shown in Fig. 7c resembles most closely that of the standard sample R-210, which indicates an almost complete transformation of the anatase form into the rutile as a result of calcination of the samples at 920°C.

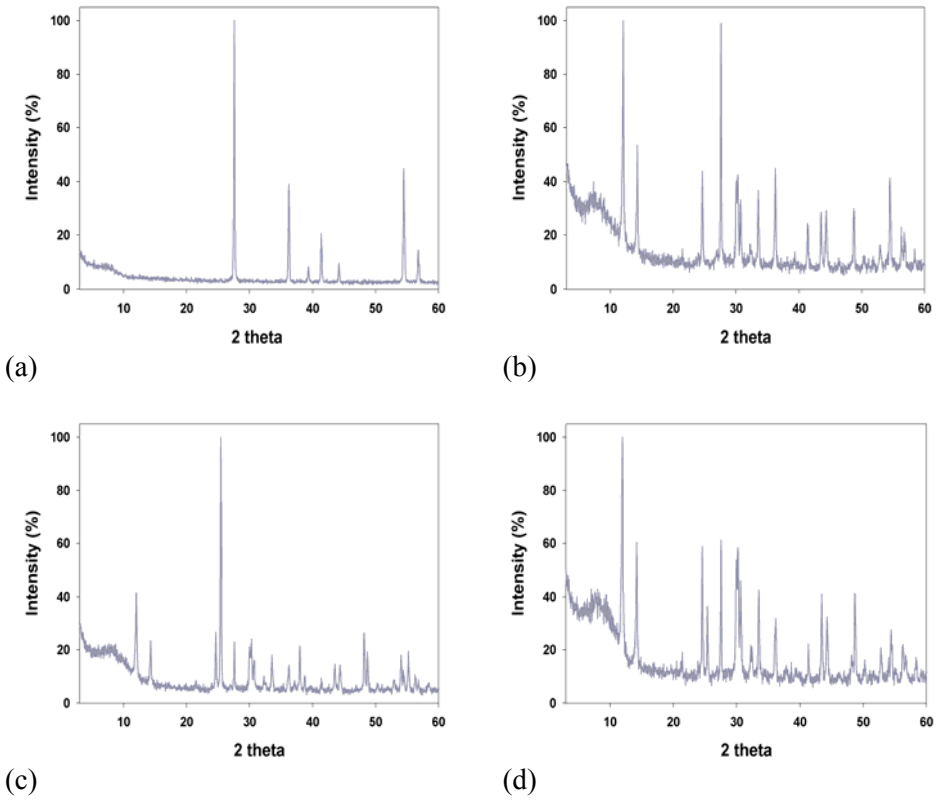

Fig. 7. XRD patterns of selected titanium dioxide samples: (a) R-210, (b) sample P3, (c) sample P4 and (d) sample P7

CONCLUSIONS

The above presented results have confirmed that titania of the rutile type structure can be obtained in the emulsion system. The properties of the TiO_2 samples obtained by precipitation are determined by the emulsifier content in the emulsion. From among all samples obtained the most similar to the standard R-210 was sample P7 precipitated from the emulsion containing 4.4 g of Rokanol K7. This sample contained the primary and secondary agglomerates of the size varying in the range 122–1990 nm, with the dominance of the particles of 342 nm in diameter, similarly as in the standard. The colour of the samples obtained was found to depend significantly on the content of the emulsifier used. The oil numbers of all samples obtained by precipitation are similar.

ACKNOWLEDGEMENTS

This publication was prepared within the key project – POIG no. 01.03.01-00-006/08 cofinanced from the funds of European Regional Development Fund within the framework of the Operational Innovative Economy. The authors thank the Chemical Works Police S.A. for the titanium dioxide standard (TYTANPOL® R-210) gift.

REFERENCES

ANDRZEJEWSKA A., KRYSZTAFKIEWICZ A., JESIONOWSKI T., 2004, *Adsorption of organic dyes on the aminosilane modified TiO_2 surface*, Dyes Pigments, 62, 121-130

ARNAL P., CORRIU R.J.P., LECLERCQ D., MUTIN P.H., VIOUX A., 1996, *Preparation of anatase, brookite and rutile at low temperature by non-hydrolytic sol-gel methods*, J. Mater. Chem., 6, 1925-1932

BRAUN J.H., 1997, *Titanium dioxide a review*, J. Coating. Tech., 69, 59-72

BRAUN J.H., BAIDINS A., MARGANSKI R.F., 1992, *TiO_2 pigment technology: a review,* Prog. Org. Coat., 20, 105-138

BURNSIDE S.D., SHKLOVER V., BARB C., COMTE P., ARENDSE F., BROOKS K., GRÄTZEL M., 1998, *Self-organization of TiO_2 nanoparticles in thin films*, Chem. Mater., 10, 2419-2425

BUXBAUM G., 1993, Industrial Inorganic Pigments, VCH, Amsterdam

CHEN Y.-F., LEE C.-Y., YENG M.-Y., CHIU H.-T., 2003, *Preparing titanium oxide with various morphologies*, Mater. Chem. Phys., 81, 39-44

DĄBROWSKI W., TYMEJCZYK A., LUBKOWSKA A., 2001, *Właściwości i zastosowanie pigmentów dwutlenku tytanu*, Materiały Firmowe Zakładów Chemicznych „POLICE" S.A., Szczecin

DOERR H., HOLZINGER F., 1989, Kronos Titandioxid in Dispersionsfarben, Kronos-Titan GmbH, Leverkusen

EIDEN-ASSMANN S., WIDONIAK J., MARET G., 2004, *Synthesis and characterization of porous and nonporous monodisperse colloidal TiO_2 particles*, Chem. Mater., 16, 6-11

HU Z.S., DONG J.X., CHEN G.X., 1999, *Preparation of nanometer titanium oxide with n-butanol supercritical dryling,* Powder Technol., 101, 205-210

JESIONOWSKI T., 2001, *Modification and characterization of titanium dioxide surface*, Pigment Resin Technol., 30, 287-295

JESIONOWSKI T., KRYSZTAFKIEWICZ A., DEC A., 2002a, *Modified Al_2O_3-treated titanium whites as pigments of acrylic paints*, Physicochem. Problems Mineral. Proc., 36, 307-316

JESIONOWSKI T., KRYSZTAFKIEWICZ A., DEC A., 2002b, *Modified titanium white covered by Al_2O_3 and SiO_2 - characteristics and application in acrylic paints*, Pigment Resin Technol., 31, 290-296

KIM K.D., KIM H.T., 2002, *Synthesis of titanium dioxide nanoparticles using a continuous reaction metod*, Colloid Surface A, 207, 263-269

LIU P., BANDARA J., LIN Y., ELGIN D., ALLARD L.F., SUN Y.P., 2002, *Formation of nanocrystalline titanium dioxide in perfluorinated ionomer membrane*, Langmuir, 18, 10398-10401

LUO Z., CAI H., REN X., LIU J., HONG W., ZHANG P., 2007, *Hydrophilicity of titanium oxide coatings with the addition of silica*, Mat. Sci. Eng. B, 138, 151-156

MANORAMA S.V., REDDY K.M., REDDY C.V.G., NARAYANAN S., RAJA P.R., CHATTERJI P.R., 2001, *Photostabilization of dye on anatase titania nanoparticles by polymer capping*, J. Phys. Chem. Solids, 63, 135-143

MORGANS W.M., 1990, Outlines of Paint Technology, Halsted Press, New York

NIEDERBERGER M., BARTL M.H., STUCKY G.D., 2002, *Benzyl alcohol and titanium tetrachloride – A versatile reaction system for the nonaqueous and low-temperature preparation of crystalline and luminescent titania nanoparticles*, Chem. Mater., 14, 4364-4370

PARALA H., DEVI A., BHAKTA R., FISCHER R. A., 2002, *Synthesis of nano-scale TiO_2 particles by a nonhydrolytic approach*, J. Mater. Chem., 12, 1625-1627

REDDY K.M., REDDY C.V.G., MANORAMA S.V., 2001, *Preparation, characterization, and spectral studies on nanocrystalline anatase TiO_2*, J. Solid State Chem., 158, 180-186

RENTSCHLER T., RELLER A., 1999, *Optimum particle size is essential*, Eur. Coating. J., 4, 80-89

SUGIMOTO T., 1987, *Preparation of monodispersed colloidal particles*, Adv. Colloid Interf., 28, 65-108

SUGIMOTO T., OKADA K., ITOH H., 1997, *Synthesis of uniform spindle-type titania particles by the gel-sol metod*, J. Colloid Interf. Sci., 193, 140-143

SUGIMOTO T., ZHOU X., 2002a, Synthesis *of uniform anatase TiO_2 nanoparticles by the gel-sol method. 2. Adsorption of OH^- ions to $Ti(OH)_4$ gel and TiO_2 particles*, J. Colloid Interf. Sci., 252, 347-353

SUGIMOTO T., ZHOU X., MURAMATSU A., 2002b, *Synthesis of uniform anatase TiO_2 nanoparticles by gel-sol method: 1. Solution chemistry of $Ti(OH)_n^{(4-n)+}$ complexes*, J. Colloid Interf. Sci., 252, 339-346

SUGIMOTO T., ZHOU X., MURAMATSU A., 2003a, *Synthesis of uniform anatase TiO_2 nanoparticles by gel-sol method: 4. Shape control*, J. Colloid Interf. Sci., 259, 53-61

SUGIMOTO T., ZHOU X., MURAMATSU A., 2003b, *Synthesis of uniform anatase TiO_2 nanoparticles by gel-sol method: 3. Formation process and size control,* J. Colloid Interf. Sci., 259, 43-52

TADROS M.E., ADKINS C.L.J., RUSSICK E.M., YOUNGMAN M.P., 1996, *Synthesis of titanium dioxide particles in supercritical CO_2*, J. Supercrit. Fluid., 9, 172-176

TANG Z., ZHANG J., CHENG Z., ZHANG Z., 2002, *Synthesis of nanosized rutile TiO_2 powder at low temperature*, Mater. Chem. Phys., 77, 314-317

THE MERCK INDEX, 1996, An Encyclopedia of Chemicals, Drugs and Biologicals, New York

WU M., LIN G., CHEN D., WANG G., HE D., FENG S., XU R., 2002, *Sol-hydrothermal synthesis and hydrothermally structural evolution of nanocrystal titanium dioxide*, Chem. Mater., 14, 1974-1980

WYPYCH G., 1999, Handbook of Fillers, 2nd ed., ChemTec Publishing, Toronto

Siwińska-Stefańska K., Krysztafkiewicz A., Ciesielczyk F., Paukszta D., Sójka-Ledakowicz J., Jesionowski T., *Badanie właściwości fizykochemicznych bieli tytanowej otrzymanej w układzie emulsyjnym* , Physicochemical Problems of Mineral Processing, 44 (2010), 231-244, (w jęz. ang), http://www.minproc.pwr.wroc.pl/journal

Przeprowadzono badania nad strącaniem bieli tytanowej w układzie emulsyjnym. Wzorcowym ditlenkiem tytanu był Tytanpol® R-210 produkowany przez Zakłady Chemiczne Police S.A. Oznaczano podstawowe parametry fizykochemiczne strąconych próbek ditlenku tytanu, takie jak: chłonności wody, oleju parafinowego i ftalanu dibutylu oraz gęstość nasypową, a także zawartość wilgoci i liczbę olejową. Określano morfologię i mikrostrukturę otrzymanego ditlenku tytanu w celu uzyskania informacji o dyspersji, morfologii ziaren oraz budowie poszczególnych cząstek, wykorzystując techniki SEM i NIBS. Ponadto strącone próbki poddano analizie rentgenograficznej i kolorymetrycznej.

słowa kluczowe: TiO_2, wytrącanie, emulsja, struktura, anataz, rutyl, aglomeracja

Physicochem. Probl. Miner. Process. 44(2010) 245-256

journal homepage
www.minproc.pwr.wroc.pl/journal/

Physicochemical Problems of Mineral Processing

Index No. 32213X ISSN 1643-1049

M. Ulewicz*, U. Lesińska**, M. Bocheńska**

TRANSPORT OF LEAD ACROSS POLYMER INCLUSION MEMBRANE WITH *p- tert* -BUTYLCALIX[4]ARENE DERIVATIVE

Received January 18, 2009; reviewed; accepted June 23, 2009

The facilitated transport of lead(II) across polymer inclusion membranes (PIMs), which consist of cellulose triacetate as polymeric support, *o*-nitrophenyl octyl ether as plasticizer and 25, 26, 27, 28 – Tetrakis(N–hydroxy-N-methylcarbamoylmethoxy)-*p-tert*-butylcalix[4]aren (***L***) as ion carrier was reported. PIM was characterized by using atomic force microscopy (AFM). The results show that Pb^{2+} can be separated very effectively from other heavy and transition metal cations as Zn^{2+}, Cd^{2+}, Co^{2+}, Ni^{2+} (each at a concentration of 10^{-3} M). The rate limiting step in the transport of Pb^{2+} across PIM doped with calix[4]aren derivative may be the diffusion coefficient of the carrier cation complex across the membrane. The stability of PIM with *p-tert*-butylcalix[4]aren derivative was described using Danesi's thermodynamic model. The apparent partition constant of the carrier was experimentally estimated and compared with different carriers.

key words: polymer inclusion membrane (PIM), lead(II), p- tert-butylcalix[4]arene-hydroxamate

INTRODUCTION

The removal of heavy metal species, particularly lead and cadmium ions, from waste waters has an important environmental aspect. Among the several methods that

* Department of Metal Extraction and Recirculation, Czestochowa University of Technology, 42-200 Częstochowa, Armii Krajowej 19 Street, e-mail: ulewicz@mim.pcz.czest.pl
** Chemistry Department, Technical University of Gdańsk, ul. G. Narutowicza 11/12, 80-952 Gdańsk

can be used to remove toxic metals from aqueous solutions, liquid membranes techniques have become important for use in separation process. Recently, polymer inclusion membranes (PIMs), first introduced by Sugiura (Sugiura, 1980), have received increasing attention as an alternative to SLM. The transport of metal ions across PIMs is accomplished by a carrier, which is essentially an ion exchanger or a complexing agent. There are several commercially available compounds, but carriers newly synthesized, especially macrocyclic compounds (Nghiem et al., 2006), have also tested. Calixarenes and calixcrowns have successfully been used for metal ions separation by solvent extraction and transport through liquid membranes systems. The use of application of macrocyclic compounds as ion carriers in liquid membranes was reviewed (Ulewicz, 2008) and (Walkowiak and Kozłowski, 2009).

Several functionalized calixarenes with different donor atoms have been used for Pb(II) ions extraction. New allyl functionalized calix[4]arene-thioamide in 1,3-alternate conformation as well as di-ionizable calix[4]arene-1,2-crown-5 ligands exhibit high extraction ability toward Pb^{2+} ions (Arena et al., 2001; Tu et al., 2008). Also, the ability to bind two lead(II) ions with a single molecule of calix[4]arene tetracarboxylic acid has been reported (Otho et al., 1999). The order of extraction selectivity to metal ions was as follows: Pb(III) >> Fe(III) > Al(III) > Cu(II) > Zn(II).

Calixarenes and their derivatives are a new generation of highly selective carrier for heavy and transition ions across liquid membranes. Hui-Min et al. (Hui-Min et al., 2001) studied the selective transport of Cu^{2+}, Fe^{3+}, Co^{2+}, Ni^{2+} and Zn^{2+} across liquid membrane with new calix[4]crowns. One of those calix crowns, 25, 27-dihydroxy-26,28-(3',6'-dioxa-2',7'-dioxooctylene)dioxy-calix[4]arene, transported Cu^{2+} cations. Efficiently. Whereas thiacalix[4]arene was found to be an effective ion carrier for the transport of Cd(II) ions (80%) across SLMs (Zaghbani et al., 2005). The transport of Pb^{2+} from an aqueous solutions across BLMs containing *p-t*-butylthiacalix[4]aren was examined (Nechifor et al., 2002).

Alpoguz et. al. (2002) studied co-transport of metal ions (Hg^{2+}, Pb^{2+}, Na^{+}) from an aqueous solution into an aqueous receiving phase through the bulk liquid membrane containing calix[4]arene nitrile derivatives as ion carriers. The transport rates show that both nitrile derivatives are efficient and selective for Hg(II) ions with respect to Na^{+} and Pb^{2+} ions and the dinitrile derivatives was a better carrier than the tetranitrile derivative. The membrane entrance and exit rate constant depend on the solvent type and are found to be of the following order: $CH_2Cl_2 > CHCl_3 > CCl_4$.

Recently, competitive transport of an aquimolar mixture of Zn(II), Cd(II) and Pb(II) cations from aqueous source phase across PIMs with calix[4]crown-6 derivatives, as ion carriers, were examined by Ulewicz et al. (2007). The maximum percentage of lead(II) removal increased in the following order of R groups attached to the compounds: -OH < $-OCH_3$ < $-OCH_2COOH$ < $OCH_2COOC_2H_5$ < $OCH_2CONHOCH_2C_5H_6$. In this paper, we describe the selective transport of heavy and transition ions across PIM doped with *p-tert*-butylcalix[4]aren with four N-methyl

hydroxamic acid moieties. Physical and chemical properties of lipophilic, functionalized *p-tert*-butylcalix[4]aren make it a potentially useful ion-carrier.

EXPERIMENTAL

REAGENTS

Inorganic chemicals such as zinc(II), copper(II), cadmium(II), nickel(II), cobalt(II), lead(II) nitrates and nitric acid were of analytical grade and were purchased from POCh (Gliwice, Poland). Organic reagents such as cellulose triacetate (CTA), *o*-nitrophenyl octyl ether (*o*-NPOE) and dichloromethane were also of analytical grade, were purchased from Fluka and used without further purification. The 25, 26, 27, 28–Tetrakis-(N–hydroxy-N-methyl-carbamoylmethoxy)-*p-tert*-butylcalix[4]aren (***L***) (Fig. 1) was synthesized according to the procedure described in (Lesińska and Bocheńska, 2006).

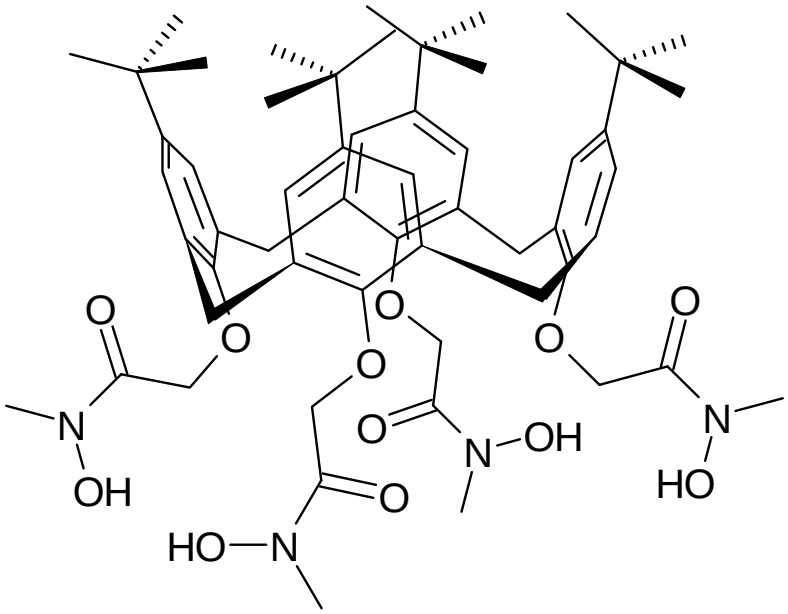

Fig. 1. Formula of studied ion-carrier L

POLYMER INCLUSION MEMBRANE PREPARATION

Membranes were prepared as previously described (Ulewicz et al., 2007). A solution of cellulose triacetate as the support, plasticizer and ion carrier L was

prepared in dichloromethane. A specified portion of this solution was poured into a membrane mould consisting of a 9.0 cm diameter glass ring placed on a glass plate with cellulose triacetate-dichloromethane glue. After slow solvent evaporation overnight, the resulting membrane was peeled off from the glass plate by immersion in cold water. The membrane was soaked for 12 hours in distilled water to achieve homogeneity. Two samples of membrane were cut from the same membrane film for duplicate transport experiments. The membrane was made of 2.6 cm^3 *o*-NPOE /1g CTA, and 0.05 M carrier ***L*** calculated on plasticizer. The average PIM thickness was estimated to be 30 μm.

MEMBRANE CHARACTERIZATION - ATOMIC FORCE MICROSCOPY

Surface characterization of the polymer membranes was carried out using atomic force microscopy (AFM). AFM was carried out on a MultiMode with NanoScope IIIa and Quadrex controllers from Veeco Instruments. Maximal scan range *x*, *y*: 10 μm, *z*: 2.5 μm. The microscope worked as AFM in the Tapping Mode using RTESP probe (Veeco). Two samples of $1cm^2$ from different regions of the same membrane were examined. For the analysis of surface pore characteristics, the AFM image processing program NanoScope v.5.12 was used. Using this program, two parameters, roughness (R_q) and porosity (ε), were calculated. Parameter R_q is the standard deviation of the *z* values within the box cursor and is calculated as:

$$R_q = \sqrt{\frac{\sum (z_i)^2}{n}} \tag{1}$$

where: z_i is the current *z* value, *n* is number of points within the box cursors.

TRANSPORT STUDIES

Transport experiments were carried out in a permeation module cell as described previously (Ulewicz et al., 2007). The membrane film (with a surface area of 4.9 cm^3) was tightly clamped between two cell compartments. Both the source and receiving aqueous phases (45 cm^3 each) were mechanically stirred at 600 rpm. The receiving phase was 0.5 M HNO_3. The PIM transport experiments were carried out at the temperature of 20 ± 0.2^0C. Small samples (0.1 cm^3 each) of the aqueous receiving phase were removed periodically via a sampling port with a syringe and analyzed to determine cation concentrations by atomic absorption spectroscopy (AAS Spectrometer, Solaar 939, Unicam). The source phase pH was kept constant (pH = 5,0) and monitored using a by pH meter (CX-731 Elmetron, with combine pH electrode, ERH-126, Hydromet, Poland). The permeability coefficients (*P*, m/s) of metal ions across polymer membranes were described using the following equation:

$$\ln\left(\frac{c}{c_i}\right) = -\frac{A}{V}\cdot P\cdot t \tag{2}$$

where c is the metal ion concentration (M) in the source aqueous phase at some given time; c_i is the initial metal ion concentration in the source phase; t is the time of transport (s); V is volume of the aqueous source phase (m^3); and A is an effective area of membrane (m^2).

The linear dependence of $\ln(c/c_i)$ in the source phase versus time was obtained and the permeability coefficients were calculated from the slope of the straight line that fits the experimental data. The initial flux (J_i) was determined:

$$J_i = P\cdot c_i . \tag{3}$$

The diffusion coefficient D_o (cm^2/s) of the metal-complex across the organic phase can be determined in the case of absence of diffusion resistances in the aqueous layer source phase/membrane by the following equation (Danesi, 1984-85) :

$$c = c_i - \frac{[L]_o\cdot A\cdot t}{n\cdot V\cdot \Delta_o} \tag{4}$$

where $\Delta_o = d_o/D_o$ (s/cm) is the resistance of transport by diffusion across the membrane, d_o (cm) is the thickness of the membrane, n - is the number of moles of the carrier in the complex (in our case n = 1);and $[L]_o$ is the initial concentration of the extractant in the organic phase (M). Plotting $[Me^{2+}]_i$-$[Me^{2+}]_t$ vs. time gives a slope equal to $([L]_o\cdot A)/(\Delta_o\cdot V)$ which can be used to calculate the diffusion coefficients D_o of the metal complex species in the membrane phase.

RESULTS AND DISCUSSION

The transport of metal ions across a liquid membrane depends on many factors. One of the important aspects of PIMs is the distribution of the organic carrier in the polymer matrix, which determines their transport efficiency (Arous et al., 2004). Atomic force microscopy was used to characterize morphology of prepared PIM. Figures 2 (a) and (b) show the AFM images of blank polymer membrane (supported with plasticizer) and polymer inclusion membrane containing 0.05M *p-tert*-butylcalix[4]aren derivative, respectively, in three-dimensional format of 1.0 x 1.0 μm. As can be seen from Fig 2b, the carrier *L* crystallizes inside the membrane matrix, which might be why the surface texture is relatively homogenous. One of the membrane features is well defined pores. The pores are clearly visible as small, well-defined dark areas.

a)

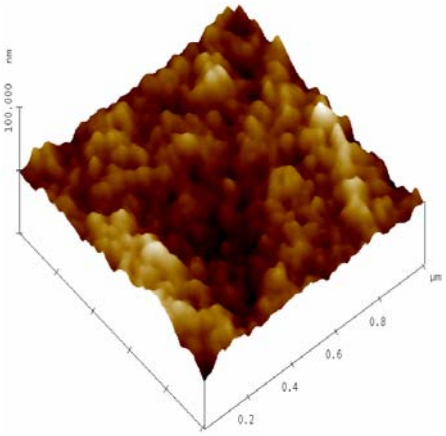
100.000 nm
0.2
0.4
0.6
0.8
µm

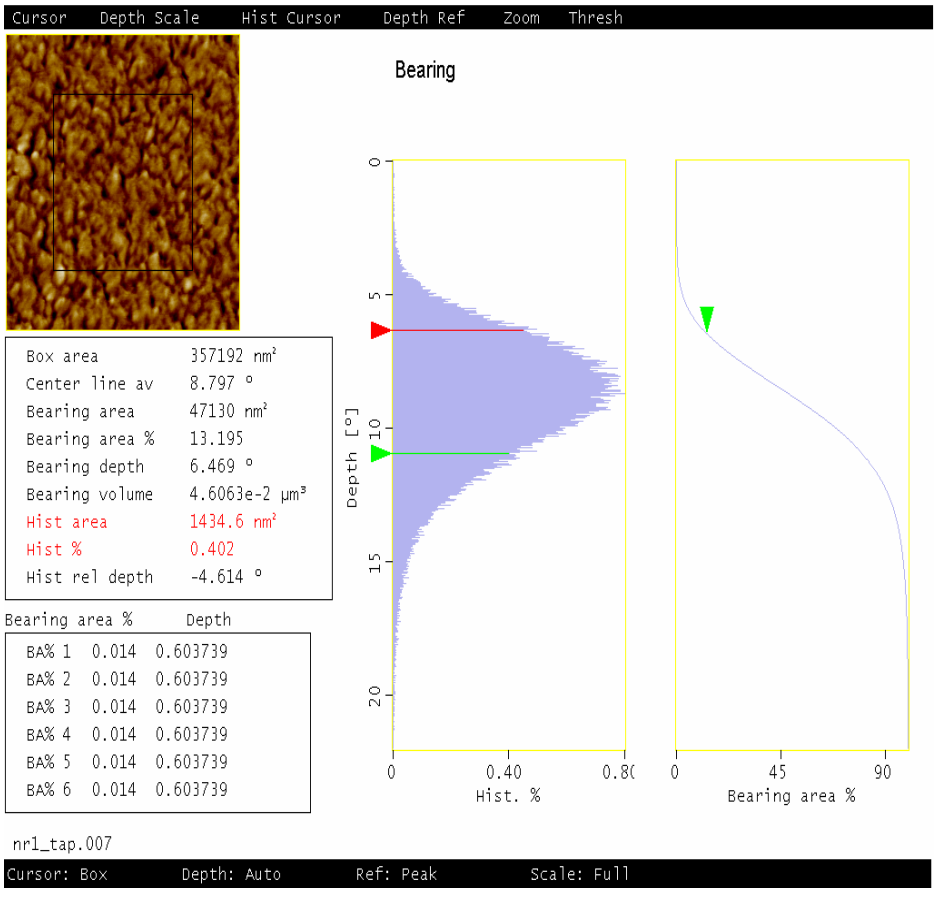
Cursor Depth Scale Hist Cursor Depth Ref Zoom Thresh
Bearing
Box area 357192 nm²
Center line av 8.797 °
Bearing area 47130 nm²
Bearing area % 13.195
Bearing depth 6.469 °
Bearing volume 4.6063e-2 µm³
Hist area 1434.6 nm²
Hist % 0.402
Hist rel depth -4.614 °
Bearing area % Depth
BA% 1 0.014 0.603739
BA% 2 0.014 0.603739
BA% 3 0.014 0.603739
BA% 4 0.014 0.603739
BA% 5 0.014 0.603739
BA% 6 0.014 0.603739
Depth [°]
0
5
10
15
20
0.40
Hist. %
45
90
Bearing area %
nr1_tap.007
Cursor: Box Depth: Auto Ref: Peak Scale: Full

b)

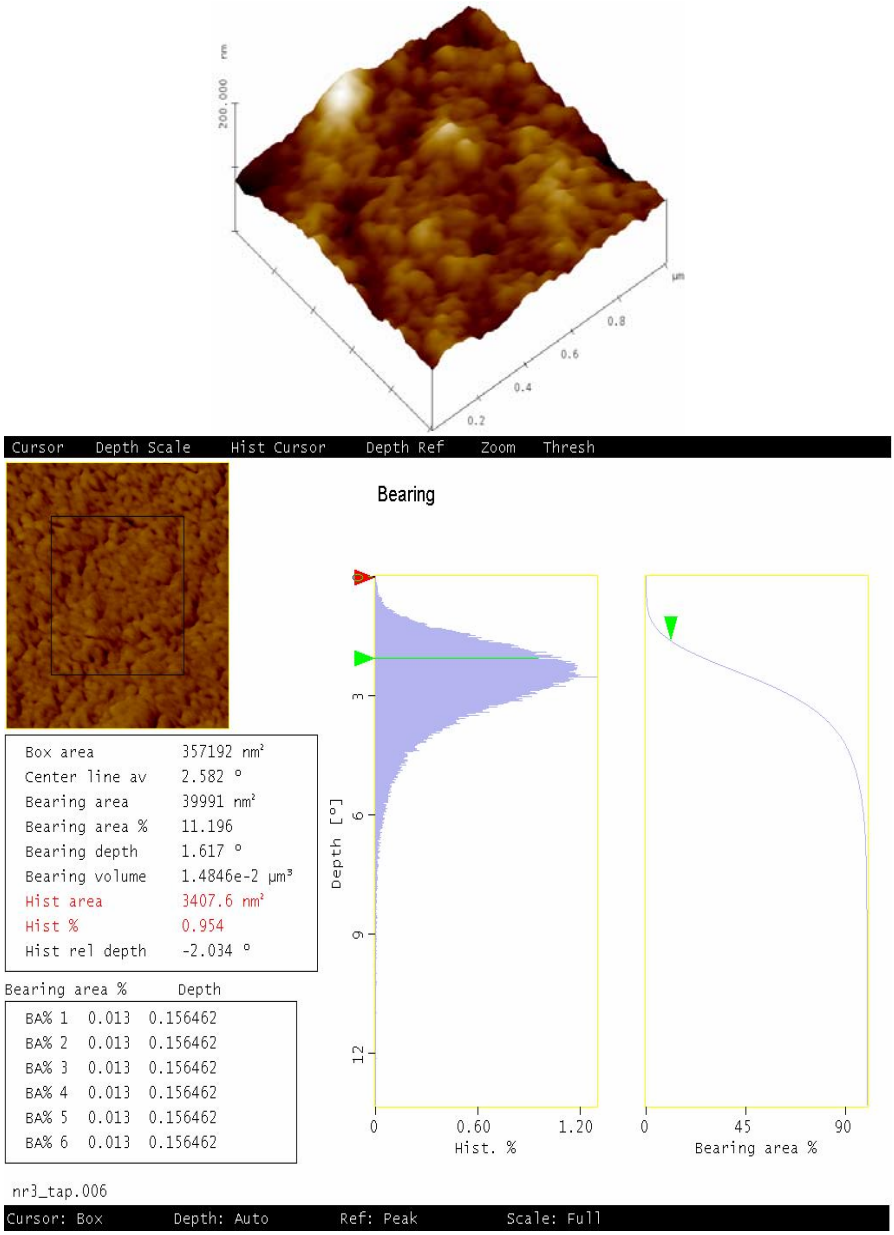

Fig. 2. 3D-view atomic force micrographs of matrix membrane - CTA-*o*NPOE (a) and polymer membrane CTA-*o*NPOE containing 0.05M carrier ***L*** (b)

Membranes without ion carrier containing only cellulose triacetate have a porous structure with a porosity of 50% (Arous et al. 2004). The pores of CTA membrane are

filled by the *o*-NPOE molecules, the membrane less porous. The calculated porosity (ε) for membrane composed only with 2.67cm^3 *o*-NPOE/1g CTA is 13.2%, whereas the porosity of this membrane with carrier is only 11.2 %. The roughness (R_q) of membrane constituted by CTA-*o*NPOE and CTA-*o*NPOE with carrier were 10.0 and 7.3 nm, respectively. The roughness of investigated PIMs with carrier is higher than that found in polymer membrane with D2EHPA (R_q = 4.6 nm) prepared by Salazar-Alvarez et al. (2005) and lower than in membranes prepared by Tor et al. (2009) for DEHPA (268 nm).

In earlier studies on heavy and transition metal ions separations, soft metal ions as Pb^{2+} or Ag^{+} display great affinity for soft coordination centres like nitrogen or sulphur atoms. Therefore, the calix[4]aren with functional group containing nitrogen atoms was used as ion carriers for the competitive heavy and transition metal ions transport from a source aqueous phase into receiving nitric acid solutions across PIM. The study included two different solutions containing of Zn(II), Cd(II), Pb(II) (mixture 1) and Co(II), Ni(II), Pb(II) ions (mixture 2) at concentration of metal equal 0.001M each. The kinetic curves of metal ions transport are shown in Fig. 3. Only Pb(II) ions were transported. Transport efficiency for the zinc(II) ions were generally less than 3%, whereas the other metal ions (Ni^{2+}, Co^{2+}, Cd^{2+}) were not transported. The driving force of Pb^{2+} cations transport was the exchange of protons from the receiving phase with metal ions from the source phase. The initial fluxes of Pb(II) from mixtures 1 and 2 were $2.69 \cdot 10^{-7}$ and $2.88 \cdot 10^{-7}$ mol/m^2·s, respectively.

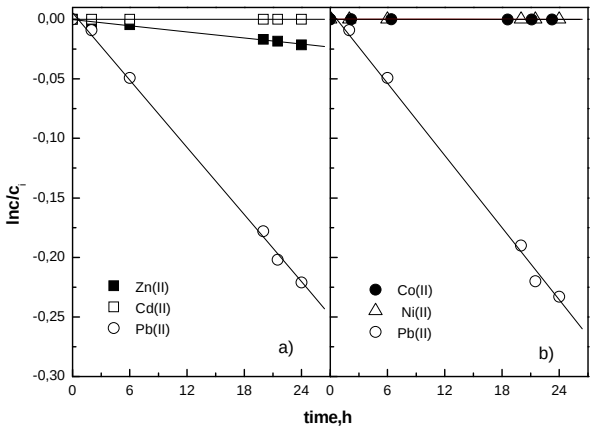

Fig. 3. Kinetics curves for metal ions transport across PIM with *p-tert*-butylcalix[4]aren derivative from different equimolar mixture of metal ions; c_{Me}= 0.001 M each, pH =5.0

In Fig. 3, the correlation graphs $[Pb^{2+}]_i$-$[Pb^{2+}]_t$ versus time of Pb(II) transport from different mixture solutions across PIM doped with ***L*** is presented. The diffusion coefficient of Pb(II) was calculated for each mixture solutions, substituting $D_o = d_o/\Delta_o$,

where d_o is the thickness of the membrane (0.003 cm), and Δ_o could be evaluated by plotting $[Pb^{2+}]_i$-$[Pb^{2+}]_t$ versus time.

The corrected (normalized) membrane diffusion coefficient $D_{o,n}$, which considers the morphological features inside the membrane (ε - porosity and τ -tortuosity), was calculated using the following equation: $D_{o,n}=D_o\cdot(\varepsilon/\tau)$ (Salazar-Alvarez et al., 2005). The membrane tortuosity was determined from the relationship developed by Wolf and Strieder (1990): $\tau = 1 - \ln \varepsilon$ and equal to 3.19 (for ε = 0.112). Diffusion coefficients are presented in Table 1. The values are comparable with previously reported values for different membranes are in the range 10^{-6} to 10^{-12} cm^2/s, and show that the limiting step of the process is the transfer of metal complex across the membrane barrier. The average value of the diffusion coefficient of Pb(II)-carrier species of $4.16\cdot10^{-9}$ cm^2/s is smaller than the value of $1.5\cdot10^{-7}$ cm^2/s reported for the lead complex with the D2EHPA in PIM reported by Salazar-Alvarez et al. (2005).

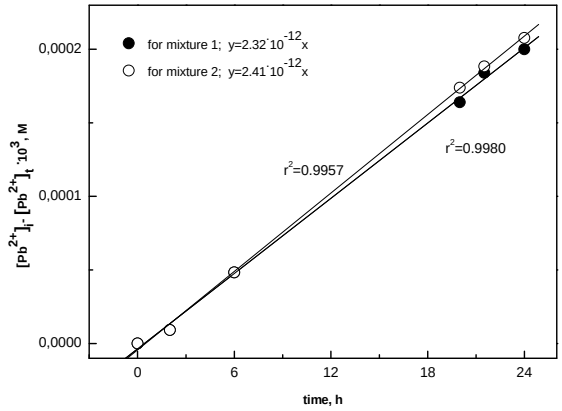

Fig. 4. $[Pb^{2+}]_i$-$[Pb^{2+}]_t$ vs. time for Pb^{2+} transport across PIM membrane doped with calix[4]arene ***L***. Conditions of experiment as in Table 1

Table 1. Permeability coefficient, diffusion coefficient normalized for competitive transport of Pb(II) ions through PIM from different mixtures, pH = 5.0

Mixture	P, (m/s)	Δ_o, (s/m)	D_o, (cm^2/s)	$D_{o,n}$, (cm^2/s)
1	$2.69\cdot10^{-4}$	$10^{7.3}$	$1.42\cdot10^{-10}$	$4.04\cdot10^{-9}$
2	$2.88\cdot10^{-4}$	$10^{7.325}$	$1.50\cdot10^{-10}$	$4.27\cdot10^{-9}$

Different approaches can be found in literature for the determination of liquid membrane lifetime or stability. The Danesi thermodynamic model to characterize the SLM with calix[4]arene derivatives stability was proposed by Hill et al. (Hill et al., 1996). According to that model, in repeated transport experiments, the decrease of permeability coefficients (P_M) is the linear function of the number of runs:

$$\log P_M^{(i)} = \log P_M^{(1)} - (i-1) \cdot n \cdot \log(1 + \frac{R}{K_p}) \quad (5)$$

where: i is the number of run experiments; $P_M^{(1)}$ and $P_M^{(i)}$ are the Pb^{2+} permeability coefficients in the first and in the i-th transport experiments, respectively; n is the stechiometric factor for ion carrier (n = 1), $R = (V_{source}-V_{receiving})/V_{PIM}$ (R = 1000); K_p – the apparent partition constant of the carrier between the PIM and both aqueous source and the receiving solutions. The slope of the linear decrease of log P_M versus (i-1) gives an idea of the carrier lipophilicity and can be use to determine and compare carrier hydrophobicities.

In Fig. 5, the semi-logarithmic variation for the permeability coefficient P_M versus the number of runs (i-1) is shown. The carrier is slowly leaching out of PIM membrane due to its apparently high partition constant, equals 105,428 ± 12,100. This value is comparable with partition constants obtained by Hill et al. (1996) for bis-(1,2-benzo) calix[4]arene-crown-6 and bis-(1,2-naphtho) calix[4]arene-crown-6_Δ , which are 106,700, and 295,000, respectively. Calix[4]arene-bis-crown-6 as well as Aliquat 336 possessing the lowest partition constant (29,100 and 37,946 respectively) were rapidly leaching from the SLM (Hill et al., 1996; Kozlowski and Walkowiak, 2005).

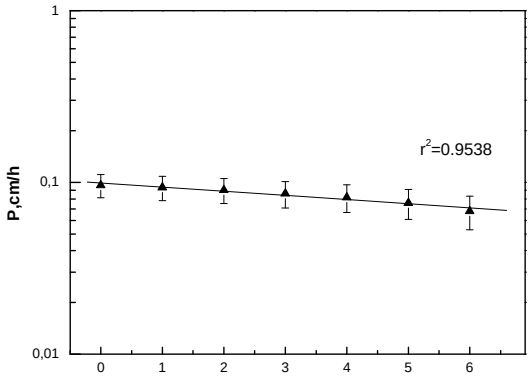

Fig. 5. Logarithmic variation of lead permeability coefficient versus the number of runs in repeated transport experiments across PIM with carrier

CONCLUSION

The studied ligand L was an efficient carrier for Pb^{2+} ions transport across PIMs. AFM of the membranes revealed that the carrier was homogeneously distributed within the membrane. The rate limiting step in transport of Pb^{2+} across PIM doped with ligand L may be the diffusion coefficient of the carrier-cation complex across the

membrane. The PIM membranes exhibited good stability using the Danesi thermodynamic model.

REFERENCES

AAMRANI F. Z. El., KUMAR A., BEYER L., FLORIDO A., SASTRE A. M. (1999), *Mechanistic study of active transport of silver(I) using sulfur containing novel carriers across a liquid membrane,* J. Membr. Sci., 152, 263-275.

ALPOGUZ K. H., SHAHABUDDIN M., MUSTAFA E., MUSTAFA Y. (2002), *Transport of Hg^{2+} through bulk liquid membrane using a bis-calix[4]arene nitrile derivative as carrier: kinetic analysis,* New Journal of Chemistry, 26, 477-480.

ARENA G, CONTINO A., LONGO E., SCIOTO D. (2001) *Selective complexation of soft Pb^{2+} and Hg^{2+} by a novel allyl functionalized thioamide calix[4]arene in 1,3-alternate conformation: A UV-visible and 1H NMR spectroscopic investigation,* J. Chem. Soc. Perkin Trans., 2001, 2, 2287-2292.

AROUS O., KERDJOUDJ H., SETA P. (2004), *Comparison of carrier –facilitated silver(I), copper(II) and gold(III) ions transport,* J. Membr. Sci., 228, 149-157.

DANESI P.R., (1984-85) *Separation of metal species by supported liquid membranes,* Sep. Sci. Technol., 19, 857-894.

KOZLOWSKI C.A., WALKOWIAK W., (2005), Applicability of liquid membranes in chromium(VI) transport with amines as ion carriers, J. Membr. Sci, 266, 143-150.

LESIŃSKA U., BOCHEŃSKA M., (2006), *Lower rim substituted tert-butylcalix[4]arenes. Part IX.** One-pot synthesis of Calix[4]arene-hydroxamates and Calix[4]arene-amides,* Synthesis, 2671-2676.

NGHIEM L.D., MORNANE P., POTTER, I.D., PERERA, J.M., CATTRALL, R.W., KOLEV, S.D. (2006), *Extraction and transport of metal ions and small organic compounds using polymer inclusion membranes (PIMs)*, J. Membrane Sci., 281, 7-41.

NECHIFOR A.C., RUSE E., NECHIFOR G, SERBAN B. (2002), *Calixarene-transportori in membrane lichide III. Transportul cationilor Pb^{2+} prin membrane lichide cu-tio-calix[4]arene,* Rev. Chim., 1, 20-26.

HILL C., DOZOL J.F., ROUQUETTE H., EYMARD S., TOURNOIS B., (1996), *Study of the stability of some supported liquid membranes,* J. Membr. Sci., 114, 73-80.

HUI-MIN M., ZHI-HUA W., QI-YU Z., LI-QUAN W., QUAN-LI M., MEI-HONG S., ZHI-TANG H. (2001), *Liquid membrane transport of transition metal ions with calix[4 crowns,* Gaodeng Xuexiao Huaxue Xuebao, 22, 1315-1318.

OTHO K., FUJIMOTO Y., INOUE K. (1999), *Stepwise extraction of two lead ions with a single molecule of calyx[4]arene tetracarboxylic acid*, Anal. Chim. Acta, 387, 61-69.

SALAZAR-ALVAREZ G., BAUTISTA-FLORES A. N., SAN MIGUEL E.R., MUHAMMED M., GYVES, T*ransport characterization of a PIM system used for the extraction of Pb(II) using D2EHPA as carrier*, J. Membr. Sci., 250, 247-257.

SUGIURA M. (1980), *Coupled-ion transport through a solvent polymeric membrane,* J. Colloid Interface Sci., 81, 385-389.

TOR A., ARSLAN G., MUSLU H., CELIKTAS A., CENGELOGLU Y., ERSOZ M., (2009) *Facilitated transport of Cr(III) through polymer inclusion membrane with di(2-ethylhexyl)phosphoric acid (DEHPA)*, J. Membr. Sci.,329, 169-174.

TU C., SUROWIEC K., GEGA J., PURKISS D.P., BARTSCH R.A. (2008), *Di-ionizable calix[4]arene-1,2-crown-5 and –crown-6 ethers in cone conformations: synthesis and divalent metal ion extraction,* Tetrahedron, 64, 1187-1196.

ULEWICZ M. (2008), *Application of macrocyclic compounds to the transport of Zn(II), Cd(II) and Pb(II) ions cross the polymer inclusion membrane (PIM),* Polish J. Chem., 82, 1237-1244.

ULEWICZ M., LESINSKA U., BOCHENSKA M., WALKOWIAK W. (2007), *Facilitated transport of Zn(II), Cd(II) and Pb(II) ions through polymer inclusion membranes with calix[4]-crown-6 derivatives,* Sep. Purif. Technol., 54, 299-306 .

WALKOWIAK W., KOZŁOWSKI C. (2009), *Macrocycle carriers for separation of metal ions in liquid membrane processes – a review,* Desalination, 240, 186-197.

WOLF J.R., STRIEDER W., (1990) *Toruosities for a random fiber bed: overlapping, parallel cylinders of several radii,* J. Membr. Sci., 49, 103-115.

ZAGHBANI A., TAYEB R., BONNAMOUR I., FELIX C., LAMARTINE R., DHAHBI M., SETA P. (2005), *Affinity membranes for the extraction of Cd^{2+} metal ions by facilitated transport ensured by a new thiacalix[4]arene complexing agent incorporated in supported liquid membranes (SLM),* J. Membr. Sci., 258, 5-7.

Ulewicz M., Lesińska U., Bocheńska M., *Transport ołowiu przez polimerową membranę inkluzyjną z pochodną p-tert-butylokaliks{4}arenem*, Physicochemical Problems of Mineral Processing, 44 (2010), 245-256, (w jęz. ang), http://www.minproc.pwr.wroc.pl/journal

Opisane zostały ułatwienia w transporcie jonów ołowiu(II) przez polimerową membranę inkluzyjną (PIMs), która składała się z trój octanu celulozy jako polimerowego suportu, eteru o-nitrofenylooktylu jako plastyfikatora i 25,26,27,28 tetra-(N-hydroksy-N-metylokarbonylo metoksy)-p-tert-butylokaliks[4]arenu jako nośnika jonów. Polimerowa membrana inkluzyjna została scharakteryzowana przy pomocy mikroskopu sił atomowych (AFM). Otrzymane wyniki wskazują, że jony Pb^{2+} mogą być efektywnie oddzielane od innych kationów metali ciężkich i przejściowych takich jak Zn^{2+}, Cd^{2+}, Co^{2+}, Ni^{2+} (przy stężeniach rzędu 10^{-3}M). Czynnikiem limitującym szybkość transportu jonów Pb^{2+} przez polimerową membranę inkluzyjna wypełnioną kaliks[4]arenem może być współczynnik dyfuzji kompleksu przenoszącego kation przez membranę. Stabilność membrany (PIM) z p-tert-butylokaliks[4]arenem była opisana przy użyciu modelu termodynamicznego Danesi. Odpowiednie stałe przenoszenia wyznaczone w sposób eksperymentalny zostały porównane z innymi stałymi przenoszenia.

słowa kluczowe: polimerowe membrany inkluzyjne, ołów(II), stabilność

Physicochem. Probl. Miner. Process. 44(2010) 257-272

journal homepage
www.minproc.pwr.wroc.pl/journal/

Physicochemical Problems of Mineral Processing

Index No. 32213X ISSN 1643-1049

M. Yildirim*, H. Akarsu**

PREPARATION OF MAGNESIUM OXIDE (MgO) FROM DOLOMITE BY LEACH-PRECIPITATION-PYROHYDROLYSIS PROCESS

Received March 3, 2009; reviewed; accepted June 12, 2009

Magnesium oxide suitable for the use in basic refractories was prepared from dolomite ($CaMg(CO_3)_2$) by hydrochloric acid leaching, precipitation with CO_2 and thermal hydrolysis. Leaching of the dolomite ore in aqueous hydrochloric acid solution was investigated with respect to the effects of time on dissolution of the dolomite sample. The dependence of the observed dissolution rate on pH was established. In the carbonation experiments changes in pH, Ca^{2+} and Mg^{2+} concentrations versus time in the effluent solution were determined. Effects of the temperature on the precipitation rate of Ca^{2+} ions as solid $CaCO_3$ were studied. Experiments were conducted to determine the kinetics of thermal decomposition of $MgCl_2.6H_2O$ during pyrohydrolysis process. From high purity magnesium chloride brine magnesium oxide containing 98.86 % MgO was obtained with the thermal decomposition recovery of 98.10 %.

key words: oxides; dolomite leaching; calcium carbonate precipitation; pyrohydrolysis; fluorescence x-ray analysis

INTRODUCTION

Magnesium oxide is usually produced by calcination of the mineral magnesite ($MgCO_3$) or magnesium hydroxide ($Mg(OH)_2$) obtained from seawater or brine by

* Corresponding author: Department of Mining Engineering, Faculty of Engineering and Architecture, Cukurova University, 01330, Balcali, Adana, Turkey, e-mail: mehyil@cukurova.edu.tr, Tel: +90 322 338 7007; fax: +90 322 338 6105

** Camis Mining Co., Is kuleleri, Kule 3, 34300, 4. Levent, Istambul, Turkey

liming. It is also produced by thermal hydrolysis of hydrated magnesium chloride ($MgCl_2$), magnesium sulfate ($MgSO_4$), magnesium sulfide (MgS), and basic carbonate (Ding et al., 2001, Duhaime et al., 2002).

One of the operations which have been widely used in the recovery of magnesium oxide from dolomite is the calcination route. Calcite and magnesite decompose at different temperatures, a stepwise decomposition permits the selective calcination in which magnesite is completely decomposed without decomposing calcite. Magnesium oxide is then separated physically from the calcined dolomite by sieving or air separation.

Magnesium bearing carbonate ores contain varying amounts of silica, iron oxide, alumina and calcium silicates, carbonates and oxides. In chemical beneficiation methods, magnesium is dissolved as salt, the insoluble impurities are removed by solid/liquid separation methods, and purified magnesia is recovered by thermal decomposition of the salt solution, which is free from the insoluble residue and the calcium component. The lime-to-silica ratio in magnesia has a major influence on its properties (Kramer, 1992).

U.S. Patent (4370422) proposes a process which comprises: a. adding calcined dolomite to a brine or bittern as a source of MgO and CaO in such amount that the molar ratio of (MgO+CaO):$MgCl_2$ is in the range of 0.66:1 to 0.05:1; b. keeping the mixture at a temperature below 90 ^oC until a solid mass is formed; c. drying the solid mass at temperature up to 200 ^oC, and d. calcining the solid mass at maximum temperature of 1200 ^oC. By this route a product of MgO was obtained and was analyzed to have purity minimum 98 % MgO, but it was an energy intensive process (Panda, Mahapatra, 1983). U.S. Patent (4720375) proposes the use of ammonium chloride to convert the calcined magnesite into $MgCl_2$. The product $MgCl_2$ solution containing also $CaCl_2$ is treated with CO_2 gas to form $CaCO_3$ that can be filtered out of the solution. The resulting $MgCl_2$ solution is then reacted with ammonium carbonate to produce $MgCO_3$ trihydrate crystals. Finally, the $MgCO_3$ is decomposed into CO_2 and MgO. The operation should be carried out in the presence of large amount of the ammonium compounds, the recovery of ammonia is costly (Ainscow, Gadgil, 1988).

In fact, all chemical processing routes based on magnesium bearing minerals rely on leaching process as the first step to selectively dissolve magnesium from the gangue minerals. This is normally followed by precipitation of magnesium from the clarified liquor. The present study pertains to a process for recovering magnesium oxide for refractory applications, and more particularly to a process for recovering precipitated calcium carbonate PCC co-product suitable for the use as a filler in paper and plastics industry.

EXPERIMENTAL

Dolomite ore from Yavca area in Icel province of Turkey was used. After grinding and sizing, its elemental analysis was performed using RIX 3000 Rigaku X-ray spectrometer and SRS 3000 Siemens X-ray fluorescence spectrometer. Mineralogical composition was determined by an electron microscope. Trace elements in the sample were determined by Perkin Elmer 2380 atomic absorption spectrometer (AAS). Analysis of thin sections indicated that dolomite was the major mineral phase whereas limonite, quartz and clay type minerals were minor mineral components of the sample. The chemical analysis results are shown in Table 1.

Table 1. Chemical analysis of the dolomite sample

Component	CaO	MgO	Al_2O_3	Na_2O	K_2O	SiO_2	Fe_2O_3
(%)	31.70	20.60	0.06	<0.002	<0.002	0.30	0.04
Component	CO_2	SO_4	Sr	Li	B	Ti	
(%)	47.30	0.13	0.06	<0.002	0.006	<0.002	

The ore sample was dissolved in hydrochloric acid solution in a 250 cm^3 Pyrex beaker. A predetermined amount of the ore at the required size (-1.7 mm) was added into HCl solution which had a starting concentration of 22 % wt. The initial solid/liquid ratio (21.70 %) was the same in all experiments, and the leaching process was conducted at room temperature (25 ^oC). After predetermined time 2 ml sample of the leach solution was withdrawn from the beaker to determine the Ca^{2+} and Mg^{2+} concentrations. pH of the leach solution was measured in each run. The necessary mixing was provided by gas evolving from the dolomite particles reacting with the acid. Filtration was made after each dissolution experiment to remove the undissolved residue and calculate the weight loss. Iron, aluminum and other ionic species were in trace amounts.

Carbonation reaction was applied to precipitate and remove the Ca^{2+} ions in the solution as PCC by using CO_2 gas at certain pressure. Magnesium hydroxide was added to adjust the pH to about 10. A batch reactor with a volume of 370 ml was used, which was equipped with magnetically driven impeller allowing the application of high stirring speed (1000 rpm) in the slurry. Injection pressure of the CO_2 gas was controlled and the temperature of the precipitation in the reactor was regulated by an automatically controlled heater underneath the stainless-steel vessel containing the solution. In each experiment Ca^{2+} concentration in the input and effluent solutions was determined by sampling from these solutions for certain precipitation period. The precipitated product PCC was filtered, dried and sampled for analysis. The experimental set up is shown in Fig. 1.

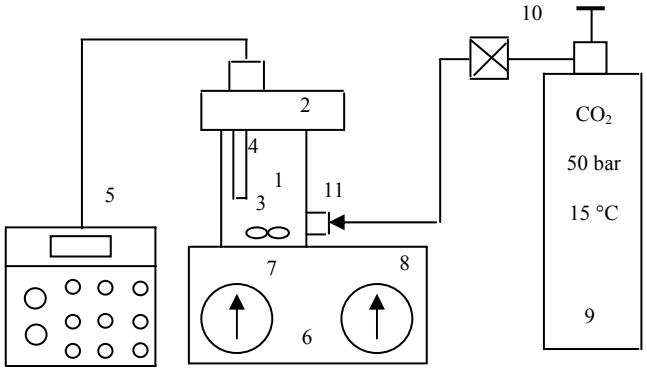

Fig. 1. Schematic diagram of the $CaCO_3$ precipitation apparatus
1. Stainless still vessel containing the leach solution, 2. Lid, 3. Magnetically driven stirrer 4. pH electrode, 5. pH meter, 6. Automatically controlled heater, 7. Stirring rate controller, 8. Temperature measuring unit, 9. CO_2 tank, 10. Gas pressure valve, 11. CO_2 inlet controller

Reference sample of $MgCl_2 \cdot 6H_2O$ (bischofite) was prepared by controlled evaporation of the purified $MgCl_2$ solution at 110 ^oC (Kashani-Nejad et al., 2005). The free water of the brine was removed from the sample at 110 ^oC. During the evaporation, pH of the solution absorbing the gaseous HCl was continuously controlled. Then 20.3 g of this sample was placed in a 500 mL heat resistant conical flask and heated at 440, 520, 560 and 600 ^oC for various periods. Gaseous HCl was absorbed in a 250 mL beaker containing 95 mL of distilled water (Fig.2). HCl concentration of this acidic solution was determined by titration with NaOH solution at the end of each experiment for the different operating temperature. Particle size analysis of the product (MgO) was determined by using the laboratory equipment Mastersizer of the Malvern Instruments Company, SEM micrographs of the sample were also obtained.

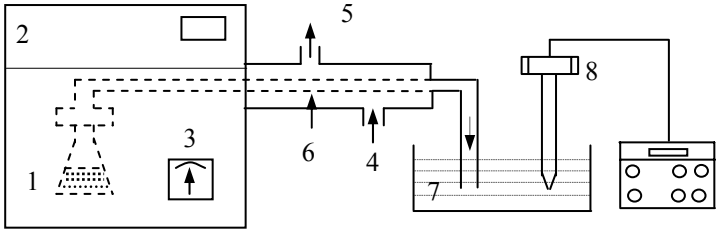

Fig. 2. Simplified view of the pyrodrolysing experiment
1. Conical flask containing $MgCl_2$ solution, 2. Heating furnace. 3. Heat control unit of the furnace (0 – 900 °C), 4. Cool water in, 5. Warm water out, 6. Flue gas ($HCl_{(g)}$) and water vapor carrying pipe, 7. Hydrochloric acid absorber, 8. pH electrode.

RESULTS AND DISCUSSION

LEACHING

The effect of leaching time on the dissolution of dolomite was studied. The results are shown in Fig. 3. Clearly, the dissolution recovery increased with time, the initial dissolution rate of Ca^{2+} and Mg^{2+} being very rapid. The recovery reached 92.43 % in the first 5 min and then, as expected, it continued to increase in the following period of time. After 30 minutes concentration of Ca^{2+} and Mg^{2+} in the leach solution increased with time and attained 1.70 mol cm^{-3} and 1.53 mol , respectively.

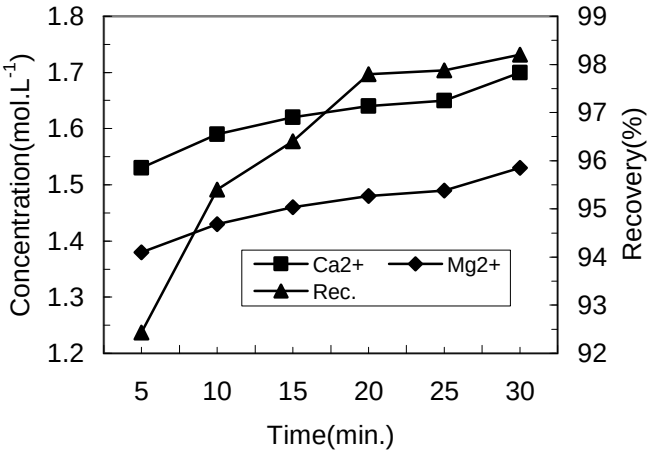

Fig. 3. Changes in the dissolution recovery, Ca^{2+} and Mg^{2+} concentrations as a function of time (HCl concentration: 22 %; solid / liquid ratio: 21.70 %; temperature: 25 °C)

The dissolution rate was calculated using Eq. (1):

$$r=(\mathrm{d}w/\mathrm{d}t)x(1/sm) \quad (\mathrm{mol\ m^{-2}s^{-1}}) \tag{1}$$

Where, dw and dt signify the weight loss of the solid sample and the time elapsed during the dissolution, respectively, s designates the unit specific surface area of the sample not dissolved at the end of the each leaching time, m represents the molecular weight of dolomite (184.41 g mol^{-1}) (Gautelier et al., 1999).

Effect of pH on the rate of dissolution of different carbonates (calcite, magnesite and dolomite) has been studied at 25 ^{o}C. At acidic conditions (pH<5), the reaction stoichiometry of dolomite dissolving in hydrochloric acid is (Chou et al., 1989, Lund et al., 1973):

$$CaMg(CO_3)_2 + 2H^+ \rightarrow Ca^{2+} + MgCO_3 + H_2O + CO_2\uparrow \tag{2}$$

$$MgCO_3 + 2H^+ \rightarrow Mg^{2+} + H_2O + CO_2\uparrow \quad (3)$$

The rate dependence of the dissolution of dolomite on pH obeys fractional order at low pH values which confirms previously published observations. The dissolution rate (r) observed can be described by the empirical relationship:

$$r=k.a^n{}_{H^+,b} \qquad (0<n<1) \quad (4)$$

Where, k is chemical reaction rate constant, n is the reaction rate order, and $a_{H^+,b}$ is the activity of hydrogen ion in the bulk of the solution. It follows from Eq. (4) that the plot of log(r) against $\log a_{H^+,b}$ for the experiments performed at constant temperature, should yield a straight line with a slope equal to n and intercept equal to log $ka_{H^+,b}$ as can be determined from Eq. 1. (Lund et al., 1973, Busenberg and Plummer, 1982; Herman and White, 1985: Alkattan et al., 1998). According to Eq. 4. log(r) is a linear function of $\log a_{H^+,b}$ and the curve drawn through these data, is consistent with this linear relationship, which was used to determine the reaction order n (Gautelier et al., 1999).

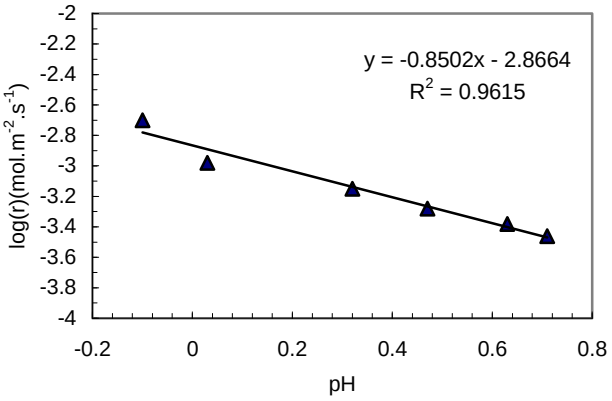

Fig. 4. Logarithm of measured dolomite dissolution rate as a function of pH

The curve illustrated in Fig. 4 was obtained from a fit of a second order functional equation to the experimental results of the dissolution. The value of the functional number n at any pH can be obtained from derivation of this functional expression with respect to the bulk pH. This calculation resulted in n value about 0.85 when pH = -0.1 at 25 ^oC. One of the researchers found n=0.75 for pH>2.5 at 25 ^0C, which is somewhat lower than found in this study (Gautelier et al., 1999). Other researchers obtained logarithm of the rate constant: log k = -2.88 and -2.59 respectively (Chou et al., 1989, Lund et al., 1973). For two component carbonates such as dolomite, the reaction order in respect to pH was determined to be 1 or 2 (Chou et al., 1989). The log$k$ value was obtained as -2.87 in this study. It is shown in Fig.4 that at very acidic conditions, dissolution rate was dependent on pH and decreased with the increase in pH value.

Hence, better dissolution conditions were achieved at high acidity. Figure 5 indicates that the rate decreased as the time increased, but the decrease was significant only up to 10 minutes, and so high recoveries (over 90 %) were achieved within 5 minutes (Fig. 3.) (Akarsu and Yildirim, 2008).

PRECIPITATION

Dissolved calcium ions in the leach solution were removed by carbonation with CO_2 gas as solid $CaCO_3$ particles. Calcium carbonate precipitation is a process of considerable industrial importance, as it is used in the production of PCC. It was performed according to the following reaction:

$$CaCl_2+H_2O+CO_2 \rightarrow CaCO_3\downarrow+2HCl \quad (5)$$

The pertinent ionic reactions which occur are represented by the following steps:

$$CO_{2\ (g)} \rightarrow CO_{2\ (aq)} \quad (6)$$

$$H_2O+CO_2 \leftrightarrow H_2CO_3 \leftrightarrow HCO_3^- + H^+ \quad (7)$$

$$HCO_3^- + Ca^{2+} \leftrightarrow CaCO_3 + H^+ \quad (8)$$

Reaction (6) is fast, but not instantaneous, and then may proceed both at the interface and in the bulk. H_2O readily reacts with CO_2 and HCO_3^- is formed in the solution (Eq. 7.). Chemical equilibrium favors the presence of CO_3^{2-} at pH 11, both CO_3^{2-} and HCO_3^- are formed at pH 8 - 11, while at pH lower than 8 only dissolved CO_2 is present. Calcium carbonate ($CaCO_3$) (reaction 8) forms at pH 7.51, while reaction (9) occurs only at pH above 10.45 (Akarsu, 2004).

$$Mg^{2+}+CO_3 \rightarrow MgCO_3 \quad (9)$$

As shown in Fig. 5, the concentration of Mg^{2+} in the effluent decreased to 1.03 mol L^{-1} during one minute, then increased again. This indicates that highest amount of Mg^{2+} ion incorporation took place during this period. On the other hand the Ca^{2+} concentration observed in the effluent was 1.6 mol L^{-1}, and then consistently decreased to 0.05 mol L^{-1}. It means that precipitation of Ca^{2+} ions as $CaCO_3$ increased with time. However, Mg^{2+} ions associated with $CaCO_3$ precipitated first, then slowly detached from the surface of the $CaCO_3$ particles into the solution.

pH of the effluent decreased as the precipitation proceeded (Fig. 5). Precipitation of calcium carbonate depends on the bicarbonate dissociation in the solution. As the sample is heated up to 70 ^oC the equilibrium between bicarbonate and carbonate (Eq. 10) is shifted towards carbonate and hence calcium carbonate begins to form and pH tends to decrease.

$$HCO_3^- \leftrightarrow CO_3^{2-} + H^+ \quad (10)$$

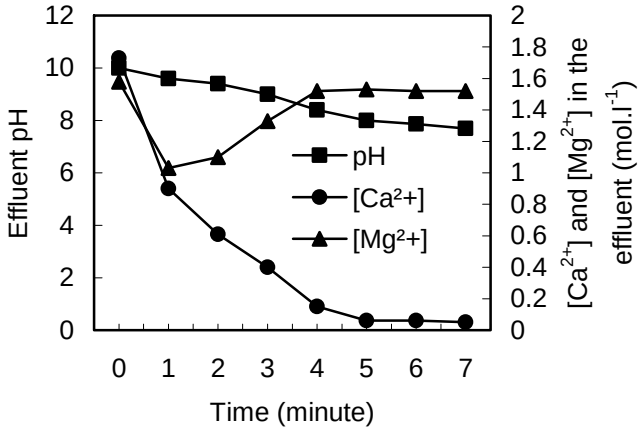

Fig. 5. Changes in pH, $[Ca^{2+}]$ and $[Mg^{2+}]$ in the effluent solution as a function of time (Temperature: 70 °C; gas (CO_2) pressure: 200 kPa)

The $CaCO_3$ precipitation rate may be given by the following equation:

$$r_p=(1/S)(N/t) \qquad (\text{mol m}^{-2}\text{s}^{-1}) \tag{11}$$

where S represents the final surface area based on the total weight of the solid $CaCO_3$ particles precipitated for the precipitation period of t, N means the number of moles of $CaCO_3$ formed at these period (Levenspiel, 1972).

The curve in Fig. 6 was obtained from a fit of a polynomial to the experimental results. It can be seen in this figure that the precipitation rates of $CaCO_3$ were low up to 50 ^oC. However the calculated rates tended to increase rapidly with increase in temperature.

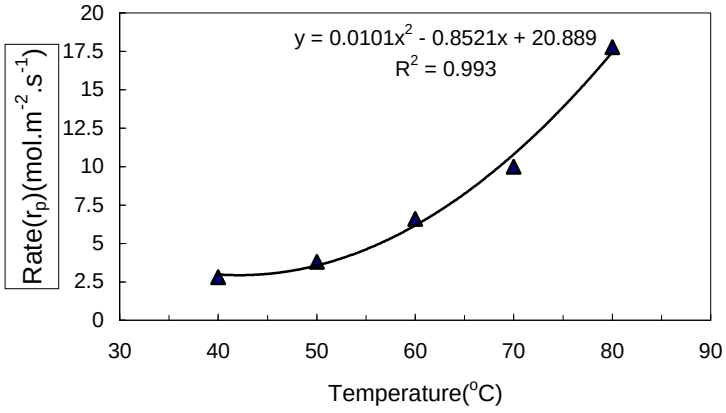

Fig. 6. Precipitation rate vs. bulk temperature (CO_2 pressure: 200 kPa; time: 5 minutes)

There was significant effect of temperature on the rate above 50 °C. It reached to $17.78 \cdot 10^{-3}$ mol $m^{-2}s^{-1}$ at 80 °C, while leaving the $MgCl_2$ solution purified from the Ca^{2+} ions. The concentration calculated was about 3.45 mol dm^{3-1}, which is about 20 times higher than that of the seawater. The precipitation rates were obtained for the temperatures using Eq. 11 and variation of $CaCO_3$ precipitation rates with temperature was determined in terms of the Arrhenius equation:

$$r_p = A e^{-Ea/RT} \tag{12}$$

Where, *Ea* is the activation energy, the term *A* is known as the pre-exponential factor, *R* designates the gas constant (8.314 $J.K^{-1}$ mol^{-1}) and *T* signifies the temperature (K). The values of the log rate computed were plotted as a function of the reciprocal temperature in Fig. 7. It follows from Eq. (12) that the slope of the straight line in Fig. 7 is equal to $-Ea/2.303R$. It can be seen from this figure that the apparent activation energy for the precipitation of $CaCO_3$ is 42.5 kJ mol^{-1}. These experiments do confirm strong temperature dependence for the precipitation reaction. In a research work it was found to be 55 kJ mol^{-1} and the *Ea* value is usually between 39 and 155 kJ mol^{-1} (Brecevic, Kralj, 2007) . A PCC product containing 96.70 % $CaCO_3$ was obtained with the precipitation recovery of 94.20 % at the optimum conditions. Its specific surface area was 0.1578 m^2 g^{-1}. The sizes d_{90} and d_{10} were 7.17 and 1.11 microns, wherein, d_{90} and d_{10} represent the particle sizes account for 90 % and 10 % by number of the total particles respectively. Chemically, it is suitable for making paint, plastic and paper due to its low SiO_2 and Fe_2O_3 contents (Table 2).

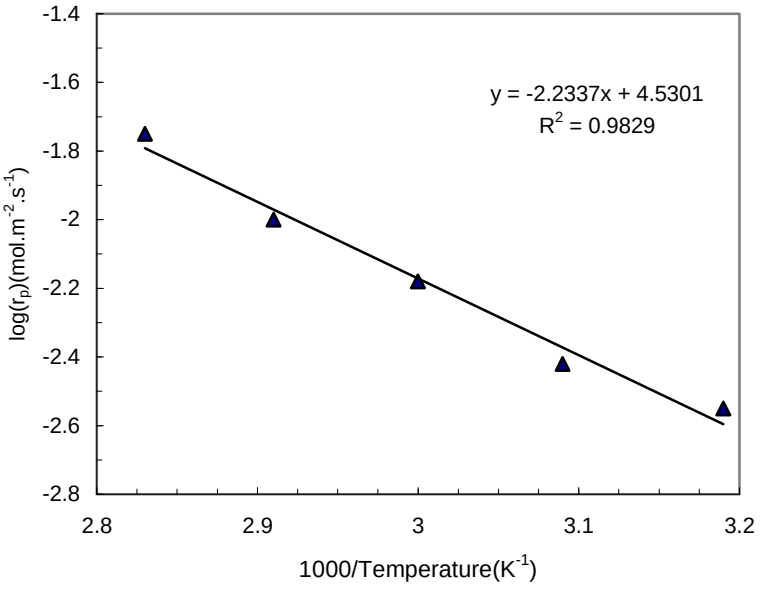

Fig. 7. Arrhenius plot for the precipitation of calcium carbonate particles

Table 2. Chemical analysis of the obtained PCC

Component	CaO	MgO	Al_2O_3	Na_2O	K_2O	SiO_2	Fe_2O_3
(%)	54.70	0.77	0.02	<0.002	<0.002	0.04	0.03
Component	CO_2	SO_4	Sr	Li	B	Ti	
(%)	44.37	0.13	0.01	<0.002	<0.002	<0.002	

PYROHYDROLYSIS

The thermal hydrolysis of hydrated magnesium chloride is a well established technology and has been commercially used for over 25 years. It is thus a proven technology even though it involves a high-temperature roast with the evolution of gaseous HCl and the attendant corrosion problems. In the pyrohydrolysis process, the purified magnesium chloride solution is heated in the pyrohydrolysing equipment shown in Fig. 2 and the hydrogen chloride gas is evolved. Under these conditions, the brine is converted to bischofite ($MgCl_2 \cdot 6H_2O$) while the gas stream is absorbed in water to reform a hydrochloric acid solution which is recycled to the leach circuit. Bischofite is decomposed into MgO and hydrogen chloride gas as shown in Eq. 13. (Kashani-Nejad et al., 2005).

$$MgCl_2 \cdot 6H2O \rightarrow MgO_{(S)} + 2HCl_{(g)} + 5H_2O \quad (13)$$

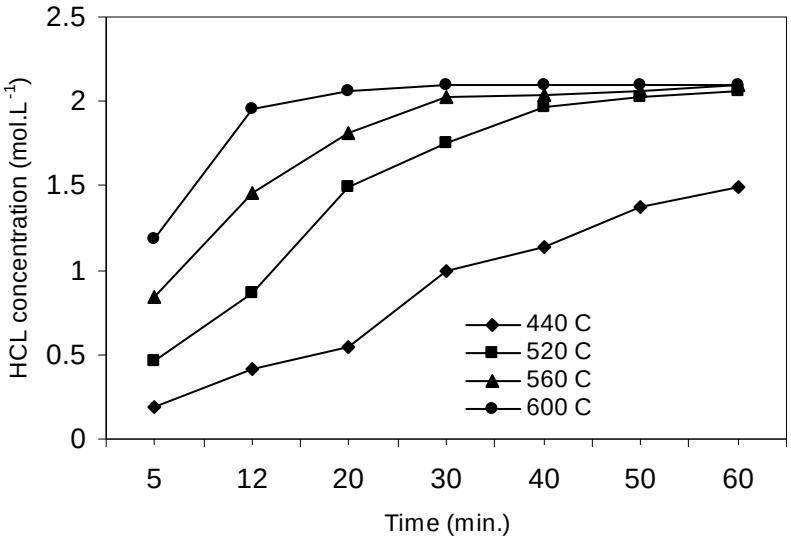

Fig. 8. HCl concentration as a function of time

It is indicated in Fig. 8 that as the time and temperature increased, HCl concentrations in the HCl absorbing solution increased. It reached 0.42 mol dm^{-3} at 440 ^oC after 12

minutes. For the same period of time at 600 °C the concentration attained 1.89 mol dm^{-3}. However it reached the value of 2.06 mol dm^{-3} at 600 °C for the 20 min. period. That corresponds to 98.10 % decomposition recovery of the HCl associated with the reference sample ($MgCl_2.6H_2O$) during this heating period. It means that one of the products of the thermal decomposition of the reference sample was HCl gas. It was consequence of the reaction shown in Eq. 13.

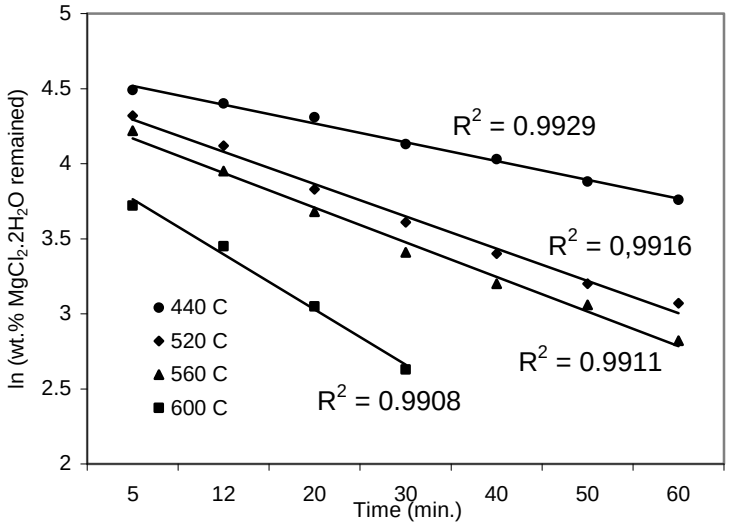

Fig. 9. Kinetics of thermal decomposition of the reference sample

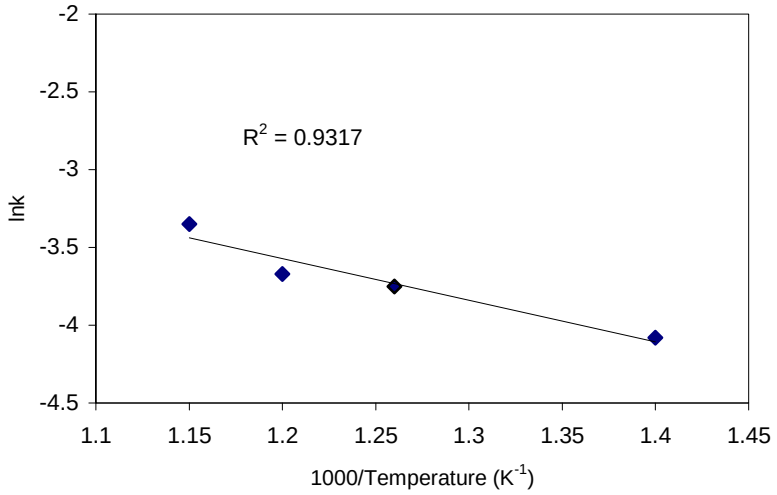

Fig. 10. Arrhenius plot of thermal decomposition of the reference sample

The weight loss of the sample determined during the decomposition process was due to the release of HCl gas and H_2O vapor. Therefore, percent of $MgCl_2.6H_2O$ remaining in the sample was found from the weight loss data. A first order kinetic plot of the results obtained in the dehydration process is shown in Fig. 9. This result is in agreement with the result obtained by the earlier researchers (Ainscow and Gadgil, 1988). Reaction rate constant (k) was obtained from the slopes of the curves in Fig. 9., and Arrhenius plot was drawn using the lnk values versus the reciprocal temperatures as shown in Fig. 10. In this figure, function of the curve was determined in terms of lnk and temperature as shown in Eq. 14. Activation energy of the thermal decomposition was obtained to be 19.95 kJ mol^{-1} by calculating the slope of the curve, which is equal to $-Ea/(1000R)$ (Fig. 10). The rate constant, k, was found to have the following dependence on temperature:

$$\ln k = -2400(1/T) + 3.27 \quad (14)$$

Table 3. Chemical composition of the purified brine

Component	Mg^{+2}	Ca^{+2}	SiO_2	Al_2O_3	Fe_2O_3	Na_2O
(g. dm^{-3})	84.32	0.78	0.03	0.02	0.02	0.001
Component	K_2O	SO_4	Sr	Li	B_2O_3	`Ti
(g dm^{-3})	0.004	0.9	0.42	0.006	0.03	0.006

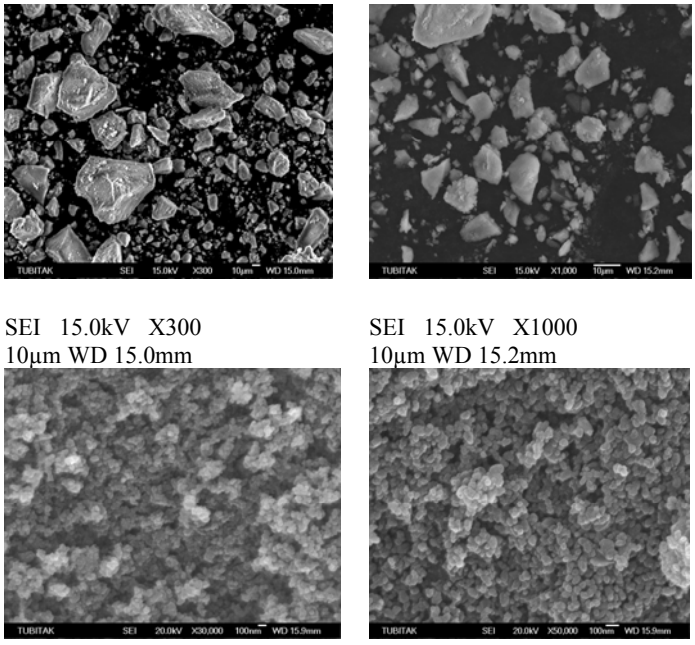

SEI 15.0kV X300 10µm WD 15.0mm

SEI 15.0kV X1000 10µm WD 15.2mm

SEI 20.0kV X30000 100nm WD 15.9mm

SEI 20.0kV X50000 100nm WD 15.9mm

Fig. 11. SEM micrographs of the submicron MgO particles

It is shown in Table 3 that basic impurity in the purified brine is calcium. It could be reduced by the improvement in the precipitation process. The carbonation is a well known process and it has been used in production of PCC in industry. This may possibly be achieved by changing the hydrodynamic conditions during the precipitation and providing better CO_2/liquid interaction. The SEM images and the particle size analysis of the particulate product MgO samples are shown in Fig. 11 and Table 4, respectively. It is evident that the shape of the particles underwent change and the sample consisted of finely divided particles displaying cubic habit. Shape of the MgO nanoparticles is important in the surface engineering.

In thermal decomposition of the sample $MgCl_2 \cdot nH_2O$; n = 1, 2, 4, 6, water can chemically bind to form a series of hydroxide compounds, and the overall reaction is:

$$MgCl_2 \cdot nH_2O \rightarrow MgOHCl \rightarrow MgO + HCl + H_2O \quad (15)$$

$$MgOHCl_{(s)} \rightarrow MgO_{(s)} + HCl_{(g)} \quad (16)$$

On the other hand, it has been known that decomposition of MgOHCl begins at 828 K, and it directly converts into MgO and HCl without undergoing any previous steps. Removal of HCl gas from the MgOHCl particle surface is a significant factor determining the rate of decomposition, and also depends on the amount of MgOHCl in the sample treated (Kashani-Nejad et al., 2005; Kipouros and Sadowayd, 2001). In this work, decomposition was 98.10% at 600 ^oC in 20 minutes. The most critical and the final reaction to form MgO is the decomposition of (MgOHCl) (Eq.16). The enthalpy of the decomposition reaction at 600 ^oC is ΔH = - 816.1 kJ mol^{-1} which means that the process is highly exothermic. The evaporation of the water is energy consuming, therefore, amount of the net energy to be supplied for formation of the MgO from the brine depends on the $MgCl_2$ concentration of the leach solution. Although the pyrohydrolysis is a highly energy intensive operation, it effectively proceeds in a single step. In the alternative process in which Mg^{2+} ions from seawater is precipitated as $Mg(OH)_2$ several unit operations are required, namely the precipitation and flocculation of $Mg(OH)_2$, dewatering, drying and calcination. The process proposed in this study does not require a pre-calcined CaO that is used to precipitate Mg^{2+} ions from seawater and other Mg^{2+} bearing solutions, which usually may increase the impurity contents of the product MgO.

When the product MgO is used in refractory and ceramic industry, the most important impurities are CaO, Al_2O_3, Fe_2O_3,, SiO_2 and B_2O_3. Generally, dolomites tend to have very low B_2O_3 contents that embrittles the magnesia refractory and ceramics during heat treatment operations. So, dolomite may be used as a raw material in manufacturing refractories and ceramic compounds. It is suitable for chemical reactions where high reactivity and rapid conversion to magnesium hydroxide are required because of its very high surface area. Its fine particle size and high purity make it an excellent magnesium source for the manufacturing of many magnesium compounds. The possible flowsheet proposed to prepare the MgO product is shown in

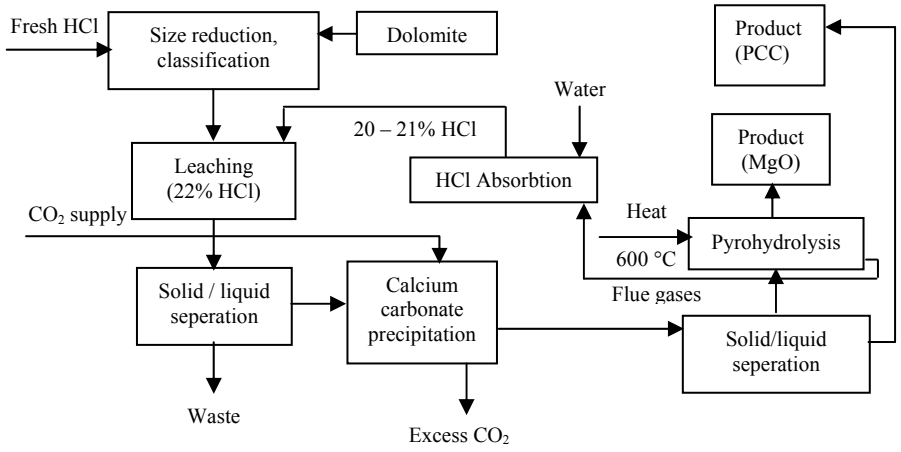

Fig. 12. Simplified flowsheet of the hydrochloric acid leach–precipitation–pyrohydrolysis process

Table 4. Physical properties of the final product MgO

Avarage particle size (microns)	36.96
Top cut	331.77
d_{90}	75.76
d_{50}	28.08
d_{10}	4.32
Surface area ($m^2 g^{-1}$)	0.5231
Whiteness (pure MgO : 100 %)	99.50

Table 5. Chemical composition of the final product MgO

Component	MgO	CaO	SiO_2	Al_2O_3	Na_2O	K_2O
(%)	98.86	0.78	0.02	0.01	0.02	<0.002
Component	SO_4	Sr	Li	B_20_3	Ti	
(%)	0.003	<0.002	0.005	0.02	<0.004	

CONCLUSIONS

I. Recovery of the dolomite dissolution increased with time and reached 92.43 % within 5 min., then 98.20% at the end of the total period (30 min).

II. The dolomite leach solution was cleaned from the Ca^{2+} ions present at 70 ^oC and 200 kPa CO_2 pressure in 5 min. with the recovery of 94.80 %..

III. Total decomposition of the purified magnesium chloride solution sample was achieved at 300-600 ^oC within 1 hour. Hydrogen chloride gas evolved was absorbed in water with the recovery of 98 % at 600 ^oC in 20 min.

IV. In the pyrohydrolysis process, kinetic data showed that removal of the product HCl gas was found to be an important factor controlling the rate of the decomposition. Kinetic data indicated that the thermal decomposition was a first order kinetic process.

V. The hydrochloric acid leach-precipitation-dehydration process offers a method of co-synthesizing high-grade MgO and PCC from a dolomite sample.

ACKNOWLEDGEMENT

The authors thank the referees who thoroughly reviewed this paper and gave valuable suggestions.

REFERENCES

AINSCOW W.S., GADGIL B.B., 1988, *Process for producing magnesium oxide*, U.S. Patent No. 4720375, January.

AKARSU H., YILDIRIM M., 2008. *Leaching rates of Icel-Yavca dolomite in hydrochloric acid solution,* Mineral Proc. Extractive Metallurgy Rev., 29, 42-56.

AKARSU A, 2004, *The Research of Obtaining High Purity MgO from Icel-Yavca Dolomite*, Cukurova University, Ph. D. Thesis, Adana, Turkey.

ALKATTAN M., OELKERS E.H., DANDURAND J.L., SCHOTT J., 1998, *An experimental study of calcite and limestone dissolution rates as a function of pH from -1 to 3 and temperature from 25 to 80 ^oC*, Chemical Geology, 151, 199-214.

BRECEVIC L., KRALJ D., 2007, *On calcium carbonates: From fundamental research application*, Croatica Chemica Acta, 80, 467-484.

BUSENBERG E., PLUMMER L.N., 1982, *The kinetics of dissolution of dolomite in CO_2-H_2O systems at 1.5 to 65 $_oC$ and 0 to 1 atm P_{CO2},* American J. Sci., 282, 45-78.

CHOU L., GARRELS M.R., WOLLAST R., 1989, *Comparative study of the kinetics and mechanisms of dissolution of carbonate minerals,* Chemical Geology, 78, 269-282.

DING Y., ZHANG G., WU H., HAI B., LIANGBIN W., QUIAN Y., 2001, *Nanoscale magnesium hydroxide and magnesium oxide powders : Control over size, shape, and structure via hydrothermal synthesis*, Chemistry of Materials, 13, 435-440.

DUHAIME P., MERCILL P., PINEAU M, 2002, *Electrolytic process technologies for the production of primary magnesium*, Transactions IMM Sect. C, 111, 53-55.

GAUTELIER M., OELKERS E.H., SCHOTT J., 1999, *An experimental study of dolomite dissolution rates as a function of pH from -0.5 to 5 and temperature from 25 to 80 ^oC,* Chemical Geology, 157, 13-26.

HERMAN J.S., WHITE W.B., 1985, *Dissolution kinetics of dolomite: Effects of lithology and fluid flow velocit,* Geochimica et Cosmochimica Acta, 49, 2017-2026.

KASHANI-NEJAD S., NG, K.-W., HARRIS R, 2005, *MgOHCl thermal decomposition kinetics,* Metallurgical and Materials Trans. B, 36B, 153-157.

KIPOUROS J.G., SADOWAYD.R., 2001, *A thermochemical analysis or the production of anhydrous $MgCl_2$,* Journal of Light Metals, 1, 111-117.

KRAMER A.D., 1992, *Magnesite and Magnesia*, Minerals Yearbook, Metals and Minerals, U.S. Bureau of Mines, Vol. 1, 163-173.

LEVENSPIEL O., 1972, *Chemical Reaction Engineering,* John Wiley & Sons, Inc., New York.

LUND K., FOGLER H.S., MCCUNE C.C., 1973, *Acidization-I. The dissolution of dolomite in hydrochloric acid,* Chemical Engineering Sci., 28, 691-700.

PANDA J.D., MAHAPATRA S.K., 1983, *Process for the production of magnesium oxide from brine or bittern*, U.S.Patent No. 4370422, January.

Yildirim M., Akarsu H., *Otrzymywanie tlenku magnezu z dolomitu za pomocą procesu ługowanie-precypitacja –pyroliza,* Physicochemical Problems of Mineral Processing, 44 (2010), 257-272, (w jęz. ang), http://www.minproc.pwr.wroc.pl/journal

Z dolomitu otrzymano tlenek magnezu przydatny do produkcji zasadowych materiałów ognioodpornych. Otrzymano go za pomocą ługowania kwasem solnym i wytrącania z użyciem CO_2 oraz stosując termiczną hydrolizę. Badano ługowanie dolomitu w roztworze kwasu solnego w odniesieniu do czasu rozpuszczania. Ustalono zależności szybkości rozpuszczania od pH. Określono zmiany pH oraz stężeń Ca^{2+} i Mg^{2+} od czasu w roztworze podczas karbonatyzacji. Badano wpływ temperatury na szybkość precypitacji jonów Ca^{2+} w postaci stałego $CaCO_3$. Przeprowadzono eksperymenty dla określenia kinetyki termicznego rozkładu $MgCl_2 \cdot 6H_2O$ podczas pirolizy. Otrzymano wysokiej czystości tlenek magnezu o zawartości 98.86% MgO z solanki zawierającej chlorek magnezu, przy sprawności termicznej dekompozycji wynoszącej 98.10%.

słowa kluczowe: tlenki, dolomity, precypitacja, piroliza, fluorescencja, analiza rtg